

**Development of a Comprehensive HPGR Model Using
Large Experimental Data Sets**

by

Chengtie Wang

B.Eng., University of Science and Technology Beijing, 2009

M.A.Sc., University of British Columbia, 2013

A THESIS SUBMITTED IN PARTIAL FULFILLMENT
OF THE REQUIREMENTS FOR THE DEGREE OF

Doctor of Philosophy

in

THE FACULTY OF GRADUATE AND POSTDOCTORAL
STUDIES

(Mining Engineering)

The University of British Columbia

(Vancouver)

April 2021

© Chengtie Wang, 2021

The following individuals certify that they have read, and recommend to the Faculty of Graduate and Postdoctoral Studies for acceptance, the thesis entitled:

Development of a Comprehensive HPGR Model Using Large Experimental Data Sets

submitted by **Chengtie Wang** in partial fulfillment of the requirements for the degree of **Doctor of Philosophy in Mining Engineering**.

Examining Committee:

Dr. Bern Klein, Department of Mining Engineering
Supervisor

Dr. Sanja Miskovic, Department of Mining Engineering
Supervisory Committee Member

Dr. Persio Rosario, Department of Mining Engineering
Supervisory Committee Member

Dr. David B Dreisinger, Department of Materials Engineering
University Examiner

Dr. Ali Madiseh, Department of Mining Engineering
University Examiner

Dr. Mauricio Guimaraes Bergerman, University of São Paulo
External Examiner

Abstract

Mining activities, particularly the crushing and grinding process, are energy intensive and energy inefficient. To meet the increasing demand in raw materials, mining companies need to focus more on energy efficiency that can enhance the operating profitability and meet the society demands for reduced carbon footprint. The High Pressure Grinding Roll (HPGR) is an important energy-efficient comminution technology with potential to significantly reduce energy consumption in the mining industry. However, a wider adoption of the HPGR is considered slow.

The goal of this research is to increase the accessibility of HPGR technology for all mining companies and their projects. A key outcome is the development of a comprehensive simulator incorporating empirical and semi-empirical models for HPGR equipment sizing, circuit design, and process simulation.

Empirical models for predicting key HPGR sizing parameters were developed based on large pilot HPGR tests conducted at the University of British Columbia (UBC). The predictions are primarily driven by feed material characteristics and HPGR operating conditions. This approach enables the sizing and selection of HPGR for cases with no specific HPGR characterization test work.

Typically, mining projects would undergo different study phases for project evaluation. A framework incorporating empirical models and small scale Piston-die Press Testing (PPT) data was proposed, which aimed at providing a low-cost option for HPGR evaluation while meeting the specific requirements per each study phase. Case studies were presented to demonstrate the use of empirical models and some specific HPGR characterization test work under the proposed framework to support different stage of studies.

Advances have also been made in addition to the semi-empirical model de-

veloped by Davaanyam (2015) that enhanced the capacity of HPGR modeling and simulation. At last, a comprehensive HPGR simulator was developed for HPGR evaluation integrating HPGR empirical models, semi-empirical models and phenomenological models.

Overall, the development of a comprehensive and reliable HPGR model and simulator provides an easier access to mining companies who may benefit from the HPGR technology. Ultimately, it is hopeful that increased number of HPGR installations can be promoted and greater energy savings can be realized.

Lay Summary

This research studied the energy efficient comminution technology, the HPGR, with an emphasis on modeling and simulation. An HPGR simulator integrating multiple empirical and semi-empirical models was developed for HPGR sizing at various project phases as well as the HPGR circuit simulation. If the simulator with corresponding laboratory testing methodology adopted, the mining industry would gain an easier access to HPGR evaluation with a greater confidence and significantly lower sample/testing requirement. It may lead to a greater number of installations of HPGR for greenfield and brownfield projects, ultimately achieving significant savings in energy usage for the mining industry.

Preface

I was responsible for developing the experimental program, conducting test work and interpreting results under the supervision of Dr. Bern Klein, professor of the Norman B. Keevil Institute of Mining Engineering, University of British Columbia. I was also responsible for all data analysis, model development and manuscript preparation.

Amit Kumar and Tulio Marques assisted with the pilot HPGR testing. Summer co-op students - Elaine Baluyut, Byrn Davies, Hassan Ahmed, and Mohamed Ashrafakl - assisted me with labor intensive tasks such as dry and wet screening tests for particle size distribution analysis.

Preliminary results of this research were published in the following papers:

- **Wang, C., & Klein, B.** (2019). A review of 10 years of HPGR pilot tests at UBC. 7th International Conference on Semi-Autogenous and High Pressure Grinding Technology, Vancouver, BC, Canada. I was the presenter and was responsible for data collection, data analysis, manuscript and presentation preparation. Dr. Klein reviewed the manuscript and presentation.
- **Wang, C., Klein, B., & Rosario, P.** (2019). Using piston-die press tests for preliminary sizing and selection of a high-pressure grinding roll. CIM Journal, Vol. 10, No. 3, 2019. <https://doi.org/10.15834/cimj.2019.10>. I was responsible for sample collection, test work, data analysis and manuscript composition. Dr. Klein and Dr. Rosario reviewed the manuscript and assisted with manuscript proofreading.
- **Wang, C., Klein, B., & Rosario, P.** (2019). Preliminary sizing and selection of an HPGR Using Piston-die press tests. 51st Annual Meeting of the Cana-

dian Mineral Processors, Ottawa, ON, Canada. I was the presenter and was responsible for sample collection, test work, data analysis, manuscript and presentation preparation. Dr. Klein and Dr. Rosario reviewed the manuscript and presentation.

- Daniel, M., Klein, B., & **Wang, C.** (2018). High-pressure Grinding Roll Technology, Mineral Processing and Extractive Metallurgy Handbook. Chapter 3. I assisted the write-up of the manuscript, provided inputs and editing assistance. Dr. Daniel and Dr. Klein were responsible for the manuscript preparation and writing.
- Klein, B., **Wang, C.**, & Nadolski, S. (2018). Energy-efficient comminution: Best practices and future research needs. In Energy efficiency in the minerals industry (pp. 197-211). Springer, Cham. I assisted the write-up of the manuscript, provided inputs and editing assistance. Dr. Klein was responsible for the manuscript preparation and writing. Dr. Nadolski reviewed the manuscript.

Table of Contents

Abstract	iii
Lay Summary	v
Preface	vi
Table of Contents	viii
List of Tables	xiii
List of Figures	xvi
List of Symbols	xxiv
List of Abbreviations	xxvii
Acknowledgments	xxix
1 Introduction	1
1.1 Problem Statement	1
1.2 Research Objectives	4
1.3 Thesis Outline	5
2 Literature Review	6
2.1 Introduction	6
2.2 High Pressure Grinding Rolls Technology	6
2.2.1 HPGR working principle	10

2.2.2	HPGR sizing and scale-up parameters	12
2.2.3	HPGR performance	14
2.2.4	HPGR advantages and disadvantages	17
2.3	Comminution Modeling	18
2.3.1	Particle-bed breakage characterization	19
2.3.2	Particle-bed breakage modeling	19
2.4	HPGR Modeling	22
2.4.1	Klymowsky-Liu HPGR model	23
2.4.2	Morrell-Tondo-Shi HPGR model	27
2.4.3	Davaanyam-Klein-Nadolski HPGR models	30
2.5	Summary of Literature Review	34
3	Experimental Program and Methodologies	36
3.1	Introduction	36
3.2	Sample Description	37
3.3	Pilot HPGR Testing	38
3.3.1	Pilot HPGR facility	38
3.3.2	HPGR test procedure	40
3.4	Piston-die Press Testing	41
3.4.1	Piston-die press test facility	41
3.4.2	Piston-die test procedure	42
3.4.3	Force-displacement analysis	44
3.5	Linear Regression Methods	46
3.6	Population Balance Modeling	52
4	Results of HPGR and Piston-die Press Testing	53
4.1	Introduction	53
4.2	Summary of HPGR Test Results	54
4.2.1	HPGR key performance indicators	55
4.2.2	Comparative HPGR testing	58
4.3	Summary of Piston-die Press Test Results	65
4.3.1	PPT calibration testing	65
4.3.2	PPT simulation testing	69

4.4	Comparison of Comminution Test Results	72
5	HPGR Database and Empirical Models	74
5.1	Introduction	74
5.2	Description of HPGR database	75
5.2.1	HPGR input variables	78
5.2.2	HPGR output variables	85
5.3	Development of Empirical Regression Models	102
5.3.1	Description of the data	102
5.3.2	Data pre-processing and exploration	103
5.3.3	Prediction of HPGR power draw	106
5.3.4	Prediction of HPGR net specific energy	110
5.3.5	Prediction of HPGR throughput	113
5.3.6	Prediction of HPGR product size and reduction ratio . . .	116
5.4	Summary and Conclusions	122
6	HPGR Sizing from Conceptual to Feasibility	125
6.1	Introduction	125
6.2	HPGR Circuit Design Considerations	126
6.2.1	Generic comminution test work	126
6.2.2	HPGR characterization test work	127
6.2.3	Process design criteria	127
6.2.4	Flowsheet development	137
6.3	HPGR Sizing Methods	140
6.4	Case Studies from Conceptual to Feasibility	146
6.4.1	Project background	146
6.4.2	Conceptual design and trade-off	147
6.4.3	Preliminary assessment	157
6.4.4	Pre-feasibility assessment	171
6.4.5	Feasibility level assessment	181
6.5	Summary and Conclusions	182
7	HPGR Modeling and Simulation	183
7.1	Introduction	183

7.2	HPGR Modeling	184
7.2.1	UBC HPGR model structure	184
7.2.2	Ore breakage characterization	186
7.2.3	Energy and size reduction model	187
7.3	Development of Ore-specific HPGR Model	190
7.3.1	Ore characterization	191
7.3.2	Pilot testing data	193
7.3.3	Model development	196
7.3.4	Simulation of HPGR processes	199
7.4	Development of Generic HPGR Model	206
7.4.1	Ore characterization database	206
7.4.2	Pilot testing data	207
7.4.3	Model development	208
7.5	HPGR Model Testing and Validation	209
7.5.1	Pilot testing and machine specification	209
7.5.2	Ore characterization	210
7.5.3	Model testing and validation	211
7.6	Summary and Conclusions	214
8	Conclusions and Recommendations	215
8.1	Main Outcomes	215
8.2	Recommendations for Future Research	219
9	Claims of Original Contribution	220
	Bibliography	222
A	HPGR Test Data	233
A.1	HPGR Test Procedure	234
A.2	HPGR Test: Cu-Mo (HB) Ore	235
A.3	HPGR Test: Cu-Mo (HC) Ore	242
A.4	HPGR Test: Cu-Au (C) Ore	255
A.5	HPGR Test: Au (G) Ore	260
A.6	HPGR Test: Quarry Sample	269

B	Piston-die Press Test Data	277
B.1	Piston-die Press Procedure	278
B.2	PPT Calibration Tests	280
C	HPGR and PPT Reproducibility	295
C.1	HPGR Test Reproducibility	295
C.1.1	Reproducibility testing	295
C.1.2	Reproducibility between labs	298
C.2	PPT Test Reproducibility	300
C.2.1	PPT calibration test	300
C.2.2	PPT simulation test	303
D	Machine Learning Approach for mdot Prediction	305
D.1	Introduction	305
D.2	Methodology	306
D.2.1	Data collection	307
D.2.2	Data pre-processing	307
D.2.3	Analytical modeling	307
D.2.4	Model evaluation and selection	309
D.3	Results and Discussion	309
D.4	Summary and Conclusions	311

List of Tables

Table 2.1	Examples of HPGR Installations	9
Table 2.2	HPGR sizing parameters	13
Table 3.1	Sample received for the research program	38
Table 3.2	Köppern HPGR specifications	39
Table 3.3	General PPT simulation test conditions	43
Table 4.1	Summary of HPGR test results	54
Table 4.2	Comparison of two HPGR tests at the same specific pressing force	60
Table 4.3	Comparison of HPGR tests on soft and hard materials	62
Table 4.4	Summary of HPGR locked-cycle tests	63
Table 4.5	Summary of Piston-die press testing program	66
Table 4.6	PPT calibration tests at piston pressure of 240 Mpa	67
Table 4.7	Summary of t_{10} breakage parameters for various ore types . . .	70
Table 4.8	Summary of the appearance parameters for various ore types .	71
Table 5.1	HPGR input and output variables	76
Table 5.2	Descriptive statistics of HPGR parameters under study	77
Table 5.3	HPGR feed top size range	78
Table 5.4	Industrial scale HPGR roll speed range	84
Table 5.5	Statistics of the HPGR feed and product sizes	98
Table 5.6	Model parameters for HPGR product normalization	101
Table 5.7	Summary results of regression for power draw	107
Table 5.8	Summary results of regression for specific energy consumption	111
Table 5.9	Summary results of regression for product size P_{80}	117

Table 5.10	Summary results of regression for reduction ratio RR_{80full} . . .	119
Table 6.1	General comminution tests	126
Table 6.2	Sizing of SAG mill and HPGR for soft and hard ores	131
Table 6.3	Example of HPGR sizing	142
Table 6.4	Examples of HPGR production machines	143
Table 6.5	Testing, sizing and selection of HPGR	145
Table 6.6	General process design criteria for Project G	146
Table 6.7	Summary of comminution tests at conceptual level	147
Table 6.8	Prediction of pilot HPGR based on given feed characteristics .	151
Table 6.9	Major comminution equipment - SAG and HPGR circuit . . .	152
Table 6.10	Comparison of pure comminution circuit specific energy	153
Table 6.11	Summary of CAPEX and OPEX	154
Table 6.12	High-level SWOT analysis	157
Table 6.13	Results of PPT on Project G composite samples	161
Table 6.14	Results of PPT on Project G variability samples	161
Table 6.15	HPGR sizing - PPT calibration method	171
Table 6.16	Summary of pilot HPGR test results - Project G	172
Table 6.17	Comparison of HPGR sizing parameters	179
Table 6.18	HPGR sizing confirmation - HPGR-PPT calibration method . .	180
Table 7.1	Summary of t_{10} breakage parameters for Project G samples . .	192
Table 7.2	Appearance function for Project G ore samples	193
Table 7.3	Summary of HPGR operating conditions - Project G	194
Table 7.4	Summary of feed and product sizes	196
Table 7.5	Fitted HPGR model parameters	196
Table 7.6	HPGR model parameters used for simulations	199
Table 7.7	Simulation summary for varying specific pressing force	200
Table 7.8	Simulation summary for varying feed size distributions	202
Table 7.9	Simulation summary for 6 variability samples	204
Table 7.10	Summary of t_{10} breakage parameters on 18 samples	206
Table 7.11	Individual and master fitted appearance function	207
Table 7.12	Summary of HPGR operating conditions	208

Table 7.13	Fitted classification function	208
Table 7.14	Köppern HPGR testing facilities	209
Table 7.15	Summary of HPGR operating conditions - Project T	210
Table 7.16	Summary of t_{10} breakage parameters for Project T samples	210
Table 7.17	Appearance function for Project T ore samples	211
Table 7.18	HPGR model parameters	211
Table C.1	Five replicates of HPGR feed PSDs - Cu-Au (C)	297
Table C.2	Nine replicates of HPGR feed PSDs - Fe (SA)	297
Table C.3	Summary of HPGR repeat tests	297
Table C.4	HPGR testing facilities	298
Table C.5	Six replicates of PPT feed and product sizes	302
Table C.6	Summary of PPT calibration repeat tests	303
Table C.7	Breakage and appearance parameters for the repeat simulation tests	304
Table D.1	Testing scores for potential mdot models	309

List of Figures

Figure 2.1	Comminution breakage mechanisms	7
Figure 2.2	Schematic of an HPGR unit	7
Figure 2.3	Schematic of particle compression and breakage in HPGR . .	10
Figure 2.4	Pressure profile in the compression zone	11
Figure 2.5	Published relationship between net specific energy and specific pressing force	14
Figure 2.6	Relationship of specific pressing force and specific throughput	15
Figure 2.7	Effect of feed moisture on the specific energy consumption . .	16
Figure 2.8	Effect of feed moisture on the roll gap and throughput	16
Figure 2.9	Energy-size reduction relationship	20
Figure 2.10	Self-similar size distributions of quartz comminuted	21
Figure 2.11	Self-similar size distributions of Au-ore comminuted in HPGR and piston-die test	22
Figure 2.12	Fraction of broken particles as a function of particle size and energy input	23
Figure 2.13	Normalized E and S	24
Figure 2.14	Breakage function parameter μ and σ as a function of size and energy absorption	25
Figure 2.15	Schematic location of three crusher zones in HPGR	27
Figure 2.16	Schematic of the Morrell-Tondo-Shi size reduction model . .	28
Figure 2.17	Whiten-Awachi-Andersen crusher size reduction model	29
Figure 2.18	A set of master curves describing $t_{10} - t_n$ relationship	32
Figure 2.19	Schematic structure of the Davaanyam size reduction model .	33

Figure 3.1	Overall structure of the research program	37
Figure 3.2	Pilot HPGR facility at UBC	39
Figure 3.3	HPGR testing facility setup	41
Figure 3.4	Schematic of the piston-die press apparatus	41
Figure 3.5	Force-displacement curve from piston-die press testing	44
Figure 3.6	Trapezoid and curve fitting method for input energy calculation	45
Figure 3.7	Comparison of trapezoid and bi-exponential integration methods	46
Figure 3.8	K-fold Cross-validation procedure (K=5)	49
Figure 3.9	Regression analysis workflow	51
Figure 4.1	Specific pressing force versus net specific energy consumption	55
Figure 4.2	Influence of specific pressing force on specific throughput constant	56
Figure 4.3	Influence of specific energy on HPGR product size	57
Figure 4.4	Influence of specific pressing force on size reduction ratio	58
Figure 4.5	Examples of HPGR feed and product PSDs ($F_{sp} = 3.6N/mm^2$)	59
Figure 4.6	Feed and product PSDs of HPGR tests on soft and hard materials	61
Figure 4.7	Feed and product PSDs of HPGR locked-cycle tests	63
Figure 4.8	Feed and product PSDs of multiple stage HPGR tests	64
Figure 4.9	Results of multiple stage HPGR testing	65
Figure 4.10	PPT feed and product PSD at 240 Mpa piston pressure	66
Figure 4.11	Specific energy versus piston pressure	68
Figure 4.12	Size reduction ratio versus specific energy	68
Figure 4.13	Specific energy and t_{10} relationship of the Cu-Au (C) ore	69
Figure 4.14	Specific energy and t_{10} relationship for various ore types	70
Figure 4.15	Relationship between t_{10} and t_n of the Cu-Au (C) ore	71
Figure 4.16	BWI and Axb	72
Figure 4.17	Comparison of various ore hardness characteristics	73
Figure 5.1	Frequency of HPGR tests per ore types within the database	75
Figure 5.2	Particle size distributions of HPGR feed	79
Figure 5.3	Examples of HPGR feed PSD model fitting	80
Figure 5.4	Distribution of feed bulk density	81

Figure 5.5	Distribution of feed moisture content	82
Figure 5.6	Moisture by weight and by volume	82
Figure 5.7	Distribution of HPGR roll speed	83
Figure 5.8	Distribution of HPGR specific pressing force	85
Figure 5.9	Simplified schematic of forces in an HPGR	86
Figure 5.10	Distribution of total power and net power draw	86
Figure 5.11	Distributions of the calculated force reaction angle	87
Figure 5.12	Distribution of HPGR operating gap	88
Figure 5.13	Operating gap and measured flake thickness	89
Figure 5.14	Distribution of estimated HPGR critical gap	90
Figure 5.15	Specific throughput constant as a function of the operating gap and flake thickness	91
Figure 5.16	Scatter plot of the calculated and recorded specific throughput constant	92
Figure 5.17	Boxplot of mdot grouped by ore type at Fsp of 4.0 N/mm ² . . .	93
Figure 5.18	Distributions of HPGR specific throughput constant by ore type	93
Figure 5.19	Boxplot of the net specific energy consumption grouped by ore type at Fsp of 4.0 N/mm ²	94
Figure 5.20	Distributions of HPGR net specific energy consumption at dif- ferent specific pressing forces	95
Figure 5.21	Particle size distributions of HPGR product	96
Figure 5.22	Distributions of HPGR product size at Fsp of 4.0 N/mm ² . . .	97
Figure 5.23	Distributions of percentage passing in HPGR product at Fsp of 4.0 N/mm ²	97
Figure 5.24	Distributions of size reduction ratios at Fsp of 4.0 N/mm ² . . .	99
Figure 5.25	HPGR product normalization	100
Figure 5.26	Reconstitution of HPGR product size distribution	101
Figure 5.27	Correlation matrix of the identified predictor and response vari- ables	105
Figure 5.28	Residual plots of the regression model for power draw	108
Figure 5.29	Residuals versus predictor variables of the power model	109
Figure 5.30	Scatter plot of the measured and predicted power draw	110
Figure 5.31	Residual plots of the regression model for specific energy	112

Figure 5.32	Residuals versus predictor variables of the specific energy model	112
Figure 5.33	Scatter plot of the measured and predicted specific energy . . .	113
Figure 5.34	Residual plots of the regression model for HPGR throughput . . .	114
Figure 5.35	Scatter plot of the measured and predicted throughput	115
Figure 5.36	Scatter plot of the measured and predicted specific throughput constant	116
Figure 5.37	Residual plots of the regression model for product size P_{80} . . .	118
Figure 5.38	Residuals versus predictor variables of the P_{80} model	118
Figure 5.39	Residual plots of the regression model for RR_{80full}	120
Figure 5.40	Residuals versus predictor variables of the RR_{80full} model . . .	120
Figure 5.41	Scatter plot of the measured and predicted P_{80}	121
Figure 5.42	Scatter plot of the measured and predicted RR_{80full}	122
Figure 6.1	SAG mill motor power as a function of operating conditions . . .	128
Figure 6.2	HPGR throughput as a function of roll diameter and speed . . .	129
Figure 6.3	Ore variability measured by DWi value	132
Figure 6.4	Estimates of potential annual power cost savings	134
Figure 6.5	SAG/HPGR design consideration	136
Figure 6.6	Greenfield HPGR flowsheet options	137
Figure 6.7	Brownfield HPGR flowsheet options	138
Figure 6.8	HPGR flowsheet options for the winter condition	139
Figure 6.9	Interrelationship between HPGR scale-up parameters	140
Figure 6.10	Simplified SABC flowsheet	148
Figure 6.11	Simplified HPGR-Ball mill flowsheet	148
Figure 6.12	SABC circuit simulation in JK SimMet™	149
Figure 6.13	Modeled HPGR feed and product PSDs	150
Figure 6.14	Sensitivity of the NPC to power cost	155
Figure 6.15	Sensitivity of the NPC to CAPEX	156
Figure 6.16	HPGR preliminary sizing methodology	158
Figure 6.17	Relation between piston pressure and specific energy	162
Figure 6.18	PPT feed and product PSDs	163
Figure 6.19	Relation between piston specific energy consumption and size reduction ratio	163

Figure 6.20	Predicted net specific energy as a function HPGR pressing force (error bars represent 95% confidence intervals)	164
Figure 6.21	Predicted reduction ratio as a function of HPGR pressing force (error bars represent 95% confidence intervals)	165
Figure 6.22	Normalized piston product size distributions	166
Figure 6.23	Predicted pilot HPGR product size distributions for composite samples	167
Figure 6.24	Predicted % -6mm of pilot HPGR product (error bars represent 95% confidence intervals)	168
Figure 6.25	Predicted circuit specific energy consumption (error bars represent 95% confidence intervals)	169
Figure 6.26	Predicted circuit throughput as a function of HPGR pressing force (error bars represent 95% confidence intervals)	170
Figure 6.27	Calibration of HPGR specific pressing force and piston pressure for Comp1 sample	173
Figure 6.28	Specific pressing force versus net specific energy consumption (error bars represent 95% confidence intervals)	174
Figure 6.29	Calibration of HPGR and piston size reduction	175
Figure 6.30	Specific pressing force versus reduction ratio (error bars represent 95% confidence intervals)	176
Figure 6.31	Normalized HPGR and piston product size distributions	177
Figure 6.32	Specific pressing force versus percent passing 6 mm (error bars represent 95% confidence intervals)	177
Figure 6.33	Predicted circuit throughput as a function of HPGR pressing force (error bars represent 95% confidence intervals)	178
Figure 6.34	Predicted circuit specific energy consumption (error bars represent 95% confidence intervals)	179
Figure 7.1	The proposed procedure for simulation to optimize design or performance	185
Figure 7.2	Proposed structure for HPGR energy-size reduction model	188
Figure 7.3	Model structure showing fitting algorithm and simulation route	191
Figure 7.4	Specific energy and t_{10} relationship on Project G ores	192

Figure 7.5	Fitted curve to tested composite and variability samples	193
Figure 7.6	Critical gap as a function of specific pressing force	194
Figure 7.7	Size distributions of HPGR feed and product	195
Figure 7.8	Comparison of measured and fitted size distributions	197
Figure 7.9	Comparison of measured and predicted values	198
Figure 7.10	Simulated product PSDs at varying specific pressing force	200
Figure 7.11	Variations of feed size distribution for the simulation	201
Figure 7.12	Simulated PSDs for different feed size distributions	202
Figure 7.13	Specific energy consumption as a function of specific pressing force for 6 variability samples based on PPT calibration tests	203
Figure 7.14	Simulated center product size for 6 variability samples	205
Figure 7.15	Master curve fitted to eighteen tested ores	207
Figure 7.16	Comparison of measured and predicted values	209
Figure 7.17	Comparison of measured and predicted values	212
Figure 7.18	Comparison of measured and fitted size distributions - Lab A	213
Figure 8.1	HPGR evaluation flow chart	218
Figure A.1	Pilot HPGR test procedure	234
Figure A.2	Feed and product PSDs of test Cu-Mo(HB)-11	235
Figure A.3	Feed and product PSDs of test Cu-Mo(HB)-12	236
Figure A.4	Feed and product PSDs of test Cu-Mo(HB)-13	237
Figure A.5	Feed and product PSDs of test Cu-Mo(HB)-14	238
Figure A.6	Feed and product PSDs of test Cu-Mo(HB)-21	239
Figure A.7	Feed and product PSDs of test Cu-Mo(HB)-22	240
Figure A.8	Feed and product PSDs of test Cu-Mo(HB)-23	241
Figure A.9	Feed and product PSDs of test Cu-Mo(HC)-A11	242
Figure A.10	Feed and product PSDs of test Cu-Mo(HC)-A12	243
Figure A.11	Feed and product PSDs of test Cu-Mo(HC)-A21	244
Figure A.12	Feed and product PSDs of test Cu-Mo(HC)-A22	245
Figure A.13	Feed and product PSDs of test Cu-Mo(HC)-A23	246
Figure A.14	Feed and product PSDs of test Cu-Mo(HC)-C11	247
Figure A.15	Feed and product PSDs of test Cu-Mo(HC)-C12	248

Figure A.16	Feed and product PSDs of test Cu-Mo(HC)-C13	249
Figure A.17	Feed and product PSDs of test Cu-Mo(HC)-C21	250
Figure A.18	Feed and product PSDs of test Cu-Mo(HC)-C22	251
Figure A.19	Feed and product PSDs of test Cu-Mo(HC)-C23	252
Figure A.20	Feed and product PSDs of test Cu-Mo(HC)-D11	253
Figure A.21	Feed and product PSDs of test Cu-Mo(HC)-D21	254
Figure A.22	Feed and product PSDs of test Cu-Au(C)-01	255
Figure A.23	Feed and product PSDs of test Cu-Au(C)-02	256
Figure A.24	Feed and product PSDs of test Cu-Au(C)-03	257
Figure A.25	Feed and product PSDs of test Cu-Au(C)-04	258
Figure A.26	Feed and product PSDs of test Cu-Au(C)-05	259
Figure A.27	Feed and product PSDs of test Au(G)-D01	260
Figure A.28	Feed and product PSDs of test Au(G)-D02	261
Figure A.29	Feed and product PSDs of test Au(G)-D03	262
Figure A.30	Feed and product PSDs of test Au(G)-D04	263
Figure A.31	Feed and product PSDs of test Au(G)-P01	264
Figure A.32	Feed and product PSDs of test Au(G)-P02	265
Figure A.33	Feed and product PSDs of test Au(G)-P03	266
Figure A.34	Feed and product PSDs of test Au(G)-P04	267
Figure A.35	Feed and product PSDs of test Au(G)-P05	268
Figure A.36	Feed and product PSDs of test Quarry SD-01	269
Figure A.37	Feed and product PSDs of test Quarry SD-02	270
Figure A.38	Feed and product PSDs of test Quarry SD-03	271
Figure A.39	Feed and product PSDs of test Quarry SD-04	272
Figure A.40	Feed and product PSDs of test Quarry SD-05	273
Figure A.41	Feed and product PSDs of test Quarry SD-06	274
Figure A.42	Feed and product PSDs of test Quarry SD-07	275
Figure A.43	Feed and product PSDs of test Quarry SD-08	276
Figure B.1	Piston-die press calibration test procedure	278
Figure B.2	Piston-die press simulation test procedure	279
Figure B.3	PPT calibration test results - Cu-Au(C)-1A	281
Figure B.4	PPT calibration test results - Cu-Au(C)-1B	282

Figure B.5	PPT calibration test results - Cu-Au(C)-2A	283
Figure B.6	PPT calibration test results - Cu-Au(C)-2B	284
Figure B.7	PPT calibration test results - Cu-Au(C)-3A	285
Figure B.8	PPT calibration test results - Cu-Au(C)-3B	286
Figure B.9	PPT calibration test results - Cu-Au(C)-4A	287
Figure B.10	PPT calibration test results - Cu-Au(C)-4B	288
Figure B.11	PPT calibration test results - Cu-Au(C)-Geo1	289
Figure B.12	PPT calibration test results - Cu-Au(C)-Geo2	290
Figure B.13	PPT calibration test results - Cu-Au(C)-Geo3	291
Figure B.14	PPT calibration test results - Cu-Au(C)-Geo4	292
Figure B.15	PPT calibration test results - Cu-Au(C)-Geo5	293
Figure B.16	PPT calibration test results - Cu-Au(C)-Geo6	294
Figure C.1	Variation in PSD of the sub-sampled HPGR feed	296
Figure C.2	Specific throughput versus specific pressing force with UBC Köppern HPGR vs Lab C Weir HPGR	299
Figure C.3	Total specific energy versus specific pressing force with UBC Köppern HPGR and Lab C Weir HPGR	300
Figure C.4	Center product size P_{80} and P_{50} versus net specific energy with UBC Köppern HPGR and Lab C Weir HPGR	301
Figure C.5	Percent passing 6 mm in the product of UBC Köppern HPGR and Lab C Weir HPGR	301
Figure C.6	Variation in PSD of the repeat PPT feed and product	302
Figure C.7	PPT simulation repeat tests - breakage curves	304
Figure D.1	Workflow for machine learning model development	306
Figure D.2	Prediction vs observation using the AdaBoost model	310
Figure D.3	Distribution of AdaBoost prediction error	311

List of Symbols

α	Nip angle or compression angle ($^{\circ}$)
β	Force reaction angle ($^{\circ}$)
C_{50}	50% passing size of the center product by weight (mm)
C_{80}	80% passing size of the center product by weight (mm)
D	Roll diameter (m)
E_{50}	50% passing size of edge product by weight (mm)
E_{80}	80% passing size of edge product by weight (mm)
E_{sc}	Specific comminution energy of impact breakage (kWh/t)
E_{sp}	Net specific energy consumption of HPGR test (kWh/t)
f_{mat}	Fitted parameter representing the material break-age property
F	Pressing or grinding force (kN)
F_{sp}	Specific pressing force (N/mm ²)
F_{8mm}	Percentage of -8mm material in the feed (%)
F_{6mm}	Percentage of -6mm material in the feed (%)
F_{4mm}	Percentage of -4mm material in the feed (%)
F_{2mm}	Percentage of -2mm material in the feed (%)
F_{1mm}	Percentage of -1mm material in the feed (%)
$F_{0.2mm}$	Percentage of -0.2mm material in the feed (%)

$F_{0.1mm}$	Percentage of -0.1mm material in the feed (%)
F_{50}	50% passing size of the feed by weight (mm)
F_{80}	80% passing size of the feed by weight (mm)
F_{95}	95% passing size of the feed by weight (mm)
L	Roll length (m)
\dot{m}	m-dot or specific throughput constant (ts/hm ³)
\dot{m}_c	Circuit-specific throughput constant (ts/hm ³)
M	Fitted representing the maximum attainable t_{10}
P	Power (kW)
P_i	No-load or idle power draw (kW)
P_{net}	Net power draw (kW)
P_{piston}	Piston pressure (MPa)
P_{50}	50% passing size of the product by weight (mm)
P_{80}	80% passing size of the product by weight (mm)
ρ_{bulk}	Feed bulk density (t/m ³)
ρ_g	Cake density (t/m ³)
ρ_f	Flake density (t/m ³)
t_{10}	Percentage passing 1/10 th the feed particle size
t_n	Percentage passing 1/n th the feed particle size
RR_{50full}	Size reduction ratios from 50% passing feed size to 50% passing full product size
RR_{80full}	Size reduction ratios from 80% passing feed size to 80% passing full product size
RR_{HPGR}	HPGR size reduction ratio
RR_{piston}	Piston size reduction ratio
T	Torque (kNm)
u	Roll peripheral speed (m/s)
u_m	Material peripheral velocity in the gap (m/s)
u_r	Roll rotational speed (rpm)
V	HPGR volumetric throughput (m ³ /h)
V_p	HPGR volumetric throughput potential (m ³ /h)
w	Moisture content (%)
W	HPGR mass throughput (t/h)

ω	Roll radial velocity (1/s)
x_c	Critical gap (mm)
x_f	Flake thickness (mm)
x_g	Operating gap (mm)

List of Abbreviations

AG	Autogenous Grinding
BBWI	Bond Ball Mill Work Index
CAPEX	Capital Expenditures
CI	Confidence Interval
COV	Coefficient of Variation, a statistical measure of the dispersion of data points in a data series around the mean
CV	Cross-Validation
DWT	Drop Weight Test
EGL	Effective Grinding Length
GHG	Greenhouse Gas
G-S	Gaudin-Schuhmann
HPGR	High Pressure Grinding Roll
KNN	K-Nearest Neighbors
LASSO	Least Absolute Shrinkage and Selection Operator
MAE	Mean Absolute Error
MSE	Mean Squared Error
NN	Neural Networks
NPC	Net Present Cost
OLS	Ordinary Least Square
OPEX	Operating Expenditures

PBM	Population Balance Modeling
PPT	Piston-die Press Testing
PSD	Particle Size Distribution
Q-Q	Quantile-Quantile
R-R	Rosin-Rammler
RMSE	Root Mean Square Error, a statistical measure of the differences between values predicted by a model or an estimator and the values observed
ROM	Run-of-Mine
RSE	Relative Standard Error
RSS	Residual Sum of Squares
SAG	Semi-Autogenous Grinding
SABC	SAG, Ball mill and pebble Crusher
LSTM	Long Short-Term Memory
SD	Standard Deviation
SE	Standard Error
SMC	SAG Mill Comminution
SVM	Support Vector Machines
SWOT	Strengths, Weaknesses, Opportunities, and Threats
VSD	Variable Speed Drive

Acknowledgments

I am deeply thankful to my supervisor Professor Bern Klein, for his guidance, drive and support throughout my research endeavor. I have immensely learned from Bern's knowledge in the field of mineral processing but more importantly for the life in general. I would also like to express my sincere appreciation to the committee members, Dr. Sanja Miskovic and Dr. Persio Rosario, for their valuable supports and technical advices on the overall research topic.

I would like to express my gratitude for the financial support from the MITACS Inc. and National Science and Engineering Research Council (NSERC). I would like to extend my sincere thanks to mining companies (anonymous) for supplying samples and operational data used in this research. I would also like to acknowledge the in-kind supports from industry sponsors, including Köppern Machinery, ALS Perth, Andritz, and Corem.

I would like to thank Pius Lo, Libin Tong, Aaron Hope and all other staffs at UBC, for providing me with the testing facility to complete my research. I would also like to thank Amit Kumar, Sijia Liu, Genzhuang Li, Tulio Marques, Santiago Seiler, Giovanni Pamparana, Cherezade Saud, Monong Huang, Mike McClintock, and Olav Mejia for giving me the mutual learning experience at UBC.

A part of this thesis was computational and owes much gratitude to the following open source software:

- scikit-learn machine learning library¹, used for multivariable linear regression analysis in Chapter 5.

¹<https://github.com/scikit-learn/scikit-learn>

- The scientific Python SciPy Stack² and Seaborn³, which were used for general computations and data visualization throughout the thesis.
- The Orange, a component-based data mining software, was used to develop the data-driven model for predicting the HPGR specific throughput (Appendix D).

Special thanks to Maren Klein and AJ Gunson, for the kind welcome to their family and life in Canada. They helped me feel at home in Canada as a new immigrant.

Lastly, I cannot forget my family, especially my lovely wife, Jiayu Guo. I couldn't have done it without her patience and emotional support over the course of this research and this challenging year of 2020. I would also like to express sincere appreciation to my parents and sisters for their love and support.

²<https://www.scipy.org/stackspec.html>

³<http://seaborn.pydata.org/>

To My loved Ones

Chapter 1

Introduction

This chapter presents the problem statement and research objectives. An outline of the thesis is also provided in this chapter.

1.1 Problem Statement

The global demand in raw materials is increasing due to rising standards of living for a growing world population. To meet the future demand for raw materials, the mining industry must overcome many challenges as follows,

- Declining ore grades due to depletion of rich mineral deposits, leads to an increase in production rates to sustain the metal production
- Increasing ore hardness as mining activities progressively transition to deeper deposits, which leads to a significant increase in energy usage to process the same tonnes of ores unless energy efficient technology is adopted
- Growing number of finely disseminated ore deposits require finer grind to achieve the desired liberation, that also increases the energy usage
- Last but not least, rising pressures from the government and society to fight the global climate change, urging the mining industry to reduce its Greenhouse Gas (GHG) emissions and respective environmental footprint

One could clearly see that all listed challenges are directly related to how energy is being used in the mining industry now and in the future. The mining activities, particularly the comminution process, are known as energy intensive and energy inefficient. Nearly 2% of total electrical energy generated on the planet is consumed by the mining industry (Napier-Munn, 2015), of which between 50% and 80% is spent on comminution (Ballantyne and Powell, 2014; Klein et al., 2018). The mining industry is becoming increasingly vulnerable to risks associated with fluctuating energy prices as well as to government regulations aimed at reducing GHG emissions (Klein et al., 2018). The impact is more profound for large tonnage low-grade deposits. Therefore, there are strong motivations to focus more on energy efficiency and energy conservation that can improve the operating profitability and meet the society demands for reduced carbon footprint.

The High Pressure Grinding Roll (HPGR) is an important energy-efficient technology with potential to significantly reduce the energy consumption of comminution circuits. This technology employs the “interparticle breakage” mechanism to compress a bed of particles in a confined environment, which is more energy efficient than conventional comminution processes. Although the HPGR has proven its efficiency, performance and durability in the cement industry and at iron ore mines since early 1980’s, the first full commercial installation in the base metal was not operating until 2007, almost 30 years later after the technology was first conceived in 1979. Historically, the mining industry was slow in adopting the HPGR technology mainly due to,

- high roll wear when processing hard and abrasive ores, which often results in significant plant downtime
- higher capital costs compared to conventional comminution circuits
- lack of knowledge and confidence on the types of application that may benefit from the HPGR technology
- low cost of energy in some jurisdictions, thus investigation of such energy efficient solutions was not motivated
- harsh winter climate posed additional design and operational challenges for the HPGR circuits, primarily due to bulk material handling and ore storage

Although many of these issues have been addressed by the industry over the years, the wider adoption of HPGR technology is still slow. In fact, many of the recent HPGR installations were executed by major mining companies with significant capital resources for project development. Early investigation with pilot scale HPGR testing was made possible for those projects to explore and capture the opportunities associated with the HPGR technology. Although the early stage testing and reports are deemed very influential to technology selection and flowsheet development, many small-medium size projects (especially junior mining companies) did not have low cost options for HPGR testing and evaluation. For pilot HPGR testing, large samples (from 1 to 10 tonnes) are often required. However, such samples may not be available for early stage projects, and may not properly represent the deposit from the geo-metallurgical perspective. Consequently, the HPGR did not arise as a possible solution, but in hindsight the HPGR would have been a technically viable and cost effective solution. Coupled with the lack of affordable small scale HPGR tests, is the lack of reliable models capable of interpreting the testing results for HPGR sizing, modeling and simulation, that can be subsequently used for the HPGR circuit design and process option trade-off.

To advance the HPGR technology, the University of British Columbia (UBC) has developed a suite of small scale laboratory tests for characterizing ores under HPGR comminution (Nadolski, 2012; Davaanyam, 2015). A set of empirical models using data obtained from those tests have been developed to provide information on the energy and resulting particle size reduction, as well as the throughput of the pilot HPGR at UBC. Apart from relating small scale testing results to pilot HPGR results, there have not been many advances in the development. There is a need to develop a comprehensive and holistic approach utilizing the obtained information from small scale test work for HPGR sizing, circuit modeling and simulation, that could advance projects with the inclusion of the HPGR.

In light of the problems, the goal of this research is to increase the accessibility of HPGR technology for all mining companies and their projects. The more mining projects are considering and adopting the HPGR technology, the more the industry can realize the energy saving potentials. The proposed research is aimed at advancing empirical and semi-empirical models to extract the sizing information from the small scale testing, and developing a holistic simulation package capable of HPGR

sizing, circuit design, and process modeling for different project phases.

1.2 Research Objectives

The main objective of this research is to develop a comprehensive model and simulator for HPGR evaluation, including equipment sizing, circuit design, and process simulation. To work towards fulfilling the stated objective of the research, the following intermediate objectives are set and form the structure of the document:

1. To understand and advance the HPGR technology through extensive bench- and pilot-scale testing for different ore types;
2. To provide practical knowledge and benchmarking information about the HPGR through a thorough analysis of the assembled HPGR test database;
3. To develop and evaluate the empirical models from the latest UBC HPGR database that can be used to generate the key HPGR sizing parameters in an absence of pilot HPGR tests;
4. To demonstrate the application of the developed empirical models with or without small scale characterization test work for HPGR assessment in all project phases, including equipment sizing and ore variability evaluation;
5. To advance and validate the semi-empirical HPGR models incorporating ore breakage characteristics through model fitting to ore specific datasets and generic datasets;
6. Eventually, to integrate the validated empirical and semi-empirical HPGR models into a comprehensive HPGR simulator, which can be used for equipment sizing, circuit design, and process simulation.

1.3 Thesis Outline

This doctoral thesis consists of the following chapters:

Chapter 2 includes a review of literature on the HPGR technology, HPGR sizing and scale-up, comminution modeling, and HPGR modeling.

Chapter 3 describes the received samples used in this research and the overall methodology for the development of HPGR models. The testing procedures and modeling methodologies are also presented.

Chapter 4 summarizes the results of pilot HPGR testing and Piston-die Press Testing (PPT) conducted in this research program. The reproducibility tests are summarized in Appendix C.

Chapter 5 presents an analysis of the latest UBC HPGR database. It summarizes the observed effects of feed properties and operating conditions on HPGR performance. The development of empirical regression models for key HPGR performance indicators is also presented.

Chapter 6 presents pragmatic approaches for HPGR sizing and selection based on available ore characteristics and design criteria. Case studies from conceptual to feasibility are presented to demonstrate the proposed assessment framework.

Chapter 7 describes the overall structure of the holistic HPGR simulator integrating the developed empirical and semi-empirical HPGR models. This chapter focuses on the refinement of the HPGR semi-empirical model, which is based on the Population Balance Modeling (PBM) method and the ore breakage characterization. The integrated simulator has the capacity of simulating the HPGR circuit and predicting the product size distributions.

Chapter 8 draws the conclusions based on the research outcomes and provides recommendations for future research and development.

Chapter 9 outlines the original claims that resulted from this doctoral thesis.

Chapter 2

Literature Review

2.1 Introduction

This chapter presents a review of literature on the HPGR technology, HPGR sizing and scale-up, comminution modeling, and HPGR modeling. A summary of the literature review is provided at the end of this chapter.

2.2 High Pressure Grinding Rolls Technology

The concept of the HPGR (also called the High-Compression Roll Mill, High Pressure Roller Mill, and High-Pressure Roll Crusher) was originated from the fundamental studies on particle breakage conducted by Prof. Schönert (1988). From his extensive research on single-particle and particle-bed breakage under compression and impact loading, Schönert (1988) concluded that slow compression of a single particle is the most energy efficient method of particle breakage. The second most efficient method is through slow compression of a confined particle bed, which is referred to as the “inter-particle” breakage. This breakage mechanism is considered more energy efficient than the loose-bed particle breakage used in tumbling mills, as shown in Figure 2.1, where energy transfer is inherently inefficient during the particle/media interaction due to the “hit-and-miss” mode (Kapur et al., 1993). The HPGR was developed based on the inter-particle breakage mechanism to break a bed of particles between two rotating rolls (Abouzeid and Fuerstenau, 2009).

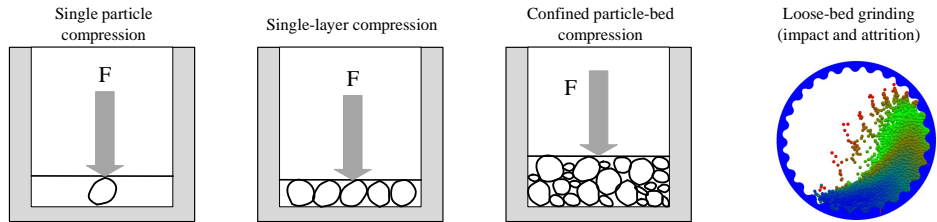


Figure 2.1: Comminution breakage mechanisms

As shown in Figure 2.2, an HPGR machine consists of a pair of counter-rotating rolls, which are mounted on a sturdy frame. The material is choke fed by gravity into the rolls, one of which is fixed and the other is floating and moves laterally when the feed material between the rolls pushes the rolls apart. The back-pressure from the feed material is counter-balanced by the hydro-pneumatic spring system, which applies the compression force directly on the bed of particles via the floating roll.

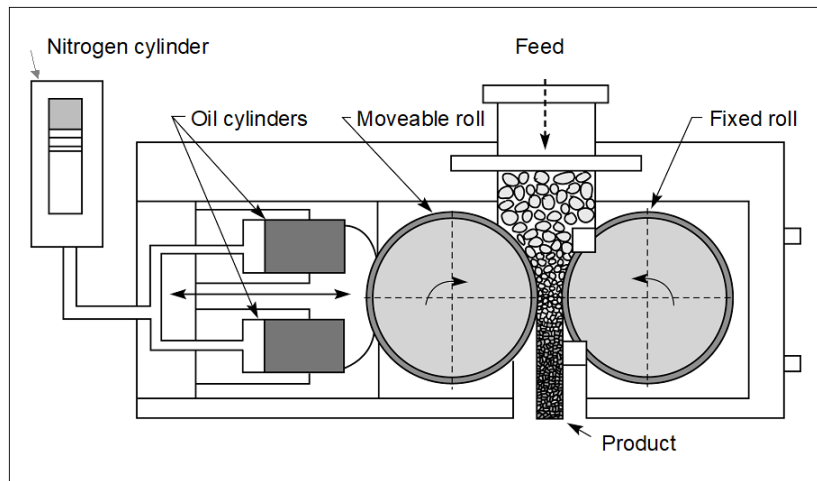


Figure 2.2: Schematic of an HPGR unit
(Source: Napier-Munn et al., 1996)

Historically, the HPGR technology has been widely used in the cement industry, and more recently found in the diamond, iron ore, copper, gold, and platinum industries. Presently, the HPGR is mainly utilized in comminution circuits to perform the following three duties that traditionally have been the role of cone crushers: (1) tertiary crushing, (2) quaternary crushing, and (3) pebble crushing. Several notable installations in hard rock mining are listed in Table 2.1. The implementation of HPGRs has been considered for both greenfield and brownfield projects.

The most pertinent HPGR-based comminution circuit, which competes with the dominant SAG mill based circuits, is the HPGR operating in the tertiary crushing duty. Feed for the tertiary HPGR operation is prepared using secondary cone crushers in either open or closed circuit. Fewer HPGR installations are in quaternary crushing duty, as this option is generally better suited for an existing three-stage crushing circuits where the goal is to increase the overall throughput by sending finer crushed product to downstream ball mills. Likewise, there are several HPGR units installed in a pebble-crushing duty, where the HPGR only handles a fraction of the fresh feed. Other alternative HPGR flowsheets are worth mentioning, such as the pellet feed grinding using HPGR (van der Meer, 2015) or HPGR dry grinding to produce the final product for downstream separation processes (van der Meer, 2011).

In terms of the flowsheet development, the industry is also actively exploring other possible HPGR applications. One is using the HPGR in coarser crushing applications (such as the secondary crushing), which will require HPGR technology providers to develop larger diameter units that can accept larger feed top sizes. Another recent trend is using the HPGR in the fine grinding stage ahead of the mineral separation, such as the secondary grinding. To enable this flowsheet, the HPGR will be operated in closed circuit with wet size classification and dewatering (Pearce et al., 2019). In either direction, the extended application of HPGR in unconventional flowsheet offers opportunities for energy savings and additional metallurgical benefits.

Table 2.1: Examples of HPGR Installations

Project	Company	Location	HPGRs	Design kt/d	Ore Type	Year	Reference
Toquepala	SPCC	Peru	2	~60	Copper porphyry	2019	(Burchardt and Mackert, 2019)
Aktogay	KAZ Minerals	Kazakhstan	1	~75 (pebble)	Copper porphyry	2017	(Burchardt and Mackert, 2019)
Bozshakol	KAZ Minerals	Kazakhstan	1	~75 (pebble)	Copper porphyry	2016	(Burchardt and Mackert, 2019)
Cerro Verde 2	Freeport	Peru	8	~240	Copper porphyry	2016	(Vanderbeek and Gunson, 2015)
Sierra Gorda	KGHM/Sumitomo	Chile	4	~110	Copper-Moly	2014	(Comi et al., 2015)
Morenci Metcalf	Freeport	USA	1	>115	Copper porphyry	2014	(Mular et al., 2015)
Tropicana	AngloGold Ashanti	Australia	1	~15	Gold	2013	(Gardula et al., 2015 and 2019)
Cuajone	SPCC	Peru	1	~90 (quaternary)	Copper porphyry	2013	(Taber and Rosell, 2015)
Karara	Ansteel	Australia	2	~50	Magnetite	2012	(Palaniandy et al., 2018)
Salobo	Vale	Brazil	2	~33	Copper, gold	2012	(Godoy, 2010)
Cadia Hill	Newcrest	Australia	1	~55 (HPGR-SAG)	Copper, gold	2012	(Engelhardt et al., 2015)
Peñasquito	Goldcorp	Mexico	1	~+100 (pebble)	Polymetallic	2010	(Lind et al., 2019)
Boddington	Newmont	Australia	4	~100	Gold, copper	2009	(Hart et al., 2011)
Mogalakwena	Anglo Platinum	S. Africa	1	~25	Platinum	2008	(Rule et al., 2008)
Grasberg	Freeport	Indonesia	2	~70 (quaternary)	Copper, gold	2007	(Villanueva et al., 2011)
Cerro Verde 1	Freeport	Peru	4	~108	Copper porphyry	2006	(Koski et al., 2011)

2.2.1 HPGR working principle

This section describes the basic working principle of the HPGR. As illustrated in Figure 2.3, the space between the two rolls generally described by three different zones, the “Acceleration Zone”, the “Compression Zone”, and the “Extrusion Zone” (Lubjuhn and Schönert, 1993; Lim et al., 1997). Feed materials are gravity fed to the HPGR, travelling through all three zones before exiting from the discharge end of the machine.

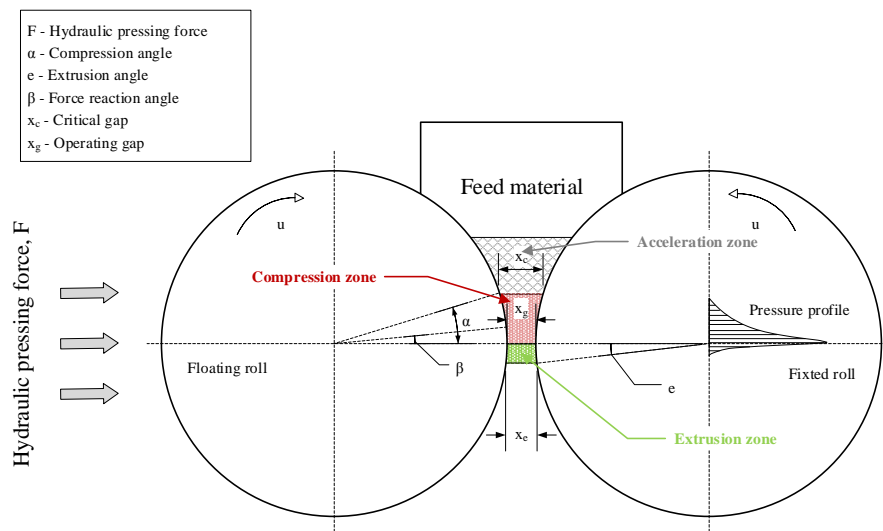


Figure 2.3: Schematic of particle compression and breakage in HPGR
(Modified from Rashidi et al., 2017)

The first zone is called the “**Acceleration Zone**” (also referred to as the deaeration, the pre-crushing, or the pre-grinding zone). The material is fed from the feed hopper into the acceleration zone, where particle re-arrangement takes place and smaller particles fill the void between the larger particles to form a particle bed. Particles larger than the critical gap (x_c), defined by the compression angle (α), are broken directly against the surfaces of the rolls until they are small enough to enter the next zone.

The second zone is the “**Compression Zone**” (also known as the grinding zone), which starts from the critical gap (x_c) and ends at the operating gap (x_g)

defined as the shortest distance between the two rolls. Within the compression zone, particle-bed is formed and broken by high compression force. The applied pressure is unevenly distributed in the radial direction and axial direction of the roll, as illustrated in Figure 2.4. Along the roll gap, the pressure starts from the compression angle and builds up sharply to its maximum pressure at the operating gap, or slightly above it. The peak pressure is typically in the order of 30-60 times the specific pressure (Schönert, 1995; De and Fuerstenau, 2012). Along the roll length, the peak pressure is located at the center of the roll and weakens towards the roll edges. Breakage at either end of rolls is different from that at the center due to the pressure difference, this is commonly referred to as the “edge effect”, where materials only experience partial compression. The shape of the pressure profile is subject to the roll length and the fit of the cheek plates (Klymowsky et al., 2002).

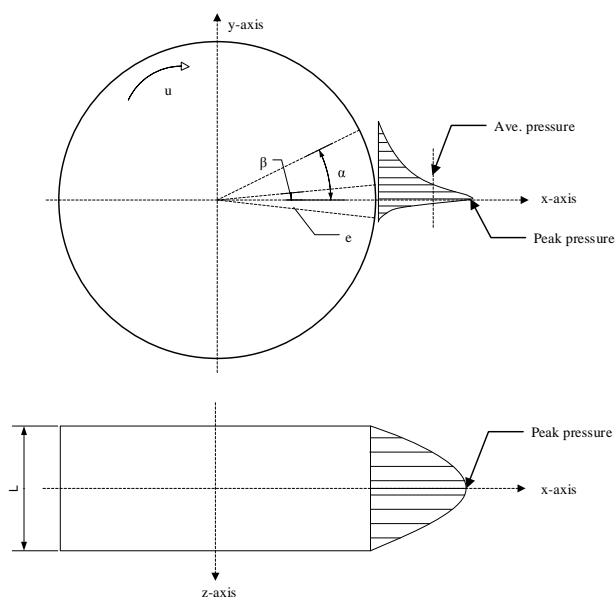


Figure 2.4: Pressure profile in the compression zone

The last zone is the “**Extrusion Zone**” (also called the relaxation, the restraining, or the expansion zone), which is located below the operating gap. The decrease of compression forces in the extrusion zone allows the compacted particles (“cake”) to expand volumetrically after exiting the compression zone.

2.2.2 HPGR sizing and scale-up parameters

Presently, HPGR manufacturers conduct a series of tests with a pilot-scale HPGR (0.7-1.0 m roll diameter) on a given ore to obtain the following HPGR sizing and scale-up parameters to establish the relationship between throughput capacity and energy/size reduction (Rashidi et al., 2017).

1. **specific throughput constant** (\dot{m} or $m\text{-dot}$), in ts/m^3h , defined as the expected throughput for an HPGR unit, with 1 m roll diameter and 1 m roll length running at 1 m/s peripheral speed (Klymowsky et al., 2002)
2. **specific pressing force or specific pressure** (F_{sp}), in N/mm^2 or kN/m^2 , defined as the average force applied on the projected area of the rolls (diameter \times length)
3. **net specific energy consumption** (E_{sp}), in kWh/t , represents the net energy requirement per tonne of ore processed
4. **operating gap** (x_c), in mm, defined as the smallest distance (gap) between the two rolls
5. **compression angle** (α), in degrees, determines the point (interface between the “Acceleration Zone” and “Compression Zone”, or at the critical gap) where a pressure increase occurs on the particles between the rolls
6. **force reaction angle** (β), in degrees, determines the point where the pressing force is applied on the roll
7. **product particle size distributions** (PSDs), for the center and edge products

Table 2.2 summarizes the key HPGR parameters in the form of equations. It is noted that the specific pressing force and specific energy consumption are independent of the machine size. However, the specific throughput constant parameter could be impacted by the size of the HPGR machine. Higher specific throughput constants have been reported for industrial scale HPGRs than for pilot units (Hart et al., 2011; Mular et al., 2015; Gardula et al., 2015 and 2019).

Table 2.2: HPGR sizing parameters

Description	Unit	Equation	Source
Specific throughput constant, \dot{m} or m-dot	[ts/hm ³]	$\dot{m} = \frac{W}{DLu}$	(Seebach and Knobloch, 1987)
Specific pressing force, F_{sp}	[N/mm ²]	$F_{sp} = \frac{F}{DL}$	
Net specific energy consumption, E_{sp}	[kWh/t]	$E_{sp} = \frac{P-P_i}{W}$	
Compression angle, α	[°]	$\alpha = \cos^{-1} \left(1 - \left(\frac{\rho_g}{\rho_f} - 1 \right) \left(\frac{x_g}{1000D} \right) \right)$	(Klymowsky et al., 2002)
Force reaction angle, β	[°]	$\beta \approx \frac{1}{2} \alpha$	(Klymowsky et al., 2002)
Mass throughput, W	[t/h]	$W = 3.6Lx_g u_m \rho_g$	(Lubjuhn and Schönert, 1993)
Volumetric throughput, V	[m ³ /h]	$V = \frac{W}{\rho} = k \left(\frac{u_m}{u} \right) V_p$	(Schönert, 1988)
Volumetric throughput potential, V_p	[m ³ /h]	$V_p = uLD$	(Schönert, 1988)
Torque, T	[kNm]	$T = DF \sin \beta \approx DF \beta = \beta D^2 L F_{sp}$	(Schönert, 1988)
Motor power, P	[kW]	$P = \omega T = \left(2\pi \frac{\omega_r}{60} \right) (DF \beta) = 2\beta V_p F_{sp}$	(Schönert, 1988)

2.2.3 HPGR performance

Figure 2.5 presents the relationship between specific energy consumption and specific pressing force published by several HPGR manufacturers and operating mines. It is evident that the specific energy consumption increases linearly with increasing specific pressing force over a typical operating range of 1-6 N/mm², however, some variations exist at a given specific pressing force. The practical specific pressing force range for studded rolls is 1.0-4.5 N/mm², and it is up to 6.0 N/mm² for smooth surface rolls (Daniel et al., 2019).

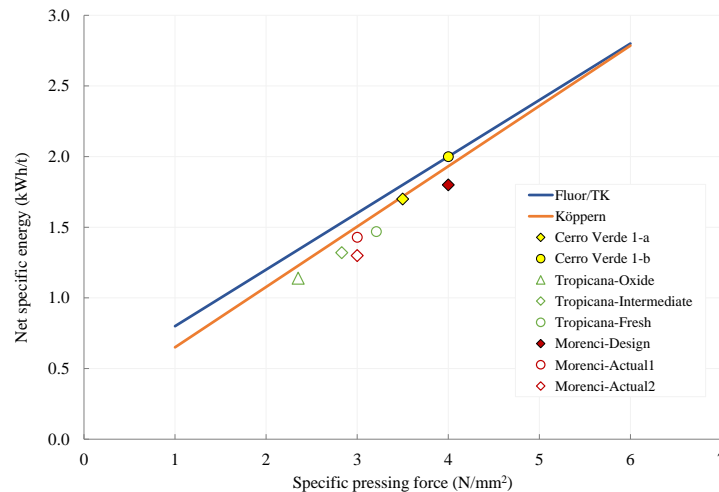


Figure 2.5: Published relationship between net specific energy and specific pressing force

(Source: Hart et al., 2011; Koski et al., 2011; Costello and Brown, 2015; Gardula et al., 2015)

The specific throughput constant is mostly influenced by the roll surface texture, feed material properties and operating conditions. It has been observed that the studded roll surface yields a higher specific throughput than the smooth surface, due to improved nipping kinetics of feed material between the rolls (Morley, 2006). The material properties have significant impacts on the specific throughput constant, particularly, the ore hardness, ore density, feed top size, fines content, and feed moisture content, all of which would require careful examination in any HPGR studies. In general, specific throughput constant increases with ore hardness, and increases slightly with an increase in feed top size, as both support a larger oper-

ating gap (Morley, 2006). Feed materials with fewer fines could decrease the specific throughput rate significantly, because truncating the feed increases the void space within the particle bed, which leads to a higher degree of compressibility and reduced operating gap (Klymowsky et al., 2002). The specific pressing force, however, has a limited impact on the throughput for most ore types except for very moist materials. As shown in Figure 2.6, a higher specific pressing force could result in formation of a narrower gap, thus a decrease in the specific throughput constant (Klymowsky et al., 2002).

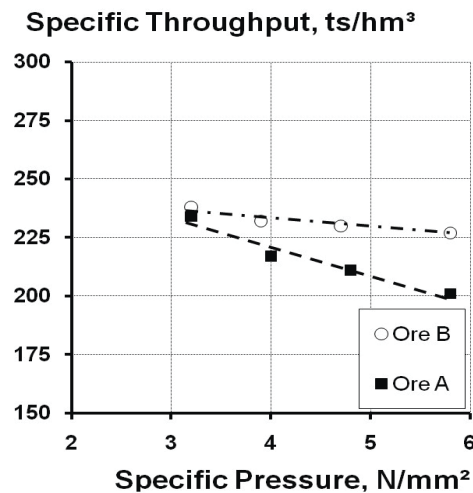


Figure 2.6: Relationship of specific pressing force and specific throughput
(Source: Van der Meer, 2010)

Moisture content in the feed has a significant effect on HPGR performance because it influences the friction and adhesion between particles as they are being squeezed in the gap (Fuerstenau and Abouzeid, 1998; Fuerstenau and Abouzeid, 2007). Some moisture would help to form an enhanced packed bed that improves the efficiency in energy transfer from particle to particle. However, too high a moisture content would provide excessive lubrication between roll surfaces and the packed bed and between particles, therefore resulting in reduced friction and causing slippage. Excessive moisture content could also wash out the autogenous layer on the studded rolls, resulting in a high roll wear. Research conducted by Saramak and Kleiv (2013) suggested that the relationship between feed moisture

and comminution efficiency could be described by a parabolic function. Therefore, an optimum comminution performance is possible with the right amount of moisture in the feed. As shown in Figure 2.7, it was observed that the specific energy consumption increased with increasing feed moisture content for a given specific pressing force.

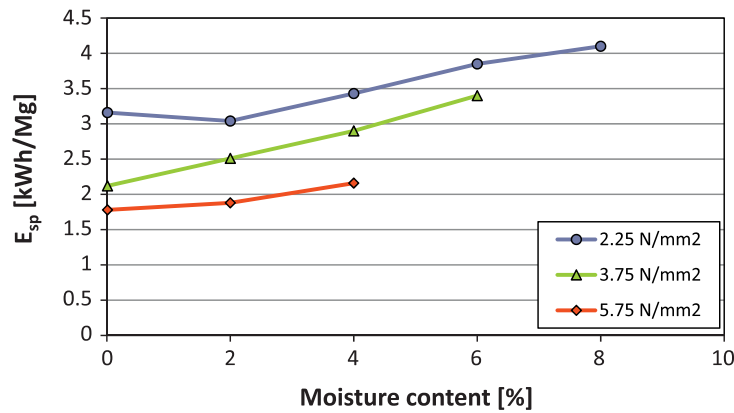


Figure 2.7: Effect of feed moisture on the specific energy consumption
(Source: Saramak and Kleiv, 2013)

As shown in Figure 2.8, the HPGR operating gap and throughput decreased with increasing moisture as materials slip on the rolls due to the increased lubrication effect at high moisture (Saramak and Kleiv, 2013; Davaanyam, 2015).

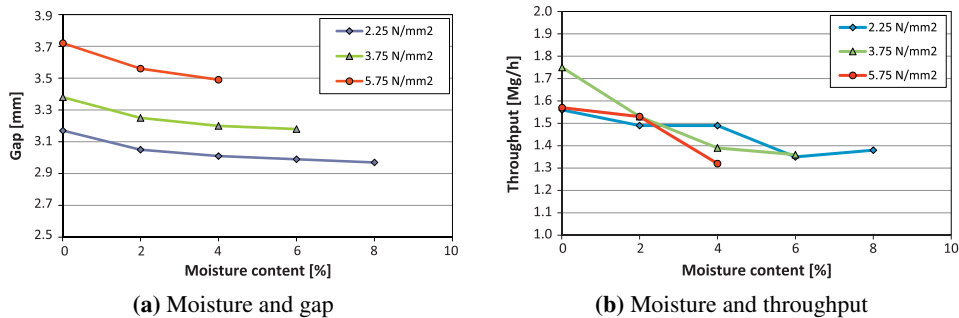


Figure 2.8: Effect of feed moisture on the roll gap and throughput
(Source: Saramak and Kleiv, 2013)

2.2.4 HPGR advantages and disadvantages

Advantages

The main benefit of using the HPGR in a comminution flowsheet is the improved energy efficiency compared to conventional circuits with tumbling mills (Rosario, 2011; Wang et al., 2013; Wang, 2013). Both energy savings and reduced media consumption in HPGR circuits translate into lower overall operating costs. This benefit increases with increasing ore hardness and electricity cost. Significant operating cost savings for HPGR-based comminution circuits have been reported, ranging from 14% to 30%, for gold, copper, platinum-group metals and iron ores (von Michaelis, 2009; Jankovic, 2015; Costello and Brown, 2015; Rosario, 2017).

Another advantage is that HPGR-circuit throughputs are relatively invariant to ore hardness when compared to the AG/SAG mill based circuits (Amelunxen et al., 2011). This is because the HPGR is a “volume limited” machine like other crushing technologies, rather than those “power limited” tumbling mills. Other reported benefits are related to the improvements in the downstream processes. The generation of micro-cracks from HPGR comminution lowers the Bond Ball Mill Work Index (BBWI) and enhances the mineral liberation, resulting in a further reduction in overall energy requirement as well as the improvement in downstream recovery (Tavares, 2005; Ballantyne et al., 2018).

As more knowledge and experience with the HPGR technology has been gained, there is an emerging consensus of the types of projects that are more likely to benefit from the adoption of HPGRs, for very hard ores where the use of SAG mills becomes less desirable or for very variable ores where HPGR circuit can bring stability into the operation. The inclusion of HPGR in a mineral processing flowsheet can provide significant potential benefits, therefore thorough evaluation of these additional benefits is essential to adequately assess the value of the technology.

Disadvantages

There are several disadvantages and limitations that act as barriers to the use of the HPGR technology. First of all, capital costs for the HPGR-based circuit are generally higher than for the equivalent SAG-based circuit due to additional upstream

feed preparation systems (secondary crushing and screening), larger footprint requirement, and increased complexity in bulk-material handling with conveyors and storage bins (Costello and Brown, 2015). Like other crushing processes, dust generation is another issue with the HPGR process, that requires sufficient dust collection and suppression systems in the design, which also adds to the overall capital costs (Vanderbeek et al., 2006). In addition, not all ores are amenable to the HPGR technology, to be specific, ores with significant clay-like content do not respond well to the HPGR because they cannot provide sufficient back-pressure to push the rolls apart. To address this issue, a mitigation solution has been developed by including a scrubber ahead of the HPGR for clay removal (Rosario, 2011). Other perceived risks with the HPGR circuit is associated with the wet and cold climate, where variations in feed moisture levels and potential freezing can cause severe operability issues.

2.3 Comminution Modeling

The energy and size reduction relationship for comminution process has been researched extensively over the last century. It has been found that the incremental energy required to produce an incremental change in particle size is a function of particle size. Its general relationship can be expressed in Equation 2.1.

$$\frac{dE}{dD} = -\frac{k}{(D)^n} \quad (2.1)$$

Understandably, the amount of energy required to break coarse particles is lower than to break fine particles for the same size reduction ratio. Equation 2.1 can be integrated to obtain a general comminution model as expressed in Equation 2.2. The most widely-accepted comminution models (often regarded as the comminution “laws”) are the Rittinger’s law ($n=2$) for fine grinding (1867), Kick’s law ($n=1$) for crushing (1885), and Bond’s law ($n=1.5$) for fine crushing and grinding (1960). However, these three models do not adequately describe the energy and size reduction relationship for the confined particle-bed breakage.

$$E = \frac{k}{n-1} \cdot \left[\left(\frac{1}{D_p} \right)^{n-1} - \left(\frac{1}{D_f} \right)^{n-1} \right], \text{ for } n \neq 1 \quad (2.2)$$

where, k is a material dependent constant (related to ore hardness), D_f and D_p are feed and product characteristic passing size.

2.3.1 Particle-bed breakage characterization

Piston-die Press Testing (PPT) has been commonly used to study the behavior of the confined particle-bed breakage (also referred to as the interparticle breakage). In fact, the HPGR development was originated from such a fundamental experiment conducted by Prof. Schönert (1988). Over the years, various researchers have used PPT for compression breakage characterization and HPGR technology assessment. Hawkins (2007) used the PPT to evaluate the performance of a lab-scale HPGR, suggesting that the PPT together with lab-scale HPGR tests have the potential to be used to simulate the industrial scale HPGR. Bulled et al. (2008) used the PPT to estimate the compression grindability index that provided a specific energy estimate for the HPGR operation. Kalala et al. (2011) used different piston-die diameters to assess the breakage behavior of particles under compression loading. He used these tests to obtain the size distribution of a piston pressed product and compared against to a lab-scale HPGR product. Davaanyam (2015) correlated the PPT results with a pilot-scale HPGR unit that could be used directly afterwards to size an industrial scale HPGR. Benzer et al. (2017) developed a simulation method for HPGR using laboratory scale piston-die tests, which was validated with the pilot HPGR testing.

2.3.2 Particle-bed breakage modeling

Schönert (1996) showed that the size reduction under confined particle-bed comminution is directly affected by the energy absorption (or specific energy input). A linear relationship between the reduction ratio ($\frac{X_{50f}}{X_{50p}}$) from median feed size X_{50f} to median product size X_{50p} and the specific energy input, expressed by Equation 2.3, was found both in PPT and lab-scale HPGR tests (Fuerstenau and Kapur, 1995; Fuerstenau et al., 1996). Fuerstenau et al. (1996) showed that this linear relationship (Figure 2.9) between the energy input and reduction ratio was valid up to an energy input of 3.5 kWh/t for dolomite, quartz, hematite, and limestone.

$$\frac{X_{50f}}{X_{50p}} = j(F_{50})E + c \quad (2.3)$$

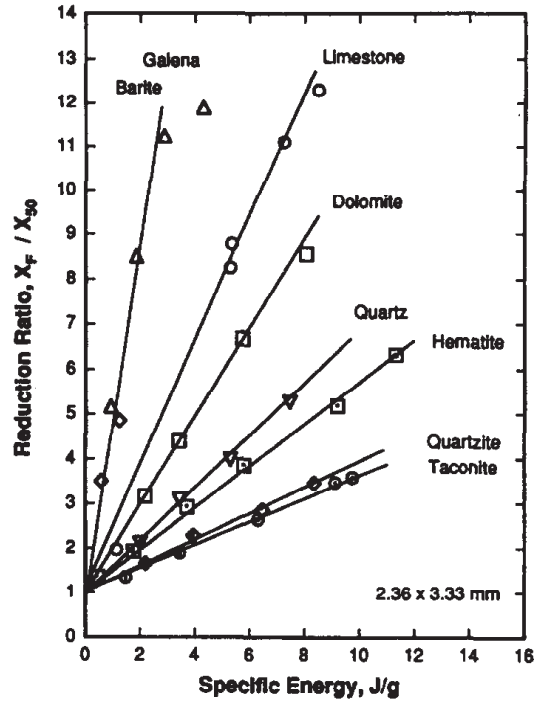


Figure 2.9: Energy-size reduction relationship
(Source: Fuerstenau et al., 1996)

In Figure 2.10a, Fuerstenau et al. (1991) showed that the cumulative size distributions of different HPGR products were “self-similar”, therefore can be normalized by plotting them against a dimensionless size X/X_{50} (product particle size divided by the product median size). Later, Fuerstenau et al. (1996) observed that the product size distributions from the PPT were also “self-similar” when plotted against the dimensionless size, as shown in Figure 2.10b.

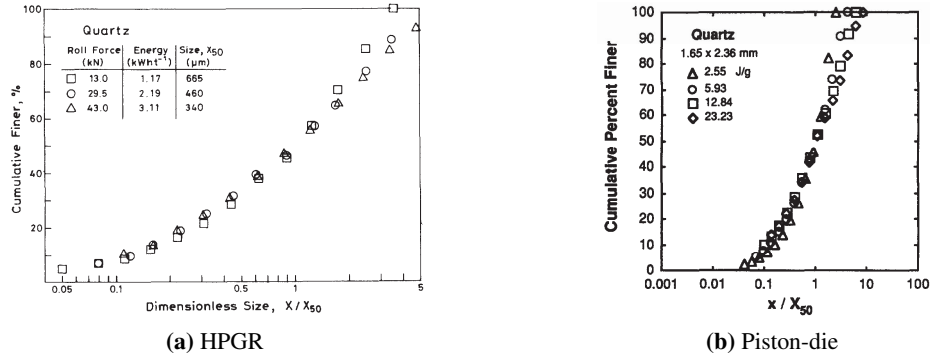


Figure 2.10: Self-similar size distributions of quartz comminuted
(Source: Fuerstenau et al., 1991; Fuerstenau et al., 1996)

As illustrated in Figure 2.11, Davaanyam (2015) confirmed that the product size distributions of both PPT and pilot-scale HPGR tests can be normalized, and the normalized curves matched well for products from the PPT on -12.5 mm samples and HPGR tests on -32 mm and -12.5 mm samples. This unique self-similar concept can be used to scale-up the HPGR product size distribution at a given specific energy input from the PPT results by fitting a master curve to the self-similar distributions (Davaanyam, 2015). An empirical equation describing this normalized master curve was proposed by Lim, Voigt, and Weller (1996), as expressed in Equation 2.4.

$$F\left(\frac{x}{X_{50}}\right) = 100 \left\{ 1 - \exp \left[-A \left(\frac{x}{X_{50}} \right)^{m \left(\frac{x}{X_{50}} \right) + n} \right] \right\} \quad (2.4)$$

where $F\left(\frac{x}{X_{50}}\right)$ is the cumulative percent passing at $\frac{x}{X_{50}}$ size; $\frac{x}{X_{50}}$ is the dimensionless size normalized by dividing by the median particle size of the product; and A , m , n are fitted model parameters.

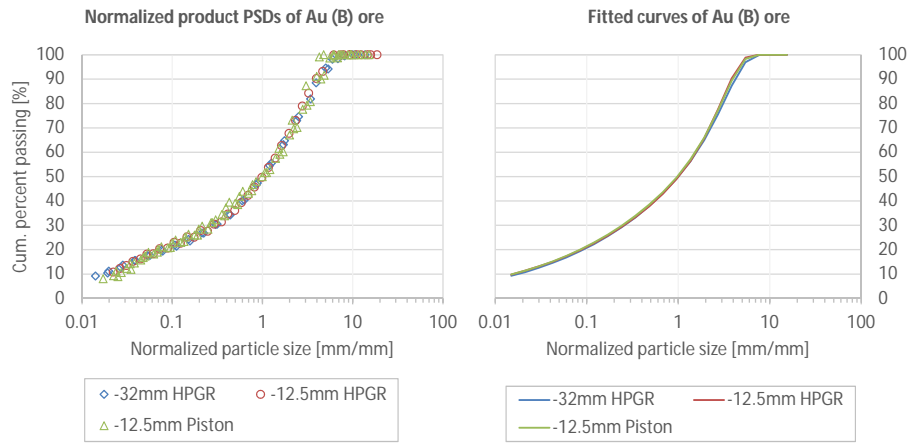


Figure 2.11: Self-similar size distributions of Au-ore comminuted in HPGR and piston-die test
(Source: Davaanyam, 2015)

2.4 HPGR Modeling

Rashidi et al. (2017) presented a comprehensive review of HPGR modeling, covering several research groups who developed HPGR models to enable predictions of HPGR throughput, power draw, and energy/size reduction (Fuerstenau et al., 1991; Austin et al., 1993; Klymowsky and Liu, 1997a and 1997b; Morrell et al., 1997a; Morrell et al., 1997b; Unland and Wang, 1998a and 1998b; Daniel and Morrell, 2004; Hinde and Kalala, 2009; Schneider et al., 2009; Torres and Casali, 2009; Dundar et al., 2013; Saramak and Naziemiec, 2013; Barrios and Tavares, 2016). However, most of the proposed models are hindered from being adopted by the industry due to their limited applicability and accuracy. Model fitting using pilot- or full-scale operating data are often required to determine the model parameters prior to simulating the HPGR circuit. In addition, the HPGR throughput models require knowledge of the operating gap or product flake thickness and density, which can only be determined through the lab- or pilot-scale HPGR testing, further limiting their application. This section details the following three groups of HPGR models which had some successes with their usage in the industry: 1) Klymowsky-Liu model; 2) Morrell-Tondo-Shi model; 3) Davaanyam-Klein-Nadolski model.

2.4.1 Klymowsky-Liu HPGR model

After performing the piston-die compression tests using various narrow-size fractions and energy inputs, Liu and Schönert (1996) came up with an interparticle breakage model, which describes the PPT product size distribution as a function of energy input. The products of the PPT using mono-sized feed were sized and the fraction of broken particles (S) versus the energy absorption (E) is displayed in Figure 2.12.

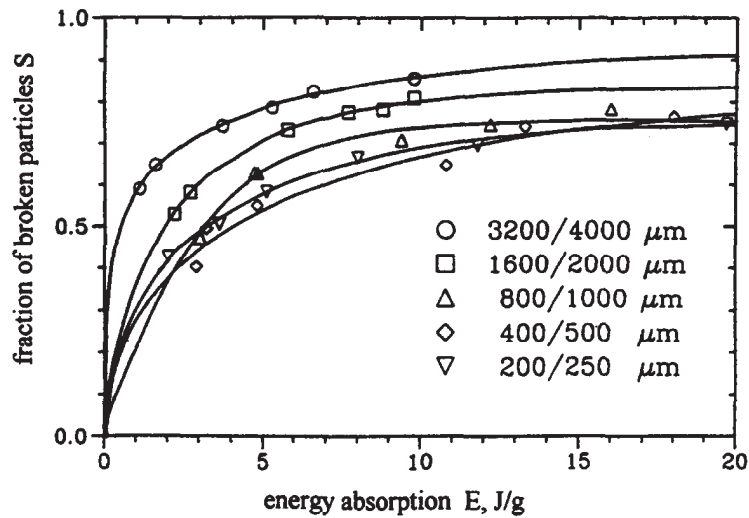


Figure 2.12: Fraction of broken particles as a function of particle size and energy input
(Source: Liu and Schönert, 1996)

An exponential function, as expressed in Equation 2.5, to describe the fraction of broken particles was selected as an approximation (Liu and Schönert, 1996).

$$S = S_{\infty} \left\{ 1 - \exp \left[- \left(\frac{E}{E_c} \right)^{\beta} \right] \right\} \quad (2.5)$$

where S_{∞} is the limiting value of S ; E_c is a characteristic energy absorption; and β is the curve shape parameter. A good fit for expressing the selection function $S(X, E)$ by Equation 2.5 was demonstrated in Figure 2.13, when plotted in a normalized form.

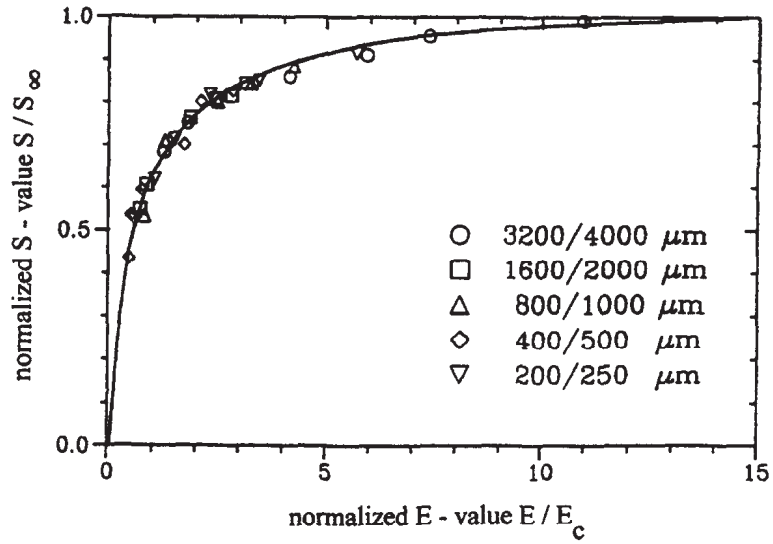


Figure 2.13: Normalized E and S
(Source: Liu and Schönert, 1996)

The breakage functions display as a truncated logarithmic normal distribution with parameter μ and σ , as expressed in Equation 2.6 and Equation 2.7, and illustrated in Figure 2.14 (Liu and Schönert, 1996).

$$\mu(X, E) = \exp \left\{ - \left[\frac{E}{E_{\mu}(x)} \right]^{\alpha} \right\} \quad (2.6)$$

$$\sigma(X, E) = \sigma^* \left(\frac{X}{X_{\sigma}} \right)^a \left(\frac{E}{E_{\sigma}} \right)^b \quad (2.7)$$

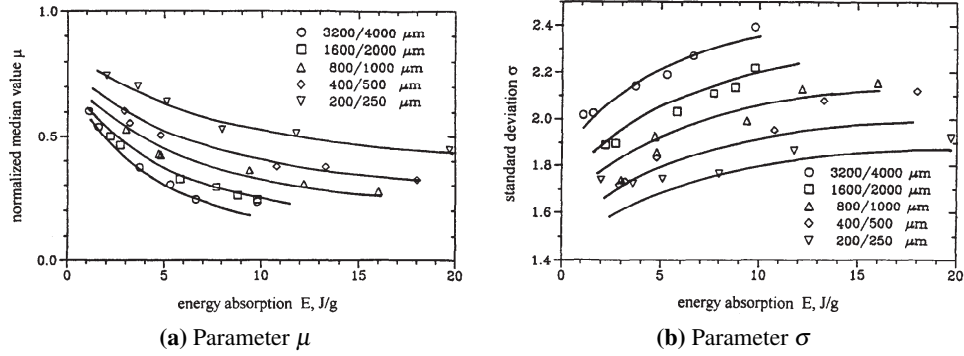


Figure 2.14: Breakage function parameter μ and σ as a function of size and energy absorption
(Source: Liu and Schönert, 1996)

In addition, Liu and Schönert (1996) introduced an energy split function to describe how the energy input is distributed to each size fraction for a given feed size distribution by Equation 2.8.

$$k_j = \frac{E_j}{E}, \sum_{j=1}^n k_j M_i(E) = 1 \quad (2.8)$$

where, k_j is the energy split factor, the ratio of the energy absorption in the size class j related to the energy absorption of the bed.

Klymowsky and Liu (1997a) further developed Liu and Schönert's model to simulate the full spectrum of Particle Size Distribution (PSD) for an industrial-scale HPGR. This model accounts for three breakage actions (pre-crushing, edge effect and center zone) within the HPGR, the product size distributions are determined by the following three steps:

Pre-crushing Predicting the product PSD in the pre-crushing zone through sequential breakage, which is similar to that used in a roller crusher. The product PSD in this zone is expressed in Equation 2.9 (Klymowsky and Liu, 1997a).

$$P_i = \begin{cases} 0 & i = 1, 2, \dots, m \\ f_i + \sum_{j=1}^m d_{ij} f_j^* & i = m + 1, m + 2, \dots, n \end{cases} \quad (2.9)$$

where, m is the number of breakage stages; f_i is the mass fraction of particles in size fraction i in the feed of m -stage breakage; P_i is the mass fraction of particles in size fraction i in the product of m -stage breakage; d_{ij} is the mass transfer coefficients; f_i^* is the relative amount of particles in the i -th stage of breakage which can be determined from Equation 2.10 (Klymowsky and Liu, 1997a).

$$f_i^* = f_i + \sum_{j=1}^{i-1} d_{ij} f_j^* \quad (2.10)$$

Center zone Predicting the product PSD in the center using the population balance model similar to Liu and Schönert (1996) model, as described earlier;

Edge zone Defining the theoretical PSD for the edge product and solving the energy balance between all three breakage zones. The breakage behavior in the edge zone is neither defined by a selection function nor breakage function, but directly by the mass transfer function $d_{i,j}$ as expressed in Equation 2.11. The size reduction for the edge zone is given by Equation 2.12 (Klymowsky and Liu, 1997a).

$$d_{i,j} = D(x_i, y_i) - D(x_{i-1}, y_j) \quad (2.11)$$

$$D(x, y) = \frac{1 - \exp\left[-\left(\frac{x}{y}\right)^u\right]}{1 - \exp^{-1}} \quad (2.12)$$

where, $D(x, y)$ is the mass fraction of particles in size fraction of top size y which appears after breakage as fragments smaller than size x ; and u is a fitted parameter which is estimated from size distribution data of the feed and edge product.

2.4.2 Morrell-Tondo-Shi HPGR model

The Morrell-Tondo-Shi HPGR model (1997b) was developed to predict the HPGR product size distribution, throughput and power draw. As illustrated in Figure 2.15, three breakage zones were defined as the pre-crusher zone, the compression zone, and the edge effect zone, which is similar to the previously discussed Klymowsky-Liu HPGR model.

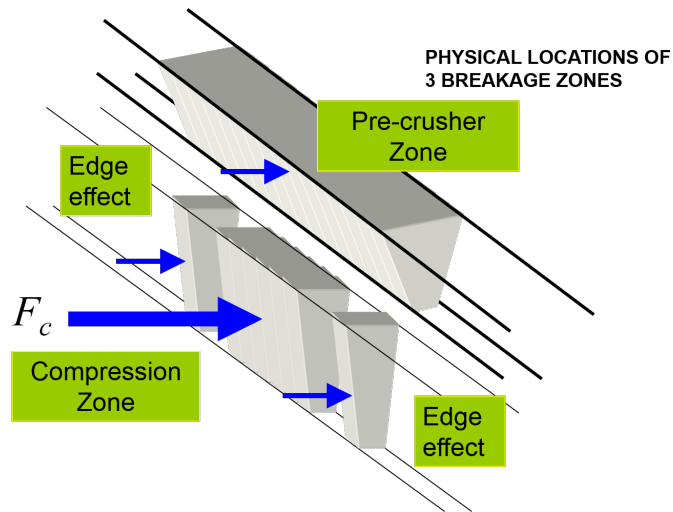


Figure 2.15: Schematic location of three crusher zones in HPGR
(Source: Daniel, 2002)

Figure 2.16 illustrates the structure of the Morrell-Tondo-Shi model for size reduction, which consists of 3 breakage functions and 1 split function. According to the location of the breakage zones, the following breakage mechanisms within the HPGR were assumed (Morrell et al., 1997a and 1997b).

1. In the pre-crusher zone, particles larger than the critical gap are broken by single particle breakage mechanism. The crushed products are combined with the remainder of the feed that bypassed the pre-crushing zone as materials are smaller than the critical gap;
2. After the pre-crusher zone, a split of the combined product enters the edge effect zone, where particles larger than the operating gap are broken by single particle breakage similar to those in the pre-crusher zone;

- The remainder of the combined product are broken in the compression zone, where particle-bed is formed and broken under interparticle compression breakage.

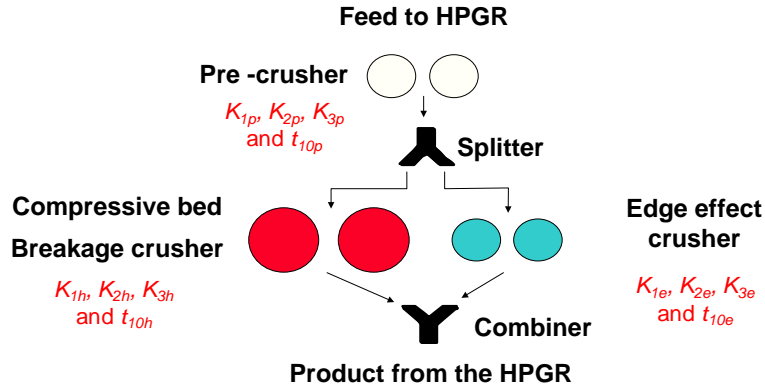


Figure 2.16: Schematic of the Morrell-Tondo-Shi size reduction model
(Source: Morrell et al., 1997b)

Morrell et al. (1997b) applied the Whiten-Awachi-Andersen crusher model for modeling three breakage zones individually, and combined the results to produce the final product. The Whiten-Awachi-Andersen crusher model (Andersen and Napier-Munn, 1988) features a classification function for each of the breakage zones. This classification, as described in Equation 2.13 and illustrated in Figure 2.17, defines the probability of particles breakage.

$$\left\{ \begin{array}{ll} C(x) = 0 & x < K_1 \\ C(x) = 1 - \left(\frac{K_2 - x}{K_2 - K_1} \right)^{K_3} & K_1 < x < K_2 \\ C(x) = 1 & x > K_2 \end{array} \right. \quad (2.13)$$

where, K_1 is defined as the size below which all particles will not be broken but enter to the product stream; and K_2 is defined as the size above which all particles will be broken; and K_3 is the shape of the classification function curve that defines the probability of breakage for size between K_1 and K_2 .

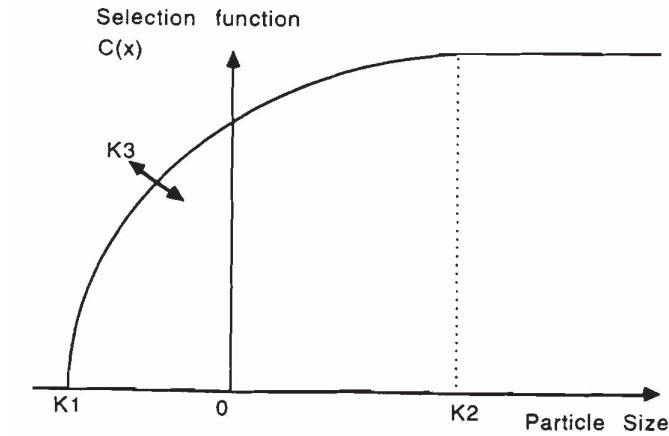


Figure 2.17: Whiten-Awachi-Andersen crusher size reduction model
(Source: Morrell et al., 1997a)

Morrell et al. (1997a) defined the critical gap as the boundary between the pre-crusher zone and the compression zone. As expressed in Equation 2.14, the critical gap is a function of the roll diameter (D), operating gap (x_g), feed bulk density (ρ_{bulk}) and cake density (ρ_g).

$$x_c = 0.5 \left\{ (D + x_g) \left[(D + x_g)^2 - \frac{4\rho_g D x_g}{\rho_{bulk}} \right]^{0.5} \right\} \quad (2.14)$$

Within the compression zone, Morrell (1997a) introduced a split function to separate the edge zone from the center zone. As expressed in Equation 2.15, the fraction of particles that undergo the edge effect is affected by the operating gap (x_g) and roll length (L).

$$f = g \frac{x_g}{L} \quad (2.15)$$

Overall, three breakage zones employ the same crusher model with different model parameters. Each breakage zone requires 4 model parameters (3 size parameter K_1 , K_2 , K_3 and one material breakage parameter t_{10}), therefore a total of 12 model parameters need to be fitted to experimental data during the model development process. The t_{10} parameter is modeled as a function of the specific energy

input, as expressed in Equation 2.16 (Napier-Munn et al., 1996). The t_{10} method for reconstructing the breakage function was developed by Narayanan and Whiten (1988) using data originally obtained from the pendulum impact test.

$$t_{10} = A \left(1 - \exp^{-bE_{sc}} \right) \quad (2.16)$$

where, t_{10} is the percentage passing $1/10^{th}$ of original narrow-size particle and represents the degree of breakage at a certain energy input; A and b are ore specific breakage parameter found through nonlinear regression, and E_{sc} is the specific energy input from impact breakage testing.

2.4.3 Davaanyam-Klein-Nadolski HPGR models

Throughput model

Nadolski (2012) developed a predictive HPGR throughput model using information obtained from a direct shear box test as well as a piston-die press test. Laboratory testing procedures were developed to obtain the frictional properties and compressibility of tested samples. Based on the test results, the HPGR operating gap and throughput can be predicted using empirical regression models shown in Equation 2.17 and Equation 2.18 (Nadolski, 2012).

$$s = \beta_0 + \beta_1 k + \beta_2 m + \beta_3 F_{sp} + \beta_4 \rho_b + \beta_5 \theta + \beta_6 z(150) \quad (2.17)$$

$$\dot{m} = \beta_7 + \beta_8 s + \beta_9 \rho_b + \beta_{10} m \quad (2.18)$$

where, s is the predicted roll operating gap; \dot{m} is the specific throughput constant; k is shear deformation modulus; m is Gaudin-Schuhmann (G-S) distribution parameter; F_{sp} is specific pressing force; ρ_b is feed bulk density; θ is shear angle; $z(150)$ is the displacement at 150 MPa pressure; and $\beta_0 \sim \beta_{10}$ are constants.

Energy-size reduction model

Following Nadolski's throughput model, Davaanyam (2015) developed a laboratory testing procedure and respective simulation method to determine the relation-

ship between energy and size reduction for the pilot-scale HPGR at the UBC. In his approach, the piston-die press tests were performed on narrowly sized fractions at various energy inputs (similar to Liu's approach) to characterize the breakage behaviors of tested materials under compressive load. The PSDs of the progeny fragments resulting from compression tests were measured to determine the breakage index t_{10} , which can be modeled as a function of specific energy shown in Equation 2.19 (Davaanyam, 2015). This is a modified model from the work of Shi and Kojovic (2007) by adding an exponent n to the particle size x . Their work was originally adapted from a model reported by Vogel and Peukert (2004) based on dimensional analysis and statistical fracture mechanics.

$$t_{10} = M \left(1 - \exp(-f_{mat} \cdot x^n \cdot E_{sp}) \right) \quad (2.19)$$

where, M is a fitted parameter representing the maximum attainable t_{10} ; f_{mat} is a fitted parameter representing the material breakage property, and E_{sp} is the specific energy input from compression breakage testing.

Davaanyam (2015) found that the relationship between t_{10} and other t_n values can be described using Equation 2.20 through Equation 2.25. Figure 2.18 shows the t_{10} and t_n relationship fitted over a range of ore types, suggesting a set of master curves can represent all ore type reasonably well. The resultant relationship between t_{10} and t_n is also referred to as the t-family curves, which is used to define the appearance function after confined particle-bed compression breakage. The appearance function for compression breakage is considered ore independent; a similar finding was reported by Narayanan and Whiten (1988) for impact breakage.

$$t_{1.2} = \frac{\beta_1 \cdot t_{10}}{(\beta_2 + t_{10})} \quad (2.20)$$

$$t_2 = \frac{\beta_3 \cdot t_{10}}{(\beta_4 + t_{10})} \quad (2.21)$$

$$t_4 = \frac{\beta_5 \cdot t_{10}}{(\beta_6 + t_{10})} \quad (2.22)$$

$$t_{25} = \beta_7 \cdot t_{10} \quad (2.23)$$

$$t_{50} = \beta_8 \cdot t_{10} \quad (2.24)$$

$$t_{75} = \beta_9 \cdot t_{10} \quad (2.25)$$

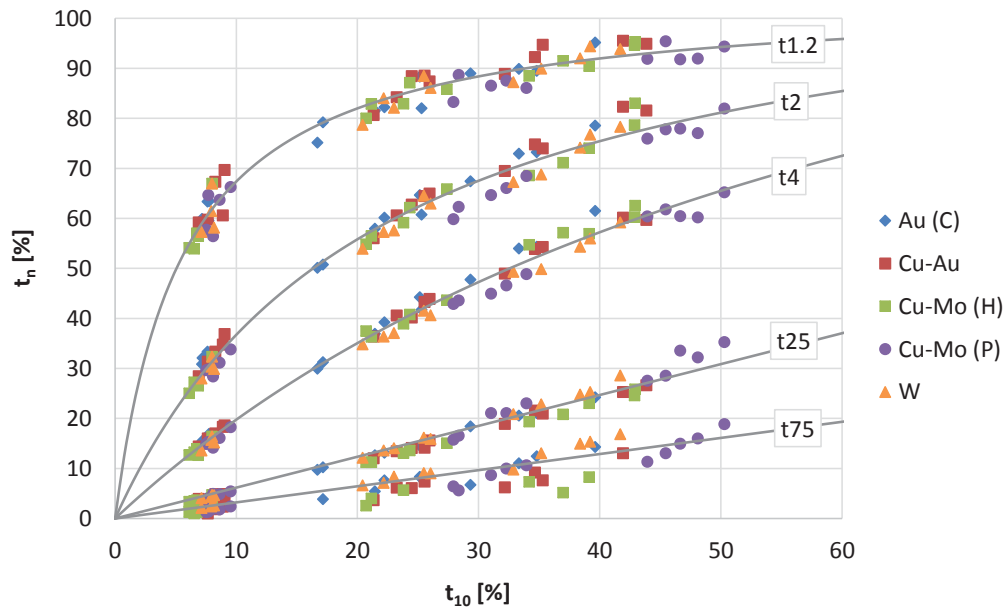


Figure 2.18: A set of master curves describing $t_{10} - t_n$ relationship
(Source: Davaanyam, 2015)

As illustrated in Figure 2.19, Davaanyam (2015) assumed only two breakage zones in the HPGR model, namely the pre-crushing zone and grinding zone (or “compression zone”). This model does not consider center and edge breakage zones separately.

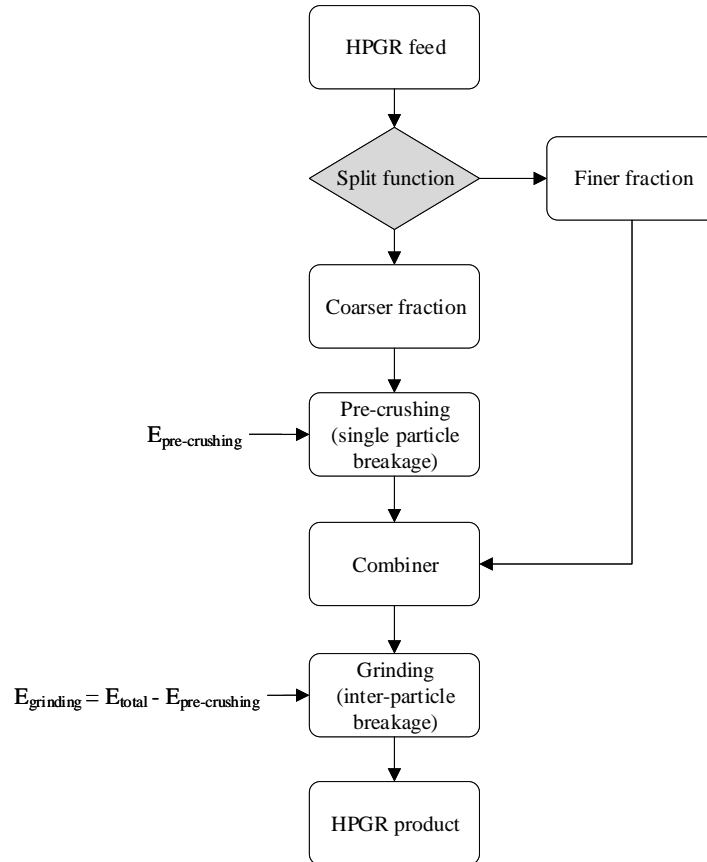


Figure 2.19: Schematic structure of the Davaanyam size reduction model
(Modified after Davaanyam, 2015)

In the pre-crushing zone, a critical size is determined by the split function that defines the coarse and fine fractions. Particles above the critical size (coarse fractions) are pre-crushed by single particle compression breakage mechanism, while fine fractions are simply bypassed. Equation 2.19 is used to calculate the size reduction within the pre-crushing zone. The specific energy to the pre-crushing

stage is described as a function of the fraction of coarser particles in the feed, as expressed in Equation 2.26.

$$E_{sp}^{crush} = \beta_{split} \cdot f_{coarse} \cdot E_{sp} \quad (2.26)$$

The product from the pre-crushing stage is combined with the finer fraction (below critical size) in the feed and the combined product is subject to size reduction in the grinding stage. This arrangement in the simulation ensures the coarse particles to break in both pre-crushing and grinding stages, while the fine particles only break in the grinding stage. In addition, the fines content in the HPGR feed was found having negative effects on particle bed compression breakage (Davaanyam, 2015). The probability of coarse particle breakage reduces with the increase of the fines in the feed. Equation 2.19 was therefore modified to obtain Equation 2.27 that takes into account the effect of fines content in the feed, which is used for simulation of the breakage in the grinding stage.

$$t_{10} = (M - c \cdot q_f) \left(1 - \exp(-f_{mat} \cdot x^n \cdot E_{sp}) \right) \quad (2.27)$$

where, c is a fitted constant to multiply the percentage of fines in the feed, q_f .

It was assumed that the total energy is distributed between the pre-crushing and the grinding stages. Therefore, the specific energy in the grinding stage can be balanced using Equation 2.28.

$$E_{sp}^{grinding} = E_{sp} \cdot (1 - \beta_{split} \cdot f_{coarse}) \quad (2.28)$$

2.5 Summary of Literature Review

Over the years, many research groups have developed HPGR models to enable prediction of the power draw, throughput, product PSD, and energy/size reduction relationship. However, few of them are being widely used in industry due to lack of validation and their limited applicability and accuracy. There are a few key takeaways from the review of literature:

1. Models to describe two different breakage zones in the radial direction (acceleration and compression zones) and two different zones in the axial direction of the roll (center and edge effect zones) within HPGR are too complex in nature. Such a model would require excessive fitting parameters thus become impractical.
2. Some models made certain assumptions that do not fully represent the fundamental breakage mechanisms in the breakage zones, resulting in inaccurate model predictions.
3. Although some models have successfully predicted the performance of a laboratory-scale HPGR, the difficulty increased for a reliable scale-up.
4. Other models still rely on model fitting from extensive pilot or full scale HPGR testing on the particular ore in question, to achieve the desired accuracy of prediction. Those models are not being adopted widely due to high cost and low accessibility of HPGR testing.
5. Concerning the HPGR throughput, these models are required to run lab-scale or pilot-scale HPGR tests, as the throughput is calculated based on the knowledge of the operating gap (or working gap), which is only available via actual HPGR testing.

The HPGR model developed by UBC (Nadolski, 2012; Davaanyam, 2015) established an experimental procedure for determining the breakage functions to describe the breakage mechanism, as well as determining the frictional properties and compressibility of the tested material to determine the throughput capacity. Large pilot-scale HPGR testing results have been used for model calibration and verification. The simplicity and accuracy of resulted models have provided potential for continuous development and further deployment.

Chapter 3

Experimental Program and Methodologies

3.1 Introduction

This chapter describes the overall methodology for the development of HPGR models. The testing facility for the pilot HPGR and PPT are described, along with the testing procedures used in this research. Towards the end of the chapter, descriptions of the regression modeling techniques and the PBM method are provided. A description of test samples is also provided in this chapter.

Figure 3.1 outlines the overall research program including experimental work and modeling work. The research program was carried out in the following phases:

- Phase 1: Conducted pilot HPGR tests and laboratory PPT;
- Phase 2: Developed empirical models for prediction of key HPGR performance (dependent) variables, based on statistical analysis of the latest HPGR database;
- Phase 3: Determined the material responses to high pressure comminution through the PPT, and enabled the investigation of ore variability using this methodology and further extended the application of PPT for HPGR sizing and design;

- Phase 4: Determined ore breakage properties under confined particle-bed comminution through the PPT simulation procedure, and enabled HPGR modeling and simulation via the PBM approach;
- Phase 5: Tested and validated the proposed methodologies using various pilot HPGR test programs. Eventually, proposed a holistic approach to facilitate the HPGR performance assessment, machine sizing and selection, and circuit design.

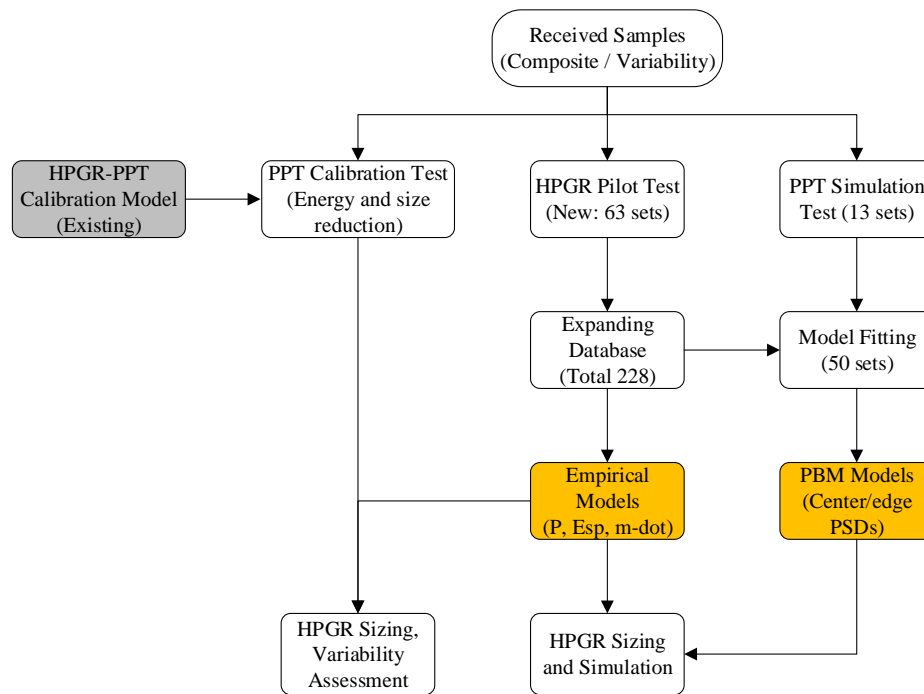


Figure 3.1: Overall structure of the research program

3.2 Sample Description

In this research program, ore samples were received from 6 operating mines and 2 mining projects. The samples represent a range of ore types including Copper-Moly (Cu-Mo) ore, Copper-Gold (Cu-Au) ore, Gold (Au) ore, Nickel (Ni) ore,

Hematite Iron (Fe) ore and Quarry sample. Table 3.1 lists the ore types and corresponding number of composite and variability samples received from each origin. The received samples were in the form of drill core, crushed Run-of-Mine (ROM) bulk sample, or mill feed collected from the respective conveyor belt. These ore samples were the primary materials used for the pilot HPGR testing and PPT programs.

Table 3.1: Sample received for the research program

No.	Ore type	Description	Composite	Variability	Axb	BBWI, kWh/t
1	Cu-Mo (HB)	Mill feed	1	0	31	18.0
2	Cu-Mo (HC)	Mill feed	3	0	65-74	13.6-13.8
3	Cu-Au (C)	Mill feed	1	6	23-40	18.0-22.0
4	Au (T)	Mill feed	2	0	32	18.0
5	Ni (G)	Drill Core	0	5	25-33	15.6-24.2
6	Au (G)	Drill Core	2	6	22-35	12.3-17.2
7	Fe (SA)	ROM	3	5	-	-
8	Quarry (SD)	ROM	1	0	-	13.5

Table 3.1 also provides the hardness characteristics of the received ore samples. JK Drop Weight Test (DWT) or its abbreviated version (SMC test[®]) are used to describe the material competency by measuring its resistance to impact breakage. The resulting Axb parameter indicates how the material will behave during the crushing process and AG/SAG milling. The standard Bond Ball Mill Work Index (BBWI) measures the ore resistance to ball milling, this parameter is widely used for ball mill sizing and capacity determination. Most of the received samples are classified as hard (competent) for AG/SAG milling and moderate to hard for ball milling.

3.3 Pilot HPGR Testing

3.3.1 Pilot HPGR facility

As shown in Figure 3.2, a pilot-scale Köppern HPGR located in the Coal and Mineral Processing Laboratory (CMPL) of UBC was used to conduct all pilot tests. This

pilot unit operates at a 32 mm feed top size and has a roll diameter of 0.75 m and roll length of 0.22 m. The pilot unit uses a Hexadur® liner that is convenient for pilot testing because an autogenous layer is not required and therefore less sample is needed. The pilot test program evaluates the influence of key operating parameters on HPGR comminution and provides information about the net energy consumption, specific throughput constant, and general ore suitability for interparticle comminution.



Figure 3.2: Pilot HPGR facility at UBC

Table 3.2: Köppern HPGR specifications

Description	Unit	Value
Roll diameter	[mm]	750
Roll length	[mm]	220
Press drive	[-]	Dual output shaft gear reducer
Feed system	[-]	Gravity
Roll wear surface	[-]	Hexadur® WTII
Installed power	[kW]	200
Maximum pressing force	[kN]	1600
Maximum specific pressing force	[N/mm ²]	8.5
Variable speed drive	[rpm]	up to 40 rpm (1.55 m/s)

3.3.2 HPGR test procedure

For all pilot HPGR tests performed at UBC, the standard Köppern testing procedure (see Appendix A.1) was followed, which involved the following steps:

1. Select testing parameters including the feed top size, feed moisture content, specific pressing force, and roll speed. Note that the specific pressing forces are typically evenly spread out, for example, 2.5, 3.5, and 4.5 N/mm².
2. Prepare the feed sample according to the required feed top size and feed moisture content, through stage-crushing, screening, homogenizing, and splitting. Subsequently, obtain representative feed samples for characterization, including the moisture, bulk density and Particle Size Distribution (PSD).
3. Perform HPGR test with, typically, a 200-litre drum of material (~250 kg to 300 kg). Start the HPGR rolls and product conveyor. Open the feed hopper slide gate (Figure 3.3) to allow the feed to enter the HPGR. Stable operation starts about five seconds after opening the slide gate, and lasts for approximately 20 seconds (subject to the total amount of feed sample), during which the feed material is being depleted. The products collected before and after the stable operation are diverted to a waste drum. The product generated during the stable operation is split into center and edge streams at approximately 70/30 mass ratio (the splitter located at the conveyor discharge is shown in Figure 3.3). During each test, product flakes are also collected.
4. Collect testing time, roll speed, torque, pressing force, operating gap, and power draw information using a data-logger connected to the HPGR programmable logic controller system.
5. Obtain representative sub-samples of center and edge product streams using a rotary splitter and then perform standard sieve testing to determine their PSDs. Measure the product flake thickness and flake density.
6. Determine HPGR sizing parameters and comminution performance using the recorded machine data alongside measurements taken from the feed and product.

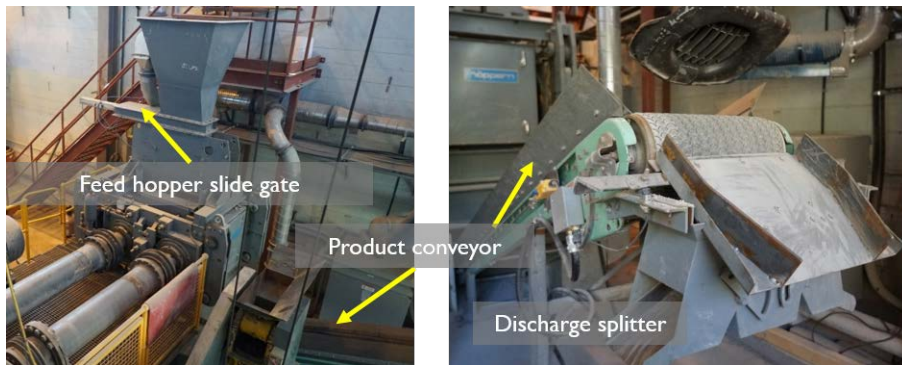


Figure 3.3: HPGR testing facility setup

3.4 Piston-die Press Testing

3.4.1 Piston-die press test facility

Piston-die Press Testing (PPT) was used to study the energy and breakage relationship in the compressive bed environment. The instrumented MTS hydraulic press (Figure 3.4) used for the PPT program can apply a maximum force of 1,400 kN, with a measurement accuracy of ± 325 N. The stress velocity ranges from 0.1 to 10.0 mm/min. The MTS test apparatus is located in the CMPL at UBC.

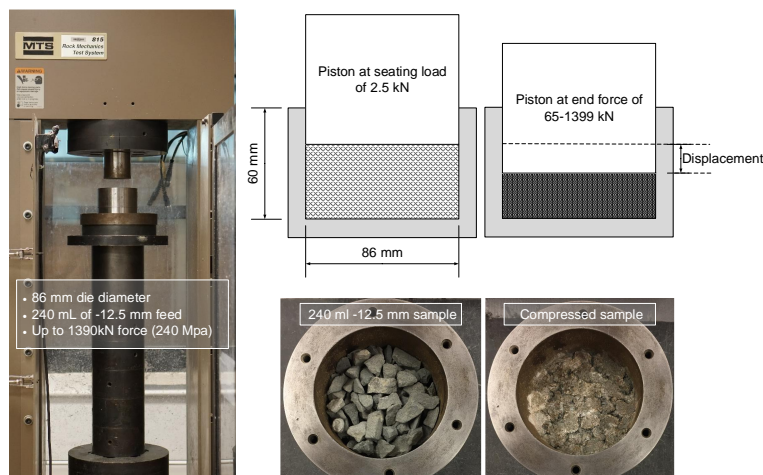


Figure 3.4: Schematic of the piston-die press apparatus

Davaanyam (2015) outlined the main considerations concerning the design and selection of the piston–die apparatus for the PPT program. The overall geometry of the testing apparatus was adjusted to match the observations from the pilot HPGR testing at UBC. The piston diameter of 86 mm was selected based on the force limit of the MTS unit, in order to reach the HPGR peak pressure requirement of 200-250 MPa (30-60 times the applied specific pressing force). The PPT feed top size of 12.5 mm was selected to match the ratio of the roll length of 220 mm to the typical feed top size of 32 mm used in the pilot HPGR testing. The test sample quantity was subject to the minimum mass requirement to ensure sample representativeness, while maintaining the alignment of the height of compressed particle bed in the PPT to the observed operating gap in the HPGR.

3.4.2 Piston-die test procedure

Two testing procedures were used for the PPT program, namely the PPT calibration test and the PPT simulation test. The former test is performed on a sample with a full PSD, and multiple tests are performed at different applied pressures. The latter test uses multiple narrowly-sized fractions with a wide range of energy input. General procedures developed by Davaanyam (2015) for PPT calibration and PPT simulation tests were followed, which can be found in Appendix B.1.

PPT calibration test

The PPT calibration test is used to measure sample responses to confined particle-bed comminution, which is similar to what occurs at the center of the HPGR. The results of the PPT calibration test can be correlated to the HPGR comminution performance. The sample requirement for the PPT calibration test is 5-10 kg. All materials are prepared to 100% passing 12.5 mm through stage-crushing and screening in a reverse closed arrangement. Representative sub-samples are obtained for feed PSD determination and subsequent compression tests. The moisture content of the sub-samples is adjusted to the desired level. The measured bulk density (packed) is used to calculate the target sample weight at 240 mL volume. Each sub-sample is then split to within ± 10 g of the target weight using a riffle splitter. The obtained sub-samples are subsequently pressed in the PPT apparatus at four different piston

pressures representing four energy inputs. The forces/pressures selected for the testing are:

- Test 1: 1,399 kN (240 MPa or N/mm²)
- Test 2: 1,100 kN (189 MPa or N/mm²)
- Test 3: 800 kN (138 MPa or N/mm²)
- Test 4: 500 kN (86 MPa or N/mm²)

For each compression test, the PSDs of the feed and product are determined through a combination of wet and dry sieving tests. After determining the specific energy input to each sample, the relationship between specific energy consumption and particle size reduction can be established.

PPT simulation test

The PPT simulation test is used to determine the size-by-size breakage characteristics of the sample under confined particle-bed comminution. It is similar to the JK DWT and involves conducting PPT on narrowly sized fractions in a multiple layer arrangement. Incremental energy levels from 0.3 to 3.0 kWh/t are applied to each size fraction, as summarized in Table 3.3.

Table 3.3: General PPT simulation test conditions

Mono-size class	Size interval [mm]	Geometric mean size [mm]	t_{10} -size [mm]	Target energy level [kWh/t]		
				3.0	1.3	0.3
1	-12.5+11.2	11.8	1.18	3.0	1.3	0.3
2	-11.2+9.5	10.3	1.03	3.0	1.3	0.3
3	-9.5+8.0	8.7	0.87	3.0	1.3	0.3
4	-8.0+6.3	7.1	0.71	3.0	1.3	0.3
5	-6.3+5.6	5.9	0.59	3.0	1.3	0.3

The PSD of the progeny fragments resulting from the PPT simulation tests are used to determine the breakage index (t_{10}), which is described by Equation 2.19 (Davaanyam, 2015).

$$t_{10} = M \left\{ 1 - \exp(-f_{mat} \cdot \chi^n \cdot E_{sp}) \right\} \quad (2.19 \text{ revisited})$$

Subsequently, the breakage parameters obtained from the PPT simulation tests are used for modeling and simulation of HPGR processes through the use of the PBM approach. The fitted HPGR model is then used to simulate the effect of variations in ore type, feed size, and operating conditions on the HPGR performance.

3.4.3 Force-displacement analysis

Both PPT procedures require the determination of specific energy input to the tested material. The compression test generates a force–displacement curve, which can be used to determine the energy input from the hydraulic press by numerical integration of the area under the force–displacement curve. Prior to the compression testing, the mechanical strain of the PPT apparatus was measured and this value is then subtracted from actual test measurements to obtain a corrected force–displacement curve. Figure 3.5 displays an example of the uncorrected and corrected force–displacement curves. The specific energy input to the sample is calculated by dividing the calculated total energy input (corrected) by the tested sample mass.

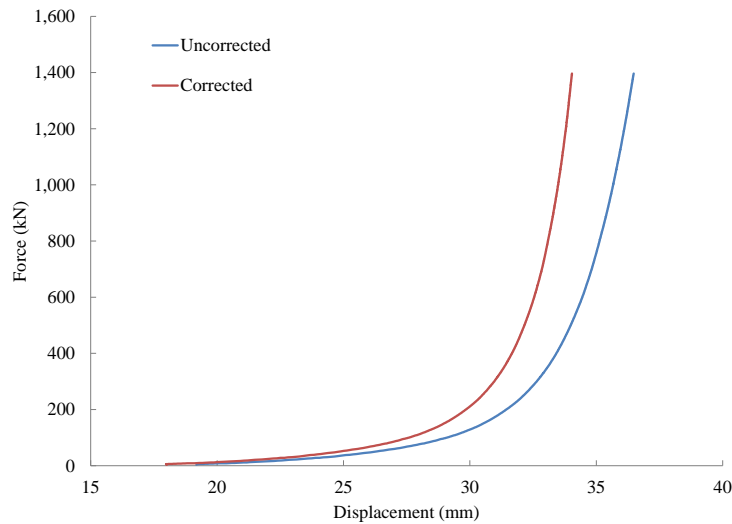


Figure 3.5: Force-displacement curve from piston-die press testing

Previously, the trapezoid method (Davaanyam et al., 2015) was used to calculate the area under the corrected force-displacement curve, which gives the total energy input to the packed particle-bed. In this research, a curve fitting method was developed by fitting a bi-exponential function (Equation 3.1) to the corrected force-displacement curve. The total energy input is therefore calculated by numerical integration of the fitted function from the initial displacement to the end displacement. Figure 3.6 shows both approaches for the determination of the input energy to the packed particle-bed.

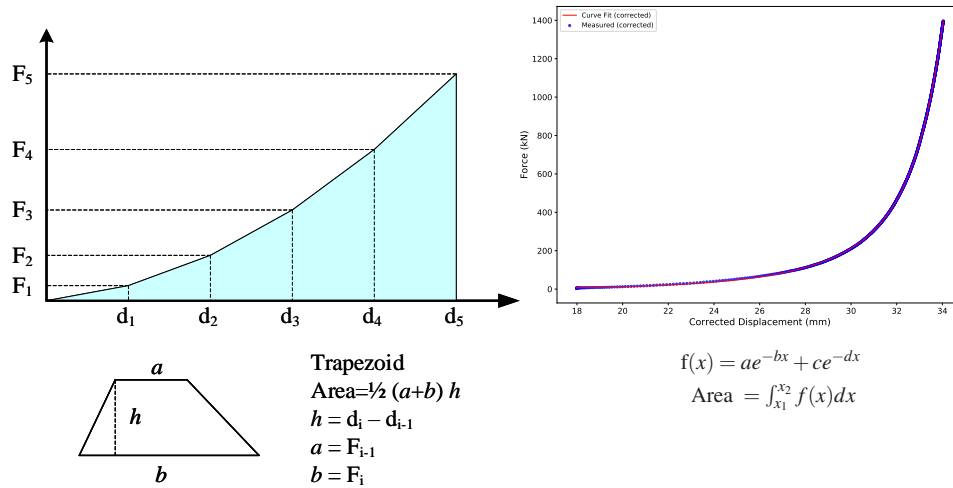


Figure 3.6: Trapezoid and curve fitting method for input energy calculation
(Modified after Davaanyam et al., 2015)

$$Area = \int_{x_0}^{x_1} (ae^{-bx} + ce^{-dx}) dx \quad (3.1)$$

Figure 3.7 compares the testing results on two different samples using both integration approaches. An increased discrepancy between the two methods was observed at higher pressure settings. Over-reporting energy input is possible due to the accumulation of noise (measurement frequency and accuracy) in the raw data when applying the trapezoid integration method.

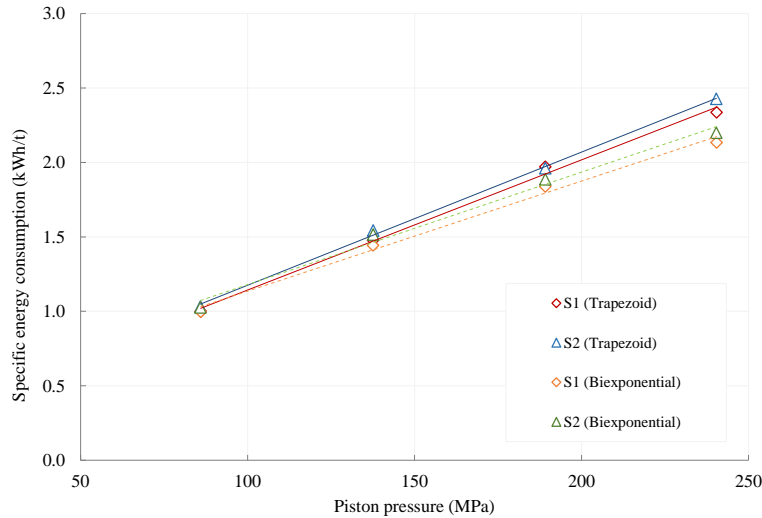


Figure 3.7: Comparison of trapezoid and bi-exponential integration methods

3.5 Linear Regression Methods

To develop empirical models for HPGR performance indicators, data collected from pilot HPGR and PPT programs were used in the regression analysis. Three multi-variable linear methods for regression were compared, namely the Ordinary Least Square (OLS), the Ridge, and the Least Absolute Shrinkage and Selection Operator (LASSO) regression. Methods were compared with respect to their predictive performance.

Description of regression models

The OLS is the simplest regression technique among the three. The other two are known as regularization regression techniques, which work by regulating or constraining the estimated coefficients of variables while minimizing the error between predictions and observations. The idea is that by shrinking the magnitude of model coefficients, the risk of over-fitting can be avoided, so that the model achieves improved prediction accuracy and increased model interpretability.

1. OLS Regression It is a statistical method to estimate the linear relationship between the predictor (independent) variables and a response (dependent) variable. An objective function is used to fit the regression, by minimizing the Residual Sum of Squares (RSS), i.e. the sum of squared errors between the predicted and observed outcomes. This can be depicted mathematically as:

$$RSS(\beta) = \hat{\beta}^{\text{OLS}} = \underset{\beta}{\operatorname{argmin}} \left\{ \sum_{i=1}^N \left(y_i - \beta_0 - \sum_{j=1}^p x_{ij} \beta_j \right)^2 \right\} \quad (3.2)$$

where, β_0 is the intercept coefficient and β_j represents the coefficient for each of the prediction variables.

2. Ridge Regression The Ridge regression is a penalized shrunken regression method developed by Hoerl and Kennard (1970). It is applied to solve the instability problem of least-squares estimation in multivariate linear models due to the existence of collinearity between predictor variables. The objective function for Ridge regression is expressed as:

$$\hat{\beta}^{\text{ridge}} = \underset{\beta}{\operatorname{argmin}} \left\{ \frac{1}{2} \sum_{i=1}^N \left(y_i - \beta_0 - \sum_{j=1}^p x_{ij} \beta_j \right)^2 + \lambda \sum_{j=1}^p \beta_j^2 \right\} \quad (3.3)$$

where, λ is the penalty term that the Ridge regression uses to impose a constraint on the coefficients β_j . The sum of squared regression coefficients is bounded in the objective function, meaning that the highest magnitude of coefficients will be penalized the most. Ridge regression shrinks coefficients and helps to reduce model complexity and multicollinearity. When the penalty term λ equals zero, the Ridge regression is effectively same as the OLS regression.

3. LASSO Regression The LASSO regression (Tibshirani, 1996) is another shrinkage method similar to the Ridge regression, except that the penalty term λ is bounded with the sum of absolute values of the coefficients. The objective function for the LASSO regression is defined as:

$$\hat{\beta}^{lasso} = \underset{\beta}{\operatorname{argmin}} \left\{ \frac{1}{2} \sum_{i=1}^N \left(y_i - \beta_0 - \sum_{j=1}^p x_{ij} \beta_j \right)^2 + \lambda \sum_{j=1}^p |\beta_j| \right\} \quad (3.4)$$

The effect of absolute values is that regression coefficients for some predictor variables might be set exactly equal to zero, while others are shrunk towards zero. Hence, one can perform LASSO regression for both model shrinkage and variable selection. Predictor variables with zero regression coefficient are effectively excluded from the model, then the remaining variables with non-zero coefficients are considered most strongly associated with the response variable. The variable selection feature of the LASSO regression is attractive for regression modeling, especially when a large number of predictor variables are involved. The predictor variables can be either quantitative, categorical, or both. Note that when the penalty term λ equals zero, the LASSO regression also becomes the OLS regression.

Variable selection and refinement

A variable selection method is a way of selecting a particular set of predictor variables for use in regression modeling. This selection is an essential step to search for a “best” model, by limiting the number of predictor variables when there are many potential variables. There are several commonly used methods for variable selection and refinement, including:

- **Expert knowledge.** Knowledge gained on the subject can be used to guide the variable selection. However, it is often overlooked in practice. Indeed, this step should always be considered before any regression modeling.
- **Stepwise selection.** During the stepwise regression process, each addition or elimination of predictor variables can be evaluated based on the selection criteria, until a “best” model is found. However, Harrell (2015) pointed out some problems associated with the stepwise method, such as statistical bias and collinearity limitation.
- **LASSO selection.** As described in the previous section, the LASSO method also features variable selection function, which is considered a better alterna-

tive than the stepwise method. The variable selection is done by performing LASSO regression with cross-validation rather than the goodness of fit.

Model assessment and selection

For regression modeling, the data can be split into training and testing data sets, so that modeling and model assessment can be performed on different subsets of data. However, the train/test split approach provides a high variance estimate, because the testing accuracy could change significantly depending on which observation was used in the testing set.

The K-fold Cross-validation technique (Anthony and Holden, 1998) is an alternative approach for model evaluation, that can obtain a more accurate estimate of model testing error, and avoid over-fitting on a small subset of data. The K-fold Cross-validation is a resampling method that, takes K replicate samples of the data set, with each model trained using $(K-1)/K$ of the data and tested on the remainder ($1/K$ of the data). This procedure repeats K times, during each iteration, every observation can only be either in the training set or the testing set. K value can be any number, but generally subject to the size of the dataset. For instance, the procedure for a 5-fold cross-validation is illustrated in Figure 3.8, when finished, the cross-validation error can be computed based on the averaged estimate of out-of-sample accuracy from the 5 iterations. Based on train/test scores and cross-validation scores, the best model can be possibly identified.



Figure 3.8: K-fold Cross-validation procedure (K=5)

Regression analysis workflow

Using the above mentioned techniques, the overall workflow for linear regression modeling is presented in Figure 3.9, and summarized below.

1. Assemble response variables (Ys) and all possible predictor variables (Xs) including quantitative and categorical variables.
2. Evaluate all data by drawing correlation/matrix plots to visually observe the inter-relationship among the data.
3. Apply engineering judgment or professional knowledge for the initial variable selection.
4. Perform data processing (e.g. data normalization/standardization) prior to the shrinkage regression and cross-validation for variable selection and refinement. All data should be normalized/standardized because variables have a wide scale of values.
5. Create regression models using the selected/refined predictor variables based on the OLS, Ridge, and LASSO methods. Note that previously normalized data sets need to be transformed back to their original scale in order to produce an interpretable model.
6. Select the “best” model by checking the training/testing scores and cross-validation scores, along with other statistics.
7. Evaluate the quality of the model by comparing the model predictions to actual observations, and examining the resulting residual plots.
8. Apply model tuning and refining, which involves rejecting outliers, adding or subtracting predictor variables prior to reiterate Step 4 through Step 7.
9. Deploy the model and report key statistics.

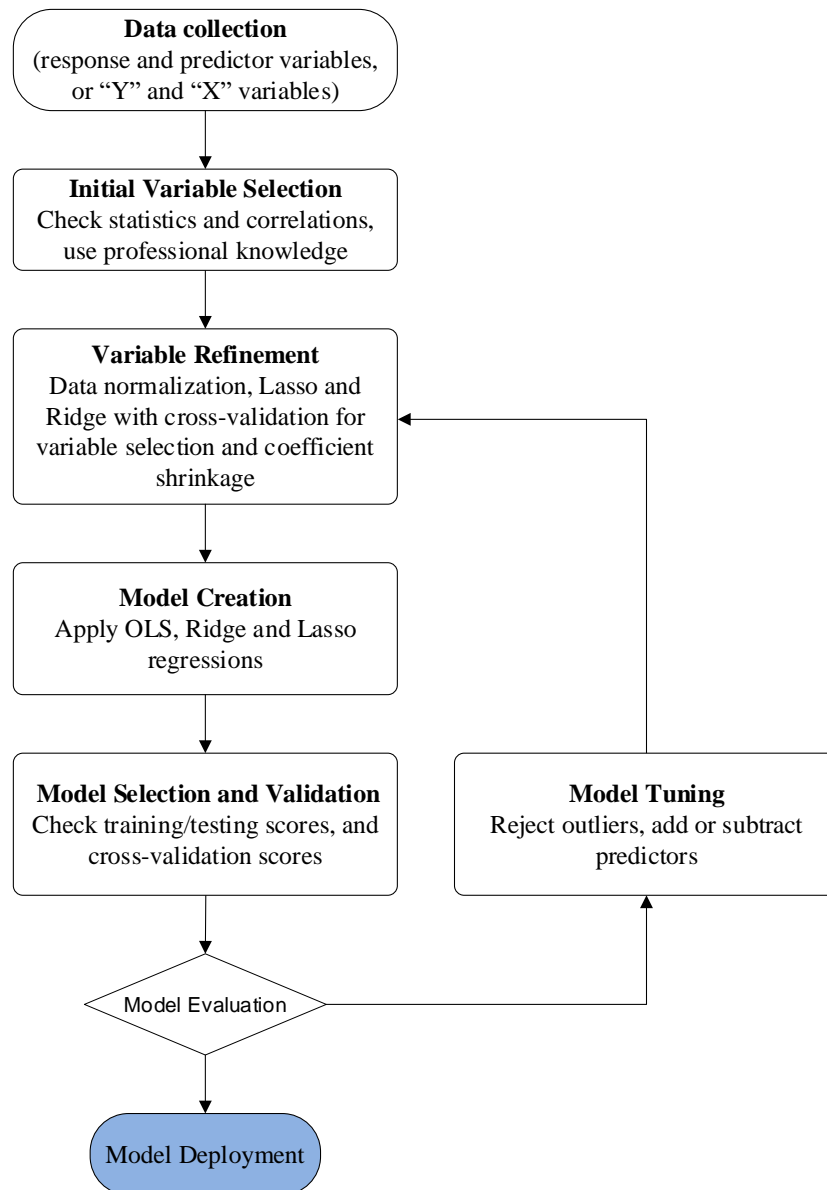


Figure 3.9: Regression analysis workflow

3.6 Population Balance Modeling

There are limitations with the empirical approach for HPGR modeling. In particular, the complete PSD of the comminution process is often difficult to predict with the empirical modeling approach. A more complex modeling approach such as the Population Balance Modeling (PBM) method is therefore used to develop the desired models that can resolve the limitation. The PBM technique involves tracking the mass and particle sizes throughout the comminution process (Wills and Finch, 2015). In addition, the population of particles in individual size fractions is continuously balanced between each stage of breakage. Advances of PBM method for comminution modeling have been well documented by researchers (Herbst and Fuerstenau, 1973; Lynch, 1977; Austin et al., 1984), which were subsequently adopted in commercial simulation programs such as JK SimMet and Moly-Cop Tools to model and simulate crusher, AG/SAG mills, and ball mills (Napier-Munn et al., 1996).

As expressed in Equation 3.5, key components of a population balance model include a selection function (S) and a breakage function (B). The selection function defines the probability that particles in a given size class are selected for breakage. The selection function is generally related to the specific comminution machine and its operating settings, for instance in a jaw crusher, larger particles have a high probability to be selected for breakage than smaller particles. The breakage function (B) describes the progeny size distribution after the breakage of parent particle sizes. The breakage function is considered as the characteristics of materials, which can be determined by laboratory tests. In the PBM, the selection function is back-calculated through model fitting for a given feed and product size distributions using the breakage function of the material.

$$\hat{p} = B\hat{S}\hat{f} + (I - S)\hat{f} \quad (3.5)$$

where, vector \hat{p} represents the mass fraction of product material in each size class; vector \hat{f} represents the mass fraction of feed material in each size class; I is an identity matrix; B is the breakage function; S is a diagonal matrix representing the selection function. Therefore, $B\hat{S}\hat{f}$ represents the portion of feed material being selected for breakage, while the unbroken portions are described by $(I - S)\hat{f}$.

Chapter 4

Results of HPGR and Piston-die Press Testing

4.1 Introduction

This chapter summarizes the results of the pilot HPGR tests and Piston-die Press Testing (PPT) conducted for this research. The objective of the pilot HPGR test programs was to characterize HPGR performance including specific energy consumption, specific throughput, and product sizes for the tested ore samples under various operating conditions. The PPT calibration tests were performed to determine the material resistance to particle-bed compression breakage, and the results from the PPT simulations were used to determine the size-by-size breakage characteristics of particles under confined compressive load.

4.2 Summary of HPGR Test Results

In total, 63 pilot-scale HPGR tests were conducted at UBC as part of this research program, and an additional 12 supplementary pilot HPGR tests were carried out at other testing facilities. Table 4.1 shows the results from each of the performed test programs, which covered a wide range of feed characteristics and operating conditions. The detailed test results are provided in Appendix A.

Table 4.1: Summary of HPGR test results

No.	Ore type	Test #	Moist %	F ₈₀ mm	F _{sp} N/mm ²	E _{sp} kWh/t	mdot ts/hm ³
1	Cu-Mo (HB)	7	3.0-5.0	4.4-23.6	2.5-4.0	1.2-2.6	172-222
2	Cu-Mo (HC)	13	0.6-5.7	4.2-21.9	2.4-4.0	1.0-3.3	154-285
3	Cu-Au (C)	5	1.1-5.6	19.9-22.8	3.1-5.0	1.8-2.9	237-253
4	Au (T)	6*	1.5-2.6	18.9-22.6	2.0-4.0	1.3-2.3	215-249
5	Ni (G)	0**	-	-	-	-	-
6	Au (G)	9+6*	2.5-5.0	25.7-27.3	2.6-5.1	1.8-3.1	182-250
7	Fe (SA)	21	2.6-8.9	4.2-14.9	2.3-5.1	1.1-2.9	224-365
8	Quarry (SD)	8	1.1-3.4	5.4-15.8	3.5-4.5	1.8-2.6	189-276

* Tests performed outside of UBC using different size pilot HPGR machines (Köppern and Weir)

** No HPGR tests conducted, but the PPT variability tests

This section summarizes the observations made during the testing program, aimed at obtaining some useful insights into the HPGR performance. The influences of the applied specific pressing force on the specific energy consumption, specific throughput constant and comminution effect were assessed. Additional testing results were included to compare the HPGR performance under different test conditions. The testing reproducibility of the UBC pilot HPGR was assessed through conducting duplicate tests at both the UBC lab and at other testing facilities. The results are summarized in Appendix C.

4.2.1 HPGR key performance indicators

Specific energy consumption

The net specific energy consumption (E_{sp}), expressed in kWh/t, corresponds to the net power draw in kW (total power draw minus no-load power) divided by the actual machine throughput rate in t/h. Figure 4.1 shows the net specific energy (E_{sp}) as a function of the specific pressing force (F_{sp}) for the selected ore samples. It shows that the net specific energy consumption increased with the increase in the applied specific pressing force, generally accepted as a linear relationship over the typical operating range of 1-6 N/mm². Although not all samples were included in this plot as some tests were not performed with a range of F_{sp} , the linear relationship is expected to hold. It is also clear that at a given applied F_{sp} , there are variations in responding E_{sp} which is largely related to the ore properties (ore type, specific gravity, hardness, size distributions, and among others).

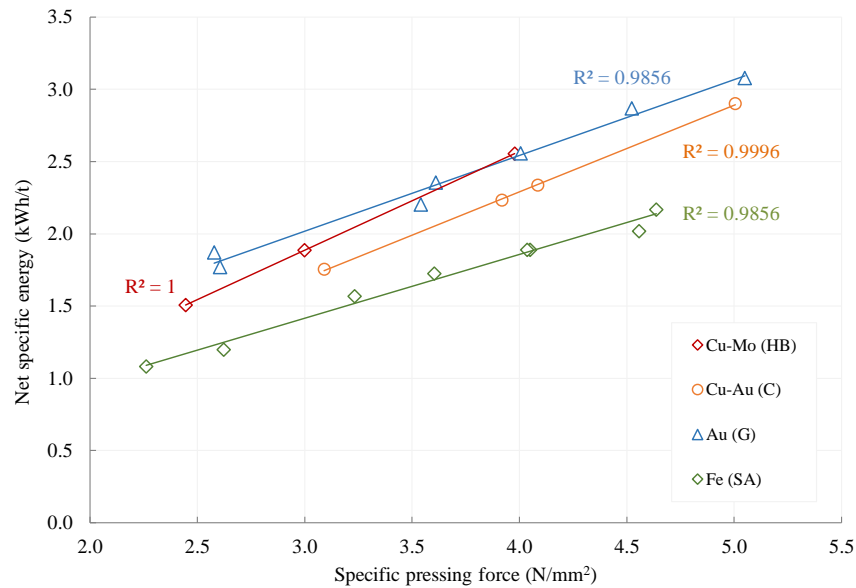


Figure 4.1: Specific pressing force versus net specific energy consumption

Specific throughput constant

The specific throughput constant (\dot{m}), expressed in ts/hm^3 , is mostly affected by material properties, operating conditions and roll surface profile. In general, the \dot{m} increases with increasing feed top size and ore hardness, but decreases with an increase in feed moisture and specific pressing force (F_{sp}). The \dot{m} is expected to be lower when the HPGR feed had fewer fines (an extreme example would be the truncated feed). It is also understood that the \dot{m} is higher for the studded roll surface than the smooth surface. Hence, the Köppern pilot HPGR at UBC is expected to give a lower \dot{m} from the testing, due to the use of Hexadur[®] liner.

Figure 4.2 shows the specific throughput constant (\dot{m}) as a function of the specific pressing force for selected ore samples. The \dot{m} value decreased slightly with higher specific pressing force due to the formation of a narrower gap at higher pressures. Tests performed on the Au (G) ores showed a lower R^2 value from the trend, possible explanations could be the experimental deviation or maybe other variables exerting an influence on the performance.

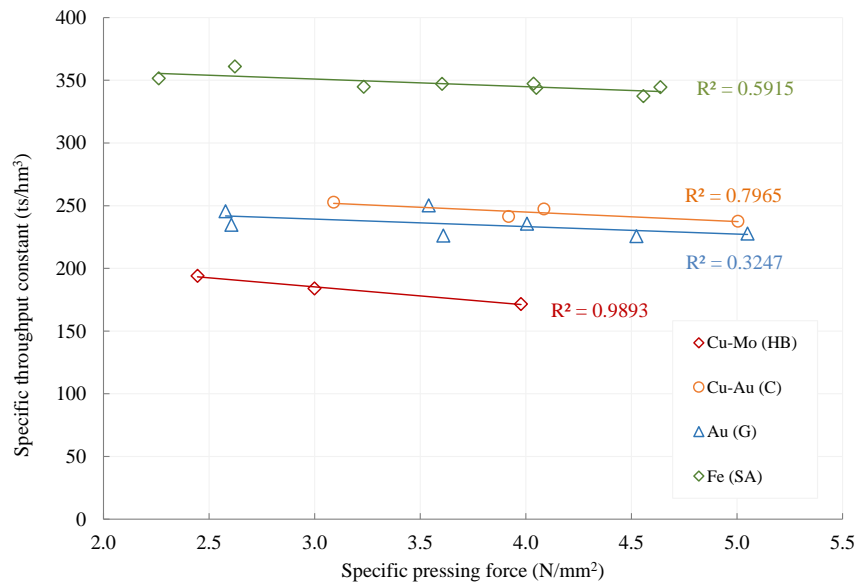


Figure 4.2: Influence of specific pressing force on specific throughput constant

Comminution effect - product size and reduction ratio

Figure 4.3 shows the relationship between the applied specific pressing force (F_{sp}) and resultant product particle sizes as measured by P_{80} and P_{50} for the tested ore samples. Clearly, the product fineness improved with higher specific energy input as a result of increased specific pressing force.

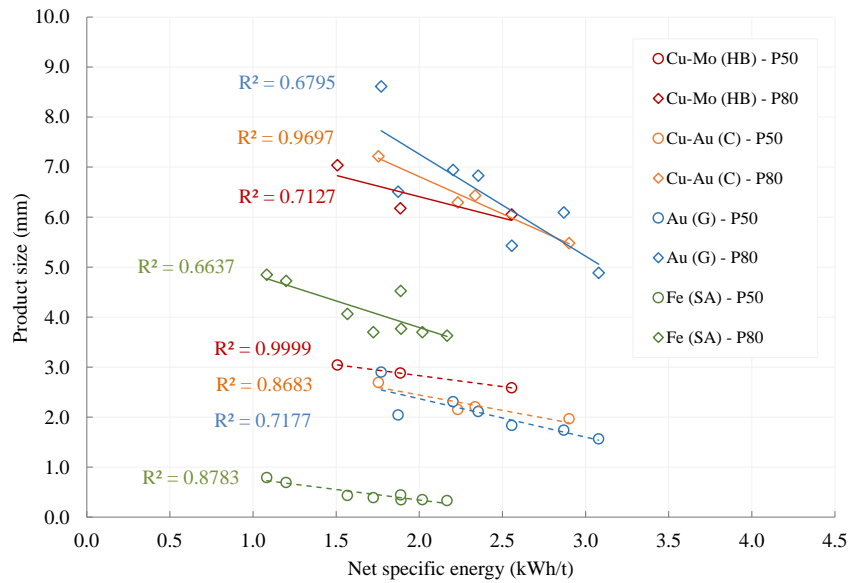


Figure 4.3: Influence of specific energy on HPGR product size

Figure 4.4 shows that the size reduction ratio, defined as F_{50} over P_{50} , improved with the increase in net specific energy input. Some ores had a more pronounced impact in size reduction than others, for instance, the size reduction for the Fe (SA) sample appeared to be more susceptible to specific energy input. This is mainly attributable to the ore type, feed PSD, ore hardness, and moisture content.

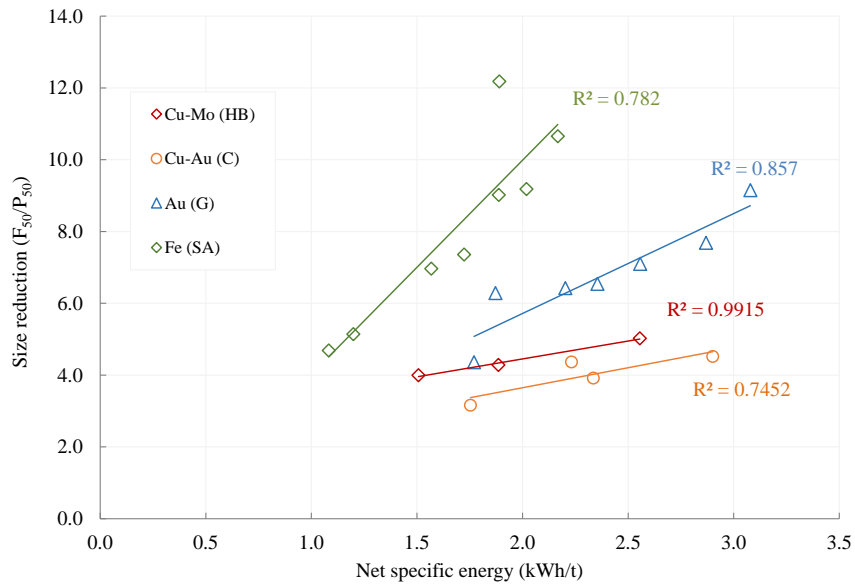


Figure 4.4: Influence of specific pressing force on size reduction ratio

4.2.2 Comparative HPGR testing

Feed particle size distributions

The feed PSD is an important process variable affecting the HPGR performance. Figure 4.5 shows examples of the HPGR feed and corresponding product PSD for Au(G)-P (Gold ore) and Fe (SA) (Hematite ore) selected from the test programs. Both tests were conducted at the same specific pressing force (F_{sp}) of 3.6 N/mm², the Au(G)-P test feed features a coarser PSD with significantly fewer fines when compared to the Fe (SA) test feed. Figure 4.5 also shows that in both cases the edge product is considerably coarser than the center product, as a result of the “edge effect”.

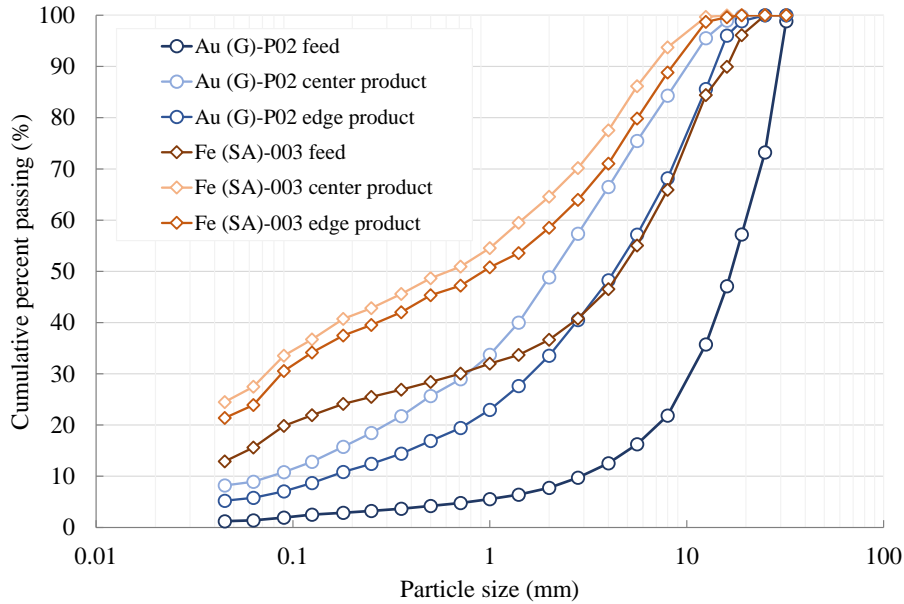


Figure 4.5: Examples of HPGR feed and product PSDs ($F_{sp} = 3.6N/mm^2$)

Table 4.2 compares the key performance indicators for the two tests including the specific energy consumption, throughput capacity and resulting product sizes. Notably, the pilot HPGR performance under different feed conditions changed substantially. Though the variation in performance is partially related to the feed PSD, it should be recognized that the Fe (SA) sample had a higher bulk density than the Au(G)-P sample, which contributed to higher specific throughput and lower specific energy consumption. Undoubtedly, the feed characteristics such as the PSD, bulk density, and moisture content have a significant impact on the HPGR performance, thus requiring careful examination before any HPGR sizing and circuit design attempts.

Table 4.2: Comparison of two HPGR tests at the same specific pressing force

Test	Unit	Au (G)-P02	Fe (SA)-003	Delta
Ore type		Gold	Hematite	
F_{80}	[mm]	26.9	11.4	-58%
F_{50}	[mm]	16.9	4.7	-72%
F_{sp}	[N/mm ²]	3.6	3.6	0%
ρ_{bulk}	[t/m ³]	1.6	2.3	44%
x_g	[mm]	19.9	19.3	-3%
E_{sp}	[kWh/t]	2.35	1.78	-24%
\dot{m}	[ts/hm ³]	226	301	33%
P_{80}	[mm]	8.2	4.7	-43%
P_{50}	[mm]	2.6	0.7	-73%
F_{80}/P_{80}	[-]	3.3	2.4	-26%
F_{50}/P_{50}	[-]	6.5	6.7	3%

Soft and hard materials

Fundamentally, the influence of ore hardness on HPGR performance should be similar to those observed on other comminution technologies. Processing harder materials would essentially require higher specific energy input to achieve the same product size target than processing softer materials. Certainly, at the same specific energy input, the system processing harder materials would produce a coarser product. So, to “reasonably” compare the performance of HPGR on soft and hard materials, two tests with similar feed PSD (as measured by F_{80} and F_{50}) at the same specific pressing force but differing in ore hardness were selected. The test results provide good evidence that the response of HPGR comminution to changing ore hardness is variable. In this case, the tested soft material is represented by the Cu-Mo (HC) sample which has an A_{xb} value of 65 and BBWI of 14 kWh/t. The tested hard material is represented by the Cu-Au (C) sample, having an A_{xb} value of 33 and BBWI of 22 kWh/t. As shown in Figure 4.6, it is important to note that the soft material has considerably more fines in the feed than the hard material, which naturally occurred during the sample preparation (crushing) process.

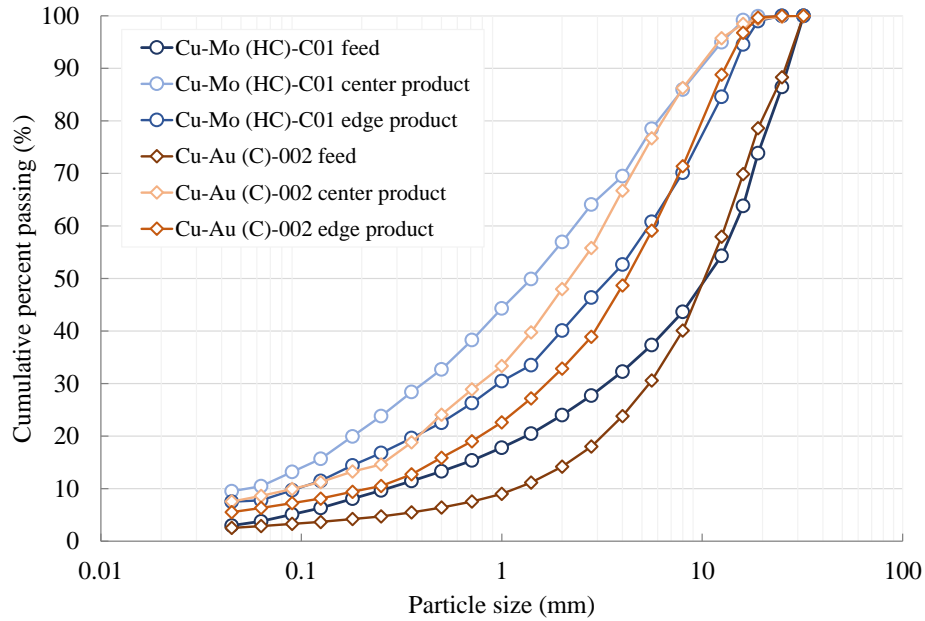


Figure 4.6: Feed and product PSDs of HPGR tests on soft and hard materials

Table 4.3 compares key performance indicators of the two tests under similar testing conditions. The resulting product P_{80} were similar, however, the recorded net specific energy consumption for the test with soft material was 38% lower than that from the hard material. The size reduction in P_{50} and generation of fines were more significant for the soft material, however, some adjustments should be made to account for the additional of fines in the soft material. Typically, harder ore can support a larger gap than softer ore provided that the feed size distributions are kept the same. In this case, it is interesting to see that the test with soft material achieved a larger operating gap than the hard material, suggesting that a wider feed PSD (with more fines) could outweigh the effect of the ore hardness in terms of supporting the operating gap.

Table 4.3: Comparison of HPGR tests on soft and hard materials

Test	Unit	Cu-Mo (HC)-C01	Cu-Au (C)-002	Delta
Sample description		Soft	Hard	
F ₈₀	[mm]	21.9	19.9	-9%
F ₅₀	[mm]	10.7	10.5	-2%
F_{sp}	[N/mm ²]	4.0	4.1	3%
x_g	[mm]	21.5	20.6	-4%
E_{sp}	[kWh/t]	1.69	2.34	-38%
\dot{m}	[ts/hm ³]	259	247	-4%
P ₈₀	[mm]	7.4	7.5	2%
P ₅₀	[mm]	1.8	2.7	52%
F ₈₀ /P ₈₀	[-]	3.0	2.6	-11%
F ₅₀ /P ₅₀	[-]	6.1	3.9	-35%

Locked-cycle testing

HPGR locked-cycle tests were performed on the Quarry (SD) sample. The testing flowsheet was configured as a direct closed circuit with 2 mm dry screen. In this case, the HPGR was tested in a quaternary stage receiving a relatively fine feed. The masses of screen oversize from the first cycle was recorded to calculate the required fresh feed to make up the combined feed for the second cycle test. Figure 4.7 shows that the second cycle feed had fewer fines (5% difference in percent passing 2 mm) than the first cycle. However, the product PSD from the two-cycle tests were only marginally different. Table 4.4 summarizes the key performance indicators of the locked-cycle tests. A reduced operating gap and subsequently lower \dot{m} were observed due to a sharper PSD recycled from the dry screening process. However, the net specific energy consumption for the two tests was practically the same.

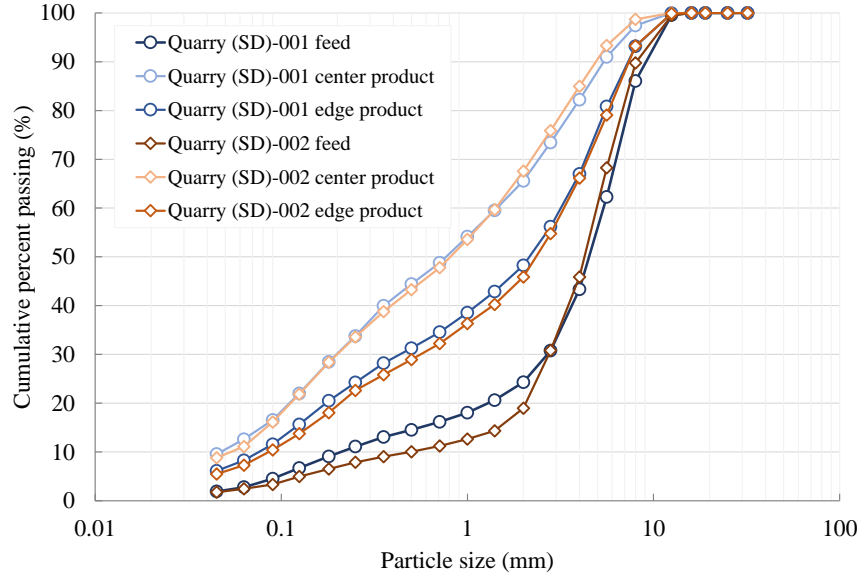


Figure 4.7: Feed and product PSDs of HPGR locked-cycle tests

Table 4.4: Summary of HPGR locked-cycle tests

Test	Unit	Quarry (SD)-001	Quarry (SD)-002	Delta
Description		Cycle 1	Cycle 2	
F ₈₀	[mm]	7.4	6.9	-6%
F ₅₀	[mm]	4.6	4.3	-6%
F _{sp}	[N/mm ²]	4.0	4.0	0%
x _g	[mm]	20.3	18.9	-7%
E _{sp}	[kWh/t]	1.95	1.93	-1%
\dot{m}	[ts/hm ³]	237	222	-7%
P ₈₀	[mm]	4.3	4.2	-5%
P ₅₀	[mm]	1.0	1.1	10%
F ₈₀ /P ₈₀	[-]	1.7	1.66	-2%
F ₅₀ /P ₅₀	[-]	4.4	3.8	-15%

as the fines generation increased. Proper reduction or removal of fines is essential step to maintain the HPGR comminution efficiency if finer product size is deemed desirable. Multiple locked-cycle HPGR test programs with different closing screen sizes may provide a clearer picture of the energy and size reduction relationship for HPGR comminution.

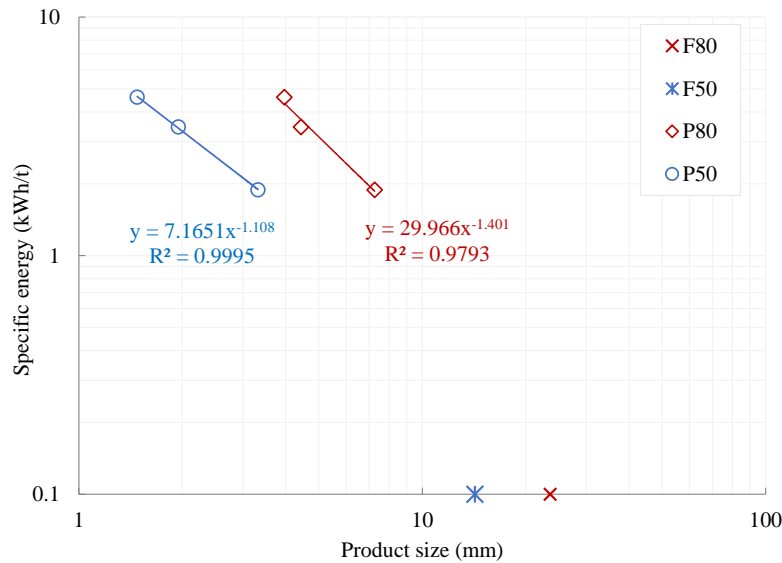


Figure 4.9: Results of multiple stage HPGR testing

4.3 Summary of Piston-die Press Test Results

The composite and variability samples listed in Table 4.5 were subject to PPT calibration tests and PPT simulation tests at UBC. Detailed PPT test results are provided in Appendix B. Additional duplicate tests were performed to assess the testing reproducibility, the results can be found in Appendix C.

4.3.1 PPT calibration testing

For those PPT calibration tests performed on the composite sample, sub-samples were taken from a split of the homogenized samples which were also fed to the pilot HPGR. Subsequent procedure (Appendix B.1) was followed to adequately

Table 4.5: Summary of Piston-die press testing program

No.	Ore type	PPT Calibration Comp. + Var.	PPT Simulation Comp. + Var.
1	Cu-Mo (HB)	-	-
2	Cu-Mo (HC)	-	-
3	Cu-Au (C)	8+6	2
4	Au (T)	2	3
5	Ni (G)	5	-
6	Au (G)	4+6	2+6
7	Fe (SA)	-	1
8	Quarry (SD)	-	-

prepare the sample for PPT calibration testing. Figure 4.10 shows examples of the PSDs of PPT calibration test feed and corresponding products. The selected tests were conducted at the same piston pressing force of 1,399 kN, which is equivalent to a piston pressure of 240 MPa (or N/mm²).

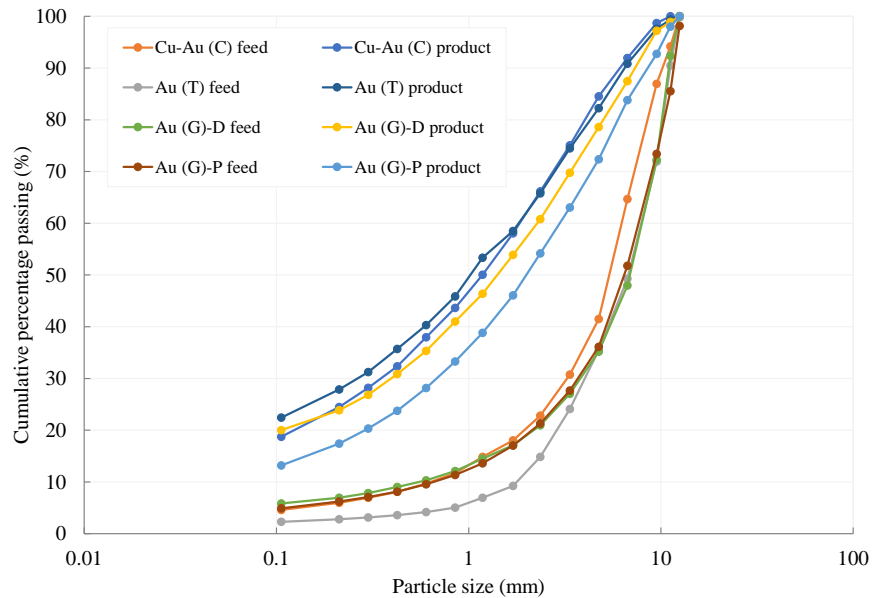


Figure 4.10: PPT feed and product PSD at 240 Mpa piston pressure

Table 4.6 summarizes the results of the selected PPT calibration tests. The combination of the energy input and resultant product size from the PPT program was considered reflective of the ore hardness under confined particle bed comminution. For instance, the resistance of Au (G)-D sample to compression breakage appeared to be weaker than Au (G)-P sample, based on the observation that Au (G)-D test yielded finer product sizes with lower specific energy requirements. This is in line with the ore characteristics measured by other comminution tests (e.g. Axb and BBWI), suggesting that the Au (G)-D sample is softer than the Au (G)-P sample under the HPGR comminution.

Table 4.6: PPT calibration tests at piston pressure of 240 Mpa

Test	Unit	Cu-Au (C)	Au (T)	Au (G)-D	Au (G)-P
Ore type		Copper-Gold	Gold	Gold	Gold
F ₈₀	[mm]	8.61	10.25	10.17	10.42
F ₅₀	[mm]	5.49	6.79	6.94	6.48
Piston pressure	[Mpa]	240	240	240	240
Specific energy	[kWh/t]	2.34	2.09	1.84	2.11
P ₈₀	[mm]	4.04	4.31	5.03	5.43
P ₅₀	[mm]	1.18	1.03	1.42	1.64
F ₈₀ /P ₈₀	[-]	2.1	2.4	2.0	1.9
F ₅₀ /P ₅₀	[-]	4.7	6.6	4.9	3.9

The energy consumed from each of the PPT was calculated from the area under the force-displacement curves at a given piston pressure. The specific energy consumption, expressed in kWh/t, is then calculated by dividing the consumed energy by the sample mass. Figure 4.11 shows the specific energy as a function of applied piston pressure. Similar to the pilot HPGR testing, the PPT is showing a linear relationship between the specific energy consumption and applied piston pressure.

Figure 4.12 shows that the size reduction ratio (F_{50}/P_{50}) improved with the increase in specific energy input. However, the susceptibility of ore samples to compression breakage could vary considerably. As shown in Figure 4.12, some ores are more susceptible (steeper slope as compared to a flatter one) to compression breakage than others.

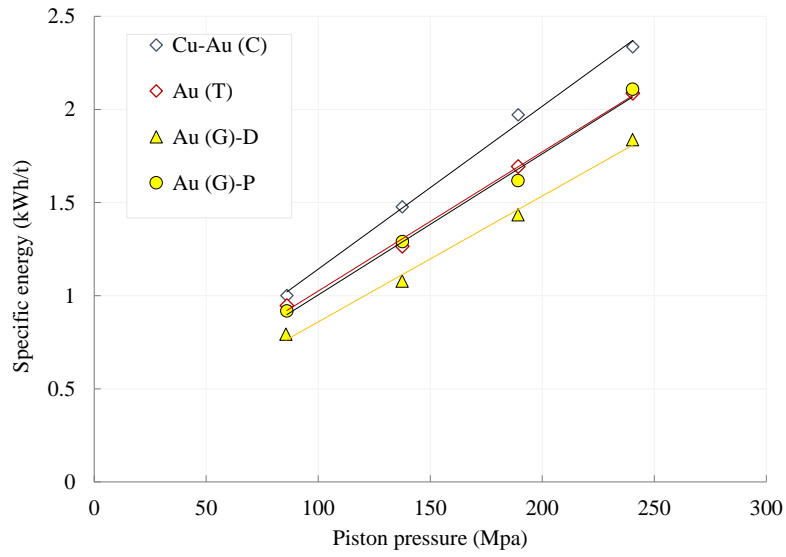


Figure 4.11: Specific energy versus piston pressure

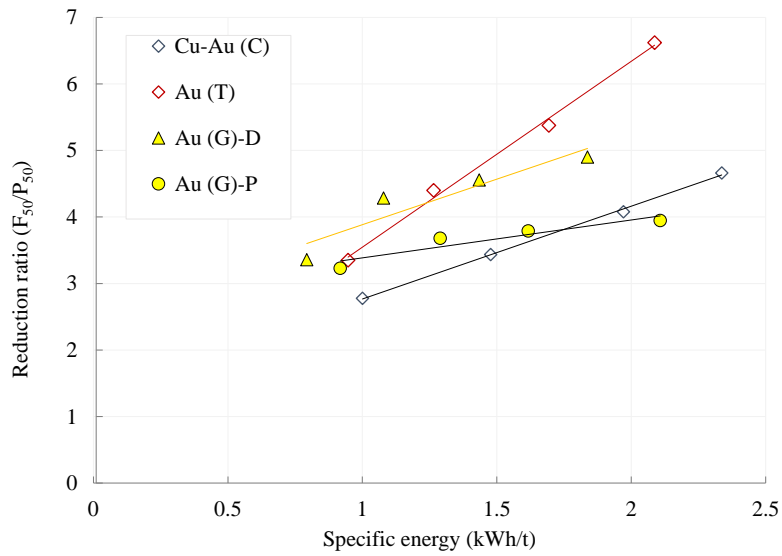


Figure 4.12: Size reduction ratio versus specific energy

4.3.2 PPT simulation testing

Results of the mono-sized PPT simulation tests were fitted to Equation 2.19 to calibrate the t_{10} -based breakage index model based on the particle size and specific energy input. Figure 4.13 shows the experimental data and a fitted t_{10} curve from the test performed on the Cu-Au (C) sample. Considering the achieved R^2 value of 0.995, the model fit is excellent in describing the experimental data for all size classes.

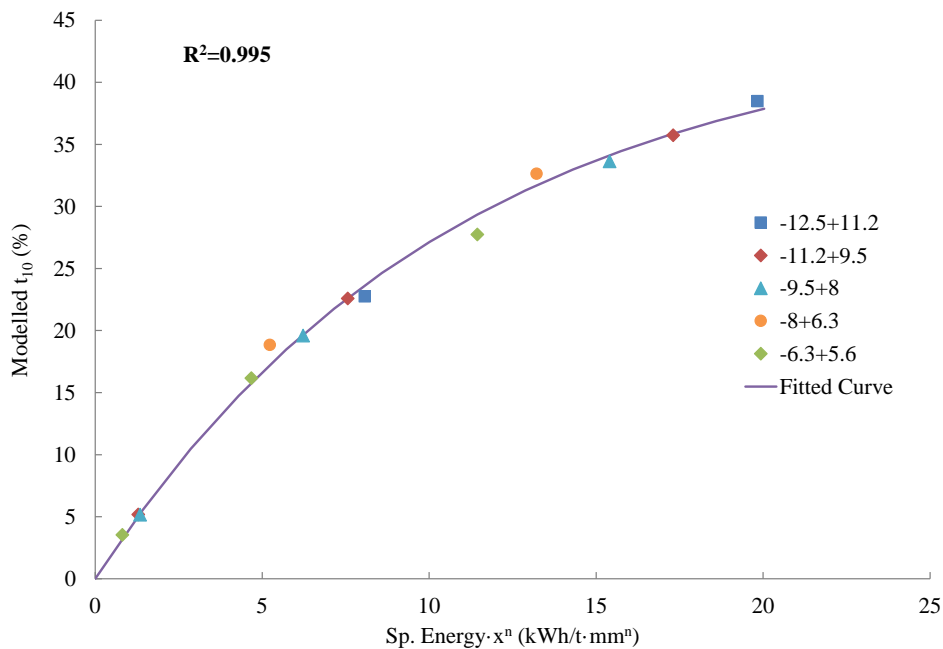


Figure 4.13: Specific energy and t_{10} relationship of the Cu-Au (C) ore

Other samples were subject to the same approach to determine their t_{10} models. The resultant breakage curves are plotted together in Figure 4.14. Table 4.7 lists the fitted t_{10} breakage parameters from the performed PPT simulation tests. The parameter M corresponds to the maximum achievable t_{10} value, f_{mat} parameter indicates how quickly t_{10} approaches the maximum threshold, and n represents the severity of particle size effect.

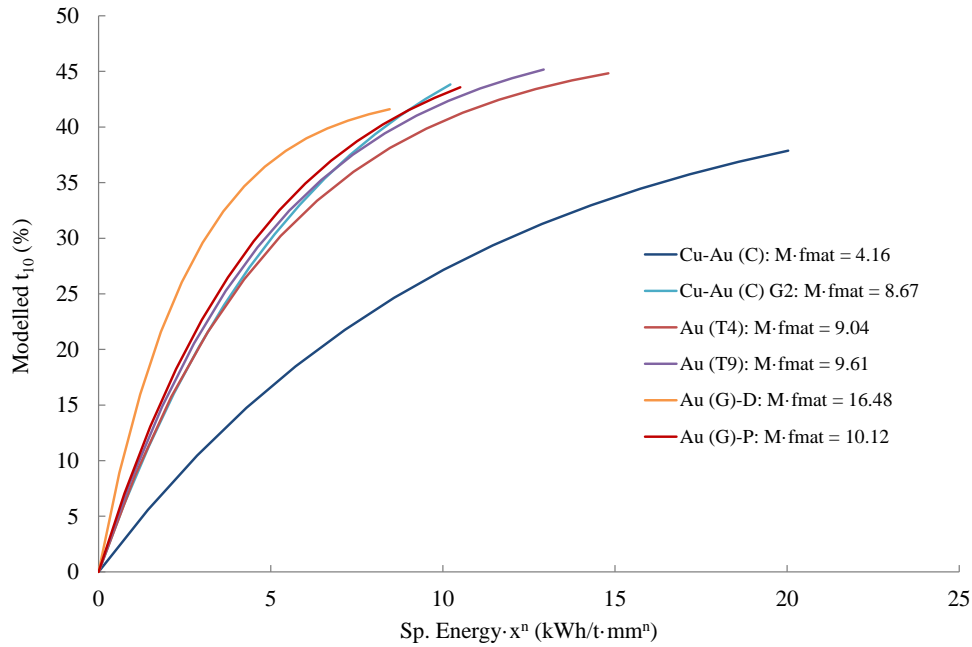


Figure 4.14: Specific energy and t_{10} relationship for various ore types

Table 4.7: Summary of t_{10} breakage parameters for various ore types

Ore type	M	f_{mat}	n	$M \cdot f_{mat}$	R^2	SSE	RMSE	95% CI
Cu-Au (C)	44.87	0.09	0.74	4.16	0.995	7.85	0.61	1.31
Cu-Au (C)-G2	54.60	0.16	0.46	8.67	0.995	20.73	0.99	2.13
Au (T4)	47.71	0.19	0.66	9.04	0.993	21.89	1.02	2.19
Au (T9)	49.08	0.20	0.60	9.61	0.992	31.20	1.22	2.61
Au (T9)-dup	49.02	0.20	0.61	9.58	0.992	30.01	1.20	2.56
Au (G)-D	43.34	0.38	0.44	16.48	0.987	39.11	1.36	2.93
Au (G)-P	49.27	0.21	0.47	10.12	0.986	40.68	1.39	2.98

Figure 4.15 shows a scatter plot of t_n and t_{10} for the Cu-Au (C) ore sample. The data were fitted to Equation 2.20 through Equation 2.25 to form the appearance curves describing the t_n and t_{10} relationship.

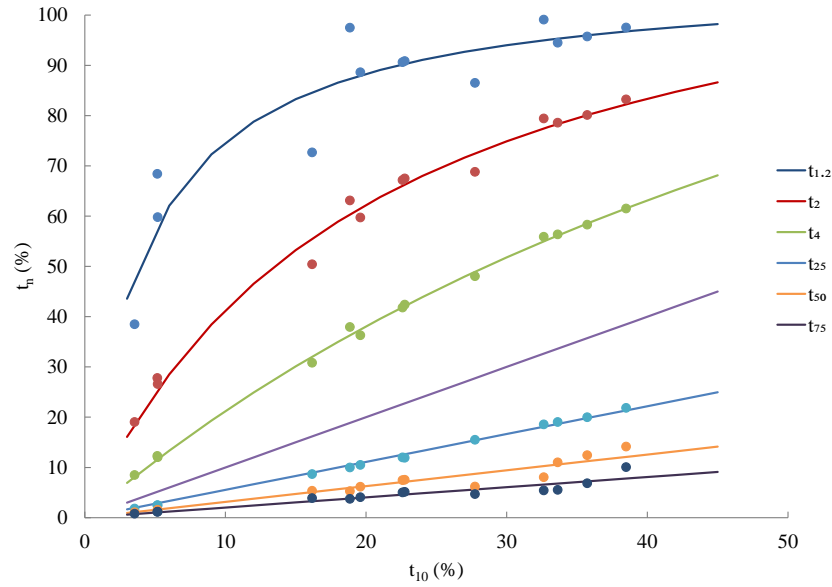


Figure 4.15: Relationship between t_{10} and t_n of the Cu-Au (C) ore

The same approach was then applied to other samples to determine their appearance curves. Table 4.8 lists the fitted appearance function parameters for tested ore samples.

Table 4.8: Summary of the appearance parameters for various ore types

Ore type	β_1	β_2	β_3	β_4	β_5	β_6	β_7	β_8	β_9
Cu-Au (C)	107.9	4.4	126.1	20.5	184.8	77.1	0.55	0.31	0.20
Cu-Au (C)-G2	104.8	4.7	115.9	19.3	167.0	71.2	0.63	0.45	0.37
Au (T4)	108.3	6.3	128.4	26.2	196.2	92.3	0.64	0.46	0.39
Au (T9)	109.9	8.0	130.6	29.4	202.6	98.8	0.66	0.49	0.41
Au (T9)-dup	109.6	7.9	129.7	29.1	203.9	99.8	0.65	0.49	0.42
Au (G)-D	111.3	7.3	137.4	30.0	222.1	109.1	0.67	0.52	0.45
Au (G)-P	110.6	7.0	136.9	28.9	205.1	96.5	0.66	0.49	0.42

4.4 Comparison of Comminution Test Results

Ore response to various breakage mechanisms is generally characterized by respective ore hardness testing. The DWT Axb parameter is an indicator of ore resistance to impact breakage, which is commonly used for sizing of crusher and AG/SAG mills. The BBWI parameter is the most widely used testing metric for ball mill sizing and performance evaluation, which measures ore resistance to ball milling (mainly attrition and abrasion). Figure 4.16 shows the BBWI as a function of Axb, including data sets obtained from the samples received at UBC. In general, the ore competency (Axb) and grindability (BBWI) for a given deposit (similar ore type, lithology, and alteration) are reasonably related as illustrated in Figure 4.16 for Ni (G) and Au (G) ores. However, no single correlation can be established to generically describe the relationship for all ore types, as some very competent ores (low Axb values) shown in the database¹ are in fact exhibiting low BBWI values.

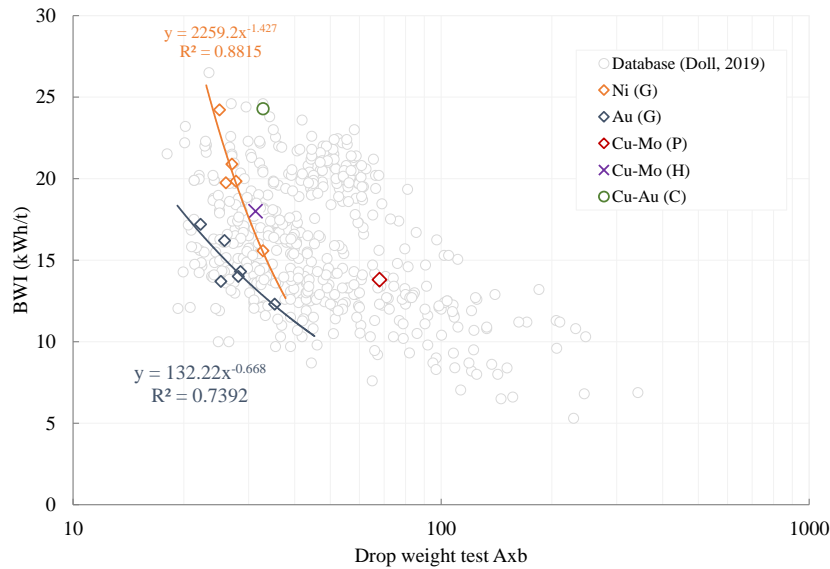


Figure 4.16: BWI and Axb
(Source: modified from Doll, 2019)

¹Retrieved from <https://www.sagmilling.com/articles/>

The $M \cdot f_{mat}$ parameter resulted from the PPT simulation test is used to characterize the ore resistance to compression breakage. Figure 4.17 shows the Axb and BBWI values as a function of the compression index ($M \cdot f_{mat}$). Clearly, no correlation was found between the ore resistance to impact breakage as measured by Axb and ore resistance to compression breakage as measured by $M \cdot f_{mat}$. But it is interesting to note that $M \cdot f_{mat}$ and BBWI are somewhat correlated. Coincidentally, an observation reported by Sepúlveda (2019) showed that the ore compressibility measured by α_0^{PPT} can be potentially expressed as a function of the BBWI value, as shown in Equation 4.1.

$$\alpha_0^{PPT} = 7.806 - 0.663 \times \text{BWI} + 0.0167 \times \text{BWI}^2 \quad (4.1)$$

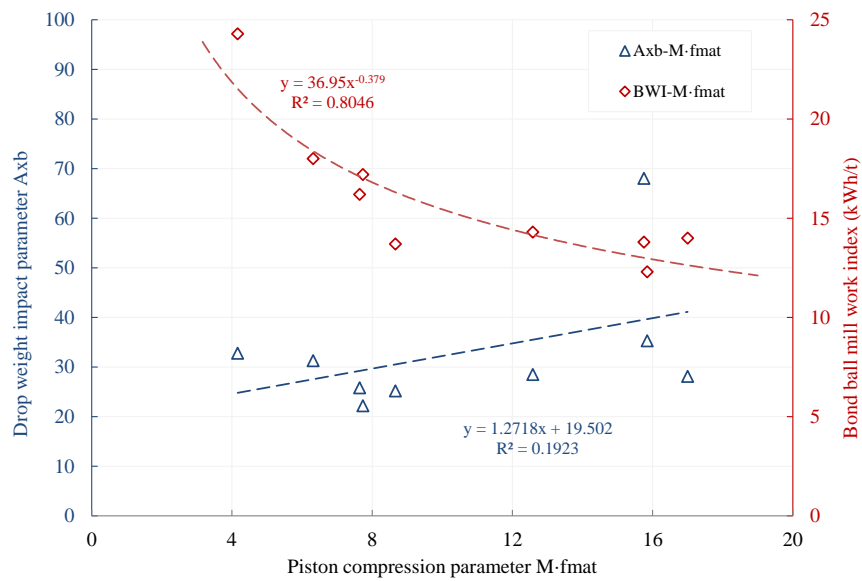


Figure 4.17: Comparison of various ore hardness characteristics

Chapter 5

HPGR Database and Empirical Models

5.1 Introduction

This chapter summarizes the key input and output variables concerning the pilot HPGR testing. Data from the performed pilot HPGR tests were incorporated into the UBC HPGR database. Based on a thorough analysis of the latest database, the observed effects of feed properties and operating conditions on HPGR performance are summarized. This chapter also presents three regression techniques used to develop empirical models for predicting the HPGR performance indicators, including the power draw, specific energy consumption, throughput, product size and size reduction ratio.

5.2 Description of HPGR database

After incorporating pilot tests performed during the current research program, the UBC HPGR database has expanded to consist of 228 HPGR data sets, covering a wide range of ore samples such as copper, gold, iron, palladium, tungsten, among others. As illustrated in Figure 5.1, the largest proportion of tested ore types is represented by copper-gold ores, followed by iron ores (mostly hematite), gold ores, and copper-molybdenum ores. As a result, the developed models might yield better prediction accuracy for those ore types that have larger shares in the database.

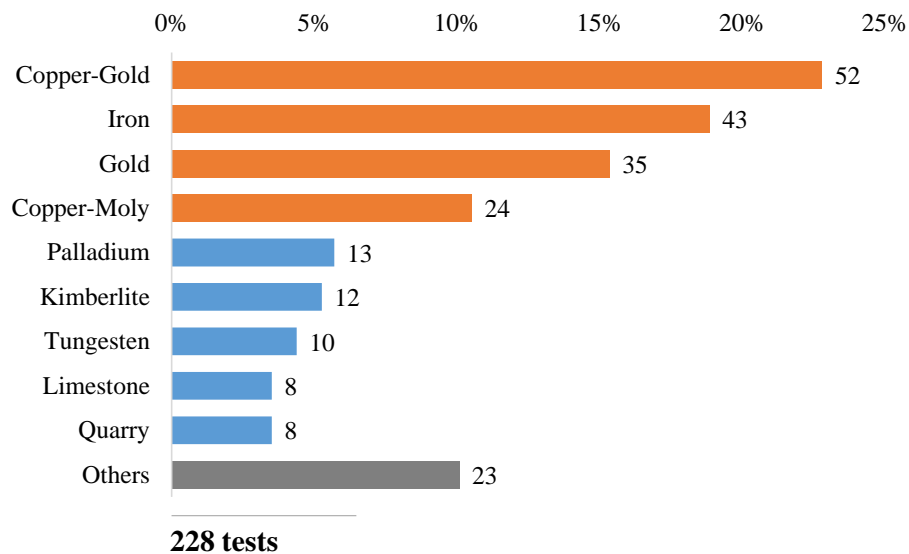


Figure 5.1: Frequency of HPGR tests per ore types within the database

Table 5.1 lists the key input and output variables from the pilot HPGR testing. The majority of the listed input variables were used to develop the empirical models for key output variables. The equipment variables (specifications) however, for the Köppern HPGR at UBC are fixed, and details can be found in Section 3.3.1. Basic statistics of recorded HPGR operating parameters were obtained and are summarized in Table 5.2.

Table 5.1: HPGR input and output variables

Feed property	Inputs Variables		Outputs Responses	
	Equipment	Operating	Product property	Operating
Size and PSDs	Roll diameter, m	Hydraulic pressure, bar	Size and PSDs	Idle (no-load) power draw, kW
Particle shape	Roll length, m	Specific pressing force, N/mm ²	Reduction ratio	Total power draw, kW
Hardness	Static gap, mm	Roll speed, m/s	Flake density, t/m ³	Nip angle or compression angle, °
Ore density, t/m ³	Surface type	Roll speed, rpm	Flake thickness, mm	Force reaction angle, °
Bulk density, t/m ³				Operating gap, mm
Moisture content, %				Critical gap, mm
Saturation moisture, %				Press throughput, t/d
Wear abrasiveness				Specific energy consumption, kWh/t
				Specific throughput constant, ts/hm ³

Table 5.2: Descriptive statistics of HPGR parameters under study

Description	Symbol	Unit	Count	Mean	SD	Min	Max	COV
Feed F_{80}	F_{80}	[mm]	221	16.66	7.30	1.84	28.06	44%
Feed F_{50}	F_{50}	[mm]	221	9.68	5.43	0.64	20.93	56%
Feed moisture content	w	[%]	228	3.0	1.8	0.0	10.0	61%
Bulk density (loose)	ρ_{bulk}	[t/m ³]	209	1.77	0.26	1.28	2.51	15%
Hydraulic pressure	P_{av}	[bar]	208	75.7	19.2	21.0	123.1	25%
Pressing force	F	[kN]	228	603	153	155	985	25%
Specific pressing force	F_{sp}	[N/mm ²]	228	3.7	0.9	0.9	6.0	25%
Roll peripheral speed	u	[m/s]	228	0.72	0.10	0.46	1.01	14%
Roll rotational speed	u_r	[rpm]	228	18.34	2.58	11.61	25.80	14%
Idle power draw	P_i	[kW]	215	8.5	2.0	3.3	12.6	24%
Power draw	P	[kW]	215	60.6	14.5	22.4	100.4	24%
Press throughput	W	[t/h]	228	27.3	5.5	12.8	43.1	20%
Specific throughput	\dot{m}	[ts/hm ³]	228	232	44	102	365	19%
Net specific energy	E_{sp}	[kWh/t]	228	1.97	0.57	0.53	4.19	29%
Operating gap	x_g	[mm]	228	18.80	2.95	7.40	25.62	16%
Flake density	ρ_f	[t/m ³]	189	2.39	0.13	2.14	2.82	5%
Flake thickness	x_f	[mm]	189	21.50	2.77	10.72	27.93	13%
Force reaction angle	β	[deg]	215	4.15	0.66	2.72	6.73	16%
Compression angle	α	[deg]	215	8.29	1.32	5.45	13.46	16%
Critical gap	x_c	[mm]	215	26.71	4.45	17.06	46.21	17%
Center product P_{80}	C_{80}	[mm]	219	4.98	1.69	1.00	10.14	34%
Center product P_{50}	C_{50}	[mm]	219	1.51	0.78	0.12	4.01	52%
Edge product P_{80}	E_{80}	[mm]	219	7.57	2.72	1.08	13.80	36%
Edge product P_{50}	E_{50}	[mm]	219	3.01	1.48	0.21	7.86	49%
% of edge portion		[%]	219	29.5	5.0	14.1	49.8	17%
Full product P_{80}	P_{80}	[mm]	219	5.74	1.93	1.02	11.28	34%
Full product P_{50}	P_{50}	[mm]	219	1.95	0.93	0.15	5.27	48%
F_{80}/P_{80} reduction	RR_{80full}	[-]	219	2.83	0.81	1.10	4.92	29%
F_{50}/P_{50} reduction	RR_{50full}	[-]	219	4.96	1.96	1.31	11.05	40%

5.2.1 HPGR input variables

Feed top size and PSD

Generally, there is a limitation on the feed top size that can be accepted by the HPGR. For smooth roll surfaces (including the Hexadur[®] liner), oversized rocks could decrease nipping efficiency and consequently compromise the HPGR comminution performance. In the case of studded rolls, too large a feed top size could cause stud breakage due to increased tangential forces applied on the roll studs. The maximum allowable HPGR feed top size is proportional to the HPGR roll diameter, meaning that a larger diameter HPGR can accept a larger feed top size. The ore hardness is another deciding factor of the maximum feed top size allowable for a given size HPGR. Burchardt (2019) reported that for a pilot HPGR with 0.95 m diameter accepting 60-100 mm feed top size for a relatively soft material caused no mechanical problems and no stud breakage during 100 hours trial period. The feed top size of 60-100 mm is far beyond the typical maximum for this size HPGR. Table 5.3 presents the ranges of the ratio of feed top size to the roll diameter at some pilot and industrial-scale HPGR facilities. In the case of the UBC-Köppern HPGR, the feed top size was limited to 32 mm, which is equal to 4.3% of the roll diameter.

Table 5.3: HPGR feed top size range

Site/Facility	HPGR Supplier	Roll Diameter (mm)	Feed Top Size (mm)	Ratio (%)
Tropicana	Köppern	2050	42	2.1
Cerro Verde	thyssenkrupp	2400	55	2.3
Morenci	Metso	3000	78	2.6
Boddington	thyssenkrupp	2400	89	3.7
Pilot	thyssenkrupp	950	35	3.7
UBC Pilot	Köppern	750	32	4.3

Figure 5.2 presents the Particle Size Distribution (PSD) of the HPGR feeds in the UBC database. The majority of the feed samples were prepared by staged crushing processes, but some were prepared by multiple stage HPGR, truncated or blended

following the specific project requirements. Feed samples prepared after multiple stage HPGR comminution typically have more fines than those prepared by conventional staged crushing. Most of the truncated feed samples were prepared by removing the fines at a specific size, and the blended feed typically features a bimodal size distribution.

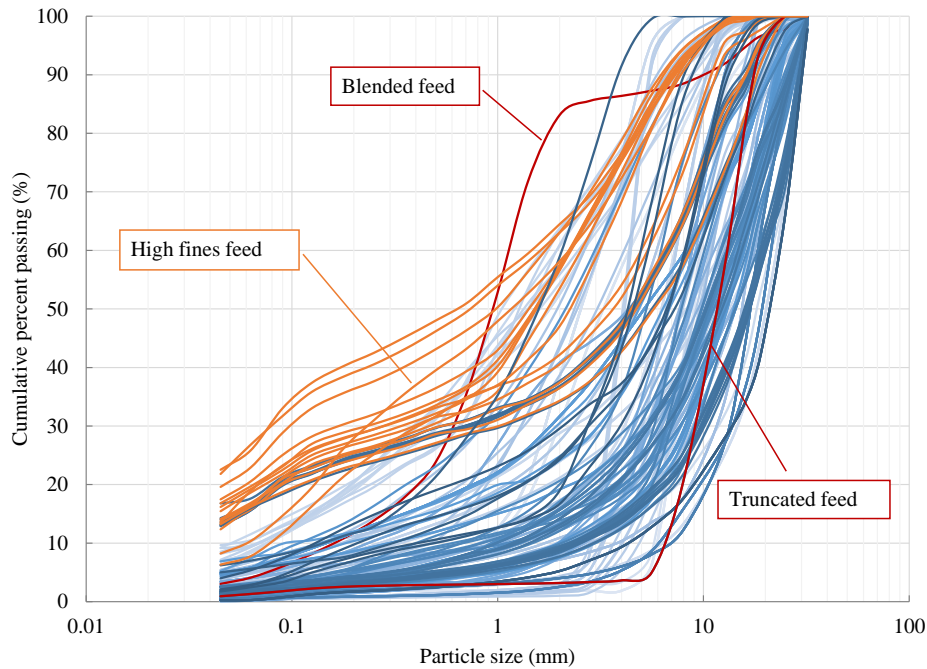


Figure 5.2: Particle size distributions of HPGR feed

No single mathematical model was found to describe all feed PSDs due to the natural fracture process under various feed preparation methods. However, the majority of the feed PSD data was found to fit reasonably well with either the Gaudin-Schuhmann (G-S) model or Rosin-Rammler (R-R) model. The G-S and R-R models are widely used to describe the particle size distribution (Macias-Garcia et al., 2004). Figure 5.3 presents examples of HPGR feed PSDs fitted to G-S or R-R models. The general understanding is that the G-S model works better for crushed drill cores, while R-R model works for the blasted bulk material.

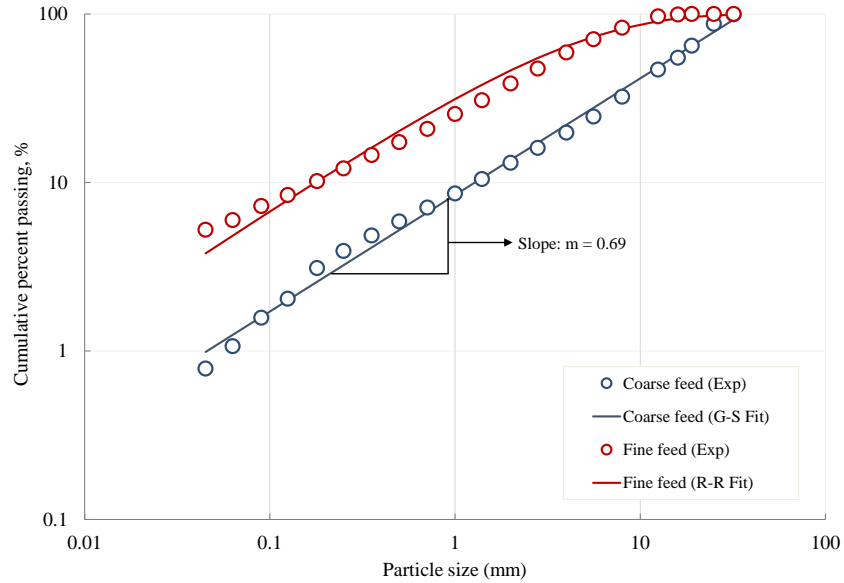


Figure 5.3: Examples of HPGR feed PSD model fitting

Feed bulk density

Figure 5.4 shows that the tested feed bulk density ranged from 1.28 to 2.51 t/m³, with an average value of 1.77 t/m³ and a Coefficient of Variation (COV) of 15%. The feed bulk density is related to material specific gravity and feed particle size distribution. Obviously, material with a high specific gravity would have a higher bulk density. Materials with a wider PSD can also feature a higher bulk density, as particles can have a higher packing density.

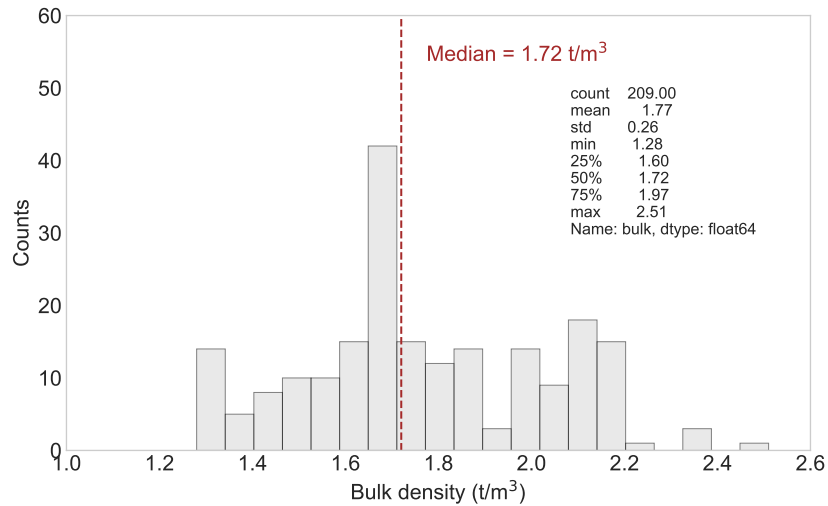


Figure 5.4: Distribution of feed bulk density

Feed moisture content

Figure 5.5 shows that the tested feed moisture content ranged from 0% to 10% by weight, averaged at 3.0% with a COV of 63%. The majority of tests were performed within 2-4% feed moisture content range, which is preferred for hard rock applications (Daniel et al., 2019).

It is understood that the HPGR cannot be operated efficiently at high feed moisture contents. The volumetric water in the feed dictates the HPGR performance, so it is important to measure and report the HPGR feed moisture by volume. However, the commonly used metric by the industry is the moisture content by weight. Figure 5.6 shows the equivalent moisture content by weight for different SG materials at the same moisture content by volume. For example, 6% moisture by weight for an ore with SG of 5.0 (e.g. iron concentrate) is equivalent to about 10% by weight for an ore with SG of 3.0.

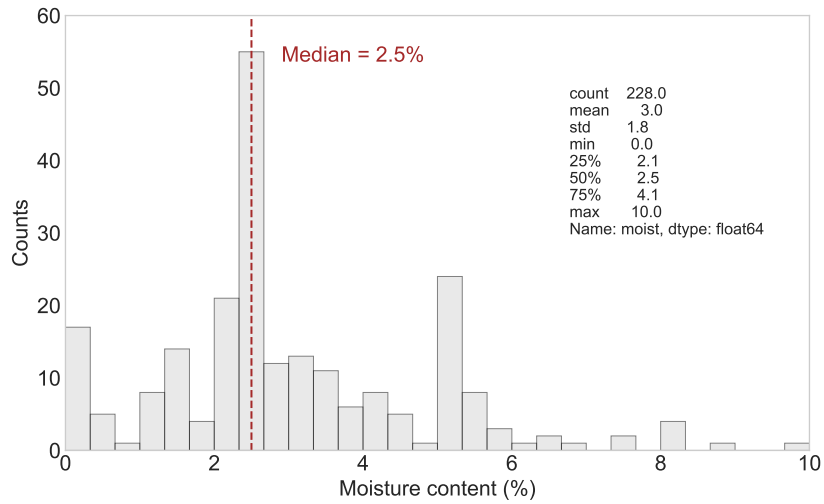


Figure 5.5: Distribution of feed moisture content

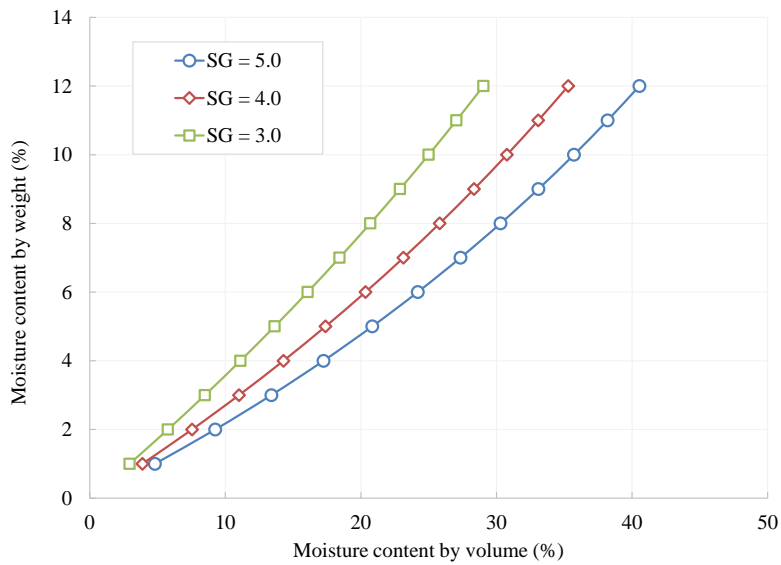


Figure 5.6: Moisture by weight and by volume

Roll speed

HPGR roll speed, controlled by Variable Speed Drive (VSD), is the primary control mechanism for adjusting machine power draw and throughput, as well as maintaining the choke feed condition. However, roll speed has a limited effect on the specific energy consumption and product particle size. Figure 5.7 shows that the roll peripheral speed (u) setpoints for the UBC pilot HPGR tests ranged from 0.46 to 1.01 m/s, with a median value of 0.76 m/s.

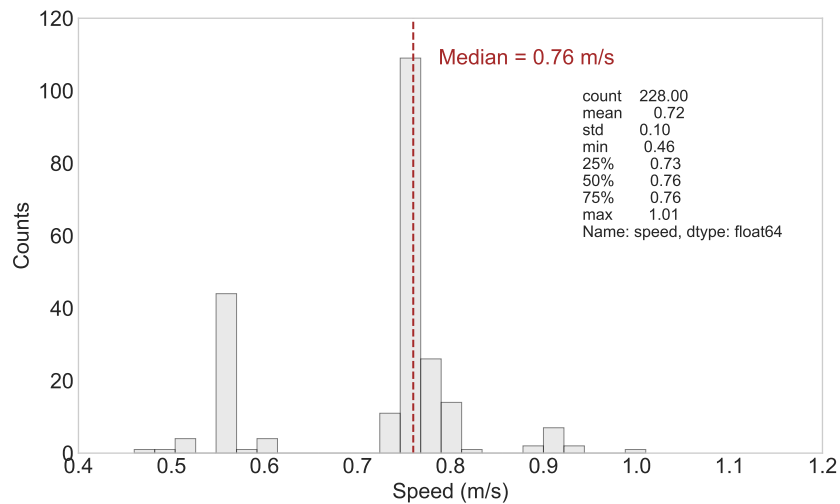


Figure 5.7: Distribution of HPGR roll speed

Industrially, the roll peripheral speed is normally set to be equivalent to the roll diameter or slightly higher (e.g. 1.0 m/s for 1.0 m diameter HPGR), which translates to an angular velocity (u_r) of 19 rpm. Table 5.4 lists ranges of roll speeds at some industrial-scale HPGR operations, which are in line with typical operating ranges between 18 and 23 rpm (Daniel et al., 2019).

Table 5.4: Industrial scale HPGR roll speed range

Project	Company	Diameter (m)	Maximum Roll Speed (m/s)	Maximum Roll Speed (rpm)
Cerro Verde	Freeport-McMoRan	2.4	2.8	22.3
Morenci	Freeport-McMoRan	3.0	3.3	21.0
Boddington	Newmont	2.4	2.7	21.3
Grasberg	Freeport-McMoRan	2.0	2.6	24.8
Tropicana	AngloGold Ashanti	2.05	2.08	19.8

Specific pressing force

The specific pressing force (“ F_{sp} ”, also known as specific grinding force or specific pressure) is defined as the force exerted across the cross-sectional area of the roll (Schönert, 1988). The specific pressing force is expressed in Equation 5.1.

$$F_{sp} = \frac{F}{D \times L} \quad (5.1)$$

The F_{sp} parameter, typically measured in N/mm² or kN/m², is the primary mechanism for controlling specific energy consumption and product particle size. Typical ranges for the F_{sp} vary considerably from 1.0 to 9.0 N/mm². The HPGR with studded rolls is normally restricted to a maximum F_{sp} of 5.0 N/mm² (Bearman, 2006). Determination of the optimum F_{sp} from the pilot test can be used to size the roll bearing and determine the required grinding force for a given HPGR geometry. Figure 5.8 shows that the tested F_{sp} set points in the database ranged from 0.9 to 6.0 N/mm², with a median value of 3.9 N/mm².

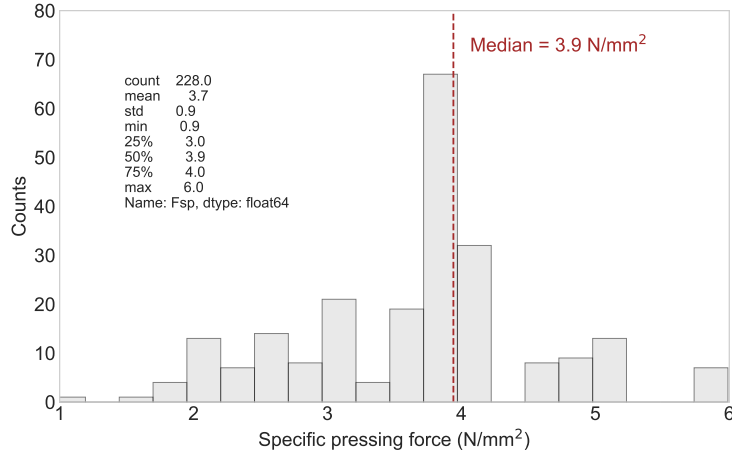


Figure 5.8: Distribution of HPGR specific pressing force

5.2.2 HPGR output variables

Power draw

HPGR power draw is directly proportional to the applied pressing forces (F , kN) on the rolls and the roll peripheral speed (u , m/s). As illustrated in Figure 5.9, the applied pressing force is split into tangential and radial components at the point defined by the force reaction angle β . Only the tangential force creates the torque that drives the rolls (Daniel et al., 2019). Therefore, the total power draw of an HPGR can be estimated by Equation 5.2 (Schönert, 1988). The β angle is required to determine the effective tangential force. Some researchers suggested that the β angle is approximately half the compression angle (α) (Klymowsky et al., 2002), though these two parameters (α and β) are completely independent of each other.

$$P = \omega T = 2Fus \sin \beta \approx 2Fus \sin \left(\frac{\alpha}{2} \right) \quad (5.2)$$

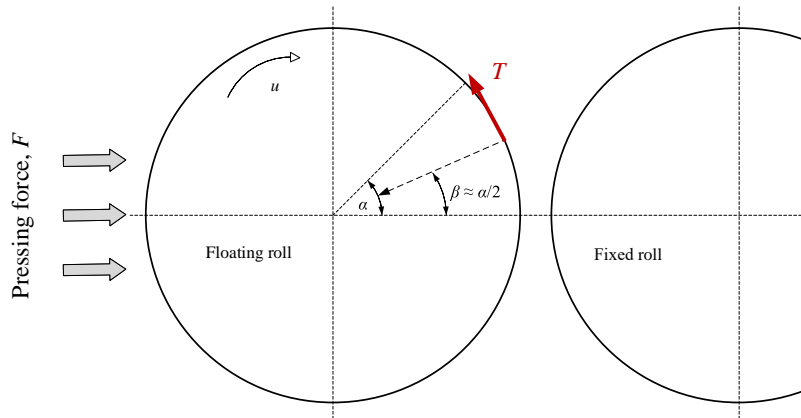


Figure 5.9: Simplified schematic of forces in an HPGR
 (Source: modified from Torres & Casali, 2009)

Figure 5.10 shows the distribution of the HPGR total power draw and the net power draw from the database. The latter one is calculated by subtracting the no-load power (or idle power, P_i) from the total power draw. It was found that the no-load power also correlates with the HPGR roll speed setting.

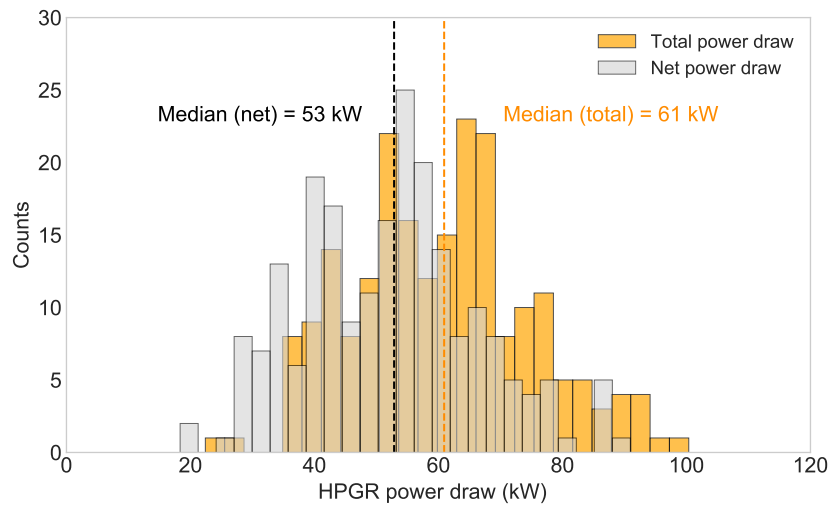


Figure 5.10: Distribution of total power and net power draw

During each pilot HPGR test, the α and β angles can be calculated based on the recorded power draw, applied pressing force, and roll speed. Frequency distribution of the calculated β in the database is shown in Figure 5.11, from which it was found that the average value was 4.2 degrees with a COV of 16%. This could translate to an average of 8.4 degrees for the compression angle (α) if Equation 5.2 is applied for the approximation. This is in good agreement with the reported compression angles ranging between 6-10 degrees (Bearman, 2006).

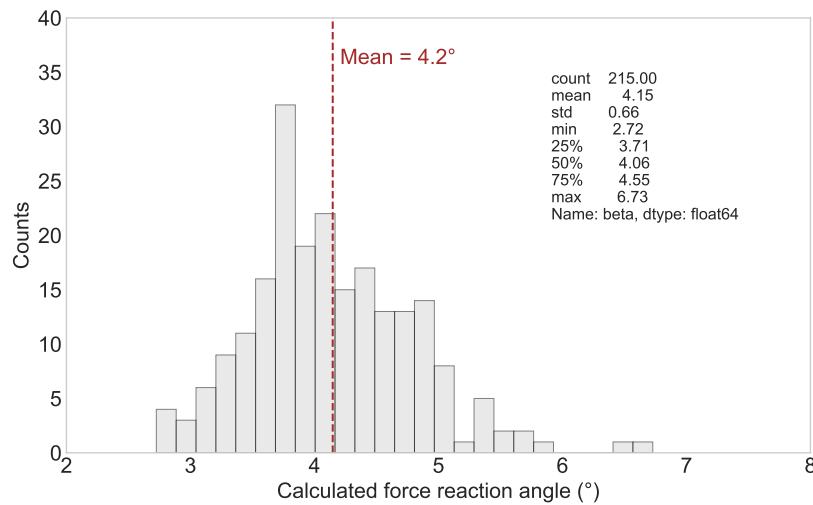


Figure 5.11: Distributions of the calculated force reaction angle

Operating gap and critical gap

Figure 5.12 shows that the measured operating gap (x_g) ranged from 7.4 to 25.6 mm, with a mean value of 18.8 mm and a COV of 15%. The operating gap is generally affected by HPGR roll diameter, applied specific pressure, feed PSD and feed moisture content. The recorded operating gap (x_g) from the UBC HPGR tests averaged at 2.5% of the roll diameter (750 mm) for all tested ore samples. This is aligned with the reported operating gap being 2-3% of the roll diameter (Klymowsky et al., 2002; Morley, 2010). A larger diameter HPGR machine is expected to offer a larger operating gap and higher throughput capacity.

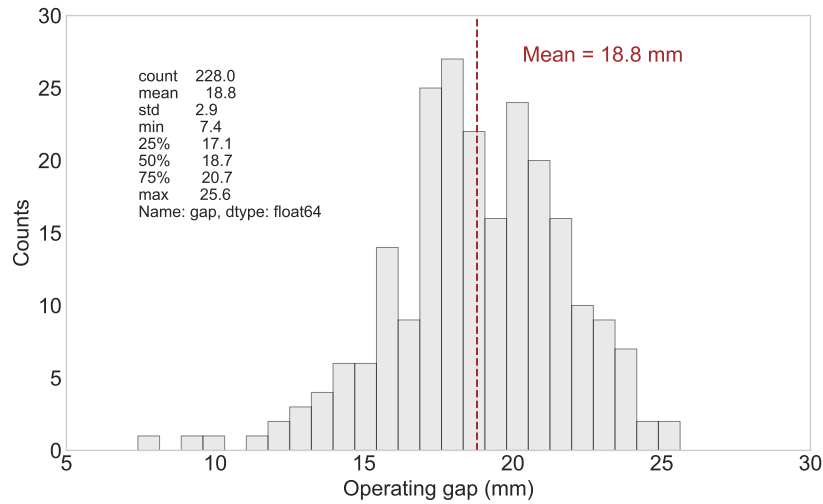


Figure 5.12: Distribution of HPGR operating gap

Figure 5.13 compares the frequency distributions of the measured flake thickness as well as the operating gap that was recorded during stable operation. The shift in distribution suggests that the flake thickness is larger than the operating gap, by approximately 12% on average. This leads to a lower bulk density for the flake material compared to the material (“cake”) between the rolls (or at the gap). The phenomenon can be explained as the compacted particle bed expanding volumetrically after exiting the compression zone, due to the relaxation of compression forces in the so-called “extrusion zone”.

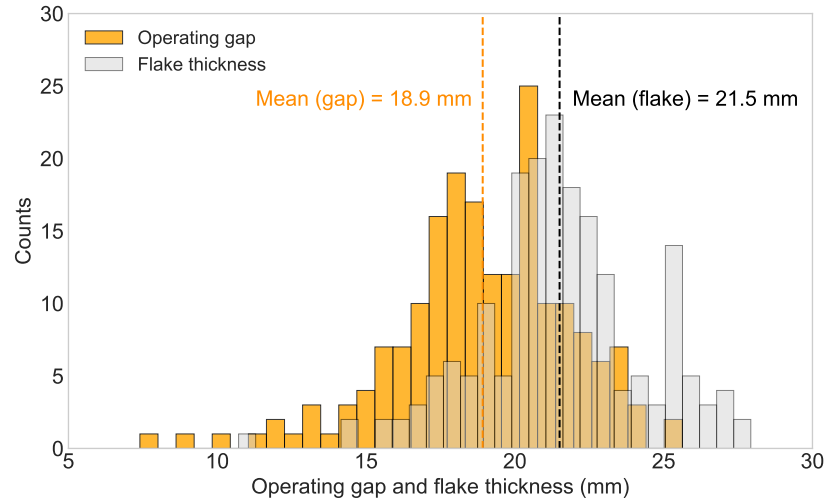


Figure 5.13: Operating gap and measured flake thickness

The critical gap (x_c) is defined as the boundary between the pre-crusher zone and the compression zone, as expressed by Equation 2.14 (Morrell et al., 1997a). Figure 5.14 shows the frequency distribution of the estimated critical gap, ranged from 17.1 to 46.2 mm, with a mean value of 26.7 mm and a COV of 16.5%.

$$x_c = 0.5 \left\{ (D + x_g) \left[(D + x_g)^2 - \frac{4\rho_g D x_g}{\rho_{bulk}} \right]^{0.5} \right\} \quad (2.14 \text{ revisited})$$

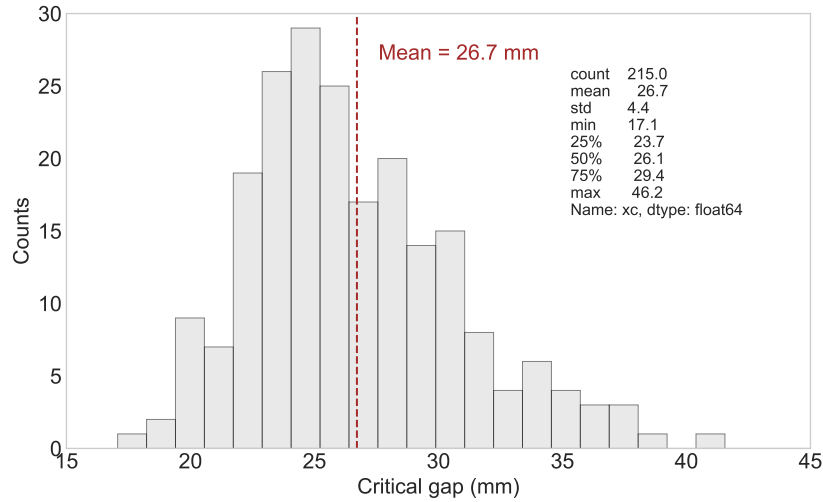


Figure 5.14: Distribution of estimated HPGR critical gap

Specific throughput constant

As expressed in Equation 5.3 (Seebach and Knobloch, 1987), the specific throughput constant (\dot{m}) is defined as the expected throughput rate per roll diameter, per roll length, and per roll peripheral speed. The \dot{m} is therefore expressed in units of ts/hm^3 . The \dot{m} value can be used to predict the throughput capacity of the HPGR with different roll geometries.

$$\dot{m} = \frac{W}{D \times L \times u} \quad (5.3)$$

Typically, there are two ways to calculate the \dot{m} , one using the HPGR geometry and roll speed expressed in Equation 5.3. An alternative approach to estimate \dot{m} is based on the operating gap (x_g) and cake density (ρ_g) at the gap, or the flake thickness (x_f) and flake density (ρ_f) using Equation 5.4 (Schönert and Lubjuhn, 1990), which is known as the “continuity equation”. It is worth noting that the cake density at the gap is usually unknown; therefore, the flake thickness and flake density are essential data to calculate the \dot{m} adequately.

$$\dot{m} = 3600 \times \frac{x_g}{D} \times \rho_g = 3600 \times \frac{x_f}{D} \times \rho_f \quad (5.4)$$

Figure 5.15 presents the measured specific throughput constant (\dot{m}) as a function of the operating gap and flake thickness. It can be seen that \dot{m} increases linearly with the increase of the operating gap or the flake thickness.

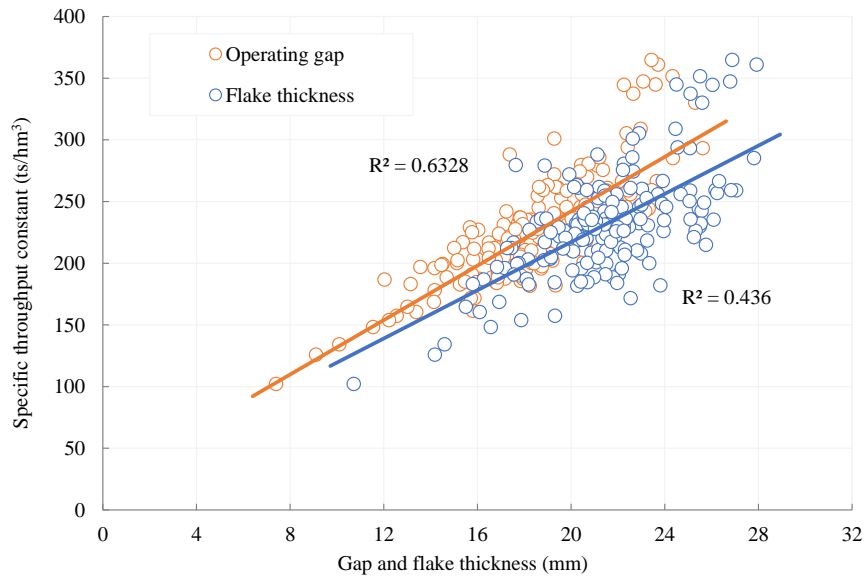


Figure 5.15: Specific throughput constant as a function of the operating gap and flake thickness

Figure 5.16 compares the calculated \dot{m} values using the continuity equation (Equation 5.4) with flake thickness and flake density to the measured values. The standard deviation of the differences between the calculated and measured values was found to be 11.8% with an overall mean difference of 7.6%. A trend line resulted from the scatter plot shows a slight deviation from the identity line (1:1 line), indicating a potential slip between the rolls surface and the feed material. At first glance, this seems to be a reasonable approach to estimate the \dot{m} value. Regrettably, the difficulties can often be encountered in determining the flake thickness and flake density with sufficient confidence if no pilot or full scale HPGR testing is conducted.

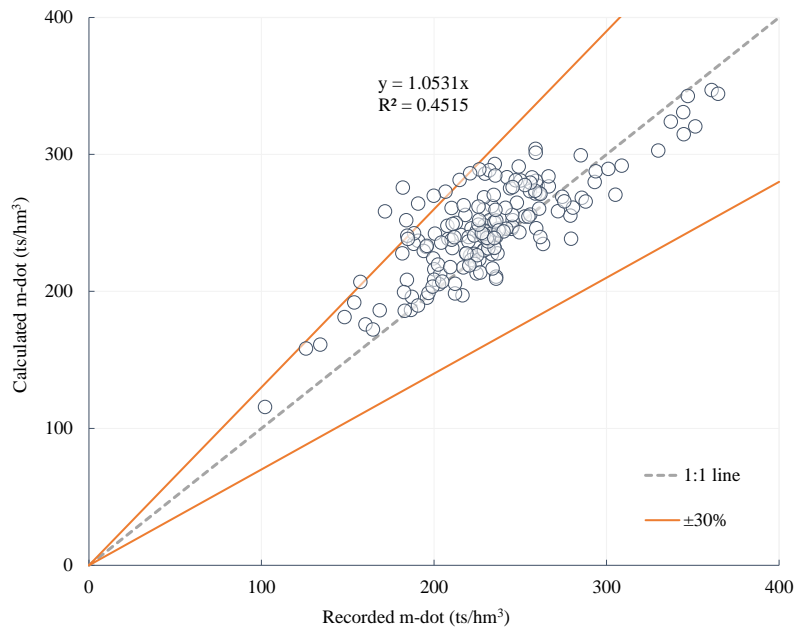


Figure 5.16: Scatter plot of the calculated and recorded specific throughput constant

Figure 5.17 presents the boxplots for the specific throughput constant grouped by ore type at a similar applied F_{sp} of around 4.0 N/mm^2 . The box covers 50% of the observations; the lower and upper box represents the 25% and 75% quartiles, respectively. The outliers are marked by the circle symbols. It is worth noting that a substantially higher \dot{m} was achieved for the Hematite and Palladium ores. This is largely driven by their higher ore density, simply because HPGR is a volumetric machine.

Distributions of the specific throughput constant by selected ore types are shown in Figure 5.18. The 80th percentile of the specific throughput constant was found to be 238 ts/hm^3 and 337 ts/hm^3 , for ore types with medium ore densities (119 data sets, including Cu-Au, Cu-Mo, Au, and Ni-Cu) and with high ore densities (56 data sets, including Fe and Pd). Their associated mean values were 220 ts/hm^3 and 280 ts/hm^3 , with COV being 11.5% and 16.5%, respectively.

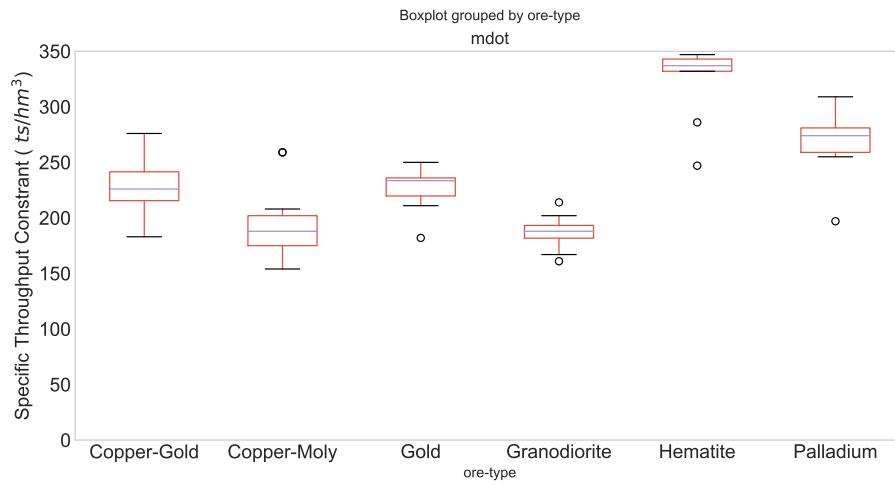


Figure 5.17: Boxplot of mdot grouped by ore type at Fsp of 4.0 N/mm²

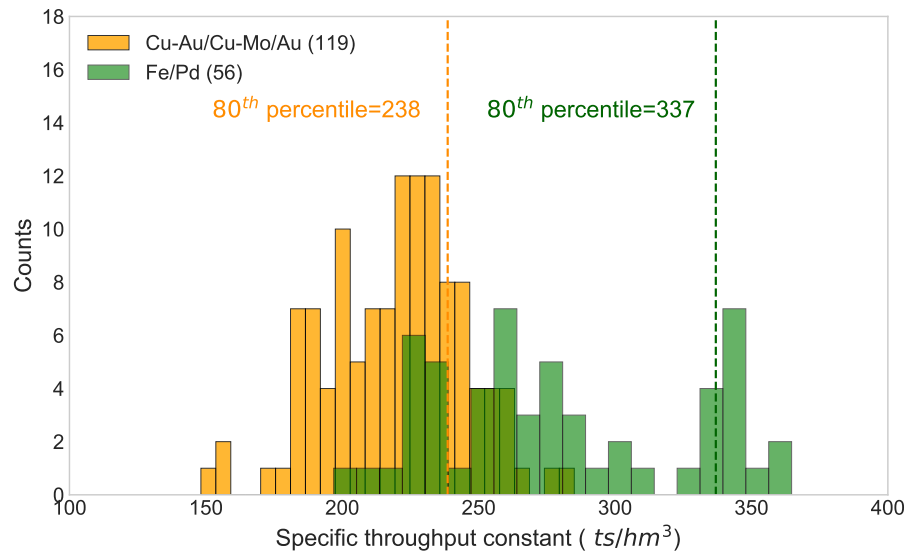


Figure 5.18: Distributions of HPGR specific throughput constant by ore type

Specific energy consumption

Net specific energy consumption (or specific energy input, E_{sp} in kWh/t) is defined as the net energy consumed by the grinding process for each tonne of processed material, which is generally expressed in Equation 5.5. The net energy input is calculated by subtracting the no-load power draw from the total power draw. The net E_{sp} is the critical HPGR sizing parameter, that is used to determine the required main motor size and gearbox design for an industrial application. Figure 5.19 presents the boxplots for the net specific energy consumption grouped by ore type at a similar applied F_{sp} of 4.0 N/mm², from which considerable variations were observed among tested ore samples suggesting that there were other influencing factors than the applied F_{sp} .

$$E_{sp} = \frac{P - P_i}{W} \quad (5.5)$$

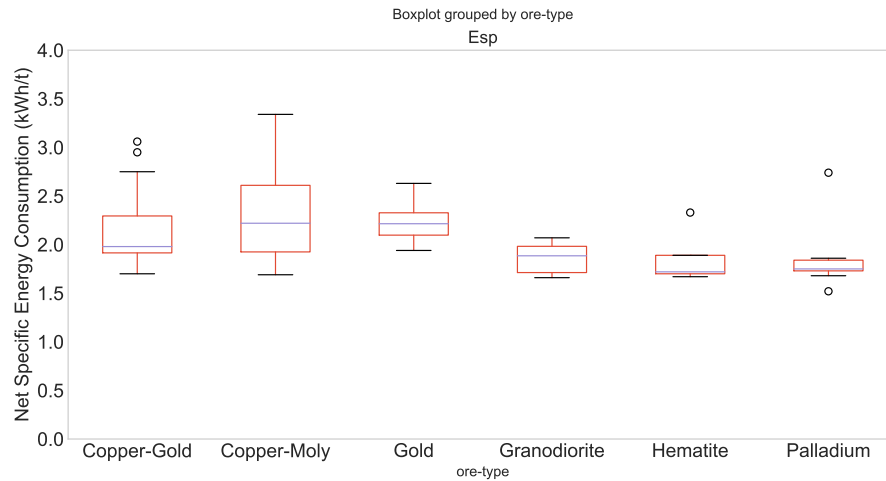


Figure 5.19: Boxplot of the net specific energy consumption grouped by ore type at F_{sp} of 4.0 N/mm²

Distributions of the net specific energy consumption are shown in Figure 5.20, from which the 50th percentile (median) of net specific energy consumption was found to be 1.58 kWh/t and 1.98 kWh/t for tests performed at the specific pressing force of 3.0 N/mm² and 4.0 N/mm². The associated mean values were 1.66 kWh/t and 2.05 kWh/t, with COV being 20% and 18%, respectively. Again, the frequency distributions confirm the large variation of the E_{sp} at a given applied F_{sp} .

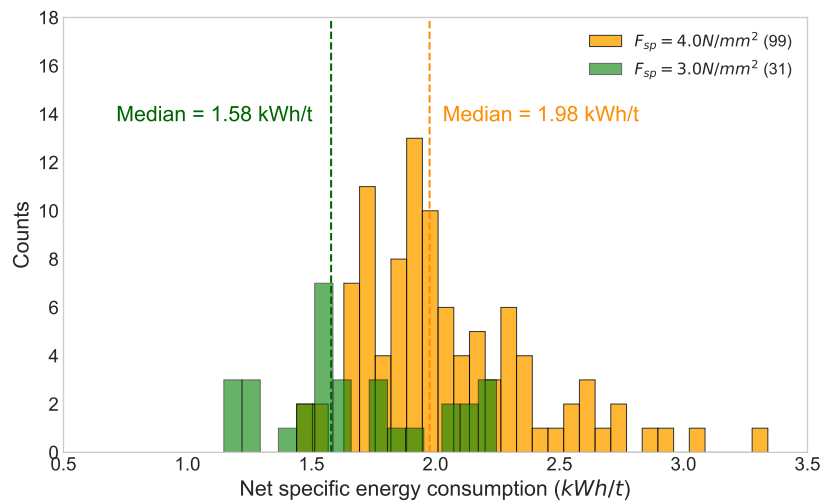


Figure 5.20: Distributions of HPGR net specific energy consumption at different specific pressing forces

HPGR product size and reduction ratio

Unlike tertiary crushers, the HPGR features a wider product particle size distribution with more fines generated, as the compressive force is applied throughout the particle bed on both coarse and fine particles. Figure 5.21 displays the PSD of the HPGR full product (referred to the combined center and edge product) in the database. Despite significant variations in the feed PSD shown in Figure 5.2, the product PSD appears to follow similar shape patterns, except for tests performed with truncated or blended feeds.

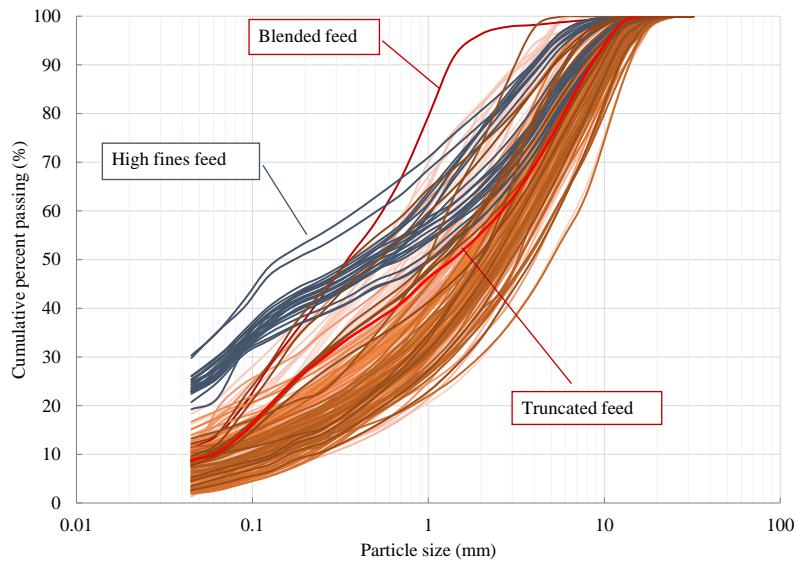


Figure 5.21: Particle size distributions of HPGR product

Distributions of the product size P_{80} and P_{50} when tested at an F_{sp} of 4.0 N/mm^2 are shown in Figure 5.22, from which the respective median values were 5.57 mm and 1.76 mm. Distributions of the percentage passing at 4 mm, 2 mm, and 0.2 mm in the full product (combined center and edge product) when tested at an F_{sp} of 4.0 N/mm^2 are shown in Figure 5.23, from which the respective median values were 72%, 55%, and 21%. The fines generation by HPGR comminution is comparable to the SAG milling, which is known to produce a higher amount of fines than conventional crushing or rod milling.

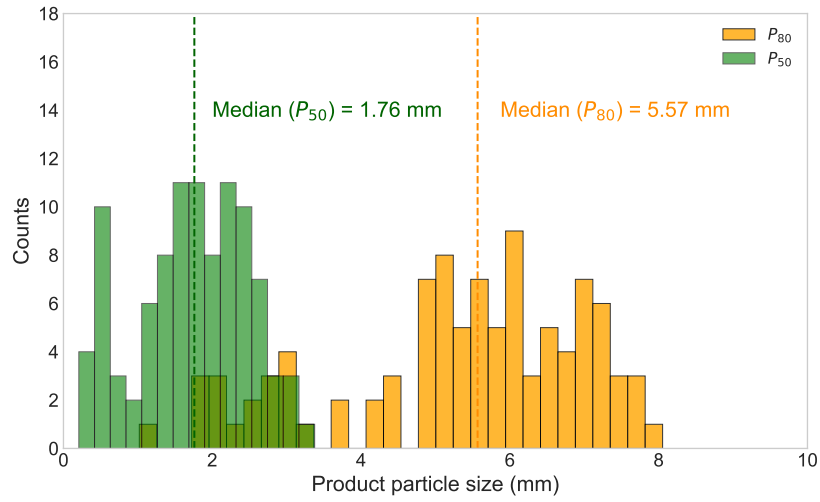


Figure 5.22: Distributions of HPGR product size at F_{sp} of 4.0 N/mm^2

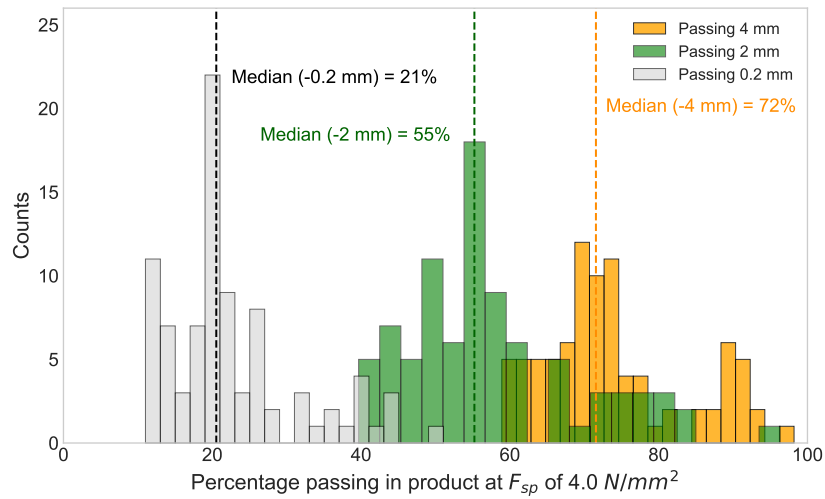


Figure 5.23: Distributions of percentage passing in HPGR product at F_{sp} of 4.0 N/mm^2

Table 5.5 summarizes the statistics of the HPGR feed and product sizes, as it can be seen that the edge product is considerably coarser than the center product. It was found that a notable portion of the coarse fraction as represented by 95% passing feed size (F_{95}) were remained unbroken in the center and edge product, indicating the limitation of HPGR comminution for top size management. To put this into perspective, a 1000 t/h HPGR operating in an open circuit would produce approximately 3 t/h of unbroken top size material (measured in F_{95}). Feeding downstream processes such as ball mills with an excessive amount of oversized particles could generate a significant amount of scats, that may be detrimental. Therefore, the most commonly adopted HPGR circuit is configured in a closed circuit with a screen or edge recycle for better control of the top size in the product. Table 5.5 also demonstrates that the HPGR generates a considerable amount of fines. The net generation of fines, calculated by the percentage in the full product minus the percentage in the feed, averaged 27% and 13% for the sub 1 mm and sub 0.2 mm size fractions.

Table 5.5: Statistics of the HPGR feed and product sizes

Description	Unit	Feed	Center	Edge	Full product
P_{95} size (mean)	[mm]	22.00	9.52	11.80	10.48
P_{80} size (mean)	[mm]	16.29	4.90	7.42	5.70
P_{50} size (mean)	[mm]	9.32	1.49	2.93	1.80
%-4 mm (mean)	[%]	31.6	75.3	61.5	71.2
%-2 mm (mean)	[%]	20.8	58.4	44.6	54.4
%-1 mm (mean)	[%]	14.5	44.5	32.9	41.2
%-0.2 mm (mean)	[%]	7.7	23.0	16.8	21.2
%-0.1 mm (mean)	[%]	5.7	16.0	11.8	14.8
Unbroken F_{95} size (mean)	[%]	-	0.20	0.49	0.28
Unbroken F_{90} size (mean)	[%]	-	0.56	1.27	0.76

Apart from fines generation, particle size reduction ratios are also used to characterize the HPGR comminution effect. Figure 5.24 shows the distribution of size reduction ratios from 80% and 50% passing feed size to 80% and 50% passing full product size, referred to as RR_{80full} (F_{80}/P_{80}) and RR_{50full} (F_{50}/P_{50}), for ores tested at an F_{sp} of 4.0 N/mm². The mean values for the RR_{80full} and RR_{50full} were 2.8 and 5.2, with associated COV being 29% and 43%, respectively. The variation in size reduction ratio is affected by the ore hardness as well as the feed particle size. It is understood that coarse feeds would require less energy to achieve the same reduction ratio compared to fine feeds.

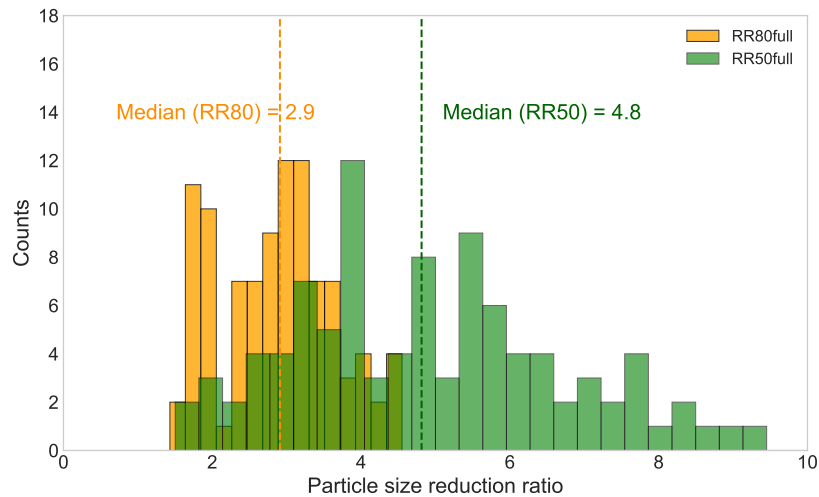


Figure 5.24: Distributions of size reduction ratios at Fsp of 4.0 N/mm²

HPGR product size normalization

As discussed in Section 2.3.2, the cumulative size distributions of different HPGR products were “self-similar”, therefore can be normalized by plotting them against a dimensionless size X/X_{50} . Figure 5.25 shows normalized PSDs of HPGR products from 125 tests performed on various ore types. Feed samples for the 125 tests had full size distributions, most of which were prepared by staged crushing. Tests performed with truncated/blended feed or feed with an excessive amount of fines were

purposely excluded, as they do not represent natural feed size distributions to the HPGR. The HPGR comminution behaviour for processing samples with little fines or excessive fines is very different than processing naturally generated feed due to differences in particle-particle interaction and particle bed formation. The selected tests were performed at different specific pressing forces and feed moisture contents, and had varying ore characteristics. Despite differences in operating conditions and feed characteristics, their normalized product PSDs matched reasonably close.

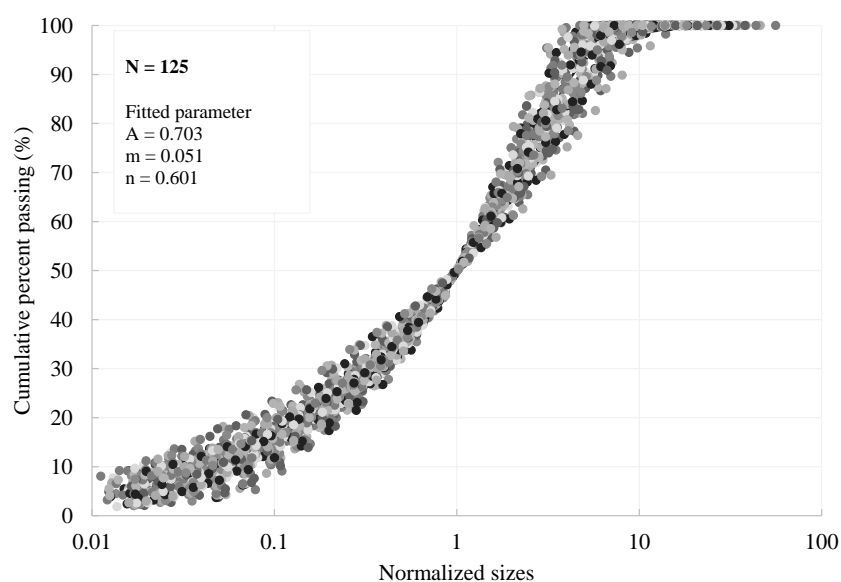


Figure 5.25: HPGR product normalization

A master normalization curve was generated after fitting the Lim's model (see Equation 2.4) individually to the selected 125 PSDs from the UBC pilot HPGR test program. Table 5.6 compares the fitted model parameters from UBC pilot tests to those obtained from industrial scale HPGR in tertiary crushing application. The master normalization curve appears to coincide with the normalized curve from industrial scale HPGR operation.

$$F\left(\frac{x}{X_{50}}\right) = 100 \left\{ 1 - \exp \left[-A \left(\frac{x}{X_{50}}\right)^{m\left(\frac{x}{X_{50}}\right)+n} \right] \right\} \quad (2.4 \text{ revisited})$$

Table 5.6: Model parameters for HPGR product normalization

Description	A	m	n
Pilot scale HPGR	0.7	0.05	0.60
Industrial scale HPGR	0.7	0.04	0.58

As described in Section 2.3.2, the normalization approach can be used to reconstruct the full product PSD if the desired product P_{50} size is known, either from specific test work or selected as per downstream process requirements. Figure 5.26 presents the generic HPGR product size distribution curves scaled from the master normalization model parameters based on selected product P_{50} sizes.

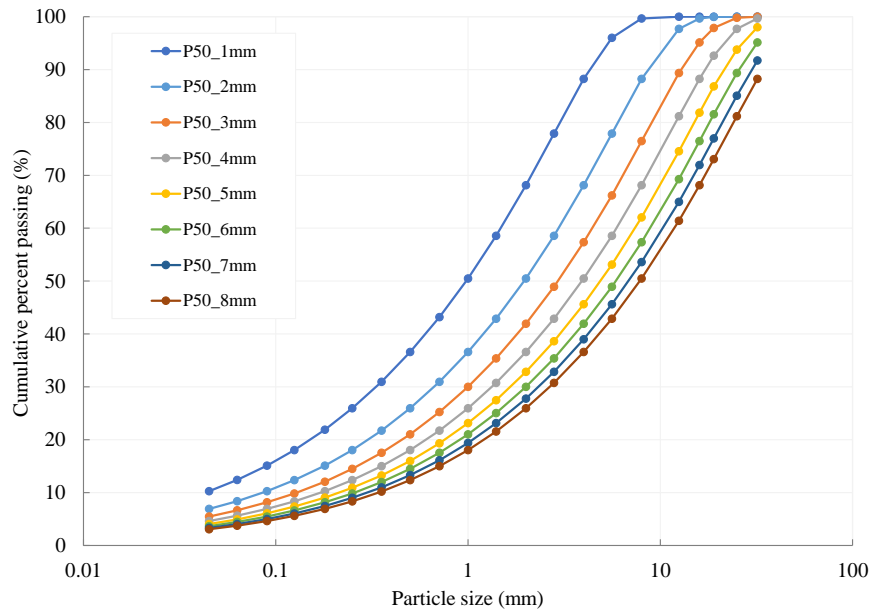


Figure 5.26: Reconstitution of HPGR product size distribution

5.3 Development of Empirical Regression Models

5.3.1 Description of the data

As discussed above, the UBC HPGR database contains many predictor variables (“Xs”) related to HPGR feed characteristics and operating conditions, and a number of important response variables (“Ys”) related to the HPGR comminution performance. One can use regression modeling techniques to determine the influence of the predictor variables on the response variables. The following key HPGR performance indicators were identified as potential response variables, which can be used for HPGR sizing and performance evaluation.

1. HPGR power draw in kW, ‘ P ’
2. HPGR net specific energy consumption in kWh/t, ‘ E_{sp} ’
3. HPGR throughput in t/h, ‘ W ’
4. HPGR specific throughput constant in ts/hm³, ‘ \dot{m} ’
5. HPGR operating gap in mm, ‘ x_g ’
6. HPGR full product sizes in mm, ‘ P_{80} ’ and ‘ P_{50} ’
7. HPGR size reduction ratio, ‘ RR_{80full} ’ and ‘ RR_{50full} ’

In developing the empirical models for prediction of the above-mentioned HPGR response variables, the following predictor variables were initially selected based on literature review and author’s experience. From Chapter 4, it was found that ore hardness and feed PSD are influencing factors, and therefore are included. Since quantitative measurements of the ore hardness were not available for all samples within the database, the “dummy variable” approach was used to provide a qualitative indicator. A dummy variable can only take the value 0 or 1 to indicate the impact of its absence or presence on the response variable. A similar approach was used for the feed PSD scenarios (truncated or blend). Remaining predictor variables are related to other feed characteristics and HPGR operating set points. In addition, several cross-products of predictor variables are included to show the effect of variable interactions.

1. Ore hardness set to “0” for soft to medium, and to “1” for the medium to hard
2. Feed PSD condition set to “0” for normal, and to “1” for abnormal conditions e.g. truncated or blended feed
3. HPGR roll peripheral speed in m/s, ‘ u ’
4. Specific pressing force in N/mm², ‘ F_{sp} ’
5. Feed moisture content by weight in %, ‘moist’
6. Feed bulk density in t/m³, ‘ ρ_{bulk} ’
7. Feed particle size in mm, ‘ F_{80} ’ and ‘ F_{50} ’
8. Feed size distribution slope module (based on G-S model), ‘ m ’
9. Percentage of selected size fraction in the feed, including ‘ F_{8mm} ’, ‘ F_{6mm} ’, ‘ F_{4mm} ’, ‘ F_{2mm} ’, ‘ F_{1mm} ’, ‘ $F_{0.2mm}$ ’, and ‘ $F_{0.1mm}$ ’. For example, ‘ F_{8mm} ’ refers to the percentage of -8mm material in the feed.

5.3.2 Data pre-processing and exploration

Following the collection of both predictor and response variables, data pre-processing including data cleaning and missing data imputation were carried out to construct a proper database for subsequent analysis. Once the database was prepared, a preliminary analysis was performed in order to gain a better understanding of the cleaned data, aimed at identifying potential correlations and determining gaps during the model development. The Spearman correlation method was used to measure the monotonic relationship between the variables. Figure 5.27 shows the Spearman correlation coefficients of all selected predictor and response variables using the heatmap function within the Python Seaborn package. The light color represents positive correlations, while the dark color indicates negative correlations. Some observations were obtained from the matrix diagram:

1. As expected, the HPGR power draw ' P ' and net specific energy ' E_{sp} ' appear strongly correlated with the specific pressing force ' F_{sp} '. The response variable ' P ' and ' E_{sp} ' are found to correlate with each other, this is referred to as variable collinearity.
2. The specific throughput constant ' m ' is reasonably correlated with feed bulk density, size module ' m ', and fines content (' $F_{0.2mm}$ ' and ' $F_{0.1mm}$ '); However, the response variable "throughput" does not reveal a similar degree of correlation with other predictor variables.
3. Operating gap has no significant correlation with other predictor variables.
4. HPGR full product sizes (' P_{80} ' and ' P_{50} ') are highly correlated with feed particle sizes (' F_{80} ' and ' F_{50} '). Of course, they are negatively correlated with the fines in the feed.
5. HPGR reduction ratios (' RR_{80full} ' and ' RR_{50full} ') are collinear, and they are related to the feed particle sizes (' F_{80} ' and ' F_{50} ').
6. Fines content as described by ' F_{1mm} ', ' $F_{0.2mm}$ ', and ' $F_{0.1mm}$ ' have correlations with the bulk density ' ρ_{bulk} '. This can be explained if one considers that feed materials with a high proportion of fines can fill the voids, thus resulting in higher bulk density.

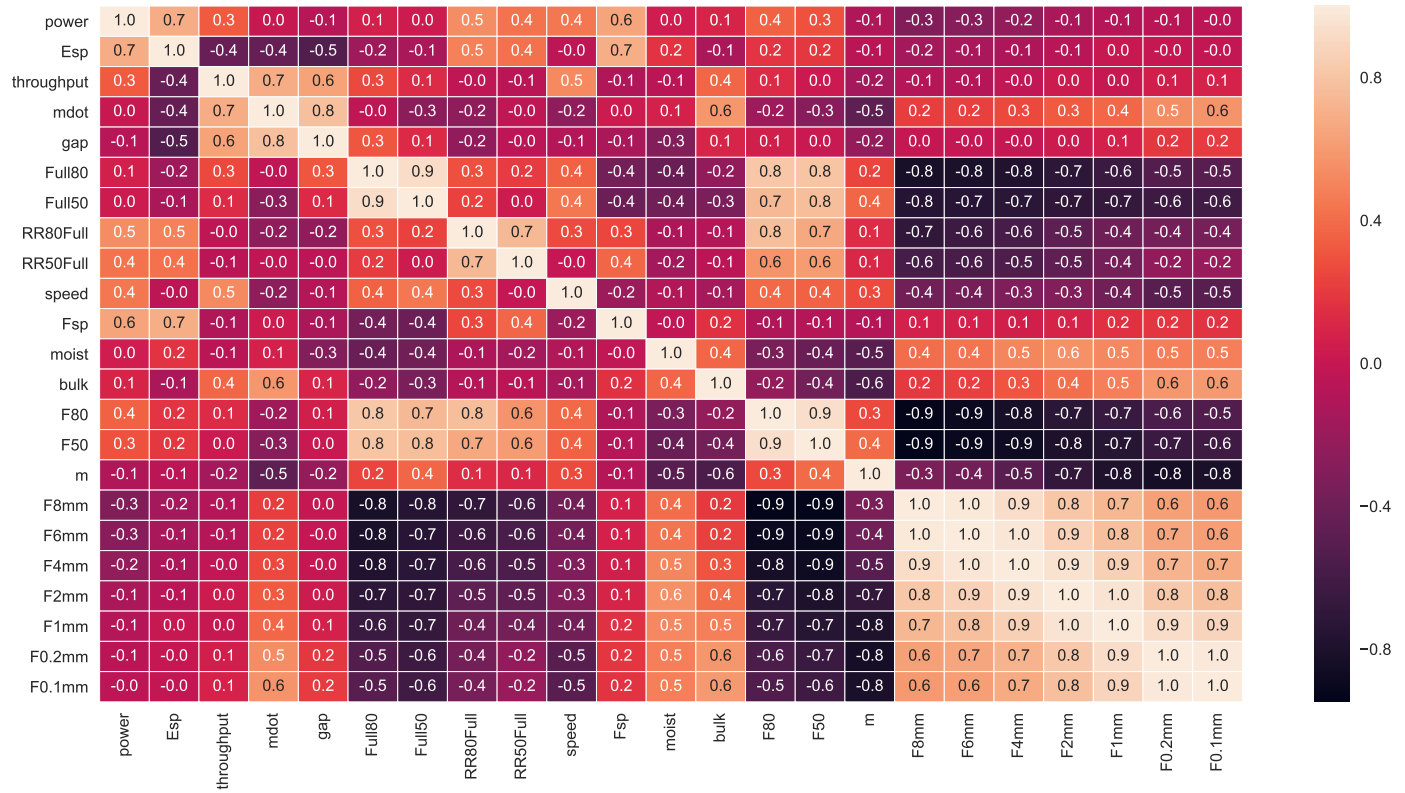


Figure 5.27: Correlation matrix of the identified predictor and response variables

5.3.3 Prediction of HPGR power draw

To develop empirical models for each of the desired response variables, regression analysis workflow presented in Figure 3.9 was followed. The particular response variable (e.g. HPGR power draw in this section) and all pre-selected predictor variables were assembled prior to regression modeling. Before executing the Ridge and LASSO regularization regression for variable selection, it was necessary to normalize all predictor variables to avoid unfair penalization of larger coefficients due to original data being on different scales.

As a result, influencing predictor variables for the HPGR power draw model were reduced to those expressed in Equation 5.6, while others were rejected due to having Ridge regression coefficients close to zero or LASSO regression coefficients equal to zero. The normalized coefficients for the influencing predictor variables are summarized in Table 5.7. Clearly, the most dominant predictor variable is the specific pressing force (F_{sp} in N/mm²). Other influencing predictor variables ranked by importance are the HPGR roll speed (u in m/s), the percent of -0.1 mm in the feed (%), the feed size F_{80} (mm), the cross-product of feed size F_{80} and feed moisture content (%), and the “feed condition” (categorized as normal and abnormal). All predictor variables have positive effect on the HPGR power draw, except the feed condition which was found having a minor negative effect, suggesting that the abnormal feed conditions (truncating feed) would result in slightly reduced power draw.

$$P = f(\text{feed}, u, F_{sp}, w, F_{80}, F_{0.1mm}) \quad (5.6)$$

After the selection of predictor variables, previously normalized data sets were transformed back to their original scale so that an interpretable model can be produced. Through the Python Scikit-learn package, three linear regression models (OLS, Ridge, and LASSO) were applied to generate empirical models for predicting the power draw.

Table 5.7 summarizes the results of the regression analysis. It was found that the regressed OLS and LASSO model reached an ultimate agreement, and gave higher predicted accuracy than the Ridge regression when fitting to the entire data sets. Regression modeling with training/testing dataset (based on 80/20 random split) and 5-fold Cross-Validation (CV) was performed to confirm the findings. The model generated by OLS and LASSO regression is considered the “best” empirical model for the power draw prediction. The coefficient of determination (regression score) for the empirical model is 0.90, meaning that the model explains 90% of the variance in the data.

Table 5.7: Summary results of regression for power draw

Variable	Normalized	OLS	Ridge	Lasso
Fitting entire data sets				
Constant		-62.31	-57.82	-62.31
Feed condition	-1.1	-1.09	-1.15	-1.09
Speed	45.3	87.14	81.33	87.14
F_{sp}	61.2	12.19	12.11	12.19
F_{80}	13.5	0.529	0.536	0.529
$F_{0.1mm}$	22.6	0.669	0.633	0.669
$F_{80} \cdot w$	12.2	0.067	0.069	0.067
Regression score		0.900	0.899	0.900
Mean Absolute Error (MAE)		3.59	3.59	3.59
Mean Squared Error (MSE)		20.03	20.28	20.03
Root Mean Square Error (RMSE)		4.48	4.50	4.48
Training/Testing (80/20 split)				
Training score		0.900	0.898	0.900
Testing score		0.881	0.877	0.881
Cross-validation				
5-fold CV score		0.826	0.819	0.826
5-fold CV RMSE		5.21	5.35	5.21

Figure 5.28 shows the residual plots for the selected model based on OLS and LASSO regression results. The histogram and Quantile-Quantile (Q-Q) plots confirmed that residuals are normally distributed as per the Anderson-Darling (1954) normality test (P-values >0.05). The majority of the residuals (measured-predicted) are within ± 10 kW, and relative errors of the model prediction are within $\pm 15\%$. In Figure 5.29, the residuals are plotted against the predictor variables selected in the model, indicating that the model does not have an inherent bias to predictor variables.

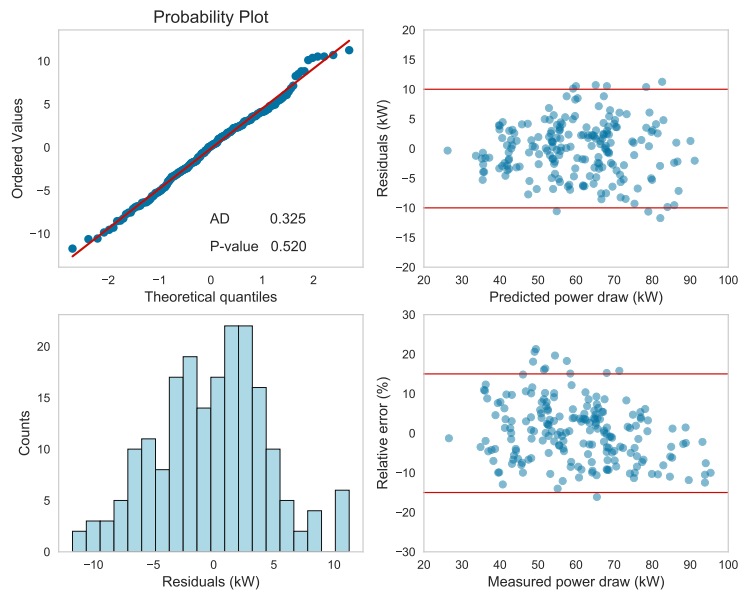


Figure 5.28: Residual plots of the regression model for power draw

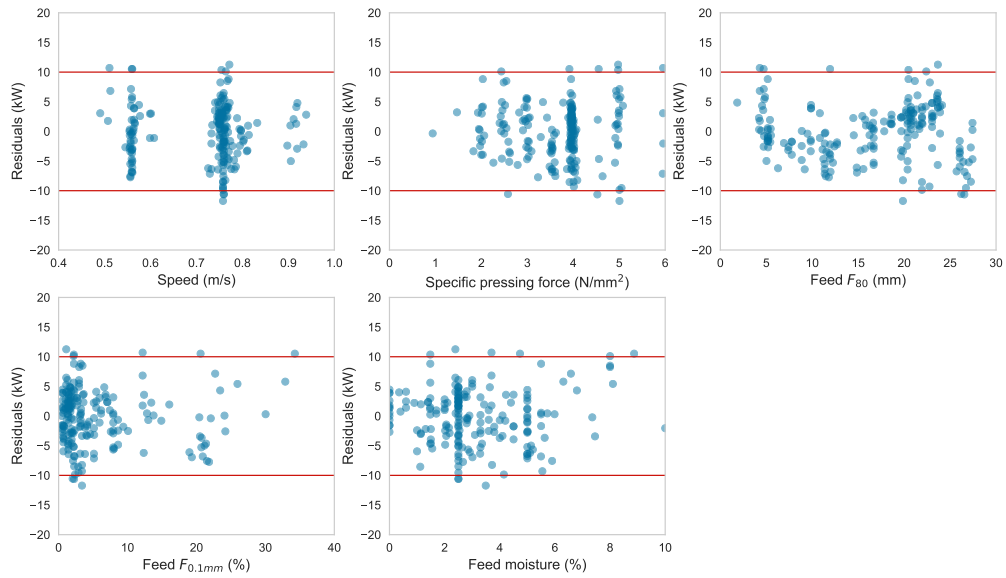


Figure 5.29: Residuals versus predictor variables of the power model

Figure 5.30 compares the predicted power draws to the measured values, with the 95% confidence intervals. The measured power draw values from pilot tests are strongly correlated to the predicted values. The standard deviation of the differences (in percentage) between the predicted and observed values was 7.5%, with an overall mean difference of 0.7%.

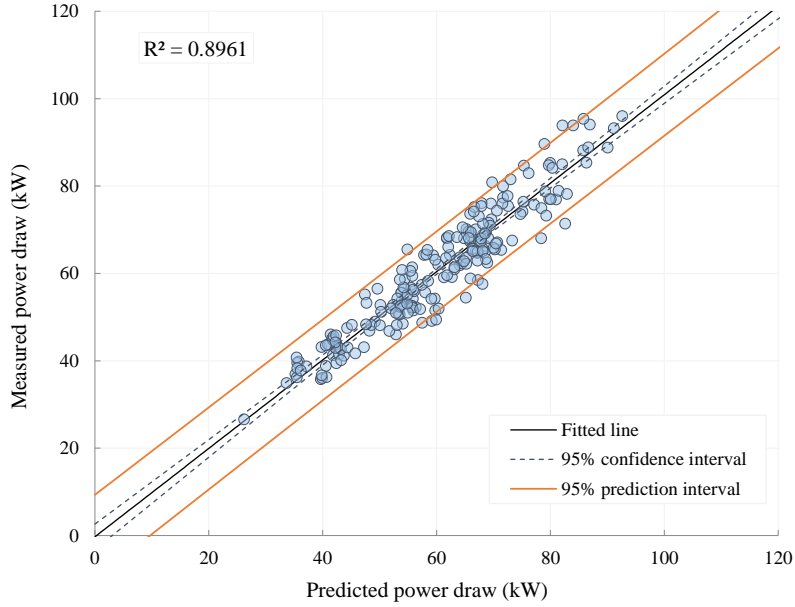


Figure 5.30: Scatter plot of the measured and predicted power draw

5.3.4 Prediction of HPGR net specific energy

Following the same methodology as described in Section 5.3.3, the critical predictor variables that affect the net specific energy consumption (E_{sp}) were refined to those contained in Equation 5.7, while others were rejected based on preliminary Ridge and LASSO regression results. As summarized in Table 5.8, the influencing predictor variables ranked by importance are the specific pressing force (F_{sp} in N/mm^2), the cross-product of feed size F_{80} and feed moisture content, the cross-product of F_{sp} and feed moisture content, the feed bulk density (ρ_{bulk}), and the feed size F_{50} (mm). Unlike the HPGR power draw model, the variation of roll speed does not affect the HPGR specific energy consumption.

$$E_{sp} = f(F_{sp}, \rho_{bulk}, w, F_{80}, F_{50}) \quad (5.7)$$

Table 5.8 summarizes the results of regression analysis for the HPGR net specific energy prediction. The best penalty term (λ) for the Ridge and LASSO regression worked out to be very close to zero and equal to zero, respectively. As

a result, all three regression methods arrived at the same model for predicting the E_{sp} . The coefficient of determination (regression score) for the empirical model is 0.823, indicating that the predictive model explains 82.3% of the variance in the data.

Table 5.8: Summary results of regression for specific energy consumption

Variable	Normalized	OLS	Ridge	Lasso
Fitting entire data sets				
Constant		0.960	0.960	0.960
F_{sp}	2.1	0.427	0.427	0.427
ρ_{bulk}	-0.8	-0.619	-0.619	-0.619
F_{50}	0.2	0.011	0.011	0.011
$F_{sp} \cdot w$	0.8	0.013	0.013	0.013
$F_{80} \cdot w$	1.1	0.006	0.006	0.006
Regression score		0.817	0.817	0.817
Mean Absolute Error (MAE)		0.170	0.170	0.170
Mean Squared Error (MSE)		0.048	0.048	0.048
Root Mean Square Error (RMSE)		0.220	0.220	0.220
Training/Testing (80/20 split)				
Training score		0.823	0.823	0.823
Testing score		0.769	0.769	0.769
Cross-validation				
5-fold CV score		0.740	0.740	0.740
5-fold CV RMSE		0.243	0.243	0.243

Figure 5.31 shows the residual plots for the selected E_{sp} model. Although the histogram and Q-Q plots showed a marginal departure from normality, the model is considered adequate for E_{sp} prediction. The majority of the residuals are within ± 0.5 kWh/t, and relative errors of the prediction are within $\pm 20\%$. In Figure 5.32, residuals are plotted against all predictor variables, confirming that the resulting model has no bias with respect to the predictor variables.

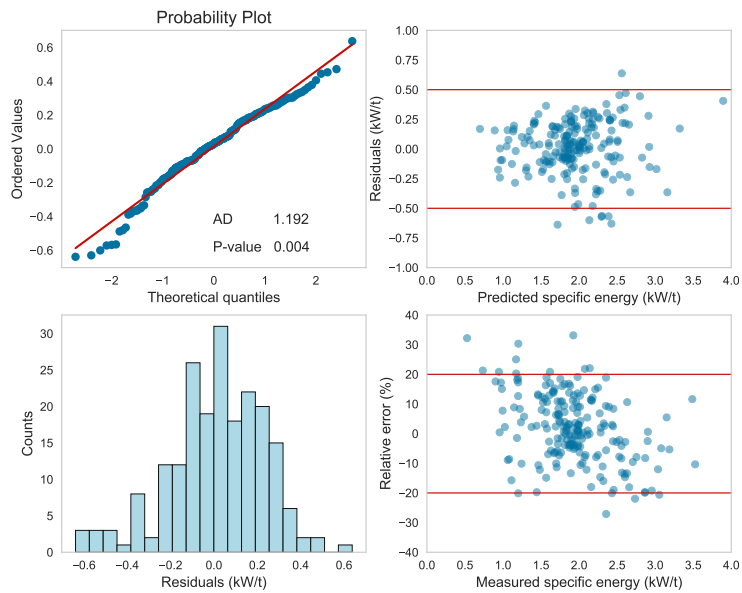


Figure 5.31: Residual plots of the regression model for specific energy

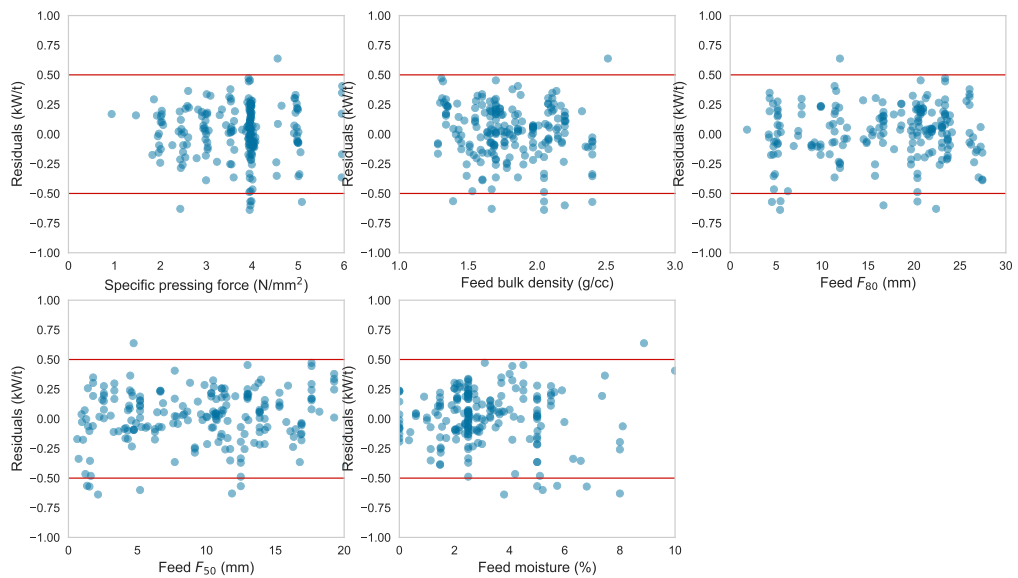


Figure 5.32: Residuals versus predictor variables of the specific energy model

Figure 5.33 compares the predicted specific energy consumption to the measured values from pilot HPGR testing, together with the 95% confidence intervals. Through the statistical examination of the data, it was found that the standard deviation of the differences between the predicted and observed values was 11.4%, and the overall mean difference was 0.7%.

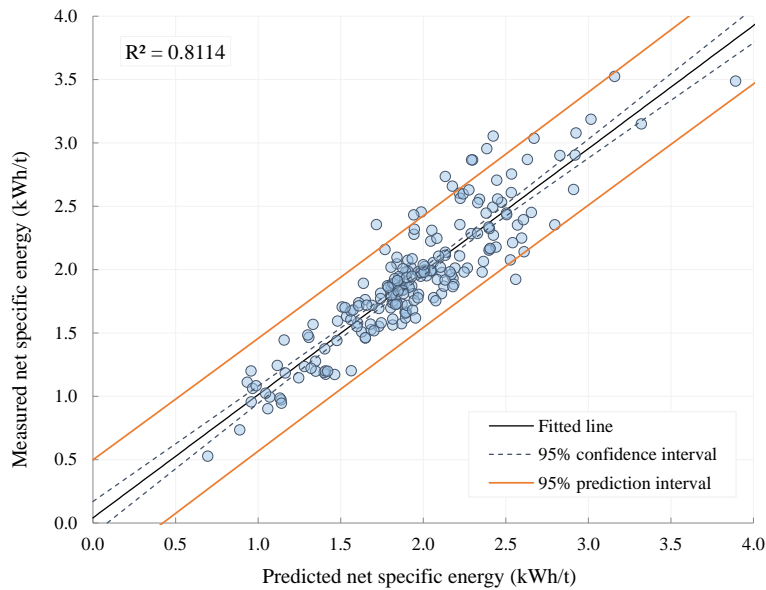


Figure 5.33: Scatter plot of the measured and predicted specific energy

5.3.5 Prediction of HPGR throughput

The HPGR throughput capacity and related parameters such as operating gap and specific throughput constant were difficult to predict from the UBC HPGR database. All three regression methods failed to produce an acceptable model for the throughput prediction. Therefore, indirect approaches (through Equation 5.8 and Equation 5.9) were adopted to calculate the HPGR throughput and \dot{m} given the knowledge of the total power draw (P) and net specific energy consumption (E_{sp}), both of which can be predicted empirically. In addition, the machine learning modeling, often regarded as the “black box” approach, was also attempted to discover the latent relationship between the HPGR throughput parameter and the predictor variables.

Details of the machine learning approach for \dot{m} model development are provided in Appendix D.

$$W = \frac{P_{\text{net}}}{E_{sp}} \tag{5.8}$$

$$\dot{m} = \frac{W}{DLu} = \frac{\frac{P_{\text{net}}}{E_{sp}}}{DLu} \tag{5.9}$$

Figure 5.34 shows the residual plots for the throughput model as a result of the indirect approach. The histogram and Q-Q plots show satisfactory results as the residuals are normally distributed (P-values >0.05 for the Anderson-Darling normality test). The majority of the residuals are within ± 8 t/h, and relative errors of the model prediction are within $\pm 25\%$.

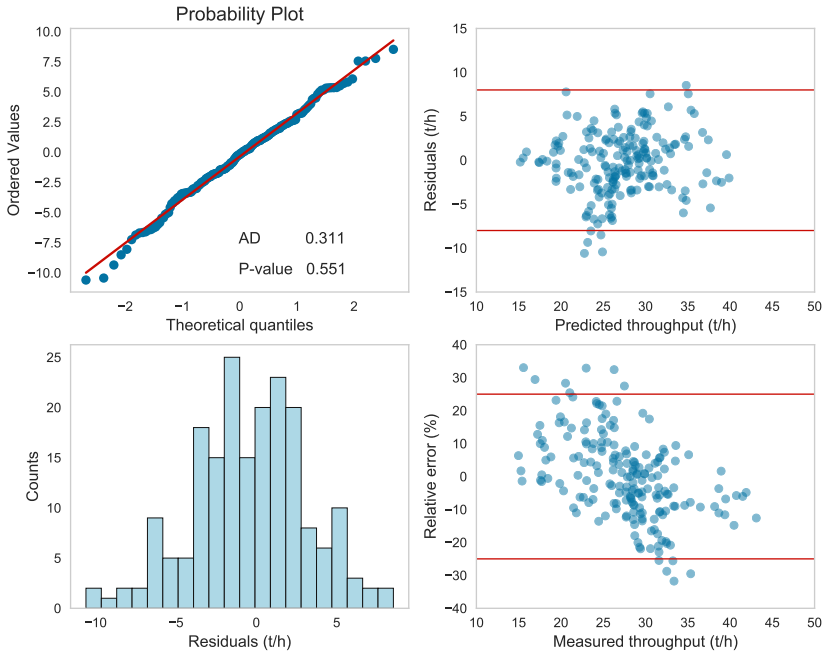


Figure 5.34: Residual plots of the regression model for HPGR throughput

Figure 5.35 compares the predicted throughput capacity (Equation 5.8) to the recorded values, with the 95% confidence intervals. The standard deviation of the differences between the observed and predicted values was 14.2%, and an overall mean difference was 2.9%.

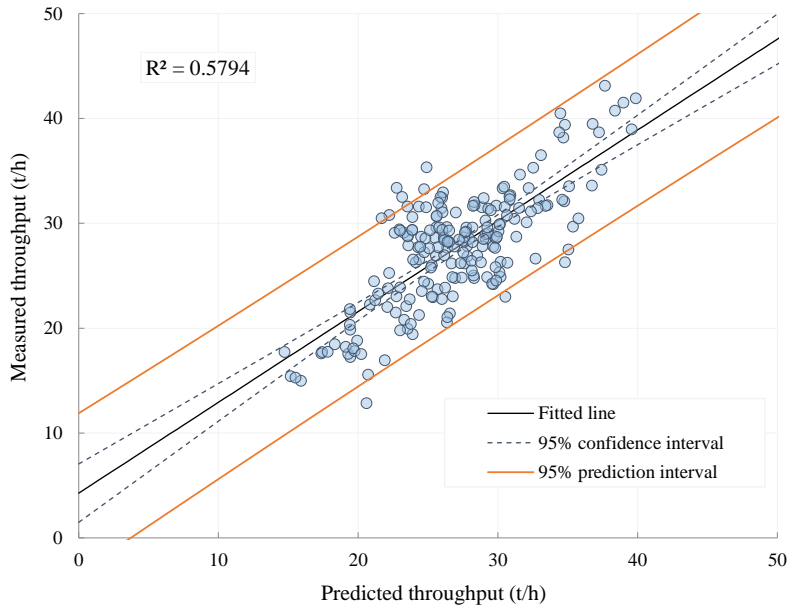


Figure 5.35: Scatter plot of the measured and predicted throughput

Figure 5.36 compares the calculated specific throughput constant (Equation 5.9) to the measured values, with the 95% confidence intervals. As can be seen, the predicted and measured \dot{m} are correlated, though to a lesser degree. However, the prediction accuracy of the \dot{m} parameter is considered adequate for preliminary HPGR sizing. Through the statistical examination of the data in Figure 5.36, it was found that the standard deviation of the differences between the observed and calculated values was 14.2%, and an overall mean difference was 3.1%.

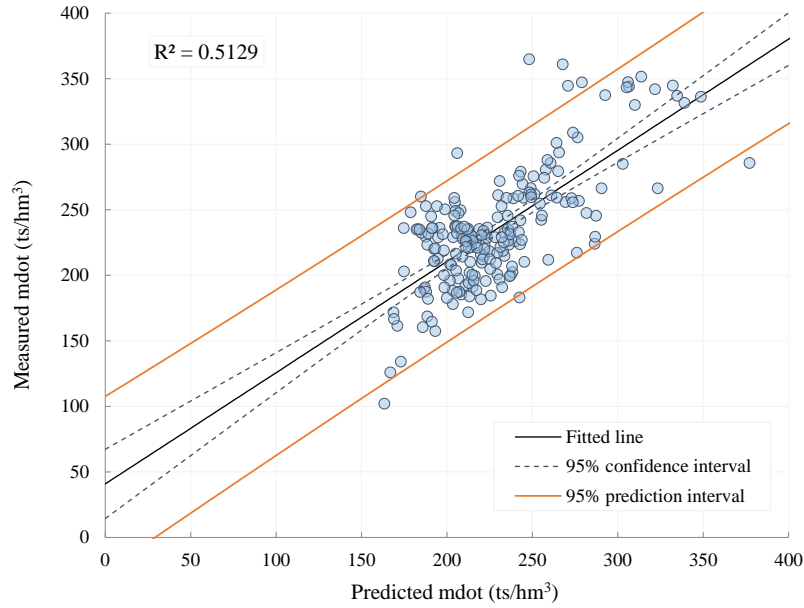


Figure 5.36: Scatter plot of the measured and predicted specific throughput constant

5.3.6 Prediction of HPGR product size and reduction ratio

The significant variables for predicting the HPGR full product size P_{80} and reduction ratio RR_{80full} were refined to those involved in Equation 5.10 and Equation 5.11. For the product size P_{80} , the influencing predictor variables ranked by importance are the specific pressing force (F_{sp}), the feed size F_{80} , the percent of -4 mm in the feed (%), the cross-product of F_{80} and feed moisture content, and the feed size distribution slope module (m). In terms of the reduction ratio RR_{80full} , the influencing predictor variables ranked by importance are the specific pressing force (F_{sp}), the feed size F_{80} , the cross-product of F_{80} and feed moisture content, and the feed size F_{95} .

$$P_{80} = f(F_{sp}, F_{80}, m, F_{4mm}, w) \quad (5.10)$$

$$RR_{80full} = f(F_{sp}, F_{80}, F_{95}, w) \quad (5.11)$$

Table 5.9 summarizes the results of regression analysis for the prediction of the HPGR full product P_{80} . The OLS and LASSO regression arrived at the same model, with higher predicted accuracy than the Ridge regression, therefore the model resulted from both methods was selected as the best model. The regression score for this empirical model is 0.827.

Table 5.9: Summary results of regression for product size P_{80}

Variable	Normalized	OLS	Ridge	Lasso
Fitting entire data sets				
Constant		8.907	7.245	8.907
F_{sp}	-3.49	-0.703	-0.639	-0.703
F_{80}	3.48	0.136	0.152	0.136
m	-1.62	-1.833	-0.55	-1.833
F_{4mm}	-3.36	-0.04	-0.03	-0.04
$F_{80} \cdot w$	-2.01	-0.011	-0.01	-0.011
Regression score		0.823	0.812	0.823
Mean Absolute Error (MAE)		0.633	0.654	0.633
Mean Squared Error (MSE)		0.637	0.676	0.637
Root Mean Square Error (RMSE)		0.798	0.822	0.798
Training/Testing (80/20 split)				
Training score		0.827	0.815	0.827
Testing score		0.784	0.773	0.784
Cross-validation				
5-fold CV score		0.677	0.636	0.677
5-fold CV RMSE		0.859	0.917	0.859

Figure 5.37 shows the residual plots for the selected P_{80} model, including the Q-Q plot confirming that the residuals were normally distributed. The majority of the residuals are within ± 1 mm, and relative errors of the model prediction are within $\pm 30\%$. Figure 5.38 compares the residuals with all predictor variables. The resulting model appeared to be satisfactory, with no particular bias found associated with the predictor variables.

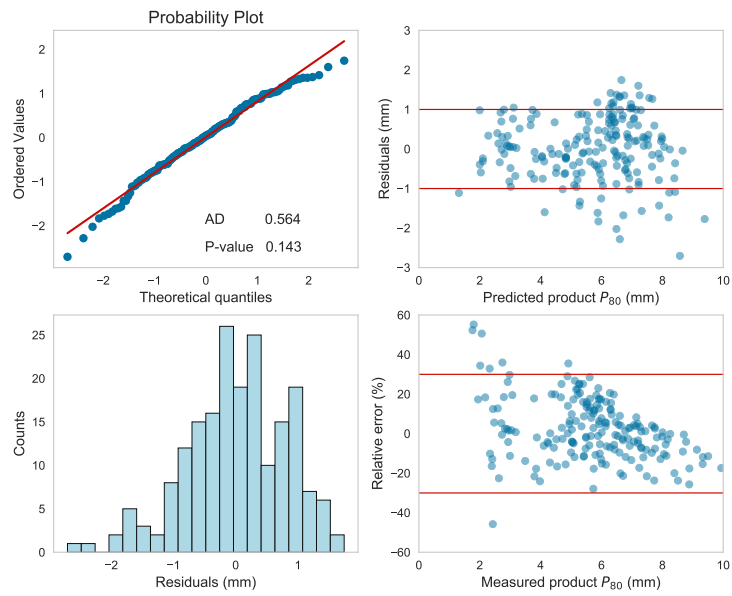


Figure 5.37: Residual plots of the regression model for product size P_{80}

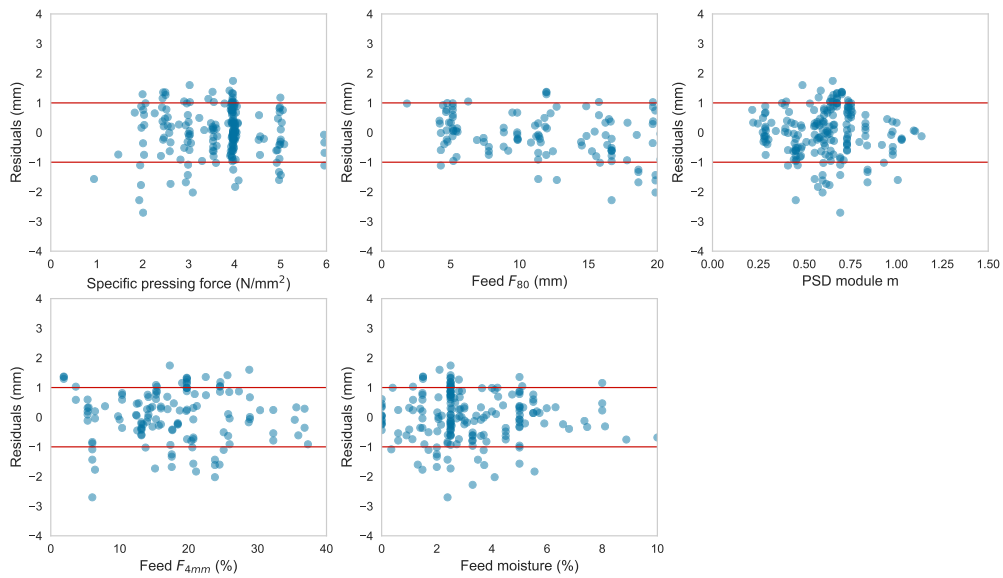


Figure 5.38: Residuals versus predictor variables of the P_{80} model

Table 5.10 summarizes the results of regression analysis for the prediction of the HPGR size reduction RR_{80full} . The resulting three regression models were similar. The OLS and Ridge model achieved a slightly higher RMSE than the LASSO model when fitting to entire data sets, but the LASSO regression showed a slightly higher predicted accuracy when the Cross-Validation (CV) is applied. It was therefore decided to choose the OLS regression.

Table 5.10: Summary results of regression for reduction ratio RR_{80full}

Variable	Normalized	OLS	Ridge	Lasso
Fitting entire data sets				
Constant		-0.015	-0.007	0.218
F_{sp}	1.37	0.309	0.307	0.255
F_{80}	1.20	0.05	0.05	0.049
F_{95}	0.75	0.027	0.027	0.027
$F_{80} \cdot w$	0.91	0.006	0.006	0.006
Regression score		0.752	0.752	0.748
Mean Absolute Error (MAE)		0.319	0.319	0.316
Mean Squared Error (MSE)		0.161	0.161	0.163
Root Mean Square Error (RMSE)		0.401	0.401	0.404
Training/Testing (80/20 split)				
Training score		0.760	0.760	0.756
Testing score		0.707	0.708	0.719
Cross-validation				
5-fold CV score		0.634	0.634	0.643
5-fold CV RMSE		0.437	0.437	0.434

Figure 5.39 shows the residual plots for the selected RR_{80full} model. The Q-Q plot shows a marginal departure from normality for the residuals, which is considered acceptable for the prediction. The majority of the residuals are within ± 1 , and relative errors of the model prediction are within $\pm 30\%$. Figure 5.40 plots the residuals against all predictor variables, confirming there was no bias associated with the predictor variables.

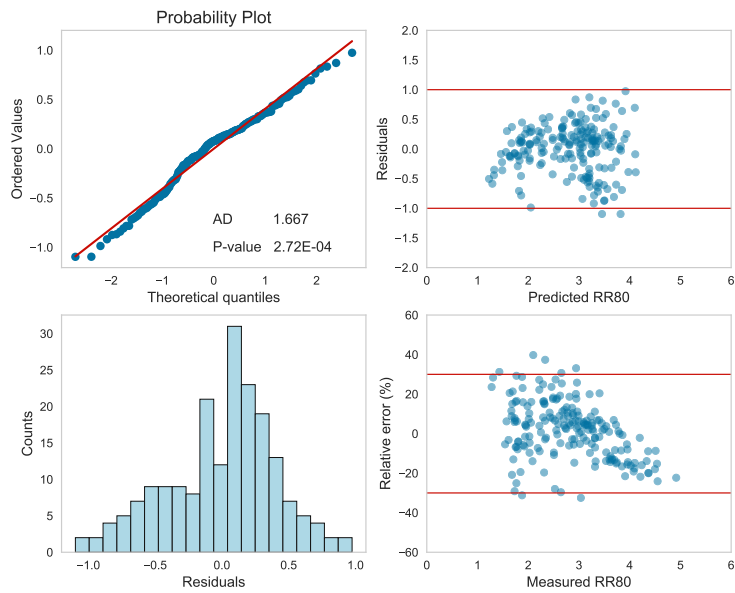


Figure 5.39: Residual plots of the regression model for RR_{80full}

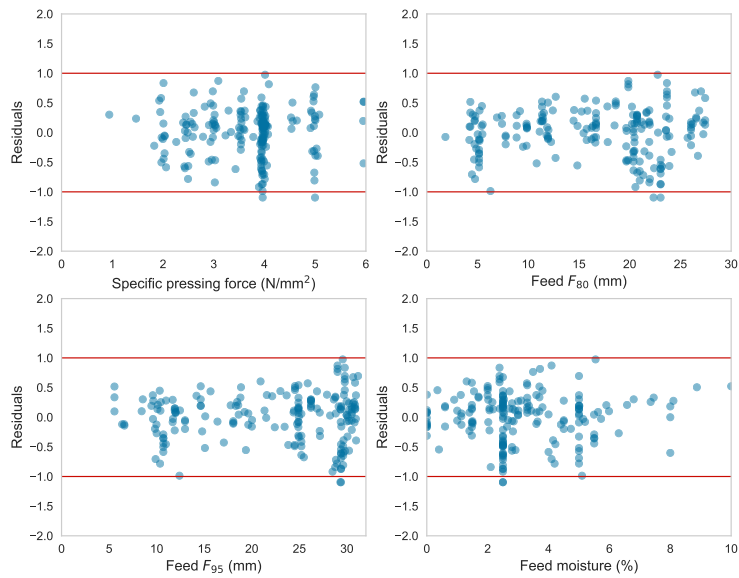


Figure 5.40: Residuals versus predictor variables of the RR_{80full} model

Figure 5.41 compares the predicted product size P_{80} to the measured values, with the 95% confidence intervals. Through the statistical examination of the data in Figure 5.41, it was found that the standard deviations of the differences between the observed and predicted values were 16% for the P_{80} , and corresponding overall means of differences were 1.0%.

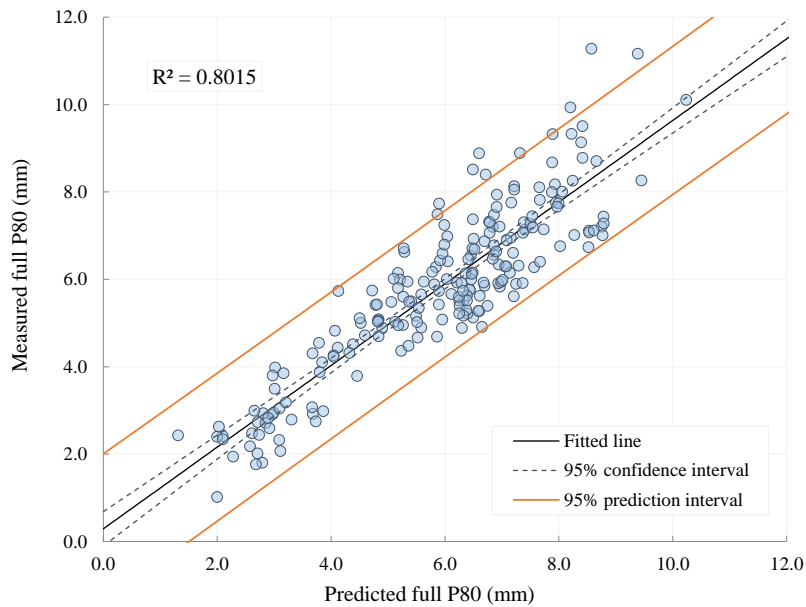


Figure 5.41: Scatter plot of the measured and predicted P_{80}

Figure 5.42 compares the predicted size reduction RR_{80full} to the measured values, with the 95% confidence intervals. It was found that the standard deviations of the differences between the observed and predicted values were 15.1% for the RR_{80full} , and corresponding overall means of differences were 1.5%.

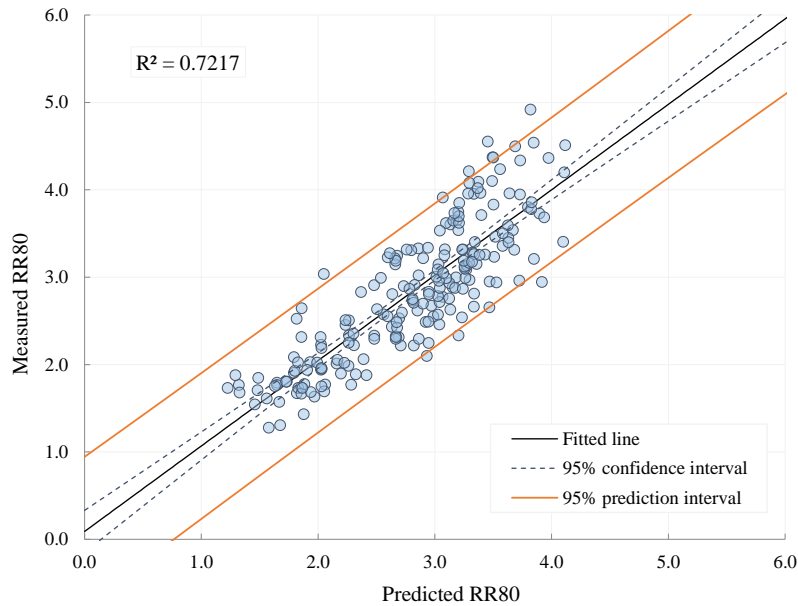


Figure 5.42: Scatter plot of the measured and predicted RR_{80full}

5.4 Summary and Conclusions

This chapter presented the data from the UBC HPGR database that contains 228 sets of pilot test data collected over 10 years. Key input and output variables from pilot HPGR testing were examined, providing corresponding frequency distributions and statistics that can be used for benchmarking comparison.

Multivariable linear regression modeling was performed to develop empirical models for the prediction of key HPGR response variables. During the course of the analysis, it was found that HPGR key performance indicators are mainly driven by the applied specific pressing force and feed material characteristics. As a result, a number of empirical models for predicting the HPGR power draw, net specific energy, specific throughput constant, product size and reduction ratio were developed and summarized below. It is shown that the developed models have adequate prediction accuracy. In the absence of pilot HPGR testing, the HPGR performance evaluation under various operating conditions is possible with the empirical models. A holistic approach consisting of these empirical models can be developed to provide the required information for HPGR sizing and circuit design.

HPGR power draw model The developed empirical model for the HPGR power draw can be expressed in Equation 5.12.

$$P = -62.31 - 1.09\text{feed} + 87.14u + 12.19F_{sp} + 0.529F_{80} + 0.669F_{0.1mm} + 0.067wF_{80} \quad (5.12)$$

HPGR specific energy model The HPGR specific energy consumption can be estimated by Equation 5.13.

$$E_{sp} = 0.96 + 0.427F_{sp} - 0.619\rho_{bulk} + 0.011F_{50} + 0.013wF_{sp} + 0.006wF_{80} \quad (5.13)$$

HPGR product size model The HPGR product P_{80} can be estimated by Equation 5.14.

$$P_{80} = 8.907 - 0.703F_{sp} + 0.136F_{80} - 1.833m - 0.04F_{4mm} - 0.011wF_{80} \quad (5.14)$$

HPGR size reduction model The HPGR size reduction ratio (RR_{80full}) can be estimated by Equation 5.15.

$$RR_{80full} = -0.015 + 0.309F_{sp} + 0.05F_{80} + 0.027F_{95} + 0.006wF_{80} \quad (5.15)$$

There are multiple assumptions and limitations that should be noted for the empirical predictions:

- It is believed that the ore hardness also impacts the HPGR performance. However, the UBC HPGR database did not contain sufficient ore hardness information to reveal its significance on model predictions.
- The model may be only suitable for ore types and projected operating conditions that are within the ranges of the parameters in the UBC HPGR database.
- The current UBC HPGR database only accounts for tests performed on tertiary-

and quaternary-stage crushing applications, the developed empirical models may not be suitable for HPGR fine grinding such as iron-ore pellet-feed preparation.

Chapter 6

HPGR Sizing from Conceptual to Feasibility

6.1 Introduction

This chapter provides pragmatic approaches for HPGR sizing and selection based on available ore characteristics and design criteria. It focuses on the HPGR sizing method and design considerations, particularly on how to reduce the sample and testing requirements for a given project setting. Case studies for different project phases, from conceptual to feasibility, are presented to demonstrate the proposed methodologies. However, justification of HPGR as opposed to other comminution technologies will typically require proper trade-off studies, from which the technical feasibility and commercial viability needs to be adequately compared.

6.2 HPGR Circuit Design Considerations

This section introduces the design considerations for HPGR circuits, covering comminution testing, process design criteria and flowsheet development.

6.2.1 Generic comminution test work

Table 6.1 lists some commonly performed comminution tests for ore hardness characterization, including JK Drop Weight Test (DWT), SAG Mill Comminution (SMC) test[®], and Bond style tests. Those tests may well suffice the requirement for conventional comminution circuit design, such as stage crushing followed by ball milling, or the Semi-Autogenous Grinding (SAG) mill based circuits. But they are not suitable for the HPGR circuit design. Occasionally, the JK DWT Axb and SMC DWi parameters are used as indicators for the HPGR evaluation (Morrell, 2009). However, these tests are based on impact breakage as opposed to the particle-bed compression breakage employed by the HPGR, and they do not generate all required parameters for HPGR sizing and selection. Very often, for early stage projects that do not have specific HPGR characterization tests, process engineers tend to use benchmark method despite that their approaches may not be ore specific.

Table 6.1: General comminution tests

Test Name	Parameters	Technology	Design Tools
Bond Crusher	Crusher Work Index (CWI)	Crushers	Excel
JK Drop Weight	Axb, ta and t ₁₀	Crushers, AG/SAG	JK SimMet TM
SMC	DWi, Mia, Mic, Mih	Crusher, AG/SAG	CITIC SMCC
SAGDesign	SAG specific pinion energy	AG/SAG	Excel
SAG Power Index	SPI, minutes (P ₈₀ of 1.7 mm)	AG/SAG	CEET
MacPherson	AWi	AG/SAG	Excel
Bond Rod Mill	Rod Mill Work Index (RWI)	Rod, AG/SAG	Excel
Bond Ball Mill	Ball Mill Work Index (BWI)	Ball Mills	Excel

* Modified after Mosher and Bigg, 2002

6.2.2 HPGR characterization test work

The HPGR circuit specific energy requirement and throughput capacity should be determined based on specific HPGR characterization test work; such tests are available and summarized in the following,

1. Piston-die press tests (PPT or P&D) for scoping level studies in cases with limited sample availability. Some HPGR manufacturers have developed methodologies such as Metso's Packed-Bed Test (Elkin et al., 2017)
2. Laboratory-scale HPGR tests for scoping studies, such as the ThyssenKrupp Labwal HPGR test
3. Pilot scale HPGR tests for more accurate HPGR sizing. All HPGR manufacturers have the capabilities conducting such tests for project evaluation. These batch tests are conducted in either open circuit or closed circuit
4. Industrial scale HPGR tests for continuous demonstration

6.2.3 Process design criteria

The selection of HPGR during the project development is primarily driven by the project economics, which should consider following aspects of the design criteria.

1. Throughput
2. Ore hardness
3. Ore variability
4. Electricity cost
5. Climate condition
6. Other considerations such as moisture and clay content in the feed

Each of the design criteria is discussed in the following section, to evaluate and compare their impact on the project when considering the SAG mill or HPGR for the comminution circuit design.

Throughput

Both SAG mill and HPGR can offer high throughput capacity for the comminution circuit. However, sizing of these technologies in a comminution flowsheet is fundamentally different. The throughput of a SAG mill is sensitive to ore hardness, to be specific the ore competency as measured by the Axb parameter or equivalent tests (e.g. DWi, SPI). The final selection of the SAG mill size has to provide sufficient power for the desired grinding duty, based on the understanding of the ore hardness and target throughput. For example, processing at a throughput rate of 1,000 t/h at a required specific energy consumption of 10 kWh/t at the motor output would need an operating power of 10 MW.

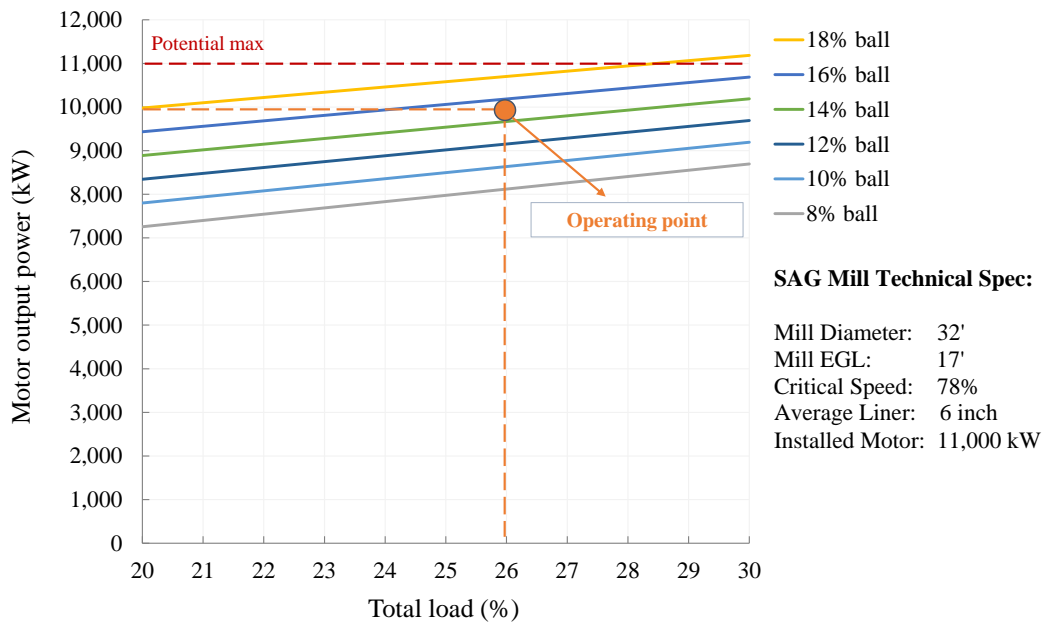


Figure 6.1: SAG mill motor power as a function of operating conditions

Figure 6.1 shows that a 32'x17' EGL SAG mill with 11 MW installed motor power can provide 10 MW power draw as required when operating at 15% ball charge, 26% total load, and 78% of critical speed. A larger mill with bigger motors may be pursued to provide additional design contingency if the specific project requires so. Depending on the ore hardness, there would be a throughput thresh-

old for a given size SAG mill. A higher throughput requirement could mean step changes in the selection of SAG mill size, such as changing from geared driven SAG mills to gearless SAG mills, or changing from a single unit to multiple units operating in parallel.

In contrast, the HPGR size is principally driven by the required volumetric flow through the machine. Figure 6.2 shows the HPGR throughput capacity as a function of roll diameter and roll speed, assuming an aspect ratio (roll diameter over roll length) of 1.5 and a specific throughput constant (m) value of 300 ts/hm³. A 3.0 m x 2.0 m HPGR can potentially process up to 7,000 t/h if operated in open circuit. For sizing an HPGR in closed circuit arrangement, it is important to obtain the information about the circulating load at the desired closing screen size, because it affects the total volumetric flow through the HPGR. For instance, the circuit capacity of a closed HPGR operation at 100% circulating load is effectively half of an open circuit using the same machine. Comparing the HPGR and SAG mill, the HPGR potentially offers a higher throughput in a single unit than the SAG mill particularly for hard ores, which may directly impact the overall project economics.

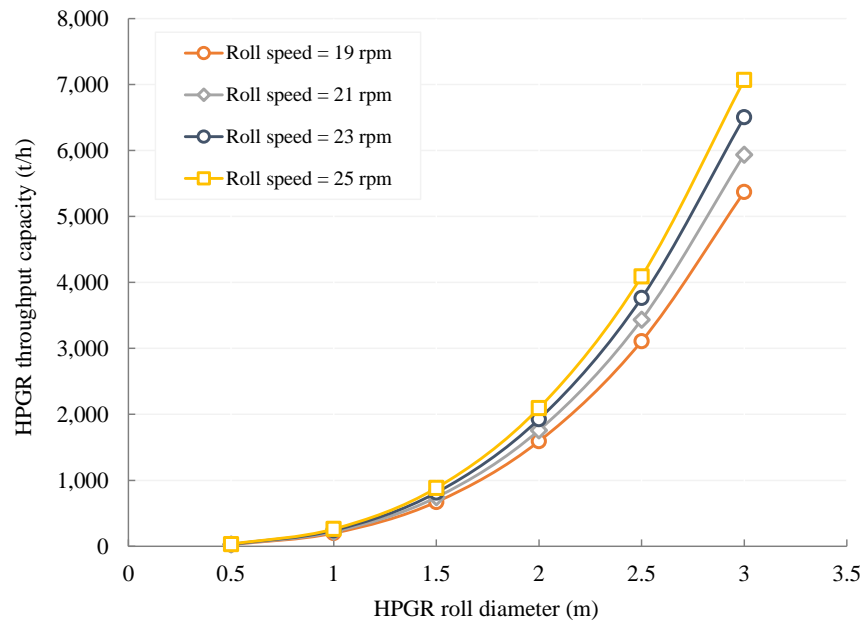


Figure 6.2: HPGR throughput as a function of roll diameter and speed

Ore hardness

It is understood that the HPGR is more resilient to variations in ore hardness as compared to the SAG mill. Changes in ore hardness often require changes of mill size and motor size for the SAG mill option, but not necessarily for the HPGR. The same size HPGR machine processing competent ores may even achieve a higher specific throughput constant than when processing soft ores as competent ores can support a larger operating gap. In contrast, a SAG mill based circuit processing more competent ores at a given throughput target would require a larger SAG mill, or sometimes even multiple units.

An example is provided here to demonstrate the influence of ore hardness for SAG mill and HPGR sizing, where data is taken from Section 4.2.2 and Table 4.3. Table 6.2 demonstrates that changing ore hardness resulted in a step change in SAG mill sizing, from a geared driven SAG mill to a SAG mill with gearless mill drives. Alternatively, two smaller geared driven SAG mills operating in parallel are needed to meet the production guideline. In either case, a substantial increase in capital cost is expected if the project retains the SAG mill in the process flowsheet. Thus, the overall economics would be negatively impacted for the SAG mill based circuit. As for the HPGR based circuit, a single line with larger installed motors may still be feasible for processing the harder ore.

Table 6.2: Sizing of SAG mill and HPGR for soft and hard ores

Description	Unit	Closed-SAG	Closed-HPGR
Design throughput	[dry t/d]	70,000	70,000
Availability	[%]	92	92
Design throughput	[dry t/h]	2,683	2,683
Scenario 1 - Soft ore			
Axb	[-]	70	70
BBWI	[kWh/t]	14	14
HPGR circulating load	[%]	-	40
HPGR circulating load	[%]	-	40
HPGR machine feed	[dry t/h]	-	3,757
Circuit specific energy	[kWh/t]	6	2.1
HPGR - \dot{m}	[ts/hm ³]	-	300
Power requirement	[MW]	16.1	5.6
Number of machine	[#]	1	1
Machine dimension	[-]	38' Dia. x 20' EGL	2.6m Dia. x 1.8m L
Installed motor power, each	[MW]	18	6
Scenario 2 - Hard ore			
Axb	[-]	30	30
BBWI	[kWh/t]	20	20
HPGR circulating load	[%]	-	70
HPGR machine feed	[t/h]	-	4,692
Circuit specific energy	[kWh/t]	10	3.4
HPGR - \dot{m}	[ts/hm ³]	-	300
Power requirement	[MW]	26.8	9.1
<u>Scenario 2 - Option 1</u>			
Number of machine	[#]	1	1
Machine dimension	[-]	40' Dia. x 26' EGL	2.6m Dia. x 1.8m L
Installed motor power, each	[MW]	28	10
<u>Scenario 2 - Option 2</u>			
Number of machine	[#]	2	
Machine dimension	[-]	38' Dia. x 17.5' EGL	
Installed motor power, each	[MW]	14	

Ore variability

Ore variability naturally occurs during the formation of ore deposit. Figure 6.3 compares the degree of ore variation for actual mining projects as measured by the DWi parameter, an indicator of the ore responses to AG/SAG milling. As can be seen, some projects (Project C and P) have significantly higher variations than others. The ore variability can also be measured in other metrics to describe the ore responses to particular unit operations (for example, the use of BBWI parameter for ball milling).

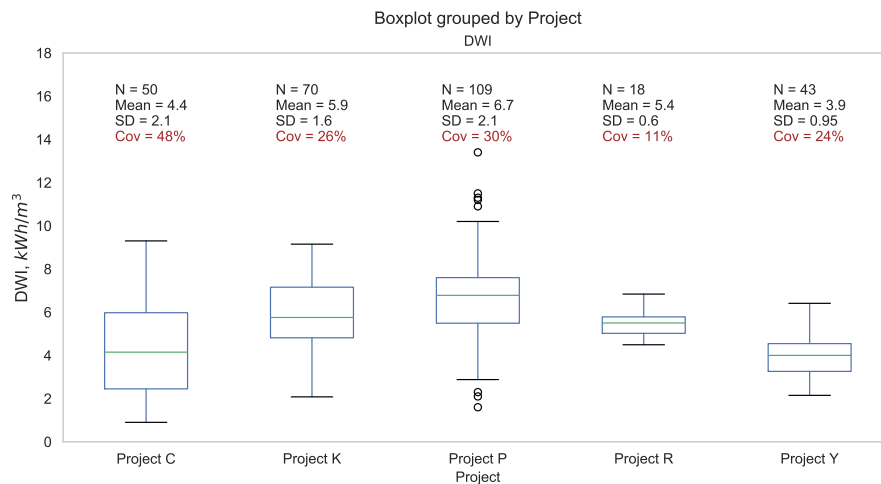


Figure 6.3: Ore variability measured by DWi value

Like other crushing technologies, the HPGR is also considered as a “constant volume” machine where the machine throughput capacity does not vary much with ore hardness. Therefore, the HPGR based circuits are less vulnerable to ore variation than the SAG mill based circuits. Although treating harder ores could result in a higher circulating load, reducing the overall circuit throughput rate, the HPGR machine itself does not see the degree of throughput variation that could be experienced with a SAG mill circuit. Two main HPGR control variables, namely the specific pressing force and roll speed, can provide flexibility and stability for a smooth operation.

Electricity cost

Power cost is one of the main components of the operating cost for any comminution circuit, which varies considerably among projects. The major contributors to the overall power cost are the unit cost of the electricity and the circuit energy intensity. The available power supply (such as hydro, diesel, LNG, or renewable sources) for any project is subject to the specific project setting, which has a significant impact on the up-front capital investment or the long term operating cost.

To demonstrate the impact of the electricity cost and circuit energy intensity, an example is provided to show the potential cost savings by employing the energy efficient circuit with the inclusion of the HPGR technology as compared to the conventional comminution circuit with SAG mills. Three SABC circuits were selected as the base cases (Case 1, Case 2 and Case 3). The assumed circuit specific energy requirements for the base cases are 10, 15, and 20 kWh/t, representing the circuit energy intensity when treating the soft, medium and hard ores. In addition, the energy savings of 10%, 20% and 30% were assumed for the HPGR based circuit. The potential power savings (in USD/t milled) for these 9 scenarios at varying electricity price are presented in Figure 6.4. It shows that greater benefits could be achieved by adopting the HPGR based circuit for harder ores and higher energy price. As a consequence, the HPGR technology has been more attractive with many installations in places like South America and Australia, where the electrical costs are exceptionally high. The energy efficiency nature of the HPGR technology provides considerable economical benefits to the projects.

In Case 3 for example, at a specific energy requirement of 20 kWh/t and unit electricity cost of 0.3 USD/kWh, the power savings achieved by the HPGR based circuit could be as high as 1.8 USD/t milled or 18 million USD per annum for a 10 million tonne per annum operation, provided that energy savings of 30% could be obtained relative to the base case. Its impact on overall project economics could be therefore assessed, prior to justifying whether or not to select such energy efficient comminution circuit for the project.

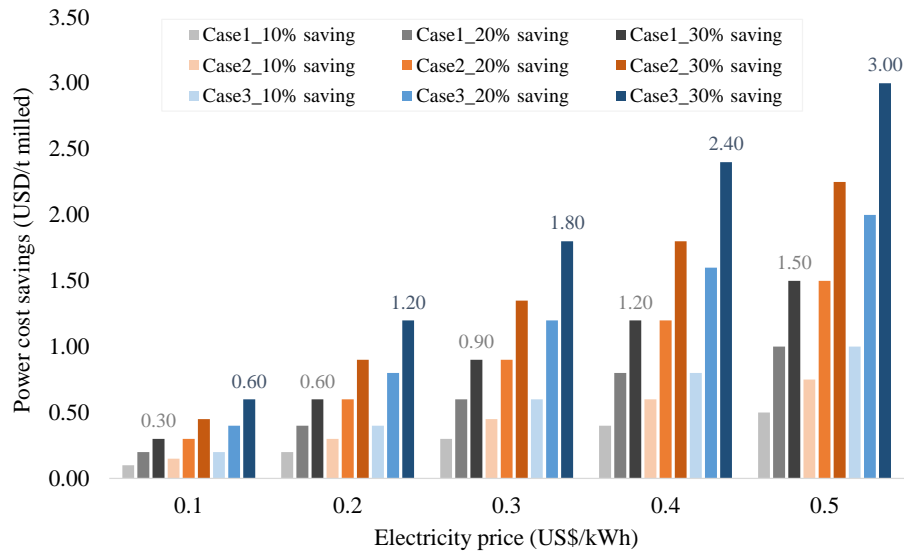


Figure 6.4: Estimates of potential annual power cost savings

Climate

The climate condition is often overlooked for potential HPGR projects in regions with extreme winter conditions, such as Canada and Russia. The SAG mill based circuit is often the “go-to” design due to its insensitivity to the weather conditions. In contrast, the “standard” HPGR flowsheet with wet classification would significantly increase the risk for operations in the cold climate regions, because frequent bin hang-ups over the HPGR and unstable conveying operation could occur as a result of mixing the cold fresh feed with the wet screen oversize materials. Without any process modification, this type of closed circuit HPGR could frequently become inoperable during the harsh winter months. To mitigate this negative effect of low temperatures, a wet disintegrator-scrubber could be integrated into the flowsheet ahead of the HPGR. Other alternatives are using the dry screens, or the edge recycle in which the screen is eliminated from the flowsheet.

For small scale HPGR operations, it may also be possible to shelter the entire HPGR circuit including the conveyors in the main process building, as such the cold weather's influence can be minimized. In this case, fresh feed to the HPGR comes from the secondary crushing and screening circuit, which removes all the ice from the feed material. The temperature inside the main process building would be above 0° C, so that freezing of cold crushed ore and wet recycled oversize can be mitigated. The drawback of this design is the capital cost due to larger building space requirement, and additional cost for the heating system (Rosario, 2010). Even though, this option could still be risky in extreme cold regions as the ore may still come at very low temperature after secondary crushing.

Others - Clays, Moisture

Generally, the HPGR does not respond well when processing ores with a significant amount of clay-like components or high moisture content. High clay presence tends to cushion the crushing action, thus make the overall comminution process inefficient (Morley, 2006). Innovative flowsheet configurations have been developed to address the clay issues (Rosario, 2011). In terms of the moisture issue, there is typically a threshold moisture level for a given material, above which the HPGR throughput capacity could be severely hampered. At moistures exceeding about 5-6%, the material may flow or extrude along the roll surfaces. Due to the flow/extrusion, it may be difficult to raise the pressure to desired high levels, so that the specific energy input could be limited. High moisture can also result in high roll wear rate, consequently higher operating costs and frequent roll change-out requirement. For a typical tertiary HPGR circuit closed with wet screening, if the screen oversize material returned to the HPGR contains mostly just surface moisture, it may not present too big a challenge to the HPGR operation.

Summary

In summary, Figure 6.5 presents a radar chart showing the breakdown of the different design attributes of the HPGR and SAG circuits. Each of the discussed design considerations is represented by the axis and divided into five levels, from low to high, to show the corresponding strength of the HPGR and SAG circuits. Clearly, the HPGR based circuits are more favorable for projects with any of the following design criteria: high throughput, hard ores, high ore variability, and expensive electricity supply.

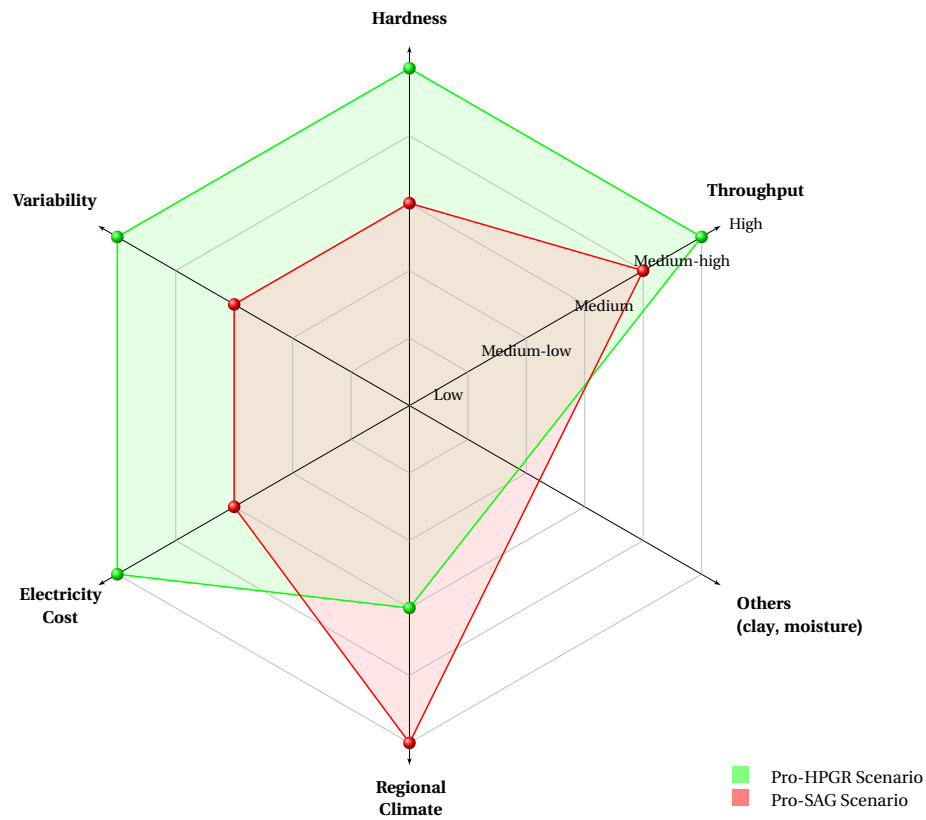
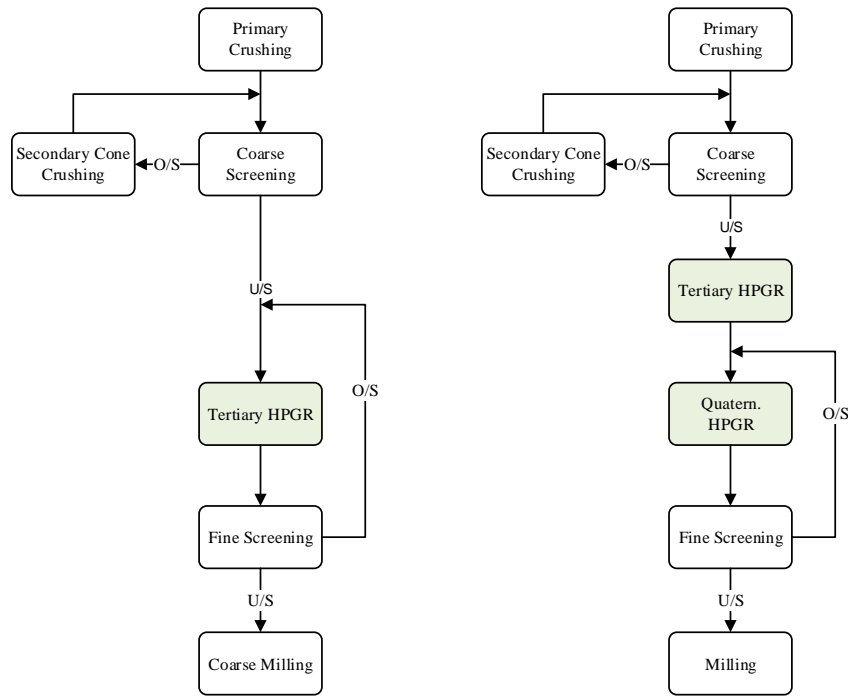


Figure 6.5: SAG/HPGR design consideration

6.2.4 Flowsheet development

Flowsheet development is an important step to ensure the comminution circuit is designed to its optimum potential for meeting project requirements (throughput and grind size, among others) and to address any potential issues for future operation (winter condition, high clay content, among others).

For greenfield projects, there are many variations of HPGR flowsheet designs. The flowsheet can use single stage HPGR or multiple stages of HPGRs. Each stage of the HPGR can be in an open circuit or a closed circuit with edge recycle or size classification that can be wet or dry (Van der Meer and Gruendken, 2010). Figure 6.6 shows some examples of the HPGR process flowsheet. The most adopted HPGR flowsheet in hard rock mining to-date is the closed circuit HPGR in tertiary crushing duty with dry or wet screening.



(Single stage, closed, tertiary)

(Multiple stages, tertiary & quaternary)

Figure 6.6: Greenfield HPGR flowsheet options

Some brownfield operations adopted the HPGR to optimize their comminution circuits. Figure 6.7 shows examples of HPGR applications for brownfield retrofit, including HPGR-SAG mill hybrid circuit (Lane et al., 2018) and HPGR in the pebble crushing circuit (Burchardt and Mackert, 2019). Possible flowsheet options for the winter condition are shown in Figure 6.8.

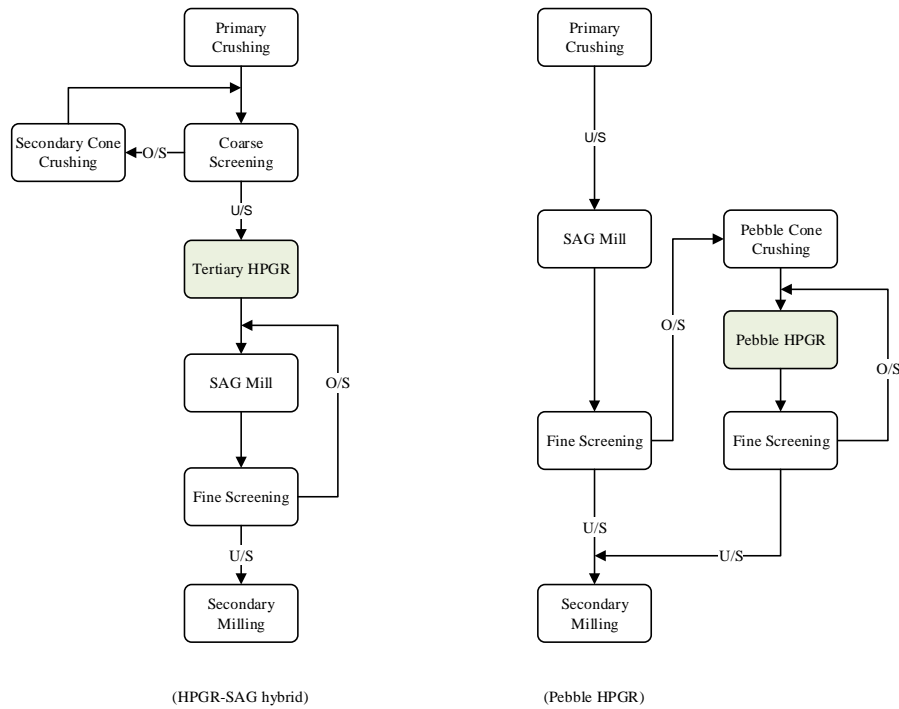


Figure 6.7: Brownfield HPGR flowsheet options

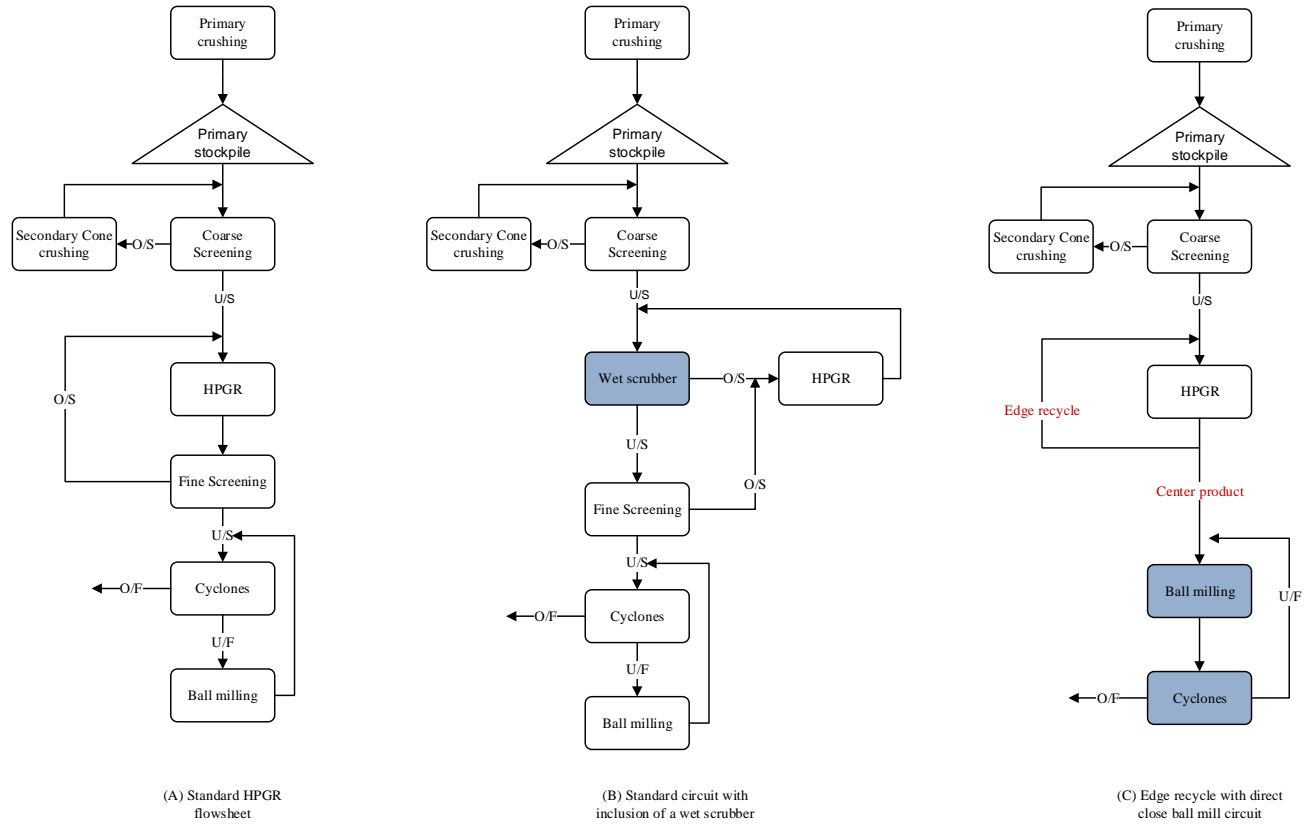


Figure 6.8: HPGR flowsheet options for the winter condition

6.3 HPGR Sizing Methods

Following the understanding of the process design criteria and flowsheet design, the HPGR machine sizing would be conducted. The conventional approach for HPGR sizing and selection is to perform a series of tests on pilot-scale HPGR (0.7-1.0 m roll diameter) and obtain scale-up parameters to predict the throughput and energy/size reduction relationship for a given ore. Large samples are generally required for such pilot test programs, typically 1-10 t, depending on the level of study and complexity of the resource. Collecting large representative samples during early-stage development is challenging and expensive. Meaningful geometallurgical studies to characterize the responses of different ore types to high-pressure comminution using pilot-scale HPGR are mostly impractical.

Ideally, the sizing and selection of the HPGR for a given application/flowsheet would be based on pilot scale HPGR test results and process design information. Figure 6.9 summarizes the interrelationship between the sizing parameters that are obtained from the pilot tests. The HPGR specific throughput constant (\dot{m}) is required to determine the HPGR roll dimension for the given project requirements. The specific pressing force information is required to determine the required grinding force. The specific energy consumption and throughput capacity information are used to decide the required motor size.

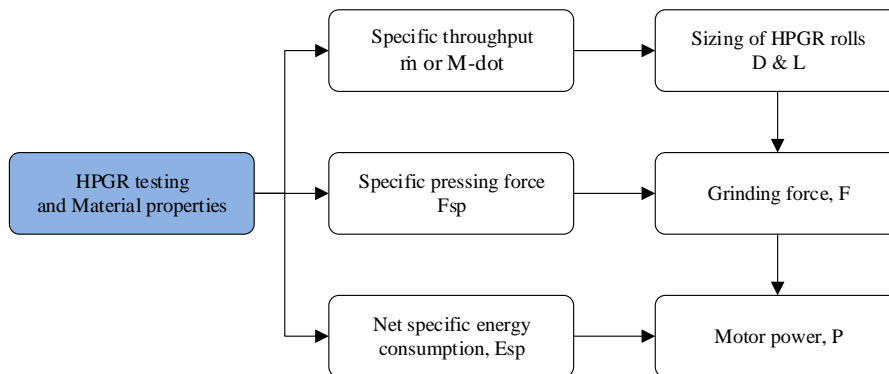


Figure 6.9: Interrelationship between HPGR scale-up parameters
(Source: Modified after Rashidi et al., 2017)

An example of a simple HPGR sizing exercise for a 40,000 t/d Copper Porphyry operation is provided in Table 6.3 with all sizing parameters obtained from the pilot HPGR tests. The first step is to determine the total HPGR machine feed, which is based on the circuit design feed and estimated circulating load. The circulating load can be recorded during a locked cycle test, or estimated based on the screen simulation with the HPGR product size from the open circuit tests. The next step is to determine the main motor power required for the design, which is based on the net specific energy and total HPGR machine feed, or the circuit specific energy and circuit throughput, followed by applying a typical drive-train efficiency of 95% and a motor design factor of 10%. Note that two motors are typical for the HPGR operation, and VSD would be required. The final step is to select the appropriate HPGR roll size for the application. This is determined based on the specific throughput constant (m) recorded from the pilot tests, and the required total machine throughput. Available roll sizes from the vendor catalog (in Table 6.4) are tried until a comfortable throughput margin could be obtained. Typically, the maximum HPGR roll speed should be no more than 23 rpm.

Table 6.3: Example of HPGR sizing

Description	Unit	Result	Comment
Step 1 Calculate total HPGR throughput			
Plant throughput	[dry t/d]	40,000	Design input
HPGR circuit availability	[%]	92	Design input
HPGR circuit feed	[dry t/h]	1,812	Design input
Screen cut-size	[mm]	6	Design input
Screen efficiency	[%]	90	Design assumption
HPGR product passing screen cut-size	[%]	70	Test work input
HPGR circulating load	[%]	59	Calculation
HPGR machine feed	[dry t/h]	2,876	Calculation
Step 2 Calculate main motor size			
Specific pressing force, F_{sp}	[N/mm ²]	3.5	Test work input
Net specific energy consumption, E_{sp}	[kWh/t]	2.0	Test work input
Total circuit specific energy consumption	[kWh/t]	3.2	Calculation
Motor drive-train efficiency	[%]	95	Design assumption
Total power requirement	[kW]	6,055	Calculation
Motor safety factor		1.1	Design assumption
Installed motor size (2 per HPGR unit)	[kW]	3,300	Calculation
Step 3 Calculate HPGR roll size			
Specific throughput constant, \dot{m}	[ts/hm ³]	280	Test work input
HPGR roll diameter	[m]	2.4	Vendor catalogue
HPGR roll length	[m]	1.65	Vendor catalogue
Roll peripheral speed - required	[m/s]	2.67	Calculation
Roll peripheral speed - max	[m/s]	2.89	Up to 23 rpm
Throughput margin	[%]	8	Calculation

Projects under different study phases would require different levels of accuracy for HPGR sizing and selection. Indicative HPGR sizing will be sufficient for projects at early stage, however, more accurate sizing will be required to increase the design confidence when projects progress to more advanced stages. The following methods provide practical solutions to facilitate the assessment of HPGR technology for a given project.

Table 6.4: Examples of HPGR production machines

Model	Working Surface		Grinding Force (kN)	Motor Power (kW)
	Diameter (mm)	Length (mm)		
9/7	950	650	2,700	2 × 220
11/8	1,100	800	3,400	2 × 450
14/8	1,400	800	4,300	2 × 500
14/10-17/12	1,400–1,700	950–1200	7,000	2 × 800
17/12-20/10	1,700–2,000	1,000–1,200	8,600	2 × 1,600
19/15-20/15	1,850–2,000	1,500	11,000	2 × 1,850
20/15-20/17	2,000	1,500–1,650	13,500	2 × 2,500
22/15-24/17	2,200–2,400	1,550–1,650	17,000	2 × 2,800
26/18	2,600	1,750	20,000	2 × 3,400
30/20	3,000	2,000	25,000	2 × 5,000

*ThyssenKrupp Polycom production machines

1. **Database method.** For an early stage project, accurate sizing of an HPGR would not be required. In the case of no available pilot HPGR test results, the database method can be used to approximate the HPGR sizing parameters. As discussed in Chapter 5, key HPGR sizing parameters can be modeled based on feed characteristics in the design criteria using the empirical models developed from the UBC HPGR database. Sometimes, the modeled value can be benchmarked against the industrial database to provide sensible sizing results. This method provides acceptable sizing information for HPGR selection that is needed for a conceptual level trade-off between a conventional comminution circuit and HPGR based circuit.
2. **PPT calibration method.** As the project progresses, higher accuracy of machine sizing and circuit design is required to improve the estimate accuracy of project economics. The PPT calibration method can provide physical information about the response of tested samples under confined particle-bed comminution. Empirical regression models (Davaanyam, 2015) developed from the previous test work conducted using UBC’s pilot HPGR unit and their PPT apparatus can be used to predict the specific energy consump-

tion, particle size reduction ratio and particle size distribution for the tested samples at varying HPGR specific pressing forces. However, previous works (Davaanyam, 2015) did not estimate the specific throughput constant (\dot{m}), an important HPGR sizing parameter. The method presented in Chapter 5 can therefore be used to model the HPGR power draw as a function of the feed material properties and applied pressure, which is estimated independently of the PPT results. Subsequently, the throughput capacity and \dot{m} can be determined using the combination of PPT results (E_{sp}) and the modeled power from the HPGR database. In addition, the PPT calibration method can be used to assess the ore variability across the deposit by performing PPT on a small amount of variability samples.

3. **HPGR calibration method.** As the project matures, performing a few pilot HPGR tests on a single composite is recommended to confirm the previous estimate of sizing parameters, since the most reliable method to estimate HPGR power requirement and throughput capacity is to test ore samples with a pilot- or full-scale HPGR unit. Furthermore, the HPGR calibration method can be applied to calibrate the previously conducted piston-die press tests to align the PPT results and pilot HPGR test results. This method is believed to provide additional confidence in HPGR circuit design, reduce the need to include conservatism in the equipment sizing and selection, as well as provide information on ore variability which is difficult to obtain through only the pilot test program.

Current industrial practices require significant amount of samples and testing for each phase of the project. A new framework for sizing the HPGR is proposed, aiming at reducing sample and testing requirements while meeting the project requirement as per the respective study phase. Table 6.5 compares the proposed HPGR sizing approach at different study phases against current industrial practices. Current practises may provide more accurate information about a particular composite sample in question, but it does not support variability evaluation so the obtained information for the deposit may be less accurate. The proposed method has the merit of testing ore variability across the deposit due to the inclusion of PPT variability tests.

Table 6.5: Testing, sizing and selection of HPGR

Study Level	Definition / Objective	Current Practices	Proposed Practices
Conceptual/Scoping	Define project options	1 single pass pilot test	Benchmark database (e.g. UBC HPGR database)
Preliminary	Amenability study, evaluate the impact of HPGR comminution on downstream processes	3-4 pilot tests at different specific pressing force	PPT calibration test PPT variability tests
Prefeasibility	Confirm sizing and selection of the machine as well as to generate data for design of the complete HPGR comminution circuit	Specific pressing force – 4 tests Moisture effect – 2 tests Top size effect – 2 tests Roll speed effect – 2 tests Closed circuit – 3 tests	Limited number of pilot HPGR testing for HPGR-Piston calibration and additional variability tests
Feasibility	Confirm selection of an HPGR in the process flowsheet, definitive cost estimate	Pre-feasibility + Ore variability	Full suite of HPGR tests

6.4 Case Studies from Conceptual to Feasibility

6.4.1 Project background

This section provides a simplified example to demonstrate the above-mentioned methods for HPGR sizing and evaluation at different project phases, from conceptual study to feasibility study. The goal is to develop a 40,000 t/d HPGR based comminution circuit for Project G (No. 6 in Table 3.1). The local climate of Project G is characterized by cold winters and warm summers. The all-in power cost for Project G is assumed to be CA\$ 0.1/kWh. The battery limit is defined as the primary crusher product to the flotation feed. Table 6.6 shows the general process design criteria defined for the processing plant.

Table 6.6: General process design criteria for Project G

Description	Unit	Project G
Project location	[-]	Northern Canada
Ore type	[-]	Gold
Mine life	[Years]	12
Throughput, Annual	[Mt/a]	14.6
Daily Throughput	[t/d]	40,000
Crushing Plant Availability	[%]	75
Process Plant Availability	[%]	92
Crushing Hourly Feed Rate	[t/h]	2,381
Process Plant Hourly Feed Rate	[t/h]	1,812
ROM Moisture Content	[wt%]	3.0
Grind Size, P_{80}	[mm]	0.10

6.4.2 Conceptual design and trade-off

The main objective of the conceptual study is to assess the possible technologies and associated flowsheet configurations in the given project setting. Very often, HPGRs do not arise as a possible solution due to limited test work available in the early stage, even though it could have been a technically viable and cost effective alternative for the project. Therefore, there is a need to allow early consideration of HPGR in the absence of specific HPGR characterization test work, so that the overall benefits and capital efficiency can be captured and quantified.

General comminution test work

During the initial phase of the project, limited comminution test work has been conducted on selected drill core samples from Project G. Test work included JK DWT and Bond-style work indices tests, but no specific HPGR characterization work has been conducted. Table 6.7 presents the comminution test work results and their selection basis for the design criteria. The general understanding of ores from Project G is fairly competent in terms of SAG milling, and medium hardness for ball milling.

Table 6.7: Summary of comminution tests at conceptual level

Description	Unit	Value	Basis
Ore Specific Gravity, SG	[g/cm ³]	2.8	Average
JK Axb Parameter	[-]	30.0	75 th percentile
Bond Crusher Work Index, CWI	[kWh/t]	20.0	75 th percentile
Bond Ball Work Index, BWI	[kWh/t]	15.0	75 th percentile
Bond Abrasion Index, Ai	[g]	0.3	Average

Flowsheet options

Based on the initial comminution test data, two conventional flowsheet options were proposed for the trade-off assessment. One is the SAG mill based circuit, as shown in Figure 6.10. This circuit is commonly referred to as the “SABC” circuit, comprising SAG mill, ball mill, and pebble crusher.

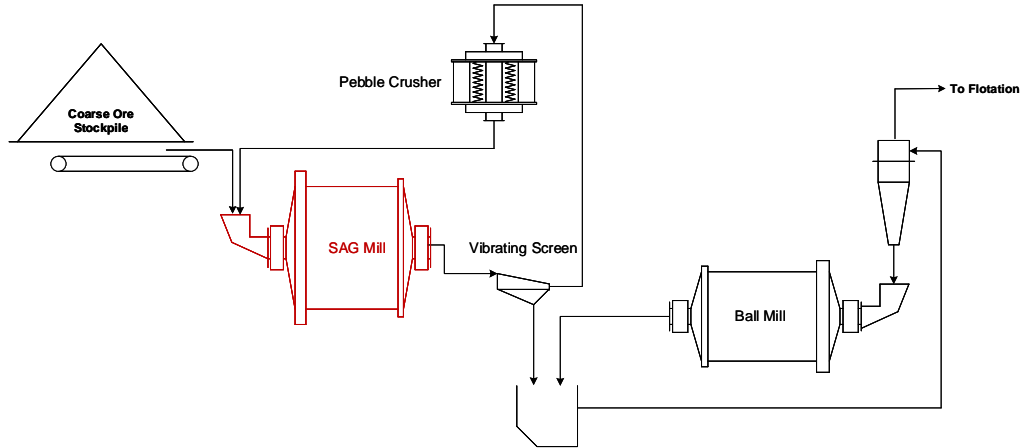


Figure 6.10: Simplified SABC flowsheet

The alternative option is a standard HPGR based circuit, as shown in Figure 6.11. This option is configured as stage crushing followed by closed circuit HPGR in tertiary crushing, and then closed ball milling circuit. This circuit is referred to as the HPGR-ball mill circuit.

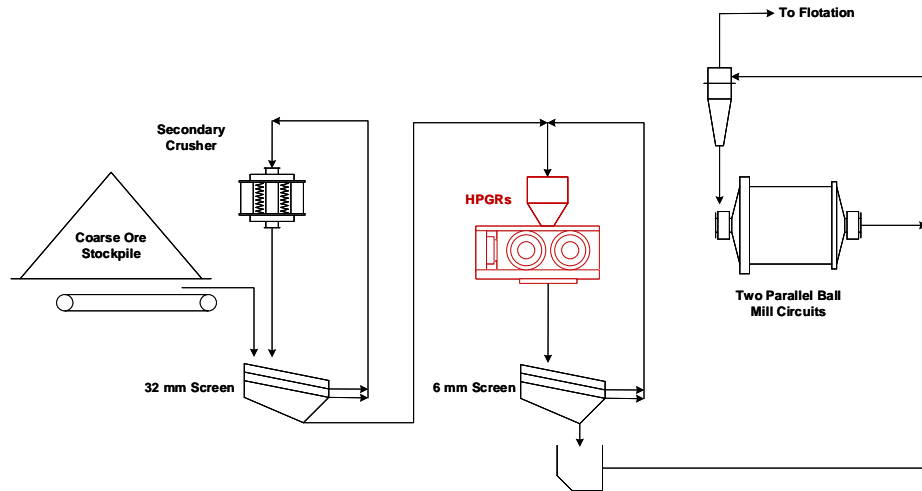


Figure 6.11: Simplified HPGR-Ball mill flowsheet

Equipment sizing, selection and quantity

The selected SABC circuit was modeled using the JK SimMet™ and the F. Bond equation. This method utilizes the A_{xb} and t_a results from the JK DWT (or SMC test) to estimate the power requirement for the SAG mill. The transfer size (T_{80}) indicated in the simulation is then used to size the ball mill based on the Bond equation with standard Bond/Rowland correction factors (Rowland, 1973). A screen snapshot of the JK SimMet™ simulation results for the SABC circuit is shown in Figure 6.12. As a result, one 40' x 22' EGL SAG mill with 22,400 kW installed motor power and two parallel 22' x 40.5' ball mills each with 11,000 kW installed power were selected to support the preliminary design.

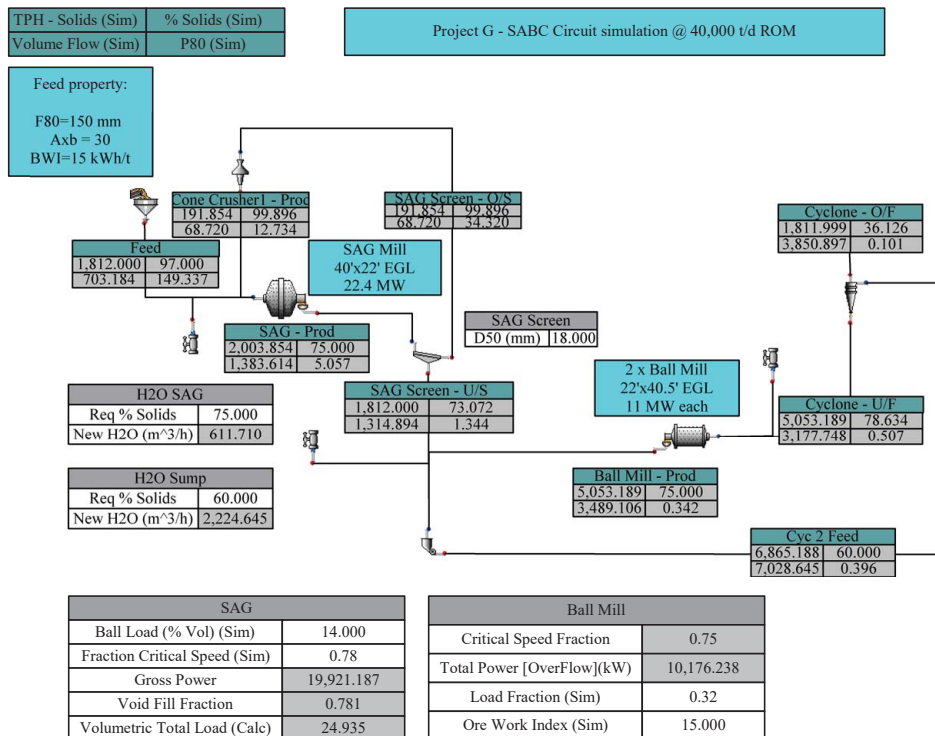


Figure 6.12: SABC circuit simulation in JK SimMet™

In designing the HPGR circuit, the secondary crushing circuit was modeled using the Metso Bruno® simulator, and the ball mill sizing was developed based on the Bond equation with standard Bond/Rowland correction factors. In the absence

of the HPGR test work, the sizing of HPGR was carried out using the “Database method”. The key sizing parameters, namely power draw, net specific energy consumption, specific throughput constant, and product PSDs can be determined for a given ore sample with the following material properties.

1. Ore type
2. Feed size distribution including F_{80} , F_{50} and $F_{0.1mm}$
3. Feed moisture content
4. Material bulk density
5. PSD normalization master curve (subject to ore type)

Empirical regression models (developed in Section 5.3) and the material properties defined in the design criteria, are used to estimate the pilot HPGR performance for Project G, as demonstrated in Table 6.8 and Figure 6.13. The HPGR circuit feed was estimated from the Bruno[®] simulation of the secondary crushing circuit.

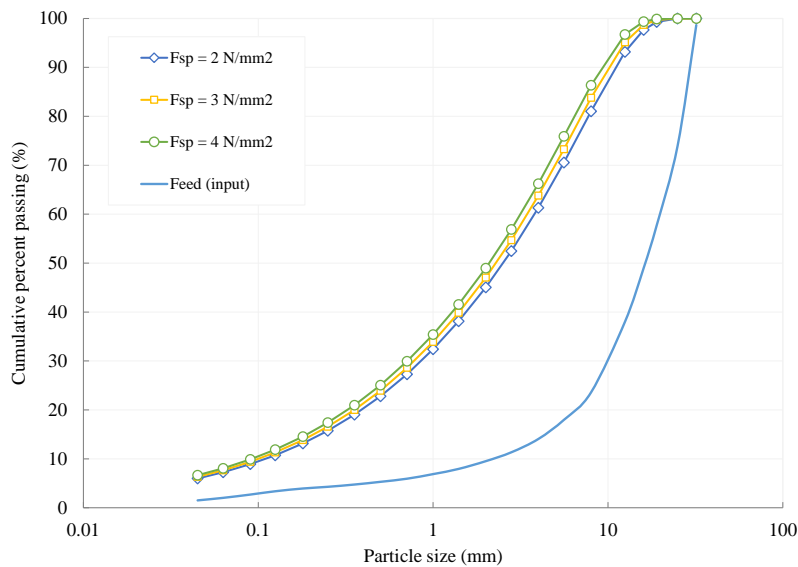


Figure 6.13: Modeled HPGR feed and product PSDs

Table 6.8: Prediction of pilot HPGR based on given feed characteristics

Description	Unit	Sim-1	Sim-2	Sim-3	Remarks
Basic Data (inputs)					
Ore type	-		Au		
Feed size F_{80}	[mm]		27		Bruno [®]
Feed size F_{50}	[mm]		16		Bruno [®]
Feed size $F_{0.1mm}$	[%]		3		Bruno [®]
Feed bulk density	[g/cc]		1.6		
Feed moisture	[%]		3		
Normalization parameter, A	[-]		0.70		Master curve
Normalization parameter, m	[-]		0.05		Master curve
Normalization parameter, n	[-]		0.60		Master curve
HPGR Parameters					
HPGR roll diameter	[m]		0.75		Pilot
HPGR roll length	[m]		0.22		Pilot
Roll peripheral speed	[m/s]	0.75	0.75	0.75	Assumed
Specific pressing force	[N/mm ²]	2.0	3.0	4.0	Input
Total pressing force	[kN]	330	495	660	Calculated
Calculations					
HPGR power draw	[kW]	48.9	61.0	73.2	Equation 5.12
Net specific energy	[kWh/t]	1.56	2.03	2.49	Equation 5.13
Specific throughput	[ts/hm ³]	206	207	208	Equation 5.9
Reduction ratio RR_{80}	[-]	3.3	3.6	3.9	Equation 5.15
Percentage passing 6 mm	[%]	72	75	78	Normalization

Table 6.9 summarizes the major comminution equipment selected for the SABC circuit and the HPGR-ball mill circuit. The information is considered preliminary but useful for the initial evaluation of the project.

Table 6.9: Major comminution equipment - SAG and HPGR circuit

Description	Unit	SABC	HPGR-ball mill
Secondary Crusher			
Quantity	[#]	-	2
Size	[-]	-	MP1000
Power (each)	[kW]	-	750
HPGR			
Quantity	[#]	-	1
Size	[-]	-	2.40 m D x 1.80 m W
Power (each)	[kW]	-	8,000
SAG Mill			
Quantity	[#]	1	-
Size	[-]	40' x 22' EGL	-
Power (each)	[kW]	22,400	-
Pebble Crusher			
Quantity	[#]	2	-
Size	[-]	MP800	-
Power (each)	[kW]	600	-
Ball Mills			
Quantity	[#]	2	2
Size	[-]	22' x 40.5'	22' x 36.5'
Power (each)	[kW]	11,000	12,000

Trade-off comparison

Table 6.10 compares the pure comminution specific energy predicted for Project G between the SABC circuit and the HPGR-ball mill circuit. The energy saving of 21.2% was obtained, which is in an agreement with other published trade-off studies (Wang et al., 2013; Costello and Brown, 2015). It should be noted that the total energy savings will be reduced when the material handling (conveyors and pumps) and other ancillary requirements (screens and fans, among others) are included.

Table 6.10: Comparison of pure comminution circuit specific energy

Description	Unit	SABC	HPGR- ball mill
Secondary Crushing	[kWh/t]	-	0.7
HPGR	[kWh/t]	-	4.0
SAG Milling	[kWh/t]	10.8	-
Pebble Crushing	[kWh/t]	0.2	-
Ball Milling	[kWh/t]	11.3	12.8
Total Specific Energy	[kWh/t]	22.2	17.5
Pure Comminution Energy Savings	[%]	-	21.2

For a conceptual study, order-of-magnitude cost estimates would typically suffice the project requirement. Following the major equipment sizing and selection, the capital and operating cost estimate for the SAG and HPGR based circuits over the proposed mine life (12 years) were developed and summarized in Table 6.11. Although the CAPEX is high for the HPGR based circuit, the OPEX is considerably lower than the SAG mill based circuit. The Net Present Cost (NPC) was then determined to compare the economics of the different options. In this case, the NPC calculation for the two options used typical discounted cash flow parameters, including a discount rate of 5% and an inflation rate of 2%. The results suggest that the HPGR based circuit is more economically favorable for Project G, as the HPGR based circuit outperformed by CAD 125 million over the life of mine.

Table 6.11: Summary of CAPEX and OPEX

Description	Unit	SABC	HPGR- ball mill
Direct Capital Cost	[\$M CAD]	200	230
Indirect Capital Cost	[\$M CAD]	100	115
Total Capital Cost	[\$M CAD]	300	345
Labour	[CAD/t milled]	0.06	0.09
Power	[CAD/t milled]	2.56	2.08
Maintenance	[CAD/t milled]	0.29	0.28
Consumables	[CAD/t milled]	2.20	1.50
Total Operating Cost	[CAD/t milled]	5.1	3.9
Total Operating Cost	[\$M CAD/a]	74.6	57.6
NPC	[\$M CAD]	1,045	920
NPC in favor of HPGR	[\$M CAD]	-	125

Following the economic comparison between the two options, several sensitivity analysis can be performed to evaluate the impact of different input variables on the trade-off. Figure 6.14 shows the sensitivity of the NPC to the unit power cost. As can be seen, the SABC circuit consistently results in a higher NPC as compared to the HPGR circuit, regardless of the unit power price. It is suggested that significant savings achieved in consumables (grinding media in particular) is another deciding factor that makes the project more favorable towards the HPGR option.

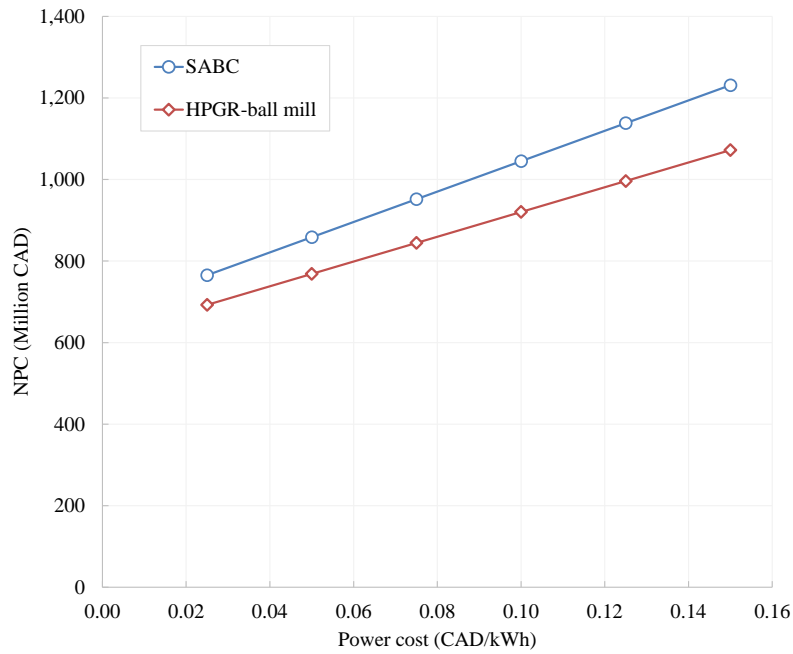


Figure 6.14: Sensitivity of the NPC to power cost

An additional sensitivity analysis was performed to assess the impact of capital cost estimate on overall project economics. Figure 6.15 reveals that for the two options to have the same NPC value, the CAPEX of the HPGR based option is required to increase by approximately 36% to CAD 469 million. This is equated to be 56.4% higher than the SAG option, and any increase below that would still favor the HPGR option.

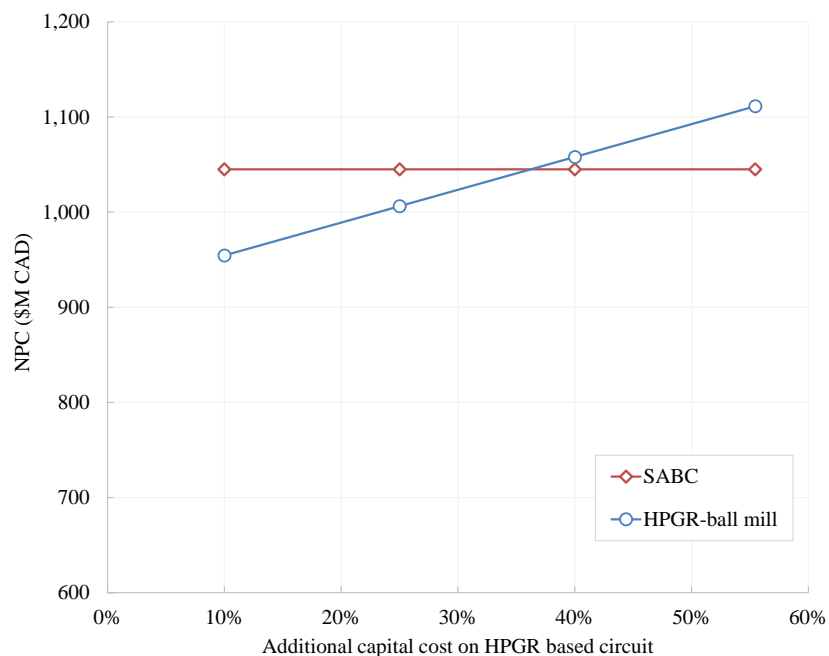


Figure 6.15: Sensitivity of the NPC to CAPEX

The process flowsheet options using the SABC circuit and HPGR based circuit were then subject to a high-level SWOT analysis. The assessment results of the major factors influencing the merits of each option are summarized in Table 6.12. The HPGR based circuit appeared to provide significant potential benefits to the project. Therefore, the HPGR is recommended to be included in the next phase of the project for a closer evaluation. A PPT test program can be recommended upon completion of this phase.

Table 6.12: High-level SWOT analysis

Description	SABC	HPGR-ball mill
CAPEX, Million CAD	300	345
OPEX, Million CAD	75	58
Strength	<ul style="list-style-type: none"> -Simple circuit -Low CAPEX -Low housekeeping effort -Low maintenance system 	<ul style="list-style-type: none"> -High energy efficiency -Low OPEX (power and media) -Circuit stability -Simple process control -No confined space entry -Fast production ramp-up -GHG emission reduction
Weakness	<ul style="list-style-type: none"> -Poor SAG mill energy efficiency -Difficult to operate and control -Lack of predictability in production -Throughput fluctuation -Throughput limitation -High OPEX (power and media) -Relining in confined space 	<ul style="list-style-type: none"> -High CAPEX -Complex circuit -Additional dust collection -Additional ore storage - Cold climate limitation -Higher earthwork requirements
Opportunity	<ul style="list-style-type: none"> -Geometallurgy program -High-energy blast -Ore sorting -Circuit expansion with pre-crusher -Process optimization 	<ul style="list-style-type: none"> -Use of energy efficient technology -Alternative flowsheet variation -Process optimization
Threat	<ul style="list-style-type: none"> -Throughput pitfall 	<ul style="list-style-type: none"> -HPGR tire damage
Overall assessment	Technically acceptable	Technically acceptable, economically favorable

6.4.3 Preliminary assessment

Advancing to the preliminary assessment, specific feed characterization test work for the HPGR should be performed to confirm the amenability of HPGR comminution and refine the design criteria. It is proposed to perform the Piston-die Press Testing (PPT) on the selected drill core samples, followed by applying the “Calibration method” to obtain useful information to refine the sizing and selection of

HPGR. Variability assessment using pilot HPGR testing is more challenging due to the large sample requirement; the PPT enables the evaluation of ore variability due to its small sample requirement. Variability assessment provides improved confidence in HPGR sizing and selection for the project.

Methodology

The PPT calibration method uses the results from the PPT program to provide the responses of tested samples to pilot scale HPGR comminution, and it then followed by the HPGR sizing. Figure 6.16 describes the overall “calibration” methodology for determining HPGR sizing parameters. The procedure involves calibrating the specific pressing force and particle size reduction ratio from the PPT according to the UBC HPGR/PPT database. The power draw and specific throughput constant parameters are estimated using empirical equations derived from the UBC HPGR database. Subsequently, the predicted net specific energy consumption, product size distribution, and specific throughput constant at varying specific pressing forces in the pilot scale can be obtained, which enables preliminary sizing of the HPGR based on the results of the PPT.

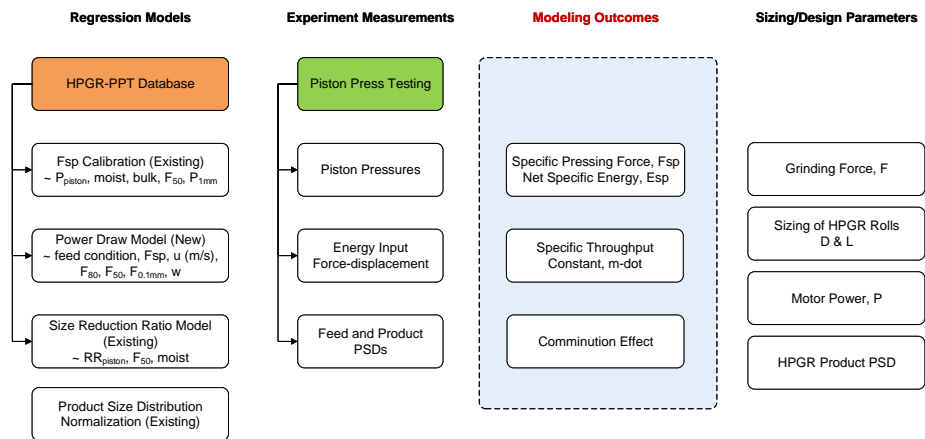


Figure 6.16: HPGR preliminary sizing methodology

Specific pressing force model The empirical model used to calibrate the specific pressing force is provided by Equation 6.1 (Davaanyam, 2015).

$$P_{piston} = 5.53 + 53.3F_{sp} + 24.3w - 86.2\rho_{bulk} + 13.1F_{50}^{HPGR} - 44.4\frac{F_{50}^{HPGR}}{F_{50}^{piston}} + 2.98P_{1mm}^{piston} \quad (6.1)$$

where P_{piston} is the PPT piston pressure in MPa; F_{sp} is the HPGR specific pressing force in N/mm²; w is the HPGR feed moisture content in % by weight; ρ_{bulk} is the feed bulk density in g/cm³; F_{50}^{HPGR} is the 50% passing size of the HPGR feed in mm; F_{50}^{piston} is the 50% passing size of the PPT feed in mm; and P_{1mm}^{piston} is the fraction passing 1 mm in the PPT test feed in %. The required PPT piston pressure can be estimated using the HPGR specific pressing force and other relevant material properties. The specific energy consumption at the corresponding specific pressing force can then be determined directly from the PPT specific energy calculation (total energy input divided by the sample mass).

HPGR power draw model As described in Chapter 5, the HPGR power draw can be estimated by Equation 5.12, which is an expanded form of Equation 5.6.

$$P = -62.31 - 1.09\text{feed} + 87.14u + 12.19F_{sp} + 0.529F_{80} + 0.669F_{0.1mm} + 0.067wF_{80} \quad (5.12 \text{ revisited})$$

where “feed” refers to feed PSD condition (“0” is normal, “1” is abnormal condition e.g. blended or truncated feed); u is the HPGR roll peripheral speed in m/s; F_{sp} is HPGR specific pressing force in N/mm²; F_{80} is the 80% passing feed size in mm; $F_{0.1mm}$ is the percentage passing 0.1 mm (fines) in the feed; w is the feed moisture content.

Throughput model As expressed in Equation 5.9, the HPGR specific throughput constant (\dot{m}) is a function of HPGR power draw and specific energy consumption. The specific energy consumption can be determined from PPT performed on the sample, which is used to estimate the \dot{m} using Equation 5.9.

$$\dot{m} = \frac{W}{DLu} = \frac{P_{net}}{E_{sp}DLu} \quad (5.9 \text{ revisited})$$

where \dot{m} is the specific throughput constant in ts/hm^3 ; W is the HPGR throughput capacity in t/h ; D is the HPGR roll diameter in m ; L is the HPGR roll length in m ; P_{net} is the HPGR net power draw in kW ; E_{sp} is the net specific energy consumption in kWh/t , and u is the HPGR peripheral roll speed in m/s .

Size reduction model The size reduction achieved in the pilot scale HPGR can be calibrated using the reduction ratio model in Equation 6.2 (Davaanyam, 2015).

$$RR_{HPGR} = 1.86 + 1.41RR_{piston} + 2.31 \frac{F_{50}^{HPGR}}{F_{50}^{piston}} - 0.41F_{50}^{HPGR} - 1.02w \quad (6.2)$$

where RR_{HPGR} is the size reduction ratio based on 50% passing feed size (F_{50}) to 50% passing the full product size (P_{50}) for the pilot HPGR testing, and RR_{piston} is the size reduction ratio (F_{50}/P_{50}) for PPT. The HPGR full product refers to the combined center and edge product based on the mass proportion observed from the HPGR test.

Size distribution normalization model As discussed in the literature review, researchers have shown that the PSD of the HPGR and PPT products for samples processed at different pressing force settings are self-similar and can therefore be normalized by dividing by their median particle size (Fuerstenau et al., 1991; Fuerstenau et al., 1996; Davaanyam, 2015). The normalized PPT product PSD is fitted to Equation 2.4 using the size reduction ratio information obtained in Equation 6.2. The normalized curves for the PPT products can then be converted to the predicted product PSDs of the pilot HPGR.

$$F\left(\frac{x}{X_{50}}\right) = 100 \left\{ 1 - \exp \left[-A \left(\frac{x}{X_{50}}\right)^{m\left(\frac{x}{X_{50}}\right)+n} \right] \right\} \quad (2.4 \text{ revisited})$$

where $F\left(\frac{x}{X_{50}}\right)$ is the cumulative percent passing at $\frac{x}{X_{50}}$ size; $\frac{x}{X_{50}}$ is the dimensionless size normalized by dividing by the median particle size of the product; and A, m, n are fitted model parameters.

Piston-die press test work

During the preliminary assessment of Project G, the PPTs were performed on two composite samples (Comp1 and Comp2). The variability testing was also performed to measure the relative ore hardness of six (6) lithologies (S1 through S6). It should be noted that S1 to S4 samples were collected from the same ore domain as the Comp1, and S5 and S6 were collected from the same ore domain as the Comp2. For each sample, four (4) different piston pressures were applied. Test results at the highest piston pressure are summarized in Table 6.13 and Table 6.14, with detailed test results provided in Appendix B.

Table 6.13: Results of PPT on Project G composite samples

Description	Unit	Comp1	Comp2
Piston Pressure	[MPa]	240	240
Specific Energy	[kW/t]	1.85	2.05
F ₈₀	[mm]	10.20	10.36
F ₅₀	[mm]	6.95	6.58
P ₈₀	[mm]	4.93	5.14
P ₅₀	[mm]	1.39	1.57
F ₈₀ /P ₈₀	[-]	2.07	2.02
F ₅₀ /P ₅₀	[-]	5.00	4.21

Table 6.14: Results of PPT on Project G variability samples

Description	Unit	S1	S2	S3	S4	S5	S6
Piston Pressure	[MPa]	240	240	240	240	240	240
Specific Energy	[kW/t]	1.84	1.80	1.90	1.81	2.13	1.99
F ₈₀	[mm]	10.71	10.44	10.39	9.80	10.34	10.46
F ₅₀	[mm]	7.42	7.20	6.82	5.89	7.20	6.60
P ₈₀	[mm]	5.08	5.57	5.18	4.85	4.98	4.85
P ₅₀	[mm]	1.47	1.56	1.58	1.37	1.47	1.54
F ₈₀ /P ₈₀	[-]	2.11	1.87	2.01	2.02	2.08	2.16
F ₅₀ /P ₅₀	[-]	5.05	4.61	4.32	4.30	4.90	4.29

Figure 6.17 shows the linear relationship between the piston pressure and piston specific energy consumption for the Comp1 and Comp2 samples. Similar trends were obtained for other tests performed on the variability samples.

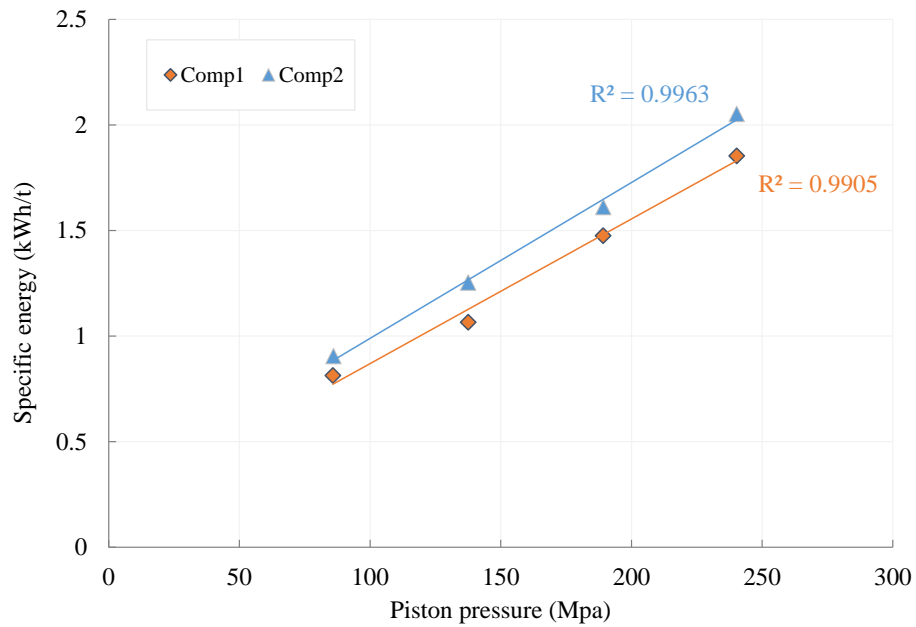


Figure 6.17: Relation between piston pressure and specific energy

Figure 6.18 shows the feed and product particle size distributions from the PPT on Comp1 and Comp2. Figure 6.19 shows that the size reduction ratio linearly correlated to the applied energy inputs for Comp1 and Comp2. By comparing Figure 6.17 and Figure 6.19, the Comp2 sample is harder than Comp1 sample, because the product size from Comp2 test was coarser even though the applied energy input was higher.

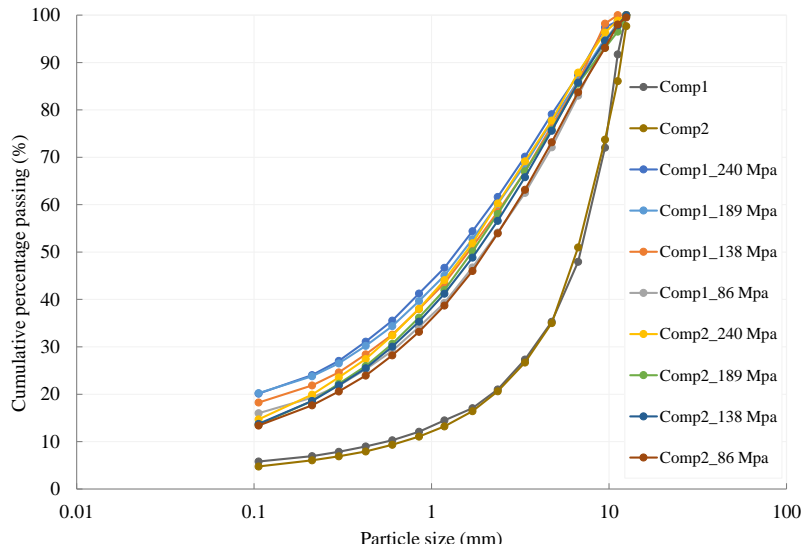


Figure 6.18: PPT feed and product PSDs

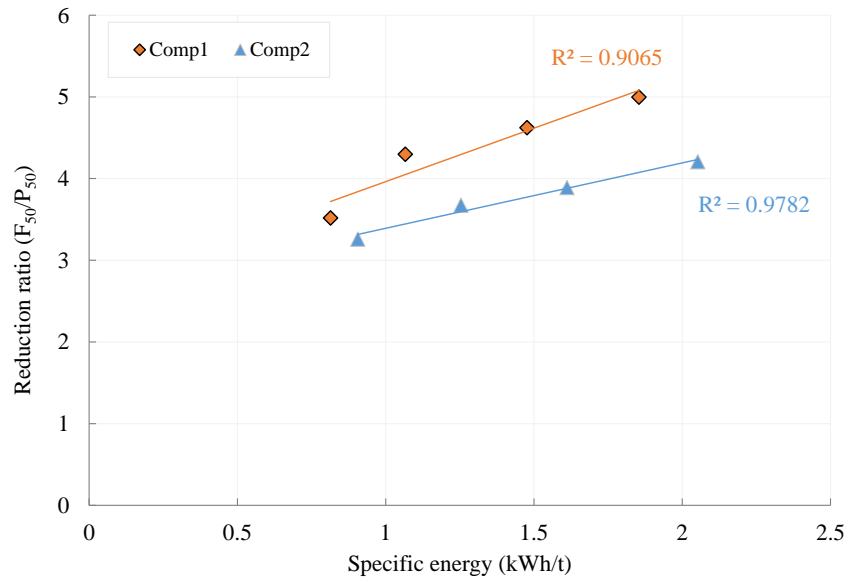


Figure 6.19: Relation between piston specific energy consumption and size reduction ratio

PPT calibration results and interpretation

The “PPT Calibration method” was used to calibrate the results obtained from the PPT and then to predict the key HPGR sizing parameters that could have been obtained from pilot scale HPGR testing. All calculations were performed for an HPGR feed F_{50} of 16 mm and a moisture content of 2.5%. This was selected based on historical HPGR test work.

To estimate the HPGR net specific energy consumption, the HPGR specific pressing force was first calibrated to the piston pressure using Equation 6.1. The corresponding PPT pressure was then used to estimate the HPGR net specific energy consumption using the relation between piston pressure and specific energy obtained from PPT. Figure 6.20 compares the net specific energy consumption predicted from the PPT for the composite and variability samples. On average, the variability samples required lower specific energy consumption compared to the composite samples at the same specific pressing force.

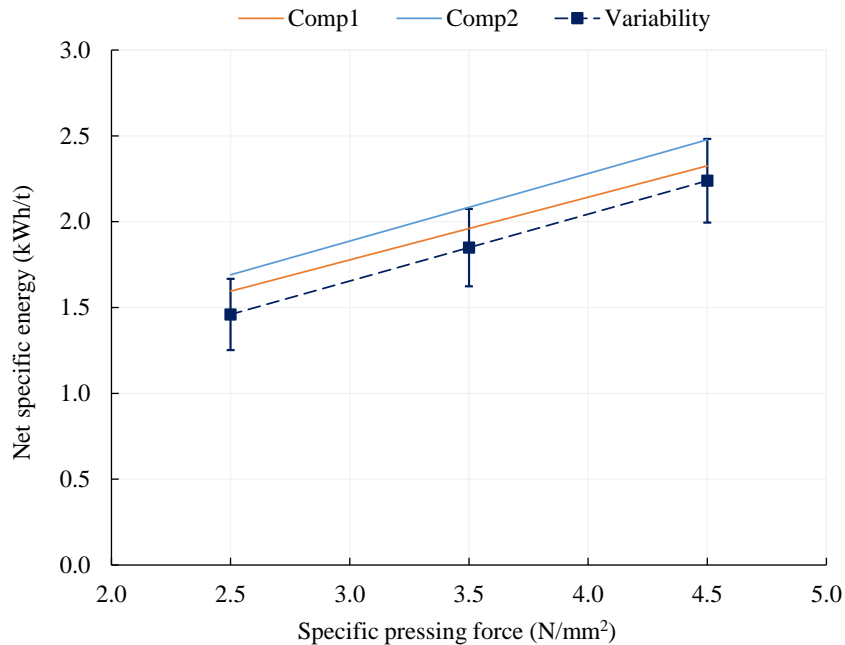


Figure 6.20: Predicted net specific energy as a function HPGR pressing force (error bars represent 95% confidence intervals)

The next step is to calibrate the HPGR reduction ratio (F_{50}/P_{50}) to the PPT reduction ratio. The relation between piston pressure and PPT reduction ratio was used to estimate the PPT reduction ratio at calibrated piston pressures and then used to estimate the HPGR reduction ratio using Equation 6.2. Figure 6.21 compares the size reduction ratio (F_{50}/P_{50}) predicted from the PPT for the composite and variability samples. As can be seen, the Comp2 sample yielded the lowest size reduction ratio at the same specific pressing force.

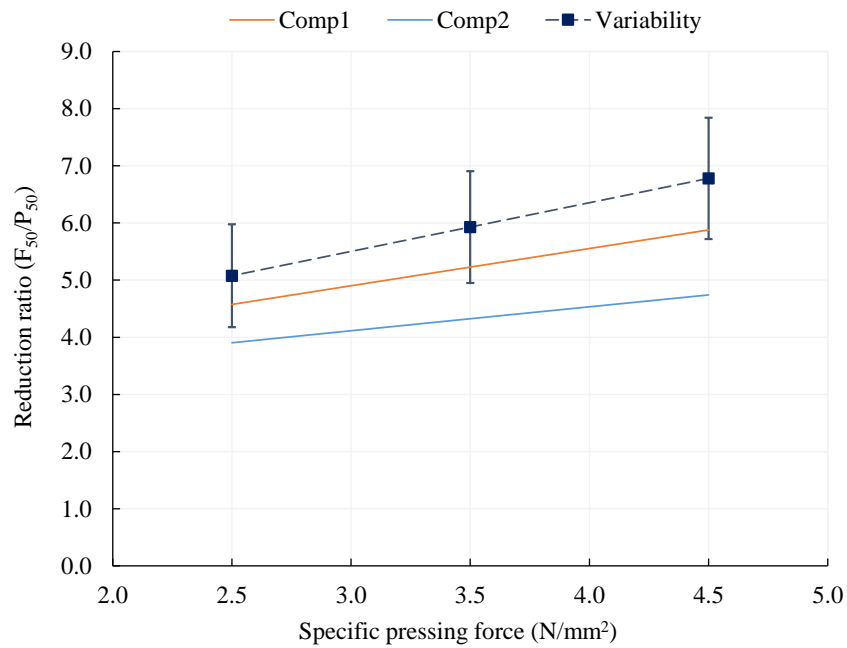


Figure 6.21: Predicted reduction ratio as a function of HPGR pressing force (error bars represent 95% confidence intervals)

After predicting the HPGR specific energy consumption and expected reduction ratio, the normalized PPT product distributions were fitted to Equation 2.4. The normalized curves for the PPT products then can be converted to the product size distribution of the HPGR. The normalized PPT product size distributions for Comp1 and Comp2 samples are shown in Figure 6.22, from which an excellent agreement among all normalized distributions was observed.

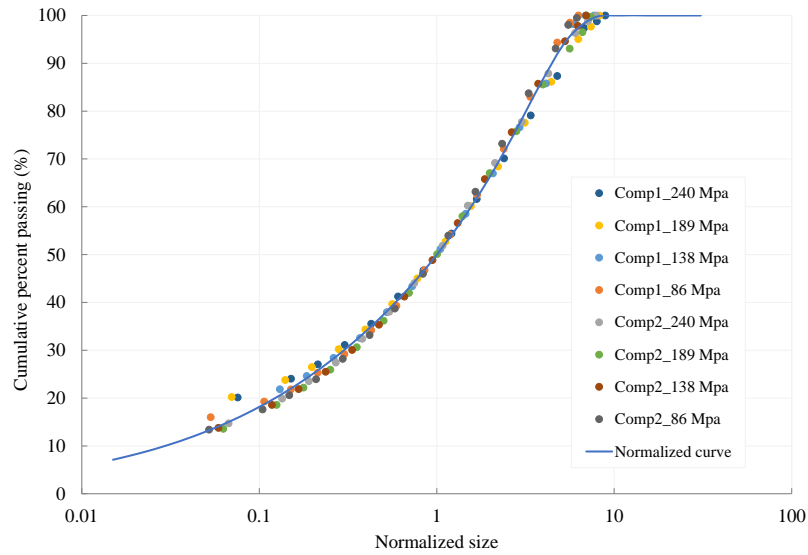


Figure 6.22: Normalized piston product size distributions

Using the fitted model, calibrated reduction ratio, and normalized sizes, the pilot HPGR product PSDs were determined for different specific pressing forces. The predicted HPGR product PSDs for Comp1 and Comp2 samples are shown in Figure 6.23. At the same specific pressing force, the Comp1 sample produced finer product PSDs.

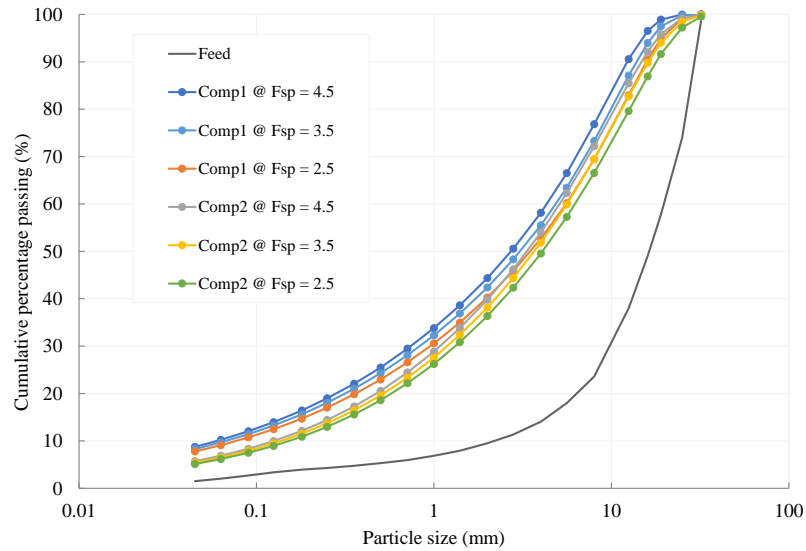


Figure 6.23: Predicted pilot HPGR product size distributions for composite samples

Figure 6.24 compares the percent passing 6 mm predicted from the PPT performed on the composite and variability samples. The percent passing 6 mm from the pilot HPGR product PSD was used to estimate the recirculating load for a closed circuit HPGR with a 6 mm screen, assuming a 90% screen efficiency. For the tested specific pressing force range, a higher specific pressing force provides a greater energy input to the sample, which results in smaller product sizes (i.e. a greater percentage passing 6 mm) and thus a smaller recirculating load.

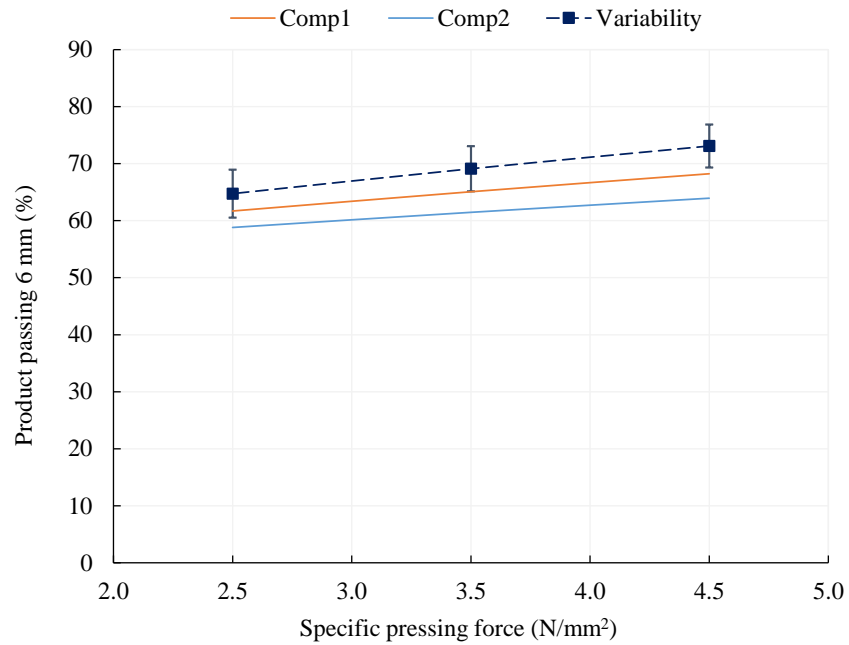


Figure 6.24: Predicted % -6mm of pilot HPGR product (error bars represent 95% confidence intervals)

The circuit-specific energy requirements for the UBC pilot HPGR operating in a closed circuit with a 6 mm screen at different specific pressing force settings were determined using the estimated recirculating load, assuming a 95% efficiency in the calculation to account for the drive-train energy loss. Figure 6.25 compares the total circuit-specific energy calculated from PPT on the composite and variability samples. It confirmed that Comp2 sample is harder than other samples, based on its highest circuit energy requirement among all tested samples. It was also found that the circuit-specific energy consumption varied considerably among the six lithological units tested using the variability samples. At a specific pressing force of 3.5 N/mm², the average circuit-specific energy consumption of 3.15 kWh/t was calculated with a coefficient of variation of 17%.

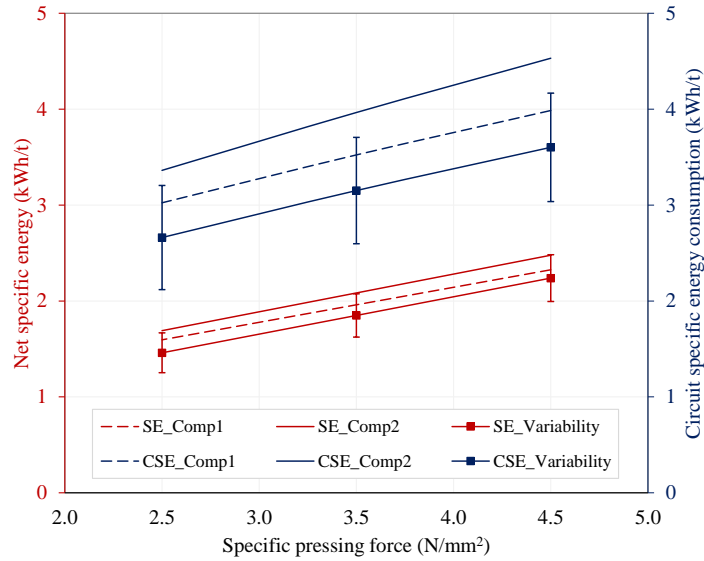


Figure 6.25: Predicted circuit specific energy consumption (error bars represent 95% confidence intervals)

To assess the overall throughput capacity of the UBC pilot HPGR operating in a closed circuit, the HPGR-specific throughput constant and the corresponding recirculating load need to be considered. This can be determined from the circuit-specific throughput constant (\dot{m}_c), which is equal to the specific throughput constant divided by 1 plus the recirculating load ratio as expressed in Equation 6.3.

$$\dot{m}_c = \frac{\dot{m}}{1 + CL} \quad (6.3)$$

where \dot{m}_c is the circuit-specific throughput constant in ts/hm^3 , \dot{m} is the specific throughput constant in ts/hm^3 , and CL is the recirculating load in %.

Figure 6.26 presents the predicted specific throughput constant (\dot{m}) and circuit-specific throughput constant (\dot{m}_c) for the composite and variability samples. Typically, a higher specific pressing force corresponds to a smaller operating gap and results in reduced specific throughput; however, the product particle size decreases in response to the higher specific energy input and higher specific pressing force. Overpredicting the specific energy input at a given specific pressing force will likely result in an underprediction of specific throughput. Figure 6.26 shows

that the circuit-specific throughput was marginally affected by the specific pressing force settings.

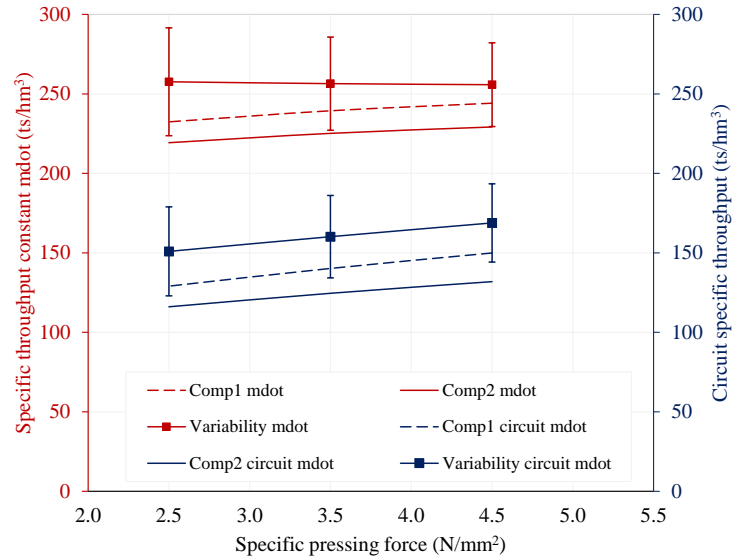


Figure 6.26: Predicted circuit throughput as a function of HPGR pressing force (error bars represent 95% confidence intervals)

Preliminary HPGR sizing and selection

In this phase, the sizing of the HPGR was carried out using the PPT calibration method. Physical tests and empirical regression models were used to determine/obtain the pilot HPGR performance and sizing parameters for Project G. The sizing parameters arising from the PPT assessment (Comp1) were used to ensure a sufficient margin of safety for the design. Table 6.15 summarizes the calculation performed for preliminary HPGR sizing based on the PPT results. As a result, a 2.4 m x 1.8 m HPGR with an installed grinding force of 17,000 kN and a total motor power of 7,700 kW (two 3,850 kW motors) was recommended for Project G. A nominal specific pressing force of 3.5–4.0 N/mm² was selected.

Table 6.15: HPGR sizing - PPT calibration method

Description	Unit	Result	Comment
Step 1 Calculate total HPGR throughput			
Plant throughput	[dry t/d]	40,000	Design Input
HPGR circuit availability	[%]	92	Design Input
HPGR circuit feed	[dry t/h]	1,812	Design Input
Screen cut-size	[mm]	6	Design Input
Screen efficiency	[%]	90	Design Assumption
HPGR product passing screen cut-size	[%]	65-68	PPT on Comp1
HPGR circulating load	[%]	63-71	Calculation
HPGR machine feed	[dry t/h]	3,041-3,189	Calculation
Step 2 Calculate main motor size			
Specific pressing force, F_{sp}	[N/mm ²]	3.5-4.5	PPT on Comp1
Net specific energy consumption, E_{sp}	[kWh/t]	2.0-2.3	PPT on Comp1
Total circuit specific energy consumption	[kWh/t]	3.5-4.0	Calculation
Motor drive-train efficiency	[%]	95	Design Assumption
Total power requirement	[kW]	6,557-7,006	Calculation
Motor size selection (2 per HPGR unit)	[kW]	3,850	Calculation
Step 3 Calculate HPGR roll size			
Specific throughput constant, m	[ts/hm ³]	239-244	Prediction
HPGR roll diameter	[m]	2.4	Vendor catalogue
HPGR roll length	[m]	1.8	Vendor catalogue
Roll peripheral speed - required	[m/s]	2.9	Calculation
Roll peripheral speed - max	[m/s]	2.9	
Throughput margin	[%]	-	Calculation

6.4.4 Pre-feasibility assessment

The purpose of a pre-feasibility study is to confirm sizing and selection of the machine as well as to generate data for design of the complete HPGR comminution circuit. Once the project advanced to the pre-feasibility level, some pilot HPGR tests should be conducted to confirm the sizing parameters. The previously conducted PPT can be directly calibrated against pilot HPGR tests to establish ore-specific calibration models. Subsequently, it would improve the prediction accuracy from the

PPT on variability samples instead of relying on the database prediction. Overall, comparing to simply conducting pilot HPGR tests, the proposed approach has the advantage of supporting more extensive variability studies.

Pilot HPGR test work

During the pre-feasibility phase of the Project G, pilot HPGR tests were performed on two composite samples (Comp1 and Comp2) that had been previously used in the PPT program. No variability tests were performed on the pilot scale due to sample availability. A summary of main test results is presented in Table 6.16, including critical indicators of HPGR comminution performance. All tests were performed with a feed moisture content of 2.5%, and a roll speed of 0.75 m/s. Again, the pilot test program confirmed that the Comp2 sample is harder than the Comp1 sample, at the same specific energy input. Comp2 tests also yielded coarser product sizes (e.g. lower size reduction).

Table 6.16: Summary of pilot HPGR test results - Project G

No.	Sample	Test #	F_{sp} N/mm ²	E_{sp} kWh/t	\dot{m} ts/hm ³	P_{80} mm	P_{50} mm	-6mm %
1	Comp1	Au(G)-D01	5.0	3.1	228	5.98	1.79	80
2	Comp1	Au(G)-D02	4.0	2.6	236	7.22	2.27	76
3	Comp1	Au(G)-D03	2.6	1.9	246	8.45	2.62	71
4	Comp2	Au(G)-P01	4.5	2.9	226	7.22	2.12	75
5	Comp2	Au(G)-P02	3.6	2.2	226	8.19	2.58	72
6	Comp2	Au(G)-P03	2.6	1.8	235	10.25	3.63	63

Test results for Comp1 showed a slight decrease in the specific throughput with the increase of specific pressing force due to a reduced operating gap. The specific throughput constant was ranging from 226 ts/hm³ to 246 ts/hm³ for tested materials, with an average value of 233 ts/hm³ and a coefficient of variation of 3%.

HPGR-PPT calibration

By now, two composite samples (Comp1 and Comp2) have been subject to both PPT and pilot HPGR testing, therefore the HPGR calibration method can be applied

to improve the assessment of ore variability. The calibration procedure involves correlating results of pilot HPGR and PPT conducted on the same feed sample. Once the specific calibration is established for the composite sample, the HPGR responses for varying ore types, lithologies and alterations can be predicted from the PPT performed on a range of variability samples. Results of the PPT were first used to calibrate the energy-size reduction models between the pilot HPGR and PPT, followed by more accurate HPGR sizing and selection. The main steps were followed for the HPGR-PPT calibration.

Step 1: Calibration of HPGR specific pressing force and piston pressure The pressure-energy relationship obtained from PPT and pilot HPGR tests can be correlated. Figure 6.27 shows the fitted regression lines for net specific energy versus HPGR specific pressing force and piston pressure. As shown in the graph, an HPGR specific pressing force of 4.0 N/mm² is equivalent to a piston pressure of 350 MPa, which deliver the same specific energy of 2.55 kWh/t to the tested sample. The obtained correlation can be used to predict the specific energy consumption at varying HPGR specific pressing forces for the variability samples.

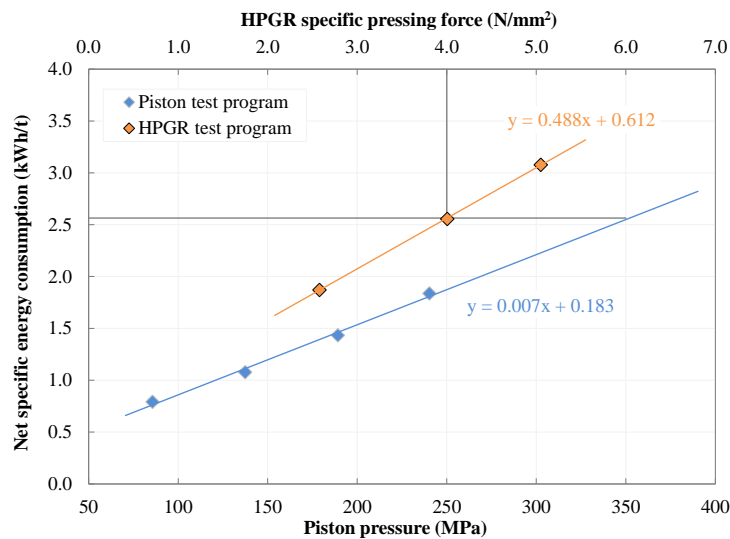


Figure 6.27: Calibration of HPGR specific pressing force and piston pressure for Comp1 sample

Figure 6.28 compares the net specific energy consumption predicted from PPT on variability samples to those recorded from pilot HPGR tests on Comp1 and Comp2 samples. As can be seen, the results from pilot tests perform on the composite samples fall into the predicted envelop based on the variability tests. The specific energy consumption does not vary significantly at the same applied specific pressing force.

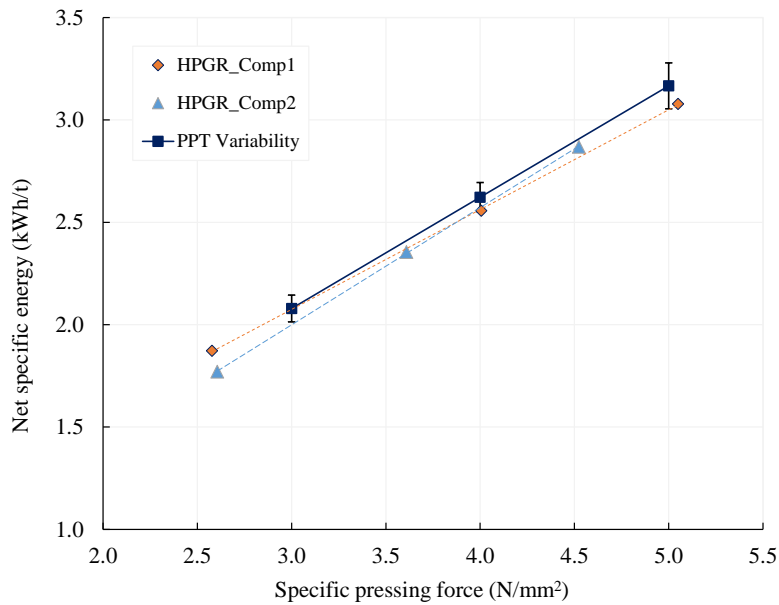


Figure 6.28: Specific pressing force versus net specific energy consumption (error bars represent 95% confidence intervals)

Step 2: Calibration of HPGR and PPT size reduction ratio The energy input-size reduction relationship for given PPT and pilot HPGR tests are correlated as shown in Figure 6.29. Unlike Bond type energy-breakage equations where the 80% passing size is used, the HPGR-PPT calibration selects the 50% passing size to describe the feed and product particle sizes. The size reduction ratios are therefore determined by the F_{50}/P_{50} . The obtained correlation can be used to predict the size reduction for the variability samples.

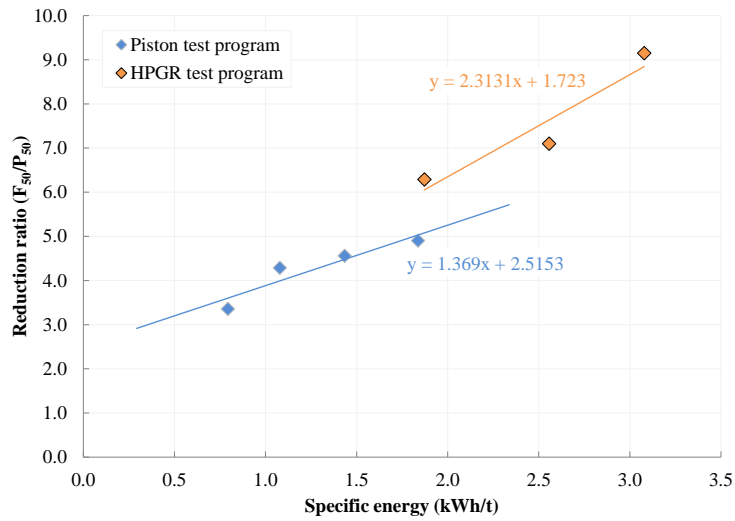


Figure 6.29: Calibration of HPGR and piston size reduction

For each lithological unit, the F_{50}/P_{50} reduction ratio was determined by applying the regression trend obtained in Figure 6.29 to corresponding PPT results. Figure 6.30 compares the size reduction ratio of HPGR tests on composite samples to those predicted from PPT on variability samples. Figure 6.30 also shows that results from pilot tests performed on the composite samples fall into the predicted envelop based on the variability tests. The mean of the predicted size reduction ratio at a specific pressing force of 4.0 N/mm^2 was 6.9 ± 1.4 with 95% confidence.

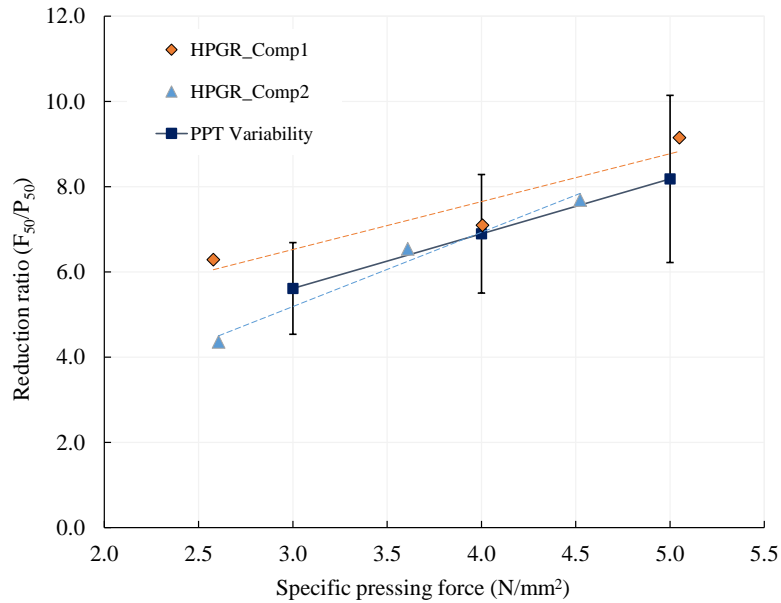


Figure 6.30: Specific pressing force versus reduction ratio (error bars represent 95% confidence intervals)

Step 3: Confirmation of matching normalized PSDs from HPGR and PPT To scale-up the product PSDs from the PPT to the pilot HPGR, the normalized product PSDs need to match, despite the differences of feed top sizes and applied pressures. Figure 6.31 shows an excellent agreement between the normalized PSDs for products from the pilot HPGR tests on -32 mm composite samples, and the PPT on -12.5 mm variability samples. The results confirmed that the normalized curves from PPT can be used to predict the HPGR product PSDs for Project G.

Figure 6.32 compares the percent passing 6 mm predicted from PPT on variability samples using the normalization parameters to those measured from HPGR tests on Comp1 and Comp2 samples. It can be seen that results from pilot tests perform on the composite samples fall into the predicted envelop based on the variability tests. The mean of the predicted percent passing 6 mm size at a specific pressing force of 4.0 N/mm² was 73±6.5% with 95% confidence. The percent passing 6 mm from the HPGR product can be used to estimate the recirculating load for an HPGR circuit closed with a 6 mm screen.

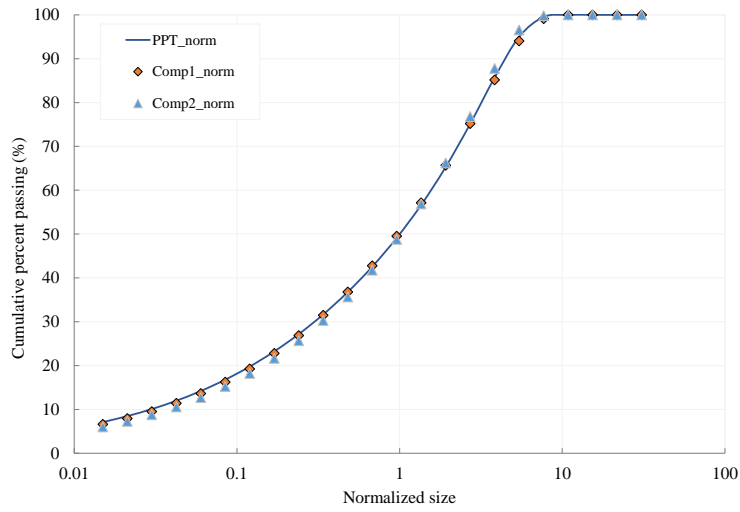


Figure 6.31: Normalized HPGR and piston product size distributions

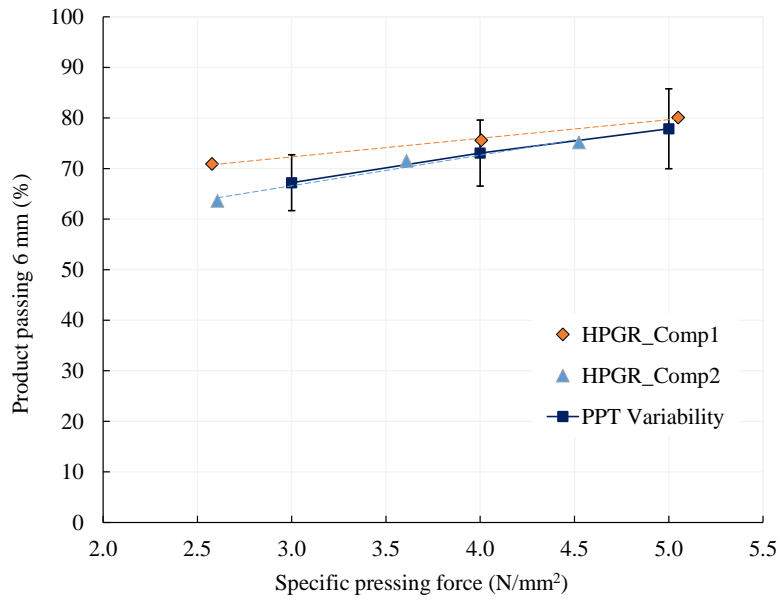


Figure 6.32: Specific pressing force versus percent passing 6 mm (error bars represent 95% confidence intervals)

Step 4: Determination of circuit throughput and specific energy Figure 6.33 compares the specific throughput constant and circuit-specific throughput constant predicted from PPT on variability samples to those determined from pilot HPGR tests on Comp1 and Comp2 samples. Overall, the specific pressing force appeared to have a limited impact on the specific throughput constant, but the circuit-specific throughput improved slightly at higher pressure settings due to reduced circulating load. The mean of the predicted specific throughput constant and circuit-specific throughput constant at a specific pressing force of 4.0 N/mm² were 256±29 ts/hm³ and 168±17 ts/hm³ with 95% confidence, respectively.

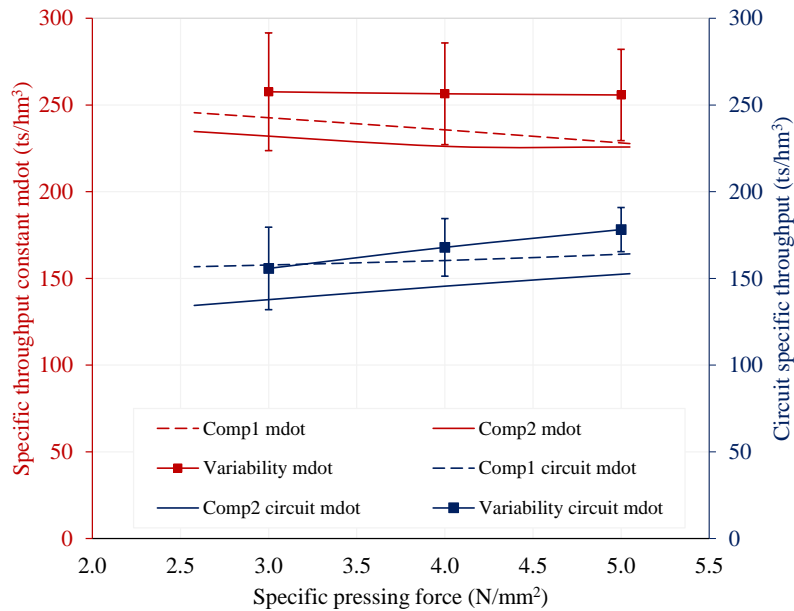


Figure 6.33: Predicted circuit throughput as a function of HPGR pressing force (error bars represent 95% confidence intervals)

Figure 6.34 compares the net specific energy consumption and circuit-specific energy consumption predicted from PPT on variability samples to those determined from pilot HPGR tests on Comp1 and Comp2 samples. The mean of the predicted circuit specific energy consumption at a specific pressing force of 4.0 N/mm² was 4.22±0.33 kWh/t with 95% confidence.

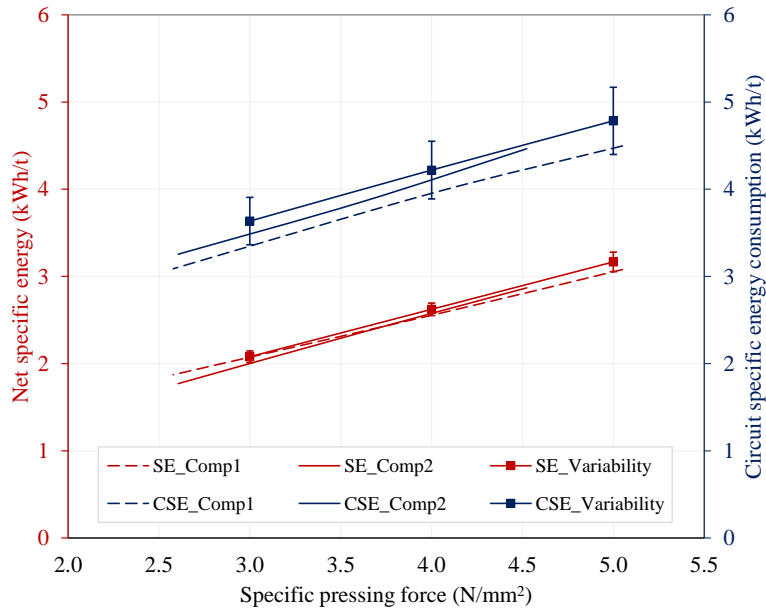


Figure 6.34: Predicted circuit specific energy consumption (error bars represent 95% confidence intervals)

Equipment sizing verification

After reviewing the results of pilot HPGR and laboratory PPT testing programs, key HPGR sizing parameters were developed and are summarized in Table 6.17. The calibrated PPT results were used to inform the ore variability.

Table 6.17: Comparison of HPGR sizing parameters

Description	Unit	Pilot HPGR tests			Piston press tests*		
		5.0	4.0	3.0	5.0	4.0	3.0
F_{sp}	N/mm ²	5.0	4.0	3.0	5.0	4.0	3.0
E_{sp}	kWh/t	3.1	2.6	2.0	3.2±0.1	2.6±0.1	2.1±0.1
\dot{m}	ts/hm ³	225	231	237	256±26	256±29	258±34
%-6mm	%	79	74	69	78±8	73±7	67±6
Circulating load	%	40	50	60	44±14	53±13	66±14

*Note: mean values with 95% confidence interval.

Table 6.18 shows the HPGR sizing results based on the results of pilot HPGR and PPT testing programs. A nominal specific pressing force of 3.5 N/mm² was selected. Consequently, a 2.4 m x 1.8 m HPGR with an installed grinding force of 17,000 kN and a total motor power of 8,000 kW (two 4,000 kW motors) was selected for Project G for processing 40,000 t/d of ores.

Table 6.18: HPGR sizing confirmation - HPGR-PPT calibration method

Description	Unit	Result	Comment
Step 1 Calculate total HPGR throughput			
Plant throughput	[dry t/d]	40,000	Design Input
HPGR circuit availability	[%]	92	Design Input
HPGR circuit feed	[dry t/h]	1,812	Design Input
Screen cut-size	[mm]	6	Design Input
Screen efficiency	[%]	90	Design Assumption
HPGR product passing screen cut-size	[%]	63-76	HPGR-PPT
HPGR circulating load	[%]	46-74	Calculation
HPGR machine feed	[dry t/h]	2,730-3,240	Calculation
Step 2 Calculate main motor size			
Nominal specific pressing force, F_{sp}	[N/mm ²]	3.5	HPGR-PPT
Net specific energy consumption, E_{sp}	[kWh/t]	2.3-2.5	HPGR-PPT
Total circuit specific energy consumption	[kWh/t]	3.3-4.3	Calculation
Motor drive-train efficiency	[%]	95	Design Assumption
Total power requirement	[kW]	6,500-8,400	Calculation
Motor size selection (2 per HPGR unit)	[kW]	4,000	Calculation
Step 3 Calculate HPGR roll size			
Specific throughput constant, m	[ts/hm ³]	226-289	HPGR-PPT
HPGR roll diameter	[m]	2.4	Vendor catalogue
HPGR roll length	[m]	1.8	Vendor catalogue
Roll peripheral speed - required	[m/s]	2.6-2.8	Calculation
Roll peripheral speed - max	[m/s]	2.9	
Throughput margin	[%]	Up to 10%	Calculation

6.4.5 Feasibility level assessment

In a feasibility study, a full suite of pilot scale HPGR tests would be typically recommended to fully understand the effect of other process variables on the HPGR comminution performance. By doing so, the project will achieve ultimate confidence with the HPGR sizing and circuit design, and improve the accuracy of the cost estimate for the proposed solution. In addition, performing these pilot test programs is required to obtain the performance guarantee from the HPGR vendors, prior to finalizing the selection of HPGR in the process flowsheet. Six major pilot scale HPGR test programs that would be examined at a feasibility level are:

1. **Specific pressing force (3-4 tests)** - These should have been undertaken during the pre-feasibility study on the composite sample.
2. **Moisture content adjustment (2 tests)** - Evaluates the effect of feed moisture content on HPGR comminution performance.
3. **Top size variation (2 tests)** - Examines the effect of feed top size on HPGR comminution performance.
4. **Variation of roll speed (2 tests)** - Evaluates the effect of roll speed on HPGR comminution performance.
5. **Re-circulating load test (3 tests)** - Evaluates the effect of the re-circulating load on HPGR performance. Essentially, the closed circuit testing is performed to simulate an HPGR operating in closed circuit with a screen under the proposed plant conditions, thus allowing sizing and selection of supporting equipment such as screens and conveyors in the comminution circuit.
6. **Wear test** - Determine the wear rate of different ores in the high pressure comminution process, and calculate the expected wear life on an industrial scale HPGR.

Upon completion of the feasibility study, all stakeholders including the owner, engineering firms and technology suppliers collaborate to prepare a comprehensive plan for the project implementation.

6.5 Summary and Conclusions

The case studies provided in this chapter demonstrate that the PPT can be used to facilitate the sizing and selection of HPGRs from scoping level to feasibility level studies. The intent is not to limit the methods that provide higher HPGR sizing accuracy, but to offer more tools to facilitate the evaluation of HPGR technology. The proposed framework requires significantly lower sample quantities for each phase of the study.

The standalone PPT calibration method is only suitable for ore types and projected operating conditions that are within the ranges represented in the UBC HPGR-PPT database. The current UBC HPGR-PPT database is limited to tertiary- and quaternary-stage crushing applications, thus the developed PPT models might not be applicable for the HPGR fine grinding or iron-ore pellet-feed preparation. Continuous effort is required to expand the database and improve the empirical models. Furthermore, the simplicity and accuracy of the PPT models, and the small sample requirement for testing, make this an ideal method for geometallurgical programs, allowing HPGR performance to be predicted for varying lithologies or ore types across a deposit.

Chapter 7

HPGR Modeling and Simulation

7.1 Introduction

This chapter describes the overall structure of the holistic UBC HPGR model incorporating the empirical regression models (Chapter 5), PPT calibration models (Chapter 6) and the energy-based PBM models. This chapter focuses on the aspect of the population balance approach, integrating the ore specific breakage characteristics and associated breakage events within the HPGR comminution process. Two HPGR PBM models are presented, an ore specific model and a generic model. Both models enable the HPGR simulation and prediction of the center and edge product PSDs for varying ore hardness and other operating conditions. The ore specific HPGR model requires model fitting to a specific pilot test program. The generic HPGR model was developed based on a model fitting to a large pool of pilot tests performed with the UBC pilot HPGR on a range of ore types. At the end of the chapter, the proposed HPGR PBM model was tested and evaluated using tests performed at a different laboratory, where a different size HPGR was used.

7.2 HPGR Modeling

The current research is built upon previous work (Davaanyam, 2015) in an effort to advance the models and to develop a holistic approach for HPGR modeling and simulation. The updated model now incorporates the critical gap model, and an energy split model in the compression zone to define the energy distribution between the center and edge zones, which in turn allows prediction of center and edge product PSD independently. A simulation package “UBC-HPGR-Simulator” was developed that bundles empirical models developed from the UBC HPGR-PPT database, and semi-empirical models based on mono-size PPT for breakage characterization.

7.2.1 UBC HPGR model structure

There are five key components for HPGR process modeling:

- HPGR power draw
- HPGR specific energy consumption
- HPGR throughput
- Ore breakage characterization
- HPGR energy-size reduction

Empirical models for predicting HPGR power draw, specific energy consumption and throughput were covered in previous chapters, based on the UBC HPGR database (Chapter 5) or PPT calibration (Chapter 6). The mono-size PPT procedure developed by Davaanyam (2015) was adopted to determine breakage characteristics of the tested material. The resulting breakage and appearance functions were used in the energy-based PBM to simulate the HPGR performance.

Figure 7.1 illustrates the proposed procedure using the UBC HPGR model. Following this procedure, it is possible to simulate and optimize the HPGR process provided that HPGR model parameters and ore characterization data are available. The HPGR modeling and simulation can be carried out using the Excel-based “UBC-HPGR-Simulator”, to assist the HPGR circuit design and process optimization.

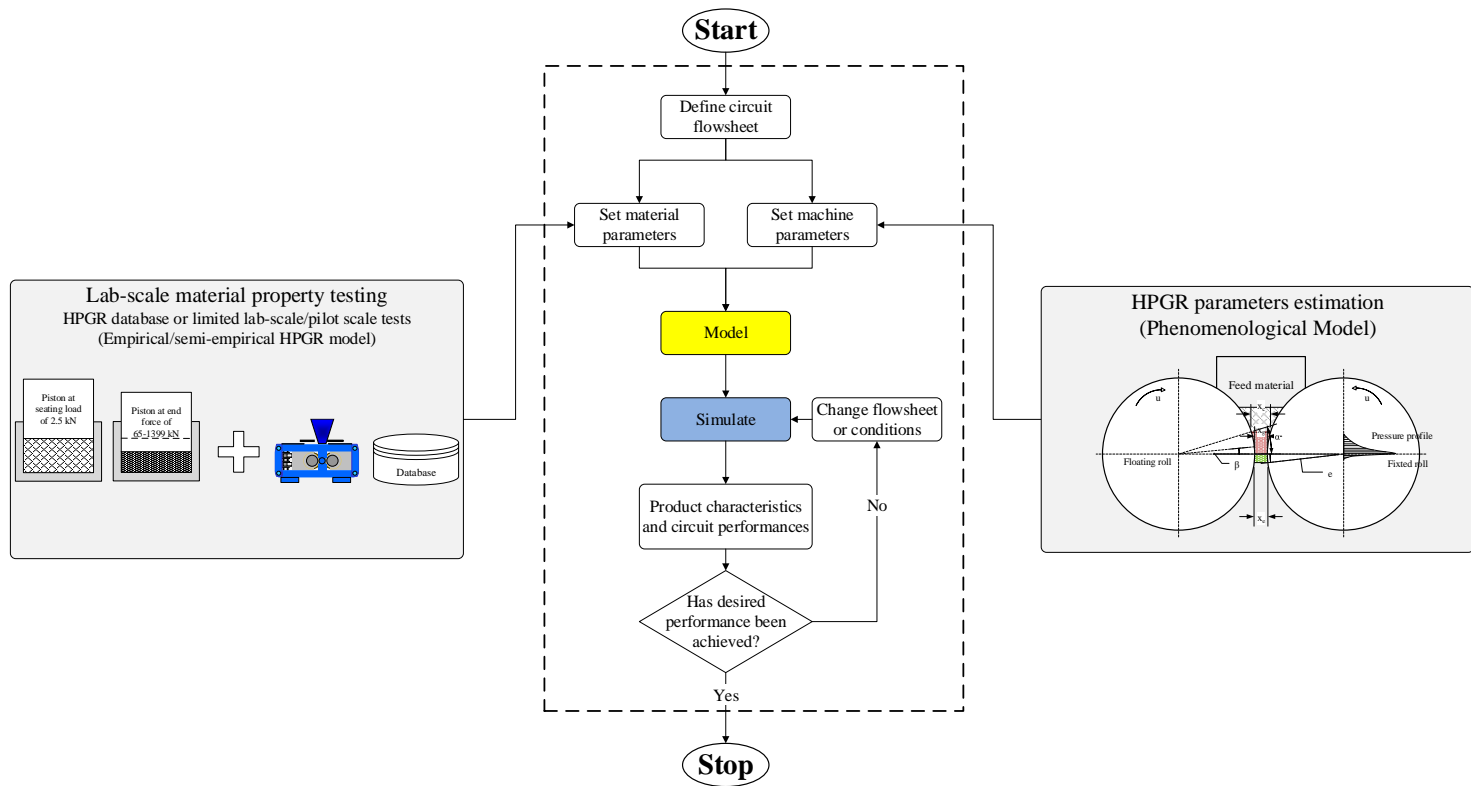


Figure 7.1: The proposed procedure for simulation to optimize design or performance

7.2.2 Ore breakage characterization

Ore characterization for compression breakage comprises three key components:

1. Compression breakage model Breakage under confined compression can be described by Equation 2.19 (Davaanyam, 2015). The relationship between applied specific energy and the progeny PSD can be determined by conducting laboratory PPT on narrowly sized particles. Results from the testing are fitted to this energy-breakage model to determine the size-by-size breakage characteristics of the sample under confined compression breakage. This model is mainly used to simulate the coarse particle breakage in the pre-crushing zone, where particles larger than the critical gap experiences compression breakage.

$$t_{10} = M \left\{ 1 - \exp(-f_{mat} \cdot x^n \cdot E_{sp}) \right\} \quad (2.19 \text{ revisited})$$

2. Fines corrected compression breakage model Due to the presence of fines in the feed, Davaanyam (2015) modified the breakage model to consider the effect of fines on the breakage performance. The modified model is referred to as the fines corrected compression breakage model, which is expressed in Equation 2.27. This model is used to simulate the particle breakage in the grinding zone (or compression zone), where the fines are present and experiencing compression breakage along with the coarse particles.

$$t_{10} = (M - c \cdot q_f) \left(1 - \exp(-f_{mat} \cdot x^n \cdot E_{sp}) \right) \quad (2.27 \text{ revisited})$$

3. Appearance function The appearance function is used to describe the breakage behavior and progeny PSD of the ore under particle bed compression. The appearance functions are represented by the relationship between t_{10} and other t_n parameters, which can be obtained from fitting the PSDs of the mono-size PPT products to Equation 2.20 through Equation 2.25. The resultant relationship can then be used to reconstruct the entire PSD after breakage based on the knowledge of the t_{10} parameter.

7.2.3 Energy and size reduction model

The most common approach for modeling of particle breakage in the HPGR is through the use of energy-based PBM techniques (Austin et al., 1993; Fuerstenau et al., 1991; Klymowsky and Liu, 1997a and 1997b; Morrell et al., 1997b; Torres and Casali, 2009; Davaanyam, 2015). The population balance approach is based on the assumption that the mass at each stage of the processes is consistently balanced, and the particle breakage occurs at each stage is subject to the applied energy and its respective breakage response (defined by the breakage function). The mass and energy split can be defined by the machine dependent parameters such as the classification function. Although the breakage function is ore dependent, it can be either determined from the well-controlled Piston-die Press Testing (PPT), or fitted to results obtained from pilot- or full-scale HPGR testing.

As discussed in the literature review, the underlying structure for most HPGR size reduction models is similar. The structure consists of three separate breakage zones namely the pre-crushing zone, the center zone, and the edge zone. The proposed UBC HPGR energy-size reduction model adopts the same concept, and uses the energy-based population balance approach to determine the breakage within each of the three HPGR breakage zones. This is a modified model from the work of Davaanyam (2015) with two additional selection functions, referred to as the critical gap model and center-edge energy split model. The modified model structure improved the definition of the three different breakage zones based on their respective breakage mechanism and physical boundaries. A schematic of the structure of the modified HPGR energy-size reduction model is provided in Figure 7.2, which consists of 2 breakage functions and 3 classification functions. Particle breakage in the pre-crushing zone is assumed to follow the compression breakage model, and particles in the grinding zone (both center and edge zones) break according to the fines corrected compression breakage model. This arrangement in the simulation allows the coarse particles to break in both pre-crushing and grinding zones, while the fine particles break only in the grinding zone. The product PSD after each stage of breakage is constructed based on the appearance function. The model can then be used to predict the PSDs of the HPGR center and edge product or the combined product under certain operating conditions.

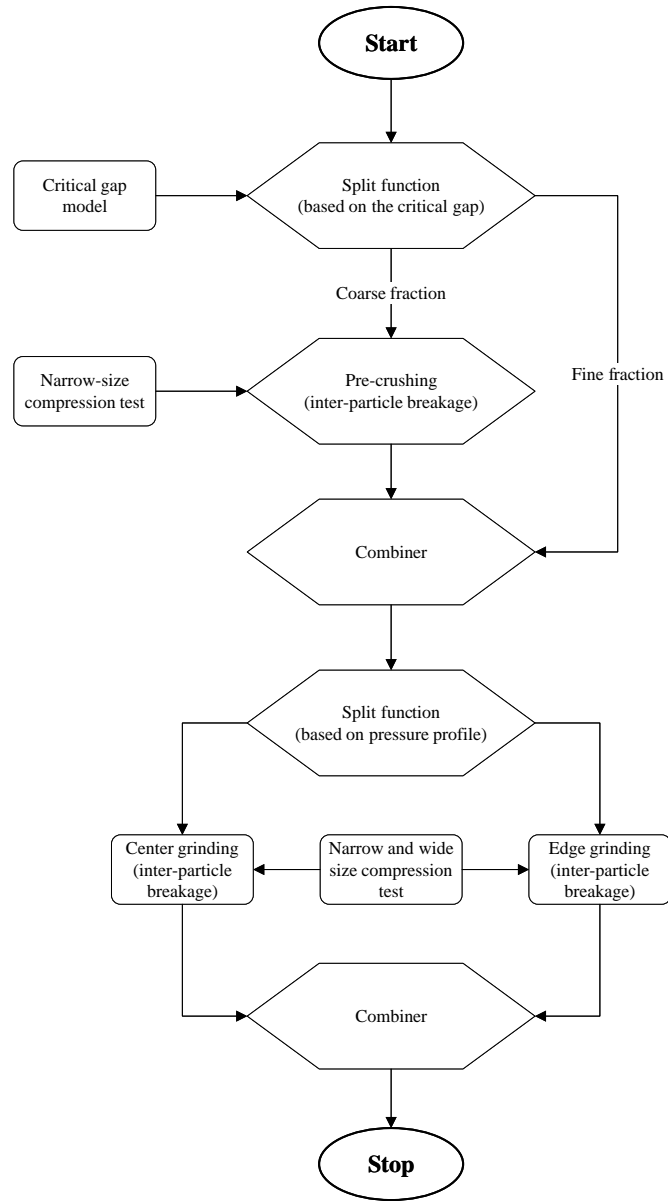


Figure 7.2: Proposed structure for HPGR energy-size reduction model

Critical gap model

It is known that the horizontal distance between the two roll surfaces at the nip angle (α) is referred to as the critical gap (x_c). Particles larger than the critical gap are broken in pre-crushing zone, while finer particles are bypassed to the subsequent breakage zone (grinding zone). This assumption is similar to Morrell et al. (1997a, 1997b), with the exception that the coarser particles in the feed are assumed to break by confined compressed bed mechanism rather than single particle impact breakage. Note that the critical gap only defines the mass split between the pre-crushing zone and the grinding zone. As shown in Equation 7.1, the critical gap (x_c) can be expressed as a function of roll diameter, operating gap and nip angle. The critical gap for each pilot HPGR test was calculated and used as an input to the HPGR model.

$$x_c = x_g + D(1 - \cos \alpha_{nip}) \quad (7.1)$$

Energy split models

Energy distribution among the three breakage zones (pre-crushing, center and edge zone) is determined by two energy split models. It was assumed that the specific energy (E_{sp}^{crush}) applied to the coarse particles (above x_c) in the pre-crushing zone is a fraction of the total applied specific energy. This relationship is expressed in Equation 7.2, where the fraction parameter β_{split}^{crush} is related to the HPGR roll diameter and feed particle size.

$$E_{sp}^{crush} = \beta_{split}^{crush} \cdot E_{sp} \quad (7.2)$$

The product from the pre-crushing zone is combined with the bypassed fines (fraction below x_c) in the feed, and the combined product becomes the feed to the grinding zone. The specific energy ($E_{sp}^{grinding}$) used for size reduction in the grinding zone is balanced using Equation 7.3. It is important to note that the sum of E_{sp}^{crush} and $E_{sp}^{grinding}$ does not equate to the total specific energy E_{sp} because the mass fractions are different in different breakage zones. Only the actual energy consumption in kW at each breakage stage is additive, and they can be summed up

to the total energy consumption.

$$E_{sp}^{grinding} = E_{sp} \cdot (1 - \beta_{split}^{crush} \cdot f_{coarse}) \quad (7.3)$$

Within the grinding zone, the energy distributed to the center and edge zones is related to the respective mass proportion that is generally pre-defined for a given HPGR unit. For the Köppern HPGR at UBC having 0.75 m roll diameter and 0.22 m roll length, a product mass split of 70% center material and 30% edge material was typical. The applied or absorbed energy on the respective center and edge proportions are balanced using Equation 7.4 and Equation 7.5. Parameter β_{split}^{edge} is a machine property and arises from differentiated pressure distribution within the compression zone of the various HPGR geometry and flange configurations.

$$E_{sp}^{edge} = \frac{E_{sp}^{grinding} \cdot \beta_{split}^{edge}}{f_{edge}} \quad (7.4)$$

$$E_{sp}^{center} = \frac{E_{sp}^{grinding} \cdot (1 - \beta_{split}^{edge})}{1 - f_{edge}} \quad (7.5)$$

7.3 Development of Ore-specific HPGR Model

This section presents an example in demonstrating the modeling and simulation of the Project G HPGR circuit using the UBC HPGR simulator. Figure 7.3 shows the model fitting algorithm and subsequent simulation route. Two important components for the model fitting process are the laboratory testing on the sample to determine the breakage function and appearance function, as well as the pilot HPGR testing on the same sample to obtain the test measurements. The objective of the model fitting is to minimize the difference between model prediction and actual measurement by altering the key model parameters. The generated model parameters from the fitting were subsequently used in the simulator to predict the HPGR performance for varying ore hardness and operating conditions as the part of the process simulation.

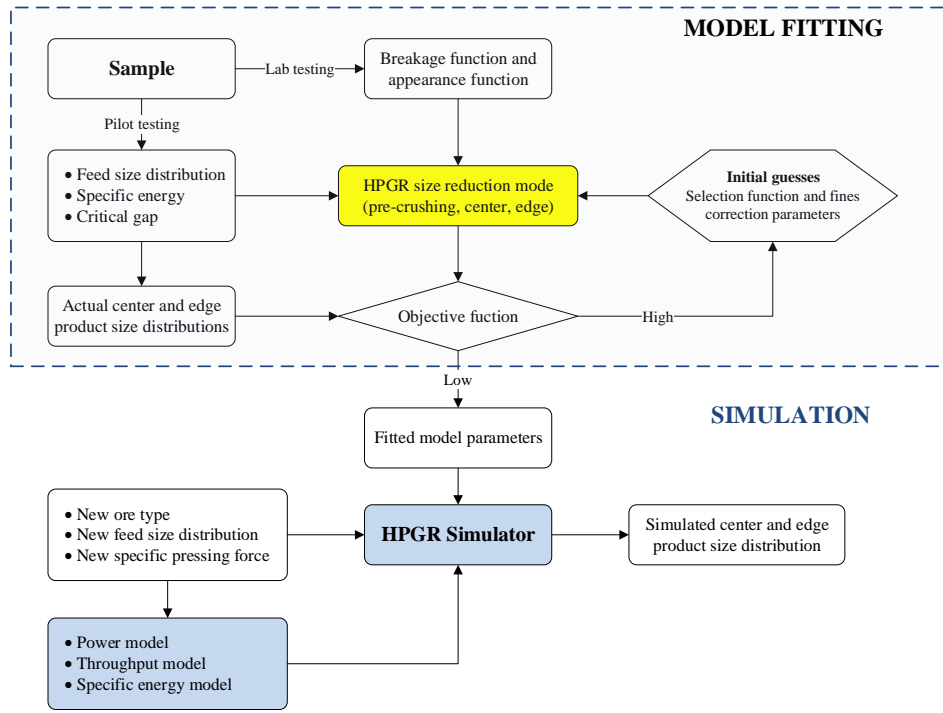


Figure 7.3: Model structure showing fitting algorithm and simulation route

7.3.1 Ore characterization

The ore characterization parameters are essential for the HPGR simulation under different operating conditions. The breakage parameters (t_{10} and t_n relationship) are ore specific, obtained from PPT on mono-size particles. In the case of Project G, two composite samples and six variability samples were subject to the mono-size PPT, characterizing their responses to particle-bed compression breakage. The experimental data were fitted to the t_{10} -based compression breakage model, from which the resultant breakage curves are plotted in Figure 7.4. Table 7.1 lists the breakage parameters obtained from the model fitting. It was found that the Comp2 sample is harder than Comp1 sample in terms of the ore resistance to the compression breakage, as measured by the ore breakage indicator $M \cdot f_{mat}$.

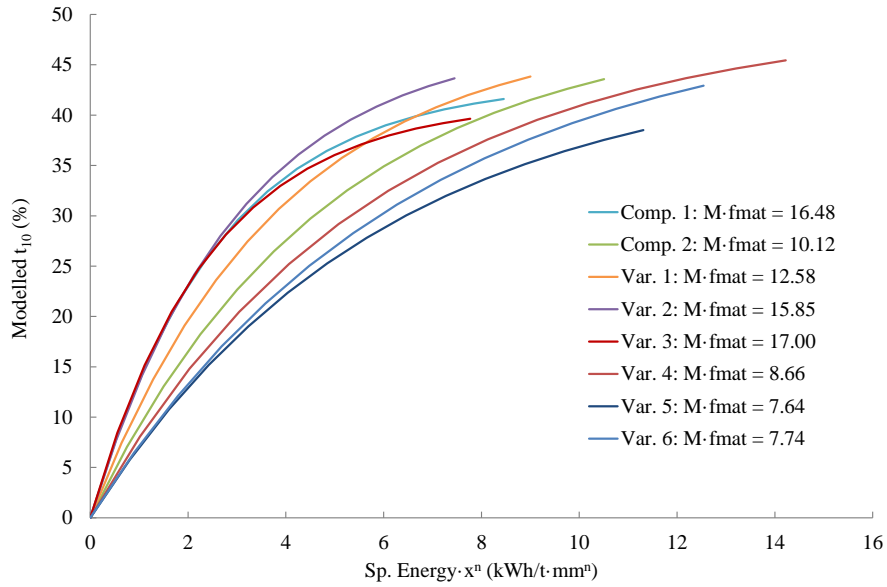


Figure 7.4: Specific energy and t_{10} relationship on Project G ores

Table 7.1: Summary of t_{10} breakage parameters for Project G samples

Sample	M	f_{mat}	n	$M \cdot f_{mat}$	R^2	SSE	RMSE	95% CI
Comp1	43.34	0.38	0.44	16.48	0.987	39.11	1.36	2.93
Comp2	49.27	0.21	0.47	10.12	0.986	40.68	1.39	2.98
Var. S1	48.54	0.26	0.45	12.58	0.986	36.41	1.32	2.82
Var. S2	47.66	0.33	0.39	15.85	0.993	21.47	1.01	2.17
Var. S3	41.33	0.41	0.39	17.00	0.986	27.53	1.14	2.46
Var. S4	49.57	0.17	0.65	8.66	0.985	52.74	1.58	3.40
Var. S5	45.19	0.17	0.53	7.64	0.992	17.34	0.91	1.95
Var. S6	50.18	0.15	0.55	7.74	0.993	19.22	0.96	2.05

Figure 7.5 shows similar t_{10} and t_n relationships for all tested samples. A single set of curves can therefore be fitted to form the master appearance function for this ore. The fitted appearance function parameters for Project G are listed in Table 7.2, that were used for simulation. The resultant relationship was then used to reconstruct the product PSD for different operating conditions.

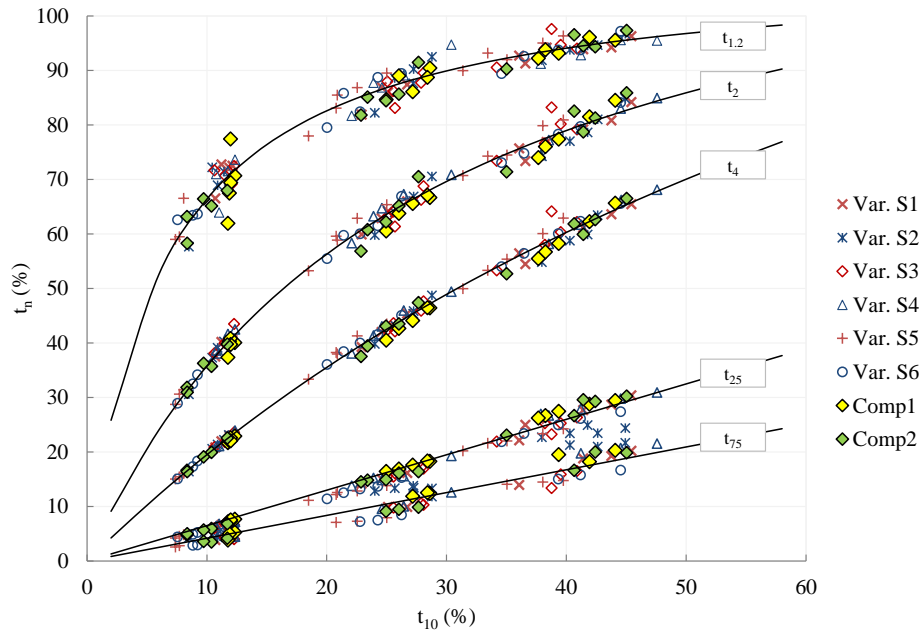


Figure 7.5: Fitted curve to tested composite and variability samples

Table 7.2: Appearance function for Project G ore samples

Description	$t_{1,2}$		t_2		t_4		t_{25}	t_{50}	t_{75}
	β_1	β_2	β_3	β_4	β_5	β_6	β_7	β_8	β_9
Fitted	109.29	6.46	132.26	26.98	198.94	91.99	0.65	0.49	0.42

7.3.2 Pilot testing data

A total of six tests were performed on the two composite samples using the Köppern pilot HPGR at UBC. Table 7.3 summarizes the operating conditions during the pilot tests. An average product mass split of 71% center material and 29% edge material was recorded. The critical gap for each test was calculated, which was found to be linearly correlated with the applied specific pressing force as shown in Figure 7.6. According to Equation 7.1, a higher specific pressing force reduces the operating gap, which in turn results in a reduced critical gap.

Table 7.3: Summary of HPGR operating conditions - Project G

No.	Sample	Test #	F_{sp} N/mm ²	u m/s	P kW	E_{sp} kWh/t	W t/h	\dot{m} ts/hm ³	x_c mm
1	Comp1	Au(G)-D01	5.0	0.75	95.4	3.1	28.4	228	27.2
2	Comp1	Au(G)-D02	4.0	0.75	81.5	2.6	29.4	236	30.0
3	Comp1	Au(G)-D03	2.6	0.75	65.5	1.9	30.7	246	37.1
4	Comp2	Au(G)-P01	4.5	0.75	89.6	2.9	28.2	226	28.8
5	Comp2	Au(G)-P02	3.6	0.75	75.4	2.2	28.2	226	30.4
6	Comp2	Au(G)-P03	2.6	0.75	60.6	1.8	29.3	235	34.2

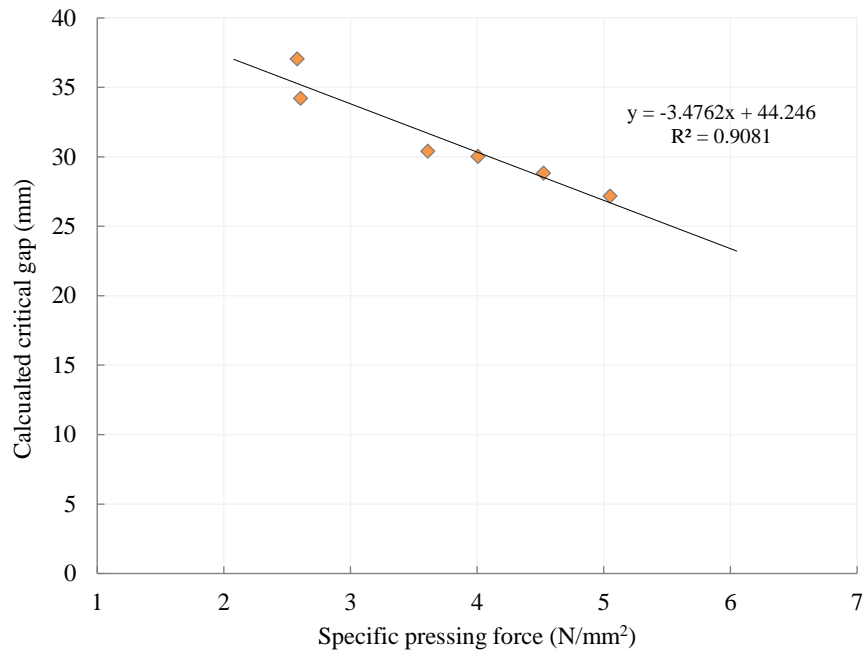


Figure 7.6: Critical gap as a function of specific pressing force

Their respective test feed and product PSDs are presented in Figure 7.7, with more information displayed in Table 7.4.

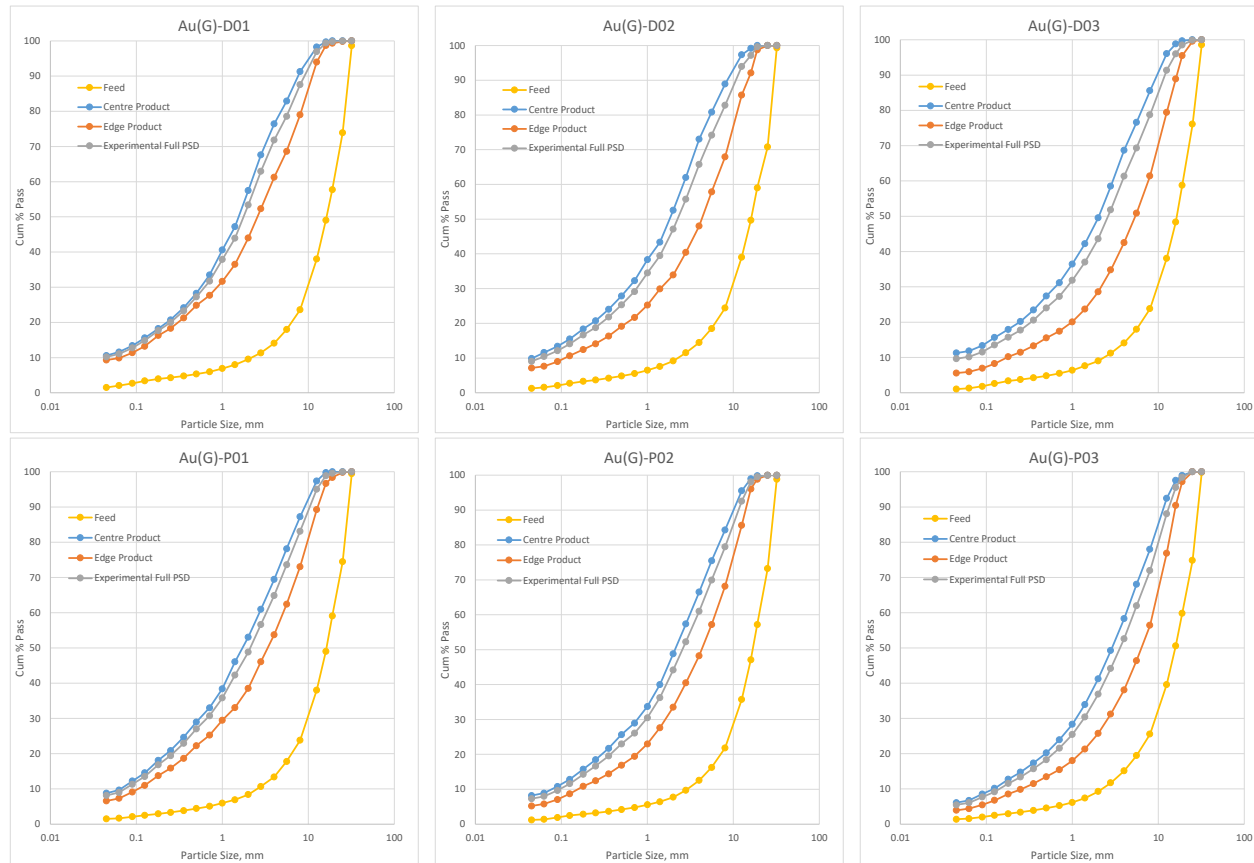


Figure 7.7: Size distributions of HPGR feed and product

Table 7.4: Summary of feed and product sizes

Description	Unit	D01	D02	D03	P01	P02	P03
F ₈₀	[mm]	26.72	27.26	26.21	26.55	26.85	26.44
F ₅₀	[mm]	16.34	16.10	16.48	16.29	16.86	15.80
Center P ₈₀	[mm]	4.88	5.43	6.51	6.09	6.83	8.61
Center P ₅₀	[mm]	1.57	1.83	2.04	1.74	2.11	2.90
Edge P ₈₀	[mm]	8.31	11.06	12.71	9.93	11.05	13.31
Edge P ₅₀	[mm]	2.58	4.32	5.43	3.41	4.31	6.46
Full P ₈₀	[mm]	5.98	7.22	8.45	7.22	4.31	10.25
Full P ₅₀	[mm]	1.79	2.27	2.62	2.12	4.31	3.63

7.3.3 Model development

Model fitting involves adjusting the model parameters based on pilot-scale HPGR test results until the best possible model parameters are obtained that achieve the minimum differences between the observations and predictions. Since the classification functions are machine specific, a method called master fitting was applied whereby all six pilot tests were used together to generate a single set of model parameters. The master fitted model parameters are shown in Table 7.5.

Table 7.5: Fitted HPGR model parameters

Description	$\beta_{\text{split}}^{\text{crush}}$	$\beta_{\text{split}}^{\text{edge}}$	X_f	c
Master fitted	0.28	0.10	1.4	0.66

Figure 7.8 provides a comparison between the measured (line) and fitted (symbol) HPGR product PSDs. Considering that a single set of model parameters was used in the simulation for all six pilot tests, the measured and predicted product PSDs had a reasonably good agreement. As a result, the fitted master model parameters can be used for subsequent process simulation.

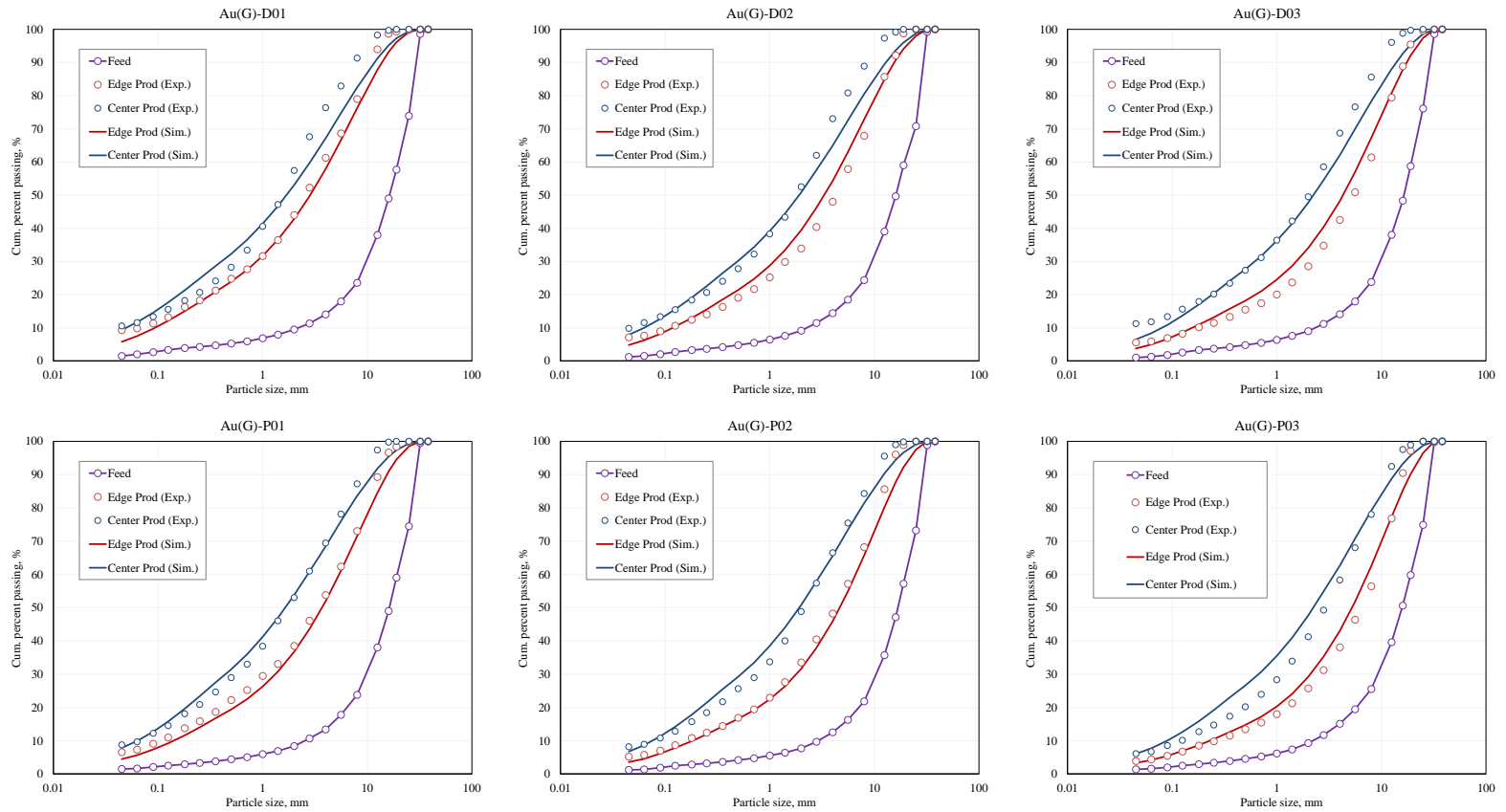


Figure 7.8: Comparison of measured and fitted size distributions

Besides the prediction of center and edge product PSDs, the HPGR power draw, specific energy consumption and specific throughput at a given specific pressing force were also predicted from the simulator based on the methodology described in Chapter 5. Figure 7.9 compares the predictions against the key operating observations. As can be seen, the majority of the predictions are within 20% error of the actual measurements, except for the center P_{80} size. The model slightly over-predicted the center P_{80} , but the overall predictions are reasonably good. Note that some of the parameters were scaled so that they all plot on a single axis.

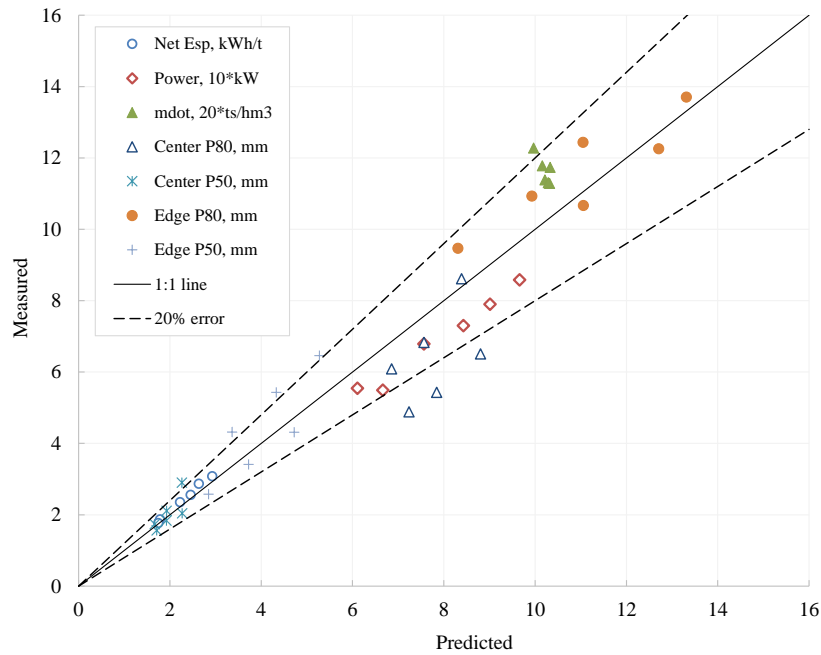


Figure 7.9: Comparison of measured and predicted values

A reasonable agreement between the measured and predicted HPGR performance for Comp1 and Comp2 samples demonstrates that the model structure described in Section 7.2.1 is suitable for HPGR simulation under varying ore hardness and operating conditions.

7.3.4 Simulation of HPGR processes

Steady-state simulation using the calibrated HPGR model provides a useful and cost-effective tool for evaluating the effect of changes to operating variables, equipment variables, and flowsheet alternatives before additional pilot scale testing. Simulation results include estimation of the HPGR power draw, throughput capacity, and center and edge product PSDs.

Table 7.6 shows the model parameters obtained from fitting the model to pilot tests with the composite samples that will be needed for HPGR simulation, including critical gap parameter, mass split between center and edge based on the HPGR machine setting, and the energy split functions. Simulation of different operating conditions was then carried out by keeping the model parameters constant.

Table 7.6: HPGR model parameters used for simulations

Description	x_c	Edge	β_{split}^{crush}	β_{split}^{edge}	X_f	c
Fitted from pilot tests	29-36	0.3	0.28	0.10	1.4	0.66

The simulation function is built into the UBC-HPGR-Simulator based on the PBM principle with following main adjustable parameters:

- Operating specific pressing force
- Feed PSD and fines content
- Ore hardness or ore breakage characterization
- Alternative comminution system and flowsheet arrangement

Once the energy–breakage relationship is defined by the mono-size PPT for a given ore sample, and the set of master curves describing the t_{10} versus t_n relationship is known, the energy–size reduction performance of the HPGR can be simulated. Using the ore characterization data and established HPGR model parameters, simulations could be run to predict pilot scale HPGR responses to changes in operating conditions.

Effect of operating specific pressing force

The specific energy consumption can be directly modeled based on a simple linear relationship between the specific pressing force and specific energy obtained from the pilot test work. Subsequently, the impact of specific pressing force on the final product sizes can be examined through conducting simulations with changes made to the applied specific pressing force. An example is provided using the fitted Comp1 model to simulate the HPGR performance for varying specific pressing forces. Note that the critical gap is also affected by the applied specific pressing force. The simulation results are summarized in Table 7.7. The resultant product PSDs for each simulation are presented in Figure 7.10. As expected, a higher specific pressing force improves the fineness of both center and edge PSDs.

Table 7.7: Simulation summary for varying specific pressing force

Simulation	F_{sp} N/mm ²	P kW	E_{sp} kWh/t	\dot{m} ts/hm ³	C ₈₀ mm	C ₅₀ mm	E ₈₀ mm	E ₅₀ mm
Sim 1	4.5	78.4	2.62	209	7.6	1.9	10.3	3.2
Sim 2	3.5	66.2	2.16	209	8.7	2.2	11.9	4.0
Sim 3	2.5	54.1	1.70	209	9.0	2.4	12.9	4.7

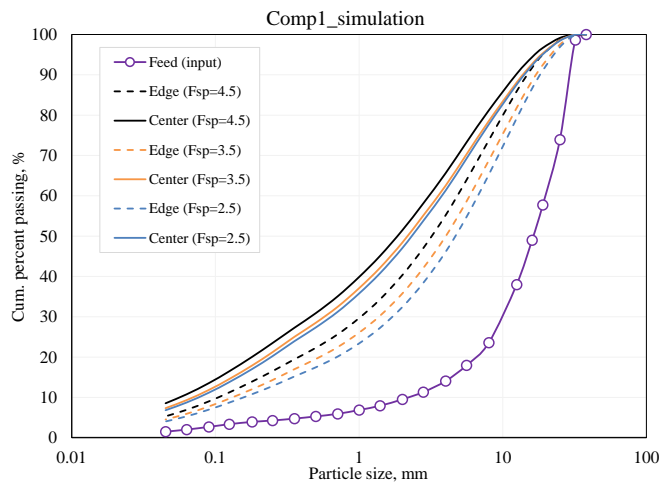


Figure 7.10: Simulated product PSDs at varying specific pressing force

Effect of feed size distribution and fines content

Based on the previous analysis conducted on the UBC HPGR database, the feed PSD is one of the most important parameters that affect the HPGR performance. Changes in HPGR feed PSD can affect the HPGR power draw and specific energy consumption at the selected specific pressing force, consequently affects the product PSDs. Although HPGR feed size is not a typical operating parameter in practice, it can be related to the upstream fragmentation process (e.g. mining method, blasting and crushing). Figure 7.11 shows feed PSDs for the following four scenarios using the Comp1 HPGR model to examine their impacts on the HPGR performance and product sizes. The fines contents were also varied among those considered feed PSD scenarios.

- A coarse feed
- A coarse feed with fines scalped at 1.4 mm
- A fine feed
- A fine feed with fines scalped at 1.4 mm

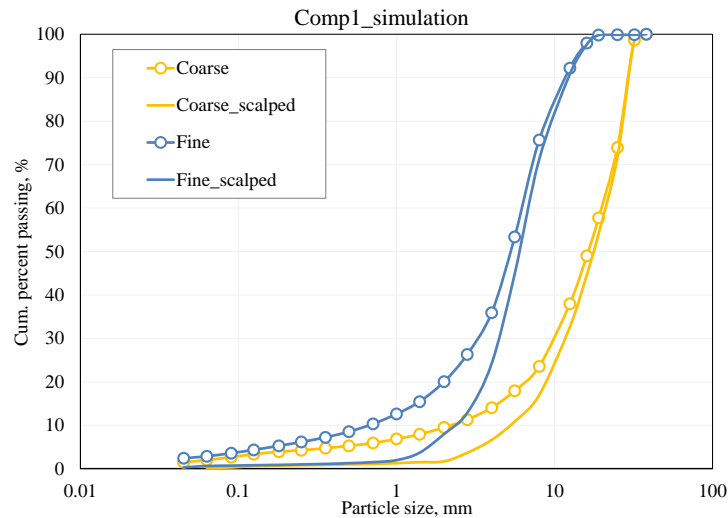


Figure 7.11: Variations of feed size distribution for the simulation

The simulation results are summarized in Table 7.8. The resultant product PSDs for each simulation are presented in Figure 7.12. This is another evidence that the feed PSD affects the HPGR performance. The pilot HPGR drew lower power when fed with finer feed PSD or when fines were scalped prior to HPGR comminution. Furthermore, fines removal has a minor negative impact on the specific throughput constant.

Table 7.8: Simulation summary for varying feed size distributions

Simulation	F_{sp} N/mm ²	Power kW	E_{sp} kWh/t	\dot{m} ts/hm ³	C_{80} mm	C_{50} mm	E_{80} mm	E_{50} mm
Coarse	3.5	66.2	2.16	209	8.7	2.2	11.9	4.0
Coarse scalped	3.5	64.9	2.18	202	8.2	2.2	11.7	4.2
Fine	3.5	54.7	1.77	202	3.7	1.1	5.3	2.2
Fine scalped	3.5	53.2	1.79	194	3.6	1.2	5.3	2.5

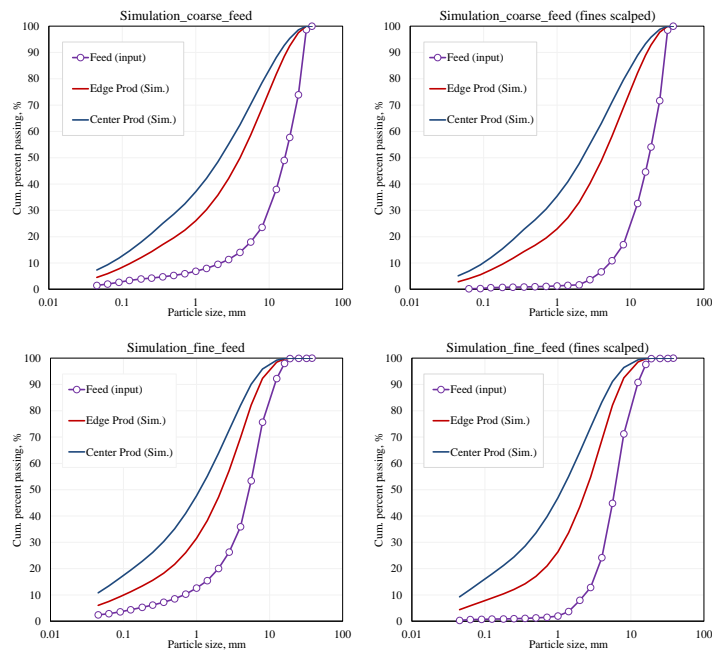


Figure 7.12: Simulated PSDs for different feed size distributions

Effect of ore hardness

In simulating the HPGR responses for all 6 variability ore samples, breakage parameters were obtained from the mono-size PPT performed on each sample. The net specific energy consumption can be either measured during an actual pilot test, or predicted from the HPGR database or predicted from the PPT calibration test. As described in Chapter 5, the empirical model developed from the UBC HPGR database does not differentiate the ore hardness when estimating the specific energy consumption. This means that the database approach will populate the same specific energy consumption regardless the ore hardness, as soon as their feed PSD and bulk density are kept the same. Consequently, the ore hardness factor is solely reflected on the product size. To properly correct the effect of ore hardness, PPT calibration tests were performed to determine the specific energy requirement for each tested ore sample at a given specific pressing force. Figure 7.13 presents the predicted specific energy consumption for all 6 variability samples as the results of the PPT calibration modeling.

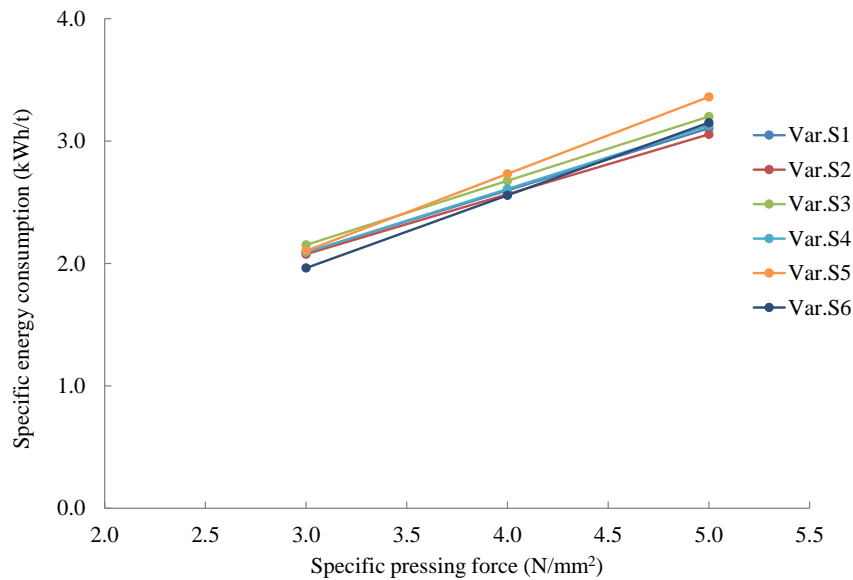


Figure 7.13: Specific energy consumption as a function of specific pressing force for 6 variability samples based on PPT calibration tests

The resultant specific energy along with other model parameters were used as inputs in the simulation. The simulation results are summarized in Table 7.9.

Table 7.9: Simulation summary for 6 variability samples

Simulation	F_{sp} N/mm²	P kW	E_{sp} kWh/t	\dot{m} ts/hm³	C₈₀ mm	C₅₀ mm	E₈₀ mm	E₅₀ mm
Var.S1 Sim1	5.0	84.5	3.10	192	6.4	1.5	9.6	3.0
Var.S1 Sim2	4.0	72.3	2.60	192	7.3	1.8	11.3	3.8
Var.S1 Sim3	3.0	60.1	2.09	193	7.9	2.0	12.6	4.6
Var.S2 Sim1	5.0	84.5	3.06	195	6.5	1.5	9.5	2.9
Var.S2 Sim2	4.0	72.3	2.57	194	7.4	1.8	11.2	3.7
Var.S2 Sim3	3.0	60.1	2.08	194	8.0	2.0	12.5	4.5
Var.S3 Sim1	5.0	84.5	3.20	186	7.6	1.9	9.7	3.0
Var.S3 Sim2	4.0	72.3	2.68	186	8.6	2.2	11.3	3.7
Var.S3 Sim3	3.0	60.1	2.15	187	9.3	2.4	12.5	4.4
Var.S4 Sim1	5.0	84.5	3.13	190	6.0	1.4	8.6	2.6
Var.S4 Sim2	4.0	72.3	2.61	191	6.9	1.6	10.2	3.3
Var.S4 Sim3	3.0	60.1	2.09	193	7.5	1.9	11.5	4.0
Var.S5 Sim1	5.0	84.5	3.36	177	7.2	1.8	10.5	3.6
Var.S5 Sim2	4.0	72.3	2.73	182	8.1	2.1	12.2	4.5
Var.S5 Sim3	3.0	60.1	2.10	191	9.2	2.5	14.0	5.5
Var.S6 Sim1	5.0	84.5	3.15	189	6.4	1.5	10.2	3.4
Var.S6 Sim2	4.0	72.3	2.56	195	7.4	1.9	11.9	4.3
Var.S6 Sim3	3.0	60.1	1.96	205	8.3	2.2	13.7	5.4

The simulated center product P_{80} and P_{50} for all 6 variability samples are compared in Figure 7.14. It is shown that for variability sample 5, coarser product was produced at higher energy input, indicating that sample 5 is harder among the variability samples.

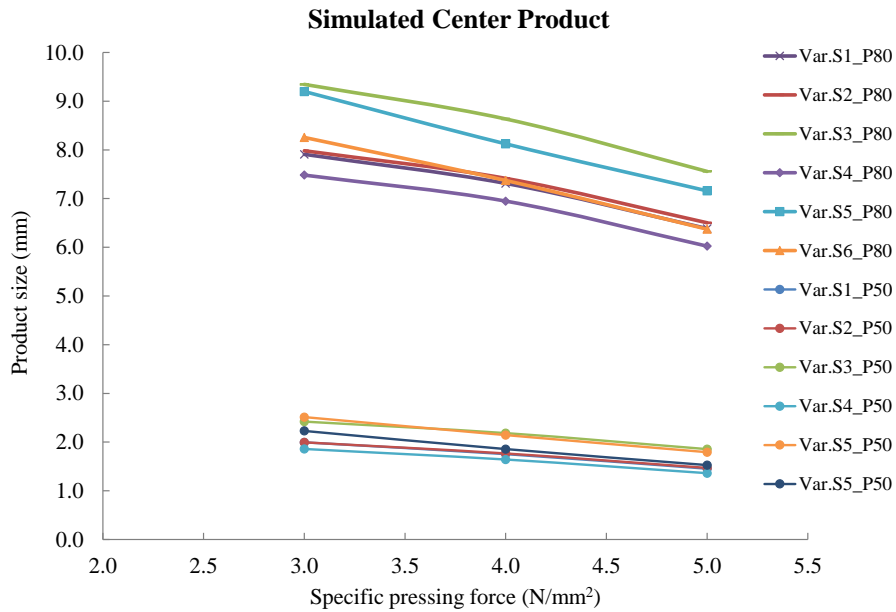


Figure 7.14: Simulated center product size for 6 variability samples

Simulation summary

The simulation study yielded the following outcomes.

- The product PSDs can be simulated for different applied pressing forces. Increasing the applied specific pressing force increases the product fineness.
- The feed PSD and fines content have a considerable impact on the HPGR power draw and comminution effect. A finer feed PSD and feed with fines removed result in lower machine power draw.
- The ore hardness has a direct impact on the specific energy requirement and resultant product PSDs. The prediction is made possible when both the PPT calibration test and the simulation test are performed on the same sample.

7.4 Development of Generic HPGR Model

A generic HPGR model was developed based on a total of 50 pilot HPGR tests on 8 different ore types, with mono-size PPT conducted on each of the feed samples for the pilot test work. Note that all pilot tests were performed in standard tertiary HPGR duty.

7.4.1 Ore characterization database

The breakage parameters (t_{10} and t_n relationship) were obtained from the mono-size PPT on all different ore types, including composite samples and some variability samples (a total of 18 samples). The fitted breakage parameters are summarized in Table 7.10.

Table 7.10: Summary of t_{10} breakage parameters on 18 samples

Sample	M	f_{mat}	n	$M \cdot f_{\text{mat}}$
Mean	47.62	0.22	0.53	10.28
SD	3.71	0.09	0.11	3.72
CV	8%	39%	20%	36%
95% CI	1.84	0.04	0.05	1.85

From the mono-size PPT, t_n against t_{10} for all tests were plotted in Figure 7.15, showing that a set of master curves can be found to describe the t_{10} - t_n relationship for all samples regardless of the ore type. The appearance function parameters from individual model fitting and master fitting to all 18 samples are provided in Table 7.11.

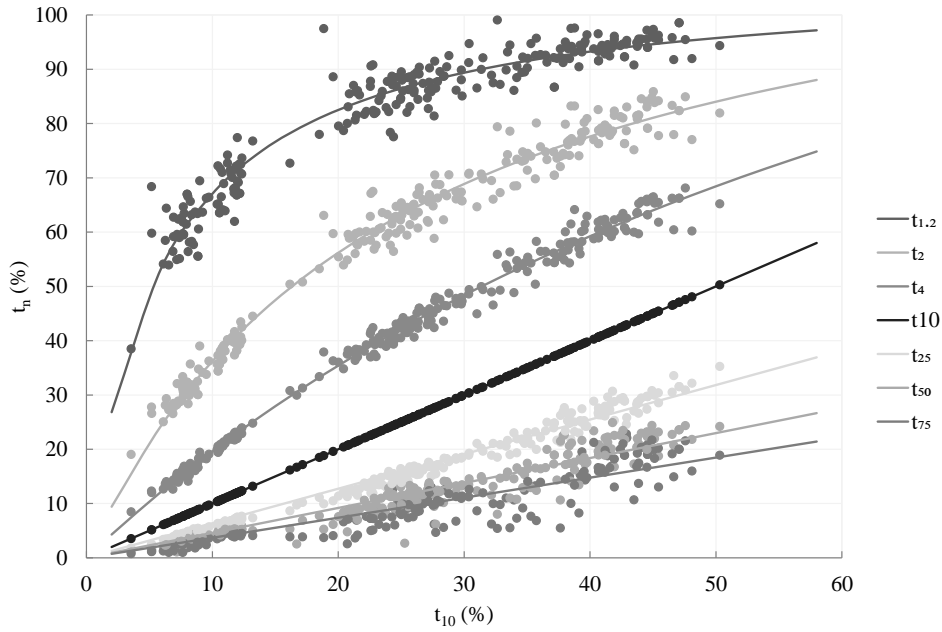


Figure 7.15: Master curve fitted to eighteen tested ores

Table 7.11: Individual and master fitted appearance function

Description	$t_{1.2}$		t_2		t_4		t_{25}	t_{50}	t_{75}
	β_1	β_2	β_3	β_4	β_5	β_6	β_7	β_8	β_9
Mean	107.9	6.2	127.3	25.4	192.3	89.1	0.63	0.45	0.37
SD	2.2	0.9	6.8	3.2	20.6	12.3	0.04	0.06	0.07
CV	2%	15%	5%	12%	11%	14%	6%	13%	19%
95% CI	1.09	0.47	3.39	1.57	10.24	6.12	0.02	0.03	0.04
Master fitted	107.2	6.0	125.4	24.6	181.0	82.2	0.64	0.46	0.37

7.4.2 Pilot testing data

Table 7.12 summarizes the key statistics of operating conditions for the 50 pilot tests performed. Tests were performed with various applied pressures, roll speeds, feed bulk densities, and feed moisture contents. An average product mass split of 70% center material and 30% edge material was recorded.

Table 7.12: Summary of HPGR operating conditions

Description	F_{sp} N/mm ²	u m/s	P kW	ρ_{bulk} t/m ³	w %	E_{sp} kWh/t	W t/h	\dot{m} ts/hm ³
Master	3.56	0.76	65.44	1.65	2.80	2.00	28.12	223.95
Max	5.05	0.92	95.36	1.82	5.55	3.08	33.50	259.04
Min	1.83	0.56	39.43	1.51	0.90	1.11	21.41	171.65
SD	0.74	0.05	13.31	0.07	1.19	0.48	3.01	21.25
CoV	21%	6%	20%	4%	43%	24%	11%	9%

7.4.3 Model development

Model fitting consists of adjusting parameters for individual pilot test and then repeating the procedure for combined data sets. The primary objective of these model fitting processes was to minimize the prediction error for the HPGR center and edge product PSDs. Key statistics of individually fitted model parameters as well as the master fitted model parameters are listed in Table 7.13. The calculated critical gap values from the test work were used as inputs to determine other model parameters.

Table 7.13: Fitted classification function

Description	Critical gap	Edge	β_{split}^{crush}	β_{split}^{edge}	X_f	c
Mean	28.14	0.30	0.40	0.14	1.47	0.44
Standard Deviation (SD)	3.84	0.04	0.12	0.10	0.55	0.36
CV	14%	14%	30%	70%	37%	81%
95% CI	1.09	0.01	0.03	0.03	0.16	0.10
Master fitted	20	0.30	0.26	0.10	1.40	1.0

Figure 7.16 compares the resultant prediction against the observed key operating outcomes. As can be seen, the majority of the predictions are within 25% of the actual measurements. This model can be used for simulating the HPGR performance for the generic purpose where no pilot HPGR test program was conducted; the only requirement would be performing the mono-size PPT in the laboratory. Note that some of the parameters were scaled so that they all plot on a single axis.

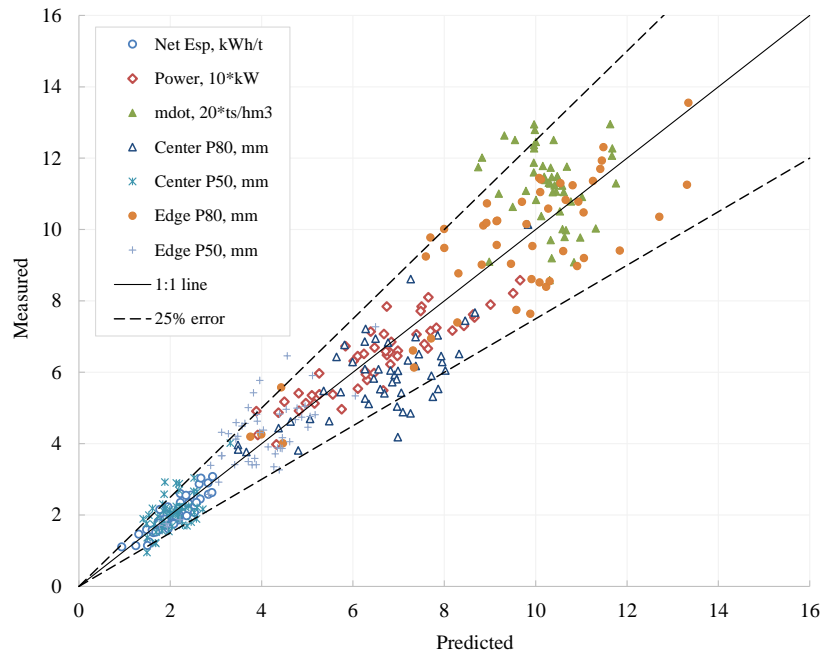


Figure 7.16: Comparison of measured and predicted values

7.5 HPGR Model Testing and Validation

7.5.1 Pilot testing and machine specification

Project T conducted pilot HPGR tests at a different lab using a larger Köppern HPGR than the UBC unit. Table 7.14 compares the machine specifications between the Köppern units at the UBC facility and Lab A.

Table 7.14: Köppern HPGR testing facilities

Description	Unit	Köppern/UBC	Köppern/Lab A
Roll diameter	[mm]	750	1,000
Roll length	[mm]	220	250
Roll wear surface	[-]	Hexadur®	Studded
Roll edge design	[-]	Cheek plate	Cheek plate
Installed power	[kW]	200	500 (250 each)

Table 7.15 summarizes the operating conditions during the pilot testing, of which 3 tests were conducted on composite sample T4, while other tests were conducted on a blend of T4 and T9 samples at a 50:50 blending ratio. An average product mass split of 70% center material and 30% edge material was recorded.

Table 7.15: Summary of HPGR operating conditions - Project T

No.	Sample	Test #	F_{sp} N/mm ²	u m/s	P kW	E_{sp} kWh/t	W t/h	\dot{m} ts/hm ³
1	T4	Au(T)1	4.0	0.75	100.7	2.30	28.4	223.0
2	T4	Au(T)2	3.0	0.75	91.8	1.90	29.4	238.0
3	T4	Au(T)3	2.0	0.75	64.7	1.30	30.7	248.6
4	Blend	Au(T)4	4.0	0.75	101.8	2.30	28.2	222.1
5	Blend	Au(T)5	3.0	0.75	76.9	1.80	28.2	217.5
6	Blend	Au(T)6	2.0	0.75	58.9	1.30	29.3	214.7

7.5.2 Ore characterization

The mono-size PPT was conducted on the T4 and T9 samples to obtain the compression breakage parameters. The resultant t_{10} -based breakage parameters are summarized in Table 7.16. It appeared that the sample T4 is slightly harder than sample T9 based on the breakage indicator $M \cdot f_{mat}$. The fitted appearance function parameters for Project T are listed in Table 7.17.

Table 7.16: Summary of t_{10} breakage parameters for Project T samples

Sample	M	f_{mat}	n	$M \cdot f_{mat}$	R^2	SSE	RMSE	95% CI
Au (T4)	47.71	0.19	0.66	9.04	0.993	21.89	1.02	2.19
Au (T9)	49.08	0.20	0.60	9.61	0.992	31.20	1.22	2.61
Au (T9)-dup	49.02	0.20	0.61	9.58	0.992	30.01	1.20	2.56

Table 7.17: Appearance function for Project T ore samples

Description	$t_{1,2}$		t_2		t_4		t_{25}	t_{50}	t_{75}
	β_1	β_2	β_3	β_4	β_5	β_6	β_7	β_8	β_9
Au (T4)	108.3	6.3	128.4	26.2	196.2	92.3	0.64	0.46	0.39
Au (T9)	109.9	8.0	130.6	29.4	202.6	98.8	0.66	0.49	0.41
Au (T9)-dup	109.6	7.9	129.7	29.1	203.9	99.8	0.65	0.49	0.42

7.5.3 Model testing and validation

The feed properties (PSD, moisture and bulk density, among others) and ore breakage characterization data were used as inputs in the UBC-HPGR-Simulator. Since the critical gap model and energy split model are subject to the machine specification, those parameters developed from the UBC database cannot be directly used for Project T. Model fitting was therefore performed by adjusting the critical gap parameter and energy split parameters to minimize the differences between the observation and prediction. The fitted model parameters are compared to the generic HPGR model resulted from the UBC pilot tests, as summarized in Table 7.18. The results suggested that the large HPGR unit at lab A, having a larger critical gap, could bypass the pre-crushing zone with a higher portion of materials (below x_c). Therefore, the specific energy split to the pre-crushing zone is expected to increase due to a smaller amount of materials remaining for the breakage in the pre-crushing zone.

Table 7.18: HPGR model parameters

Description	Critical gap	Edge	β_{split}^{crush}	β_{split}^{edge}	X_f	c
UBC HPGR	20	0.30	0.26	0.10	1.40	1.0
Lab A HPGR	24	0.30	0.73	0.06	1.40	1.0

Figure 7.17 compares the resultant prediction against the key operating observations from Lab A. Note that the power model was scaled proportionally to reflect the machine dimension at Lab A, as the empirical regression model was developed for the UBC pilot HPGR unit. As can be seen, the majority of the predictions fall within 20% of the actual measurements. Note that some of the parameters were scaled so that they all plot on a single axis. Comparison of the measured and predicted power draw shows an excellent agreement.

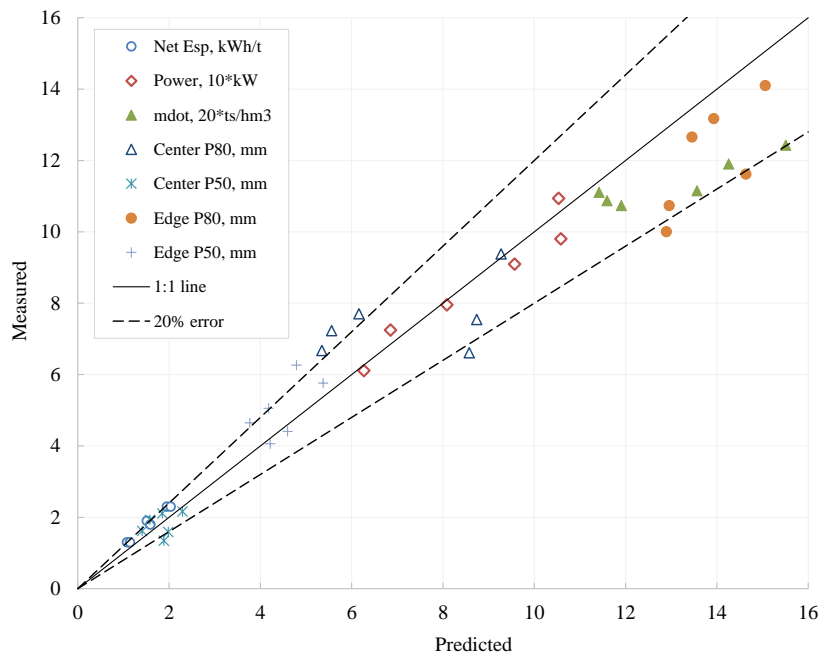


Figure 7.17: Comparison of measured and predicted values

The comparison between the measured (line) and simulated (symbol) HPGR product PSDs is provided in Figure 7.18. There are some deviations in the prediction of center and edge products, particularly towards the finer size fraction. The model has the potential to be improved by incorporating the fines correction model that is specific to the HPGR unit at Lab A.

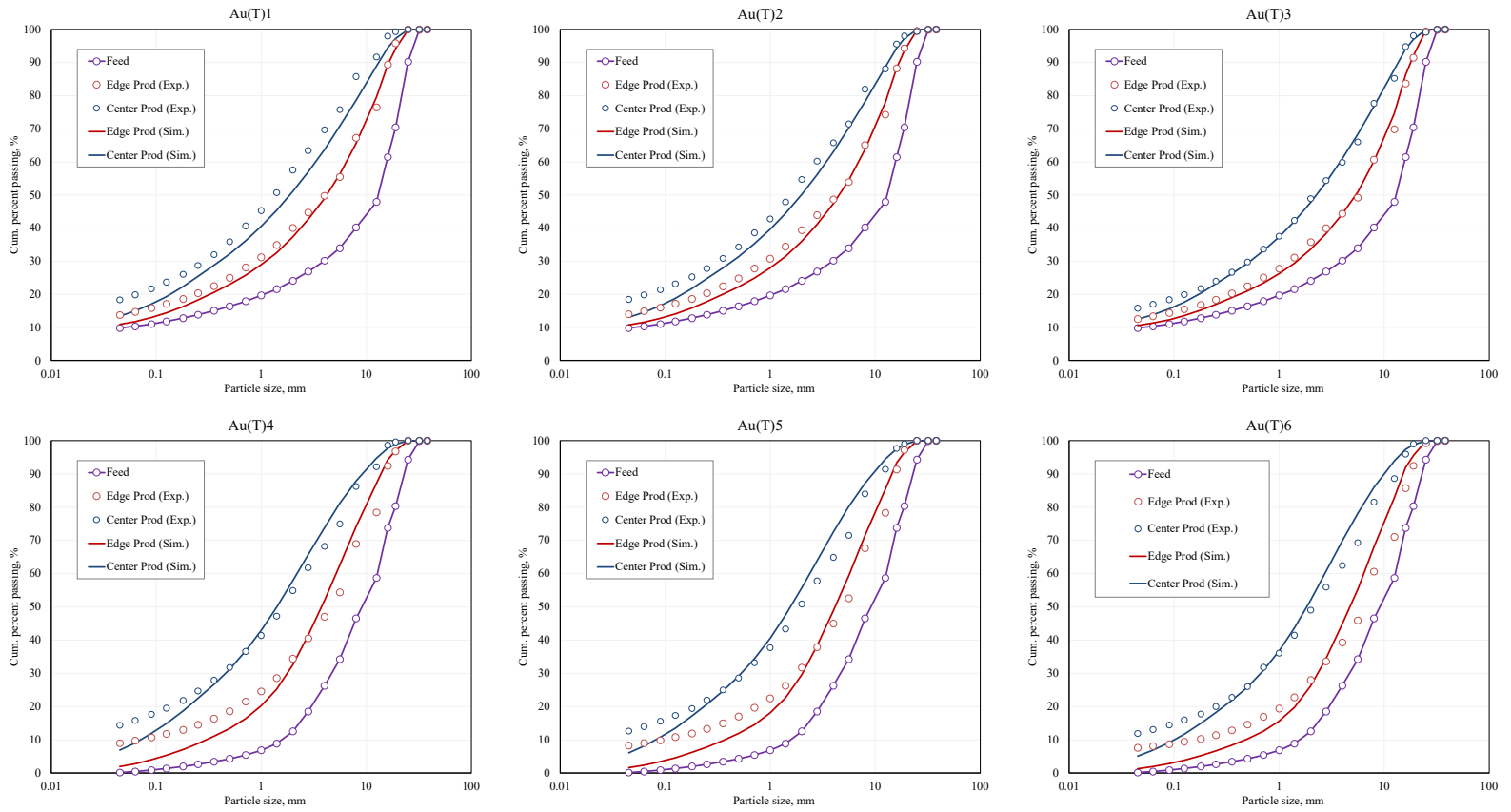


Figure 7.18: Comparison of measured and fitted size distributions - Lab A

7.6 Summary and Conclusions

This chapter presented a simulation package “UBC-HPGR-Simulator” that incorporates a holistic model for HPGR process simulation. The developed framework contains a set of empirical models developed from the UBC HPGR-PPT database, a breakage characterization model based on mono-size PPT, and an HPGR energy-size reduction model. The difficulty of predicting the center and edge product PSD has been addressed by adding an energy split sub-model that defines the energy distribution between the center and edge zones. The “UBC-HPGR-Simulator” allows the full breakage progeny PSD to be modeled directly from the feed particle size and energy input using selected model parameters.

Two HPGR PBM models were presented in this chapter, an ore specific model and a generic model, both enable the simulation and prediction of HPGR center and edge product PSD for varying ore hardness and other operating conditions. For simulating the HPGR product sizes, it is always advisable to use the ore specific model with model parameters developed from limited pilot HPGR tests, as some of the model parameters change with the testing conditions. Due to a lower prediction accuracy, the use of the generic HPGR model is only advisable when there is no HPGR test data available. The UBC-HPGR-Simulator can be used to aid the design of HPGR circuits based solely on laboratory breakage tests and/or in conjunction with some pilot scale HPGR test data.

Some aspects of the HPGR operating variables were not evaluated in this chapter but are considered to have impacts on HPGR performance, including HPGR roll speed, HPGR feed moisture content, HPGR roll surface type, and closing screen size in closed circuit arrangement. Those variables should be further investigated through model fitting and simulation.

Chapter 8

Conclusions and Recommendations

8.1 Main Outcomes

The main research findings of the research are listed in the following areas:

HPGR empirical models

Empirical HPGR models were developed based on the latest UBC HPGR database. In the absence of pilot HPGR tests, one can apply these empirical models for predicting the HPGR power draw, the net specific energy, the specific throughput constant, the product size distribution and the size reduction ratio based on feed material characteristics and the applied specific pressing force settings. The main outcomes of this part of the research are the following,

- Provided benchmark information for key operating variables;
- Carefully selected the input variables for regression modeling including the ore hardness and feed PSD condition;
- Established empirical regression models based on more than 200 pilot tests conducted at UBC;

- Developed analytical model based on the machine learning approach for modeling the m parameter, as provided in Appendix D;
- Confirmed the applicability of the “self-similar” normalization approach for re-constructing HPGR product size distribution based on the predicted size reduction ratio.

HPGR sizing and selection

Proposed the framework for HPGR sizing and selection incorporating empirical models and small scale PPT test data for each study stage of the project. The proposed framework is aimed at providing a low cost option for metallurgical facilities and engineers to evaluate the HPGR comminution circuit as the basis for comparison to alternative flowsheet. The main outcomes of this part of the research are the following,

- Used empirical models to reduce sample size for testing, and improved the accuracy of model predictions for HPGR sizing and selection;
- Implemented PPT programs to support HPGR circuit design that can lead to significant savings in sample quantity and testing, as well as provide improved confidence that reduces the need to include conservatism in the equipment sizing and selection;
- Demonstrated the application of the PPT for ore characterization under compressive load, that led to its use for ore variability assessment which is difficult to obtain through only the pilot test program.

HPGR modeling and simulation

Developed an integrated simulator based on empirical models, PPT calibration test results and PPT simulation test results for HPGR modeling and simulation. The main outcomes of this part of the research are the following,

- Refined the semi-empirical HPGR models by integrating the critical gap model in the model structure;

- Added an energy split function in the model to define the energy distribution between center and edge zones, allowing prediction of the center and edge product PSD individually;
- Validated the proposed semi-empirical HPGR model based on ore breakage characterizations through model fitting to ore specific dataset and generic dataset;
- Validated the proposed semi-empirical HPGR model using the pilot tests performed at a different laboratory, where a different size of HPGR was installed.

Figure 8.1 provides a guidance for HPGR sizing and circuit design depending on available test work. The simplicity and accuracy of the developed models and proposed evaluation framework significantly reduce the sample requirement and associated costs in drilling and testing for metallurgical programs that consider the HPGR as a potential alternative to conventional technologies, particularly for project at the early stage. It could ultimately lead to increased application of HPGR for a significant reduction in comminution energy usage in the mining industry.

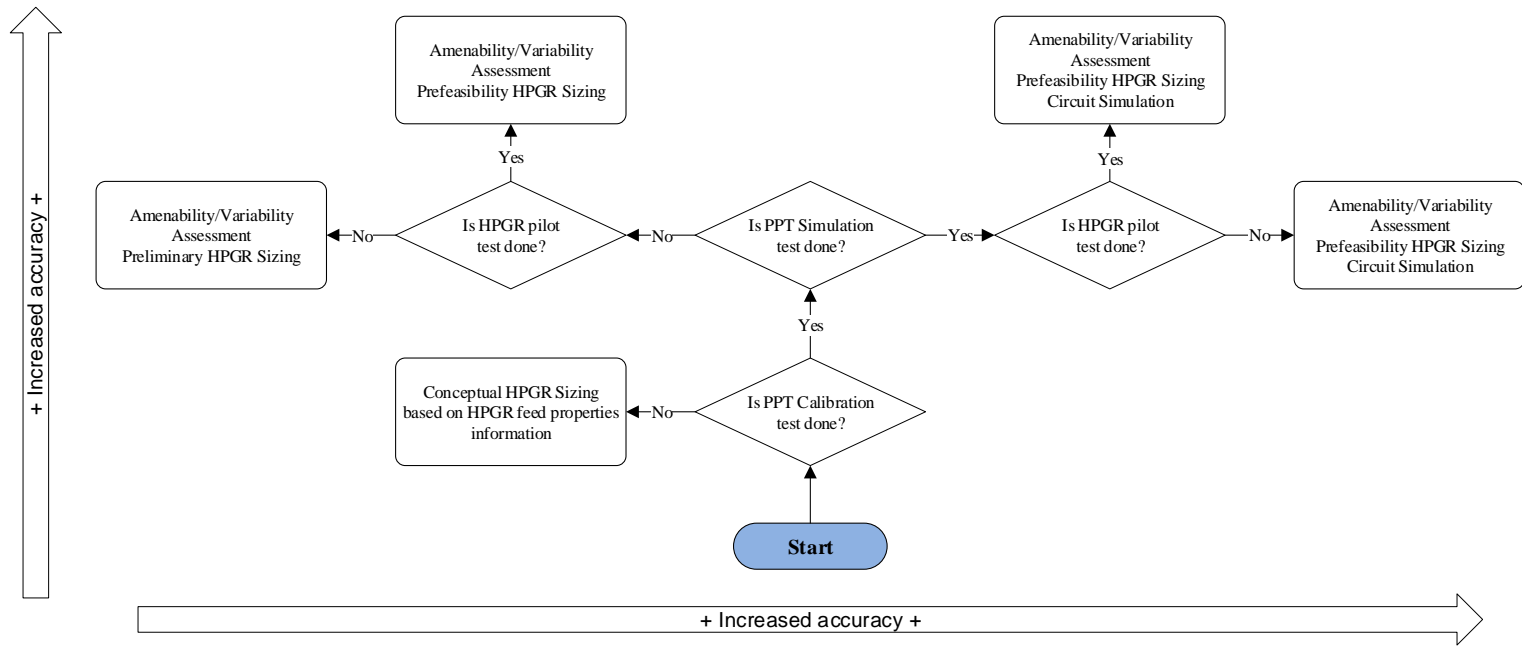


Figure 8.1: HPGR evaluation flow chart

8.2 Recommendations for Future Research

Advances in the following areas will lead to further improvements to the HPGR models:

1. Further expanding the database, engage industry/metallurgical companies by sharing the methodology and increase the database to continue the model development.
2. It is believed that the ore hardness has a considerable impact on the HPGR performance. Incorporating quantitative ore hardness parameters as model inputs would improve the model prediction.
3. Developing empirical models for HPGR performance evaluation and machine sizing in specific applications based on ore type (e.g. copper porphyry) and respective comminution flowsheet (e.g. open circuit tertiary stage).
4. Developing empirical models based on locked-cycle PPT for simulating HPGR in closed circuit. Conducting locked cycle tests at different closing screen sizes to confirm the energy and product size relationship for the compression breakage.
5. Developing a compression breakage model for fine crushing and grinding applications, by extending the mono-size PPT testing to finer size fraction.
6. Validating the empirical and semi-empirical models to full scale HPGR operations. Performing model fitting using the proposed PBM method to enable process simulation and optimization.

Chapter 9

Claims of Original Contribution

Overall, the development of a comprehensive and reliable HPGR model and simulator will provide the following significance:

1. To advance the HPGR technology, and contribute the knowledge and understanding of this energy-efficient comminution device, in hope to support broader implementation of the HPGR within the mining industry;
2. To provide the tool for mining companies to investigate and evaluate the suitability of HPGR technology for processing their ore bodies at early stage;
3. To provide a tool for plant designers to size and select an HPGR as well as design an HPGR circuit;
4. To provide a tool for existing HPGR operations to evaluate their HPGR circuit performance and enable simulation studies for process optimization.

To support the development of a comprehensive HPGR simulator, the following original contributions were made:

HPGR general knowledge

1. Significantly expanded the HPGR database from previous 154 sets to current 228 sets

2. Conducted HPGR repeatability tests within the lab and between labs, proving the reliability of the UBC test results and increasing the confidence in the developed empirical models
3. Provided key performance metrics from the HPGR database such as specific energy consumption, size reduction, product size, throughput capacity, among others. Increased knowledge of HPGR technology and provided information for HPGR benchmarking comparison.
4. Discussed the major design consideration for the HPGR circuit, and compared with the conventional SAG mill circuit design.

HPGR sizing and selection

1. Empirical models were developed for predicting the key HPGR operating parameters including power draw, specific energy consumption, specific throughput constant and product sizes.
2. Developed a framework that is vendor independent for HPGR evaluation in different phases of studies with significant reduction in sample and testing requirements.

HPGR modeling and simulation

1. Improved the accuracy of energy estimate from the force-displacement curve using the bi-exponential function, instead of the trapezoid approach.
2. Applied the machine learning approach for HPGR specific throughput constant modeling and prediction.
3. Developed an enhanced semi-mechanistic model incorporating HPGR design for prediction of HPGR center and edge product particle size distribution.
4. Validated the proposed HPGR model using the pilot tests performed with a different size of HPGR at a different laboratory.
5. Developed an integrated HPGR simulator for one-stop HPGR process modeling and circuit simulation.

Bibliography

- [1] Abouzeid, A. M. and Fuerstenau, D. W. (2009). Grinding of mineral mixtures in high-pressure grinding rolls. *International Journal of Mineral Processing*, 93(1):59–65. → page 6
- [2] Ahmadzadeh, F. and Lundberg, J. (2013). Remaining useful life prediction of grinding mill liners using an artificial neural network. *Minerals Engineering*, 53:1–8. → page 305
- [3] Altman, N. S. (1992). An introduction to kernel and nearest-neighbor nonparametric regression. *The American Statistician*, 46(3):175–185. → page 308
- [4] Amelunxen, P., Mular, M., Vanderbeek, J., Hill, L., and Herrera, E. (2011). The Effects of Ore Variability on HPGR Trade-off Economics. In *Proceedings of the 5th International Conference on Semi-Autogenous Grinding Technology*, Vancouver, BC, Canada. → page 17
- [5] Andersen, J. and Napier-Munn, T. J. (1988). Power prediction for cone crushers. *Australasian Institute of Mining and Metallurgy*. → page 28
- [6] Anderson, T. W. and Darling, D. A. (1954). A test of goodness of fit. *Journal of the American statistical association*, 49(268):765–769. → page 108
- [7] Anthony, M. and Holden, S. B. (1998). Cross-validation for binary classification by real-valued functions: theoretical analysis. In *Proceedings of the eleventh annual conference on Computational learning theory*, pages 218–229. → page 49
- [8] Austin, L., Weller, K., and Lim, W. (1993). Phenomenological modelling of the high pressure grinding rolls. → pages 22, 187
- [9] Austin, L. G., Klimpel, R. R., and Luckie, P. T. (1984). *Process engineering of size reduction: ball milling*. American Institute of Mining, Metallurgical, and Petroleum Engineers. → page 52

- [10] Ballantyne, G. and Powell, M. (2014). Benchmarking comminution energy consumption for the processing of copper and gold ores. *Minerals Engineering*, 65:109–114. → page 2
- [11] Ballantyne, G. R., Hilden, M., and van der Meer, F. P. (2018). Improved characterisation of ball milling energy requirements for hpgr products. *Minerals Engineering*, 116:72–81. → page 17
- [12] Barrios, G. K. and Tavares, L. M. (2016). A preliminary model of high pressure roll grinding using the discrete element method and multi-body dynamics coupling. *International Journal of Mineral Processing*, 156:32–42. In Honor of Professor Heinrich Schubert on his 90th birthday. → page 22
- [13] Bearman, R. (2006). High-Pressure Grinding Rolls - Characterising and Defining Process Performance for Engineers. In Kawatra, S. K., editor, *Advances in comminution*. SME. → pages 84, 87
- [14] Benzer, H., DüNDAR, H., Altun, O., Tavares, L. M. M., Powell, M., Mazzinghy, D. B., and Russo, J. F. C. (2017). Hpgr simulation from piston-die tests with an itabirite ore. *REM-International Engineering Journal*, 70(1):99–107. → page 19
- [15] Bond, F. C. (1960). Confirmation of the third theory. *AIME transactions*, 217:139–153. → page 18
- [16] Breiman, L. (2001). Random forests. *Machine learning*, 45(1):5–32. → page 307
- [17] Bulled, D. and Husain, K. (2008). The development of a small-scale test to determine work index for High Pressure Grinding Rolls. In *Proceedings 2008*, Ottawa, ON, Canada. → page 19
- [18] Burchardt, E. and Mackert, T. (2019). Hpgrs in minerals: What do more than 50 hard rock hpgrs tell us for the future? (part 2 - 2019). In *Proceedings of the 7th International Conference on Semi-Autogenous and High Pressure Grinding Technology*, Vancouver, BC, Canada. → pages 9, 78, 138
- [19] Comi, T., Garcia, C., Potulsha, A., and Opazo, J. (2015). Sierra Gorda Chile's New Copper-Molybdenum Operation. *Mining Engineering*, 67(7):23–23. → page 9
- [20] Cortes, C. and Vapnik, V. (1995). Support-vector networks. *Machine learning*, 20(3):273–297. → page 308

- [21] Costello, B. and Brown, J. (2015). A tabletop cost estimate review of several large hpgr projects. In *Proceedings of the 6th International Conference on Semi-Autogenous and High Pressure Grinding Technology*. → pages 14, 17, 18, 152
- [22] Daniel, M., Klein, B., and Wang, C. (2019). High-Pressure Grinding Rolls Technology. In Young, C. A., editor, *SME Mineral Processing and Extractive Metallurgy Handbook*. SME. → pages 14, 81, 83, 85
- [23] Daniel, M. J. (2002). *HPGR model verification and scale-up*. MASc, The University of Queensland, Brisbane, Queensland, Australia. → page 27
- [24] Daniel, M. J. and Morrell, S. (2004). HPGR model verification and scale-up. *Minerals Engineering*, 17(11–12):1149–1161. → page 22
- [25] Davaanyam, Z. (2015). *Piston Press Test Procedures for Predicting Energy - Size Reduction of High Pressure Grinding*. Ph.D., The University of British Columbia, Vancouver, BC, Canada. → pages iv, 3, 16, 19, 21, 22, 30, 31, 32, 33, 34, 35, 42, 43, 143, 144, 159, 160, 184, 186, 187
- [26] Davaanyam, Z., Klein, B., Nadolski, S., and Kumar, A. (2015). Predicting the energy requirements of High Pressure Grinding Rolls using piston press testing procedures. Ottawa, ON, Canada. → page 45
- [27] De, A. and Fuerstenau, D. (2012). Simulation of macroscopic variables related to comminution in high-pressure grinding rolls. In *XXVI International Mineral Processing Congress (IMPC), New Delhi*, pages 1075–1090. → page 11
- [28] Dundar, H., Benzer, H., and Aydogan, N. (2013). Application of population balance model to HPGR crushing. *Minerals Engineering*, 50–51:114–120. → page 22
- [29] Elkin, N., Pate, W., Alkac, D., Suarez, D., and Noriega, R. (2017). The applicability of the packed bed test (pbt) to assess ore hardness variability in the hrc™ hpgr. In *Procemin GEOMET*, Santiago, Chile. → page 127
- [30] Engelhardt, D., Seppelt, J., Waters, T., Apfelt, A., Lane, G., Yahyaei, M., and Powell, M. (2015). The cadia hpgr-sag circuit—from design to operation—the commissioning challenge. → page 9
- [31] Freund, Y. and Schapire, R. E. (1995). A decision-theoretic generalization of on-line learning and an application to boosting. In *European conference on computational learning theory*, pages 23–37. Springer. → page 308

- [32] Fuerstenau, D. and Abouzeid, A.-Z. (2007). Role of feed moisture in high-pressure roll mill comminution. *International Journal of Mineral Processing*, 82(4):203–210. → page 15
- [33] Fuerstenau, D., Shukla, A., and Kapur, P. (1991). Energy consumption and product size distributions in choke-fed, high-compression roll mills. *International Journal of Mineral Processing*, 32(1-2):59–79. → pages 20, 21, 22, 160, 187
- [34] Fuerstenau, D. W. and Abouzeid, A.-Z. M. (1998). The performance of the high pressure roll mill: Effect of feed moisture. *Fizykochemiczne Problemy Mineralurgii*, 32:227–241. → page 15
- [35] Fuerstenau, D. W., Gutsche, O., and Kapur, P. C. (1996). Confined particle bed comminution under compressive loads. *International Journal of Mineral Processing*, 44-45:521–537. → pages 19, 20, 21, 160
- [36] Fuerstenau, D. W. and Kapur, P. C. (1995). Newer energy-efficient approach to particle production by comminution. *Powder Technology*, 82(1):51–57. → page 19
- [37] Gardula, A., Das, D., DiTrento, M., and Joubert, S. (2015). First year of operation of hpgr at tropicana gold mine—case study. In *Proceedings of the 6th International Conference on Semi-Autogenous and High Pressure Grinding Technology*. → pages 9, 12, 14
- [38] Gardula, A., Das, D., Viljoen, J., Tickner, C., and Piscicelli, S. (2019). Hpgr at tropicana gold mine - case study. In *Proceedings of the 7th International Conference on Semi-Autogenous and High Pressure Grinding Technology*, Vancouver, BC, Canada. → pages 9, 12
- [39] Godoy, M. L. S. (2010). Development of the Salobo project. In *Canadian Institute of Mining, Metallurgy and Petroleum*. → page 9
- [40] Gonzalez, G., Miranda, D., Casali, A., and Vallebuona, G. (2008). Detection and identification of ore grindability in a semiautogenous grinding circuit model using wavelet transform variances of measured variables. *International Journal of Mineral Processing*, 89(1-4):53–59. → page 305
- [41] Harrell Jr, F. E. (2015). *Regression modeling strategies: with applications to linear models, logistic and ordinal regression, and survival analysis*. Springer. → page 48

- [42] Hart, S., Parker, B., Rees, T., Manesh, A., and McGaffin, I. (2011). Commissioning and ramp up of the HPGR circuit at Newmont Boddington gold. In *Proceedings of the 5th International Conference on Semi-Autogenous Grinding Technology*, Vancouver, BC, Canada. → pages 9, 12, 14
- [43] Hawkins, R. (2007). *A Piston and Die Test to Predict Laboratory-scale HPGR Performance*. M.Phil., University of Queensland. → page 19
- [44] Herbst, J. and Fuerstenau, D. (1973). Mathematical simulation of dry ball milling using specific power information. *Trans. AIME*, 254:343. → page 52
- [45] Hinde, A. and Kalala, J. (2009). The application of a simplified approach to modelling tumbling mills, stirred media mills and HPGRs. *Minerals Engineering*, 22(7-8):633–641. → page 22
- [46] Hoerl, A. E. and Kennard, R. W. (1970). Ridge regression: Biased estimation for nonorthogonal problems. *Technometrics*, 12(1):55–67. → page 47
- [47] Hoseinian, F. S., Faradonbeh, R. S., Abdollahzadeh, A., Rezai, B., and Soltani-Mohammadi, S. (2017). Semi-autogenous mill power model development using gene expression programming. *Powder Technology*, 308:61–69. → page 305
- [48] Jaime E. Sepúlveda, Edson Tobar, . S. F. (2019). Model-based laboratory / plant scale-up of hpgr circuit performance. In *Proceedings of the 7th International Conference on Semi-Autogenous and High Pressure Grinding Technology*. Vancouver, BC, Canada. → page 73
- [49] Jankovic, A. (2015). Developments in iron ore comminution and classification technologies. In *Iron Ore*, pages 251–282. Elsevier. → page 17
- [50] Kalala, J., Dong, H., and Hinde, A. (2011). Using piston-die press to predict the breakage behaviour of HPGR. In *Proceedings of the 5th International Conference on Semi-Autogenous Grinding Technology*, Vancouver, BC, Canada. → page 19
- [51] Kapur, P., Gutsche, O., and Fuerstenau, D. (1993). Comminution of single particles in a rigidly-mounted roll mill part 3: particle interaction and energy dissipation. *Powder technology*, 76(3):271–276. → page 6
- [52] Kick, F. (1885). Das gesetz der proportionalen widerstande und seine anwendung felix. *Leipzig, Germany*. → page 18

- [53] Klein, B., Wang, C., and Nadolski, S. (2018). Energy-efficient comminution: Best practices and future research needs. In *Energy efficiency in the minerals industry*, pages 197–211. Springer. → page 2
- [54] Klymowsky, I. and Liu, J. (1997a). Modelling of the comminution in a roller press. In *XX International Mineral Processing Congress (IMPC), Aachen*, pages 141–154. → pages 22, 25, 26, 187
- [55] Klymowsky, I. and Liu, J. (1997b). Progress in the modelling of comminution in a roller press. *ZKG INTERNATIONAL*, 50(9):500–510. → pages 22, 187
- [56] Klymowsky, R., Patzelt, N., Knecht, J., and Burchardt, E. (2002). Selection and sizing of high pressure grinding rolls. *Mineral processing plant design, practice and control proceedings*, 1:636–668. → pages 11, 12, 13, 15, 85, 87
- [57] Klymowsky, R., Patzelt, N., Knecht, J., and Burchardt, E. (2006). An overview of HPGR technology. In Allan, M., editor, *International autogenous and semiautogenous grinding technology, 2006*. University of British Columbia Dept. of Mining Engineering, [Vancouver]. → page 298
- [58] Koski, S., Vanderbeek, J., and Enriquez, J. (2011). Cerro Verde concentrator-Four years operating HPGRs. In *Proceedings of the 5th International Conference on Semi-Autogenous Grinding Technology*. → pages 9, 14
- [59] Lane, G., Seppelt, J., and Wang, E. (2018). Quantifying the energy efficiency transformation at cadia due to hpgr crushing. In *Proceedings 14th AusIMM Mill Operators' Conference*, Melbourne, Victoria, Australia. → page 138
- [60] Li, H., Evertsson, M., Lindqvist, M., Hulthén, E., Asbjörnsson, G., and Bonn, G. (2019). Dynamic modeling of a sag mill-pebble crusher circuit by data-driven methods. In *Proceedings of the 7th International Conference on Semi-Autogenous and High Pressure Grinding Technology*. Vancouver, BC, Canada. → page 305
- [61] Lim, I., Voigt, W., and Weller, K. (1996). Product size distribution and energy expenditure in grinding minerals and ores in high pressure rolls. *International Journal of Mineral Processing*, 44-45(0):539–559. → page 21
- [62] Lim, W. I., Campbell, J. J., and Tondo, L. A. (1997). Extrusion effect in the high pressure grinding rolls. → page 10

- [63] Lind, P., Erwin, K., Chandramohan, R., Tweed, D., Lane, G., Staples, P., Hille, S., Foggiatto, B., Awmack, J., and Patterson, B. (2019). Optimisation opportunities at newmont goldcorp’s peñasquito operation. In *7th International Conference on Semi-Autogenous and High Pressure Grinding Technology*, Vancouver, BC, Canada. → page 9
- [64] Liu, J. and Schönert, K. (1996). Modelling of interparticle breakage. *International Journal of Mineral Processing*, 44-45:101–115. → pages 23, 24, 25, 26
- [65] Lubjuhn, U. and Schönert, K. (1993). Material flow in the acceleration zone and throughput of high pressure roller mills. In *XVIII International Mineral Processing Congress (IMPC), Sydney*, pages 161–168. → pages 10, 13
- [66] Lynch, A. (1977). Mineral crushing and grinding circuits: Their simulation, optimization, design and control. *Elsevier*, page 340. → page 52
- [67] Macías-García, A., Cuerda-Correa, E. M., and Díaz-Díez, M. (2004). Application of the rosin–rammler and gates–gaudin–schuhmann models to the particle size distribution analysis of agglomerated cork. *Materials Characterization*, 52(2):159–164. → page 79
- [68] McCoy, J. and Auret, L. (2019). Machine learning applications in minerals processing: A review. *Minerals Engineering*, 132:95–109. → page 305
- [69] Morley, C. (2006). High-Pressure Grinding Rolls - A Technology Review. In Kawatra, S. K., editor, *Advances in comminution*. Society for Mining Metallurgy & Exploration. → pages 14, 15, 135
- [70] Morley, C. (2010). Hpgr-faq. *Journal of the Southern African Institute of Mining and Metallurgy*, 110(3):107–115. → page 87
- [71] Morrell, S. (2009). Predicting the overall specific energy requirement of crushing, high pressure grinding roll and tumbling mill circuits. *Minerals Engineering*, 22(6):544–549. → page 126
- [72] Morrell, S., Lim, W., Shi, F., and Tondo, L. (1997a). Modelling of the HPGR crusher. In Kawatra, S. K., editor, *Comminution Practices*. → pages 22, 27, 29, 89, 189
- [73] Morrell, S., Shi, F., and Tondo, L. (1997b). Modelling and scale-up of high pressure grinding rolls. In *Proc. XX International Mineral Processing Congress*, eds. HB von Blottnitz and H. Hohberg. → pages 22, 27, 28, 187, 189

- [74] Mosher, J. and Bigg, A. (2002). Bench-scale testing and pilot plant tests for comminution circuits design. *Proceedings of the SME Mineral Processing Plant Design, Practice and Control*, 1:123–135. → page 126
- [75] Mular, M., Hoffert, J., and Koski, S. (2015). Design and operation of the metcalf concentrator comminution circuit. In *Proceedings of the 6th International Conference on Semi-Autogenous and High Pressure Grinding Technology*. → pages 9, 12
- [76] Nadolski, S. (2012). *Development of laboratory scale procedure for predicting throughput of High Pressure Grinding Rolls*. MASC, University of British Columbia, Vancouver, BC, Canada. → pages 3, 30, 35
- [77] Napier-Munn, T. (2015). Is progress in energy-efficient comminution doomed? *Minerals Engineering*, 73:1–6. → page 2
- [78] Napier-Munn, T. J., Morrison, R., Morrell, S., and Kojovic, T. (1996). *Mineral Comminution Circuits: Their Operation and Optimisation*. Julius Kruttschnitt Mineral Research Centre. → pages 7, 30, 52
- [79] Narayanan, S. and Whiten, W. (1988). Determination of comminution characteristics from single-particle breakage tests and its application to ball-mill scale-up. *Trans. IMM*, 97:C115–C124. → pages 30, 31
- [80] Palaniandy, S., Halomoan, R., and Ishikawa, H. (2018). Shifting the comminution workload from the primary ball mill to TowerMill circuit. In *14thAusIMM Mill Operators' Conference*, Brisbane, Australia. → page 9
- [81] Pearce, P., Gagnon, C., Klein, B., McIvor, R., Makni, S., Wang, F., and Kumar, A. (2019). Investigation of novel hpgr and size classification circuit. In *7th International Conference on Semi-Autogenous and High Pressure Grinding Technology*, Vancouver, BC, Canada. → page 8
- [82] Rashidi, S., Rajamani, R. K., and Fuerstenau, D. W. (2017). A review of the modeling of high pressure grinding rolls. *KONA Powder and Particle Journal*, page 2017017. → pages 10, 12, 22, 140
- [83] Rosario, P. (2010). A structured approach to the evaluation of the energy requirements of hpgr and sag mill circuits in hard ore applications. *Journal of the Southern African Institute of Mining and Metallurgy*, 110(3):117–123. → page 135

- [84] Rosario, P. (2011). *Comminution Circuit Design and Simulation for the Development of a Novel High Pressure Grinding Roll Circuit*. Ph.D., The University of British Columbia, Vancouver, BC, Canada. → pages 17, 18, 135
- [85] Rosario, P. (2017). Technical and economic assessment of a non-conventional hpgr circuit. *Minerals Engineering*, 103:102–111. → page 17
- [86] Rowland, C.A., J. (1973). Comparison of work indices calculated from operating data with those from laboratory test data. In *Proceedings of the 10th Commonwealth Mining and Metallurgy Congress*, Ottawa, ON, Canada. → page 149
- [87] Rule, C., Smit, I., COPE, A., and HUMPHRIES, G. (2008). Commissioning of the polycom 2.2/1.6 5.6 mw hpgr at anglo platinum's new mogalakwena north concentrator. *Comminution 2008*. → page 9
- [88] Saramak, D. and Kleiv, R. A. (2013). The effect of feed moisture on the comminution efficiency of hpgr circuits. *Minerals Engineering*, 43:105–111. → pages 15, 16
- [89] Saramak, D. and Naziemiec, Z. (2013). Determination of the nip zone angle in high-pressure grinding rolls. *Physicochemical Problems of Mineral Processing*, 49(1):243–253. → page 22
- [90] Schneider, C. L., Alves, V. K., and Austin, L. G. (2009). Modeling the contribution of specific grinding pressure for the calculation of HPGR product size distribution. *Minerals Engineering*, 22(7-8):642–649. → page 22
- [91] Schönert, K. (1988). A first survey of grinding with high-compression roller mills. *International Journal of Mineral Processing*, 22(1-4):401–412. → pages 6, 13, 19, 84, 85
- [92] Schönert, K. (1995). Comminution from theory to practice. In Herbst, J., editor, *Proceedings of the XIX International Mineral Processing Congress.*, volume 1. Society for Mining Metallurgy and Exploration, Littleton Colo. → page 11
- [93] Schönert, K. (1996). The influence of particle bed configurations and confinements on particle breakage. *International Journal of Mineral Processing*, 44-45:1–16. → page 19

- [94] Schönert, K. and Lubjuhn, U. (1990). Throughput of high compression roller mills with plane and corrugated rollers. In *Proceedings of 7th European Symposium on Comminution*, pages 213–217. → page 90
- [95] Seebach, M. v. and Knobloch, O. (1987). High pressure grinding rolls in industrial application. In *SME Annual Meeting*. → pages 13, 90
- [96] Shi, F. and Kojovic, T. (2007). Validation of a model for impact breakage incorporating particle size effect. *International Journal of Mineral Processing*, 82(3):156–163. → page 31
- [97] Taber, Q. and Rosell, E. (2015). Aplicación de la tecnología hpgr en la operación de conminución implementada en la concentradora cuajone. → page 9
- [98] Tavares, L. (2005). Particle weakening in high-pressure roll grinding. *Minerals Engineering*, 18(7):651–657. → page 17
- [99] Tibshirani, R. (1996). Regression shrinkage and selection via the lasso. *Journal of the Royal Statistical Society: Series B (Methodological)*, 58(1):267–288. → page 47
- [100] Torres, M. and Casali, A. (2009). A novel approach for the modelling of high-pressure grinding rolls. *Minerals Engineering*, 22(13):1137–1146. → pages 22, 187
- [101] Unland, G. and Wang, G. (1998a). Model of high pressure roller mills a phenomenological-mathematical approach, part 1. *ZKG INTERNATIONAL*, 51(7):347–353. → page 22
- [102] Unland, G. and Wang, G. (1998b). Model of high pressure roller mills-a phenomenological-mathematical approach, part 2. *ZKG INTERNATIONAL*, 51(11):600–+. → page 22
- [103] Van der Meer, F. (2010). High pressure grinding rolls scale-up and experiences. In *XXV International Mineral Processing Congress (IMPC), Brisbane*, pages 1319–1331. → page 15
- [104] van der Meer, F. (2011). Feasibility of dry high pressure grinding and classification. In *Autogenous and Semi-autogenous Grinding Technology Conference. Vancouver*. → page 8
- [105] van der Meer, F. P. (2015). Pellet feed grinding by hpgr. *Minerals Engineering*, 73:21–30. Special issue: Comminution. → page 8

- [106] Van der Meer, F. P. and Gruendken, A. (2010). Flowsheet considerations for optimal use of high pressure grinding rolls. *Minerals Engineering*, 23(9):663–669. → page 137
- [107] Vanderbeek, J. and Gunson, A. (2015). Cerro verde 240,000 t/d concentrator expansion. In *Proceedings of the 6th International Conference on Semi-Autogenous and High Pressure Grinding Technology*. → page 9
- [108] Vanderbeek, J. L., Linde, T. B., Brack, W. S., and Marsden, J. O. (2006). HPGR Implementation at Cerro Verde. In Allan, M. J., Major, K., Flintoff, B. C., Klein, B., and Mular, A. L., editors, *International Autogenous and Semiautogenous Grinding Technology 2006*, volume IV. Vancouver, BC, Canada. → page 18
- [109] Villanueva, A., Banini, G., Hollow, J., Butar-Butar, R., and Mosher, J. (2011). Effects of hpgr introduction on grinding performance at pt freeport indonesia’s concentrator. In *Proceedings of the 5th International Conference on Semi-Autogenous Grinding Technology*, Vancouver, BC, Canada. → page 9
- [110] Vogel, L. and Peukert, W. (2004). Determination of material properties relevant to grinding by practicable labscale milling tests. *International Journal of Mineral Processing*, 74, Supplement(0):S329–S338. → page 31
- [111] von Michaelis, H. (2009). How energy efficient is HPGR? The Southern African Institute of Mining and Metallurgy. → page 17
- [112] von Rittinger, P. (1867). *Lehrbuch der aufbereitungskunde*. → page 18
- [113] Wang, C. (2013). *Comparison of HPGR - Ball Mill and HPGR - Stirred Mill Circuits to the Existing AG/SAG Mill - Ball Mill Circuits*. MASc, The University of British Columbia, Vancouver, BC, Canada. → page 17
- [114] Wang, C., Nadolski, S., Mejia, O., Drozdiak, J., and Klein, B. (2013). Energy and cost comparisons of hpgr based circuits with the sabc circuit installed at the huckleberry mine. In *45th Annual Canadian Mineral Processors Operators Conference, Ottaea, Ontario*. → pages 17, 152
- [115] Wills, B. A. and Finch, J. (2015). *Wills’ mineral processing technology: an introduction to the practical aspects of ore treatment and mineral recovery*. Butterworth-Heinemann. → page 52

Appendix A

HPGR Test Data

A.1 HPGR Test Procedure

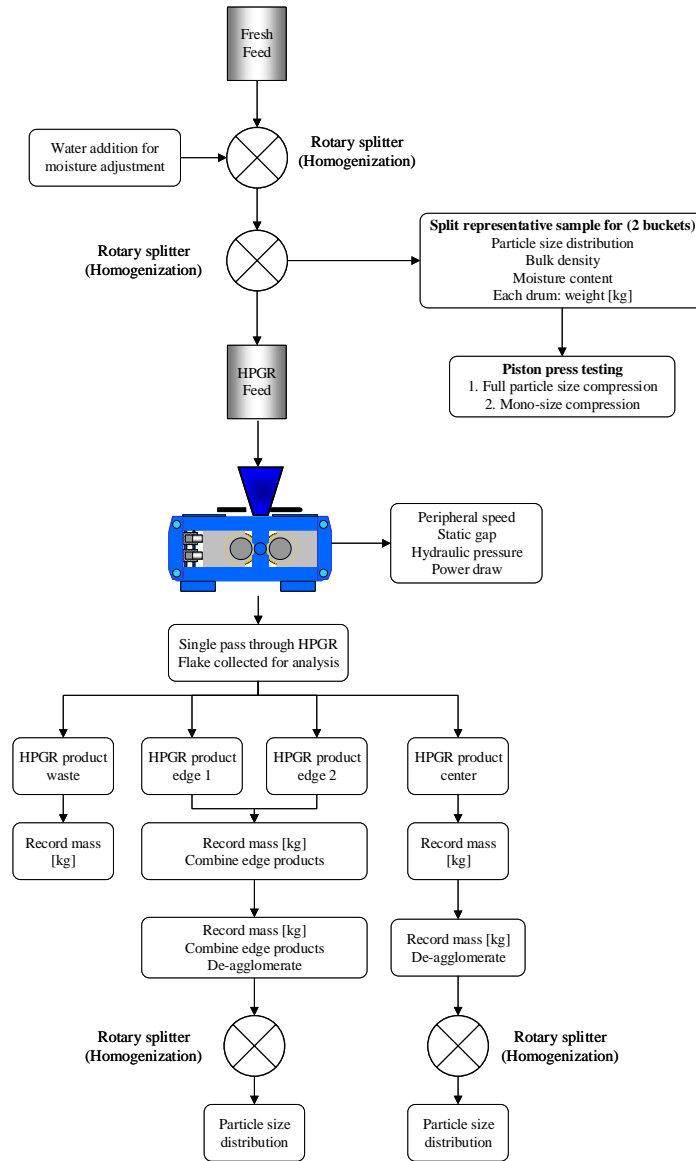


Figure A.1: Pilot HPGR test procedure

A.2 HPGR Test: Cu-Mo (HB) Ore

HPGR Test PSD Summary

Project	Cu-Mo (HB)		Total Feed	235.50	Kg
Sample ID	SAG feed belt cut		Center Product	84.50	Kg
Test ID	Cu-Mo(HB)-11		Edge Product	38.00	Kg
Moisture:	3.00	%			
Bulk:	1.70	g/cc	Waste	102.00	Kg
Dry Proctor:		g/cc	Center Product %	69%	
Pressure:	4.00	N/mm2	Edge Product %	31%	

Test No.		Feed		Centre Product		Edge Product		Experimental Full PSD	Scaled HPGR Product
Cu-Mo(HB)-11		Retained	Cum % Pass	Retained	Cum % Pass	Retained	Cum % Pass	Cum % Pass	90% Center + 10% Edge
Sieve #	Particle Size, mm								Cum % Pass
1.00	32.000	62.50	99.52	0.00	100.00	0.00	100.00	100.00	100.00
2.00	25.000	2013.30	83.94	0.00	100.00	0.00	100.00	100.00	100.00
3.00	19.000	2146.80	67.32	0.00	100.00	0.00	100.00	100.00	100.00
4.00	16.000	1368.50	56.73	32.80	99.67	27.80	99.60	99.60	99.67
5.00	12.500	1722.00	43.41	133.60	98.34	183.70	96.99	97.92	98.20
6.00	8.000	2166.20	26.64	990.00	88.45	1074.00	81.71	86.36	87.77
7.00	5.600	844.70	20.11	1042.30	78.04	941.50	68.32	75.02	77.06
8.00	4.000	533.40	15.98	1255.10	65.50	953.00	54.76	62.17	64.42
9.00	2.800	398.10	12.90	1300.00	52.51	803.70	43.33	49.66	51.59
10.00	2.000	257.20	10.91	933.30	43.19	611.80	34.63	40.53	42.33
11.00	1.400	243.00	9.03	910.00	34.10	521.00	27.22	31.96	33.41
12.00	1.000	160.60	7.78	599.10	28.11	307.20	22.85	26.48	27.59
13.00	0.710	136.10	6.73	527.80	22.84	292.80	18.68	21.55	22.42
14.00	0.500	102.80	5.93	389.30	18.95	201.40	15.82	17.98	18.64
15.00	0.355	91.10	5.23	314.80	15.81	178.60	13.28	15.02	15.55
16.00	0.250	90.00	4.53	278.70	13.02	148.80	11.16	12.44	12.84
17.00	0.180	76.80	3.94	214.30	10.88	117.00	9.50	10.45	10.74
18.00	0.125	83.20	3.29	193.30	8.95	113.50	7.88	8.62	8.84
19.00	0.090	58.80	2.84	123.90	7.72	69.90	6.89	7.46	7.64
20.00	0.063	71.40	2.29	127.00	6.45	79.10	5.76	6.24	6.38
21.00	0.045	0.80	2.28	73.20	5.72	41.50	5.17	5.55	5.67
	Pan	294.70		572.80		363.50			
	Total mass	12922.00		10010.30		7029.80			
Size Distribution Interpolations									
	%passing 8 mm		26.64		88.45		81.71		86.36
	%passing 6 mm		21.19		79.77		70.55		76.91
	%passing 4 mm		15.98		65.50		54.76		62.17
	%passing 1 mm		7.78		28.11		22.85		26.48
	%passing 0.2 mm		4.11		11.49		9.97		11.02
	%passing 0.1 mm		2.97		8.07		7.17		7.98
Linear P80	[mm]		23.58		6.05		7.69		6.65
Linear P50	[mm]		14.23		2.58		3.50		2.83

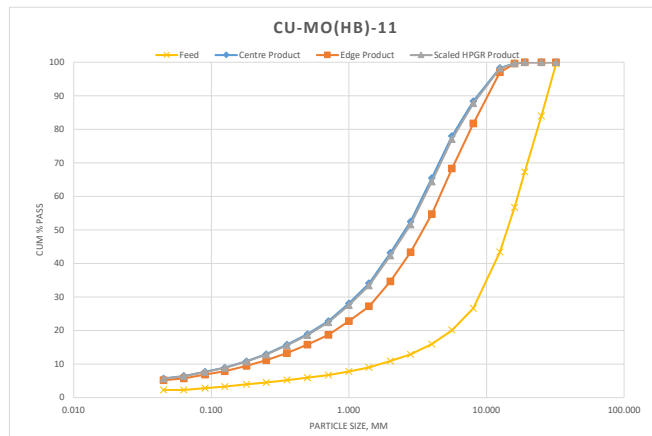


Figure A.2: Feed and product PSDs of test Cu-Mo(HB)-11

HPGR Test PSD Summary

Project	Cu-Mo (HB)	Total Feed	246.00	Kg
Sample ID	SAG feed belt cut	Center Product	75.50	Kg
Test ID	Cu-Mo(HB)-12	Edge Product	43.50	Kg
Moisture:	3.00			%
Bulk:	1.70	Waste	122.50	Kg
Dry Proctor:		Center Product %	63%	
Pressure:	3.00	Edge Product %	37%	

Test No.		Feed		Centre Product		Edge Product		Experimental Full PSD	Scaled HPGR Product
Cu-Mo(HB)-12		Retained	Cum % Pass	Retained	Cum % Pass	Retained	Cum % Pass	Cum % Pass	Cum % Pass
Sieve #	Particle Size, mm								
1.00	32.000	62.50	99.52	0.00	100.00	0.00	100.00	100.00	100.00
2.00	25.000	2013.30	83.94	0.00	100.00	0.00	100.00	100.00	100.00
3.00	19.000	2146.80	67.32	18.80	99.89	8.60	99.92	99.90	99.89
4.00	16.000	1368.50	56.73	18.60	99.70	75.80	99.20	99.52	99.65
5.00	12.500	1722.00	43.41	194.60	97.74	448.20	94.94	96.72	97.46
6.00	8.000	2166.20	26.64	993.50	87.74	1984.50	76.09	83.48	86.57
7.00	5.600	844.70	20.11	1011.60	77.55	1421.50	62.58	72.08	76.05
8.00	4.000	533.40	15.98	1526.20	62.17	1480.90	48.51	57.18	60.81
9.00	2.800	398.10	12.90	1296.90	49.11	1281.70	36.33	44.44	47.83
10.00	2.000	257.20	10.91	939.10	39.65	848.90	28.27	35.49	38.51
11.00	1.400	243.90	9.03	858.40	31.00	634.40	22.24	27.80	30.13
12.00	1.000	160.60	7.78	558.50	25.38	434.00	18.12	22.73	24.65
13.00	0.710	136.10	6.73	456.00	20.79	361.20	14.69	18.56	20.18
14.00	0.500	102.80	5.93	374.70	17.01	264.10	12.18	15.25	16.53
15.00	0.355	91.10	5.23	284.20	14.15	207.80	10.20	12.71	13.75
16.00	0.250	90.00	4.53	253.80	11.59	174.10	8.55	10.48	11.29
17.00	0.180	76.80	3.94	190.70	9.67	139.30	7.23	8.78	9.43
18.00	0.125	83.20	3.29	176.40	7.90	134.30	5.95	7.18	7.70
19.00	0.090	58.80	2.84	112.10	6.77	84.40	5.15	6.17	6.60
20.00	0.063	71.40	2.29	115.60	5.60	98.60	4.21	5.09	5.46
21.00	0.045	0.80	2.28	64.60	4.95	54.40	3.70	4.49	4.83
	Pan	294.70		491.50		389.00			
	Total mass	12922.00		9927.80		10525.70			
Size Distribution Interpolations									
	%passing 8 mm	26.64		87.74		76.09		83.48	86.57
	%passing 6 mm	21.19		79.25		64.83		73.98	77.80
	%passing 4 mm	15.98		62.17		48.51		57.18	60.81
	%passing 1 mm	7.78		25.38		18.12		22.73	24.65
	%passing 0.2 mm	4.11		10.22		7.61		9.26	9.96
	%passing 0.1 mm	2.97		7.09		5.38		6.46	6.92
Linear P80	[mm]	23.58		6.18		8.93		7.27	6.50
Linear P50	[mm]	14.23		2.88		4.17		3.32	3.00

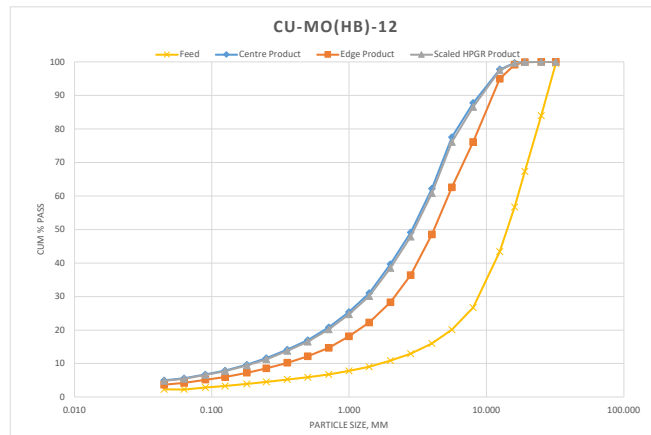


Figure A.3: Feed and product PSDs of test Cu-Mo(HB)-12

HPGR Test PSD Summary

Project	Cu-Mo (HB)	Total Feed	249.00	Kg
Sample ID	SAG feed belt cut	Center Product	81.00	Kg
Test ID	Cu-Mo(HB)-13	Edge Product	47.50	Kg
Moisture:	3.00			%
Bulk:	1.70	Waste	111.00	Kg
Dry Proctor:		Center Product %	63%	
Pressure:	2.50	Edge Product %	37%	

Test No.		Feed		Centre Product		Edge Product		Experimental Full PSD	Scaled HPGR Product
Cu-Mo(HB)-13		Retained	Cum % Pass	Retained	Cum % Pass	Retained	Cum % Pass	Cum % Pass	90% Center + 10% Edge
Sieve #	Particle Size, mm								
1.00	32.000	62.50	99.52	0.00	100.00	0.00	100.00	100.00	100.00
2.00	25.000	2013.30	83.94	0.00	100.00	0.00	100.00	100.00	100.00
3.00	19.000	2146.80	67.32	31.50	99.72	0.00	100.00	99.82	99.75
4.00	16.000	1368.50	56.73	94.10	98.87	193.50	98.25	98.64	98.81
5.00	12.500	1722.00	43.41	285.10	96.31	766.90	91.31	94.47	95.81
6.00	8.000	2166.20	26.64	1327.10	84.41	2357.60	69.99	79.08	82.97
7.00	5.600	844.70	20.11	1224.00	73.42	1525.10	56.19	67.05	71.70
8.00	4.000	533.40	15.98	1460.70	60.32	1308.20	44.35	54.42	58.72
9.00	2.800	398.10	12.90	1441.10	47.39	1176.80	33.71	42.33	46.02
10.00	2.000	257.20	10.91	1062.20	37.86	757.40	26.86	33.79	36.76
11.00	1.400	243.90	9.03	868.30	30.07	638.70	21.08	26.74	29.17
12.00	1.000	160.60	7.78	673.70	24.02	433.50	17.16	21.48	23.33
13.00	0.710	136.10	6.73	511.70	19.43	361.70	13.89	17.38	18.88
14.00	0.500	102.80	5.93	400.20	15.84	266.60	11.47	14.23	15.40
15.00	0.355	91.10	5.23	310.90	13.05	213.40	9.54	11.75	12.70
16.00	0.250	90.00	4.53	268.20	10.64	179.90	7.92	9.64	10.37
17.00	0.180	76.80	3.94	202.20	8.83	142.60	6.63	8.01	8.61
18.00	0.125	83.20	3.29	191.10	7.11	134.70	5.41	6.48	6.94
19.00	0.090	58.80	2.84	119.30	6.04	90.70	4.59	5.51	5.90
20.00	0.063	71.40	2.29	130.40	4.87	100.30	3.68	4.43	4.75
21.00	0.045	0.80	2.28	62.80	4.31	56.00	3.17	3.89	4.20
	Pan	294.70		480.30		350.90			
	Total mass	12922.00		11144.90		11054.50			
Size Distribution Interpolations									
	%passing 8 mm		26.64		84.41		69.99		79.08
	%passing 6 mm		21.19		75.26		58.49		69.06
	%passing 4 mm		15.98		60.32		44.35		54.42
	%passing 1 mm		7.78		24.02		17.16		21.48
	%passing 0.2 mm		4.11		9.35		7.00		8.48
	%passing 0.1 mm		2.97		6.35		4.82		5.78
Linear P80	[mm]		23.58		7.04		10.11		8.27
Linear P50	[mm]		14.23		3.04		4.76		3.56

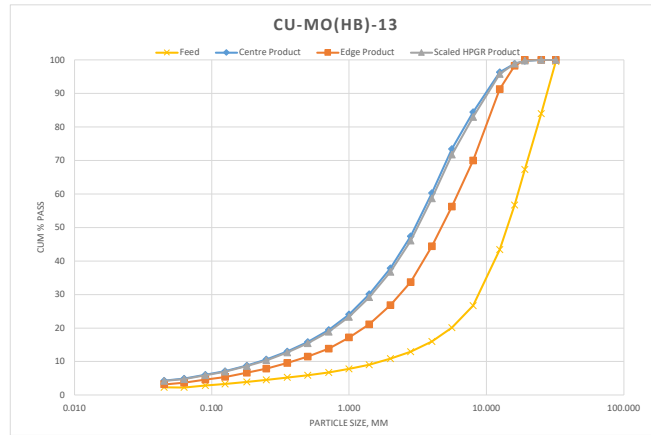


Figure A.4: Feed and product PSDs of test Cu-Mo(HB)-13

HPGR Test PSD Summary

Project	Cu-Mo (HB)	Total Feed	309.83	Kg
Sample ID	SAG feed belt cut	Center Product	73.40	Kg
Test ID	Cu-Mo(HB)-21	Edge Product	45.00	Kg
Moisture:	5.00			%
Bulk:	1.74	Waste	179.00	Kg
Dry Proctor:		Center Product %	62%	
Pressure:	3.00	Edge Product %	38%	

Test No.		Feed		Centre Product		Edge Product		Experimental Full PSD	Scaled HPGR Product
Cu-Mo(HB)-21		Retained	Cum % Pass	Retained	Cum % Pass	Retained	Cum % Pass	Cum % Pass	Cum % Pass
Sieve #	Particle Size, mm								
1.00	32.000	0.00	100.00	0.00	100.00	0.00	100.00	100.00	100.00
2.00	25.000	0.00	100.00	0.00	100.00	0.00	100.00	100.00	100.00
3.00	19.000	0.00	100.00	0.00	100.00	0.00	100.00	100.00	100.00
4.00	16.000	95.90	99.38	0.00	100.00	0.00	100.00	100.00	100.00
5.00	12.500	397.20	96.79	12.30	99.91	16.50	99.84	99.88	99.90
6.00	8.000	2127.70	82.94	519.40	95.99	378.90	96.14	96.05	96.00
7.00	5.600	1857.60	70.85	978.40	88.61	826.00	88.08	88.41	88.55
8.00	4.000	1817.10	59.02	1570.70	76.75	1130.90	77.04	76.86	76.78
9.00	2.800	1776.10	47.46	2020.30	61.51	1386.30	63.52	62.27	61.71
10.00	2.000	1347.00	38.69	1518.30	50.06	1171.20	52.09	50.83	50.26
11.00	1.400	1218.90	30.76	1287.40	40.34	982.40	42.50	41.16	40.56
12.00	1.000	812.10	25.47	1065.70	32.30	699.60	35.67	33.58	32.64
13.00	0.710	717.90	20.80	842.30	25.95	731.80	28.53	26.93	26.20
14.00	0.500	529.80	17.35	611.40	21.33	519.50	23.46	22.14	21.55
15.00	0.355	429.90	14.55	481.20	17.70	434.40	19.22	18.28	17.85
16.00	0.250	375.70	12.10	491.40	13.99	420.90	15.11	14.42	14.11
17.00	0.180	294.50	10.19	346.20	11.38	310.00	12.09	11.65	11.45
18.00	0.125	272.80	8.41	320.70	8.96	286.90	9.29	9.09	9.00
19.00	0.090	180.00	7.24	186.70	7.55	162.40	7.70	7.61	7.57
20.00	0.063	195.00	5.97	201.80	6.03	160.30	6.14	6.07	6.04
21.00	0.045	112.90	5.24	116.90	5.15	105.90	5.10	5.13	5.15
Pan		804.40		682.50		523.10			
Total mass		15362.50		13253.60		10247.00			
Size Distribution Interpolations									
%passing 8 mm		82.94		95.99		96.14		96.05	96.00
%passing 6 mm		72.86		89.84		89.42		89.68	89.80
%passing 4 mm		59.02		76.75		77.04		76.86	76.78
%passing 1 mm		25.47		32.30		35.67		33.58	32.64
%passing 0.2 mm		10.74		12.13		12.95		12.44	12.21
%passing 0.1 mm		7.58		7.96		8.16		8.03	7.98
Linear P80	[mm]	7.42		4.44		4.43		4.43	4.44
Linear P50	[mm]	3.06		2.00		1.87		1.95	1.98

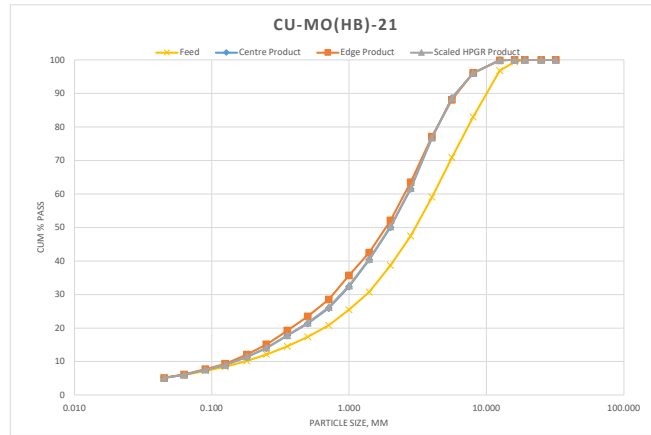


Figure A.5: Feed and product PSDs of test Cu-Mo(HB)-14

HPGR Test PSD Summary

Project	Cu-Mo (HB)	Total Feed	256.50	Kg
Sample ID	SAG feed belt cut	Center Product	82.90	Kg
Test ID	Cu-Mo(HB)-22	Edge Product	78.00	Kg
Moisture:	5.00			%
Bulk:	1.74	Waste	88.00	Kg
Dry Proctor:		Center Product %	52%	
Pressure:	3.00	Edge Product %	48%	

Test No.		Feed		Centre Product		Edge Product		Experimental Full PSD	Scaled HPGR Product
Cu-Mo(HB)-22		Retained	Cum % Pass	Retained	Cum % Pass	Retained	Cum % Pass	Cum % Pass	Cum % Pass
Sieve #	Particle Size, mm								
1.00	32.000	0.00	100.00	0.00	100.00	0.00	100.00	100.00	100.00
2.00	25.000	0.00	100.00	0.00	100.00	0.00	100.00	100.00	100.00
3.00	19.000	0.00	100.00	0.00	100.00	0.00	100.00	100.00	100.00
4.00	16.000	28.90	99.82	0.00	100.00	0.00	100.00	100.00	100.00
5.00	12.500	81.50	99.30	13.90	99.87	30.50	99.78	99.83	99.87
6.00	8.000	1046.30	92.64	288.30	97.26	526.30	96.03	96.66	97.14
7.00	5.600	1478.20	83.23	650.40	91.38	859.20	89.89	90.66	91.23
8.00	4.000	2020.00	70.37	1203.80	80.48	1377.40	80.06	80.28	80.44
9.00	2.800	2386.00	55.18	1778.90	64.38	1922.30	66.35	65.33	64.58
10.00	2.000	1870.80	43.27	1366.10	52.02	1657.30	54.52	53.23	52.27
11.00	1.400	1751.10	32.13	1257.50	40.64	1558.60	43.40	41.97	40.91
12.00	1.000	1453.00	22.88	938.20	32.14	1114.50	35.44	33.74	32.47
13.00	0.710	1180.90	15.36	771.90	25.16	1011.90	28.22	26.64	25.46
14.00	0.500	766.40	10.48	556.30	20.12	797.20	22.53	21.29	20.36
15.00	0.355	279.20	8.70	406.70	16.44	545.80	18.64	17.51	16.66
16.00	0.250	240.40	7.17	352.60	13.25	488.90	15.15	14.17	13.44
17.00	0.180	178.20	6.04	252.10	10.97	366.10	12.53	11.73	11.13
18.00	0.125	170.90	4.95	231.10	8.88	338.60	10.12	9.48	9.00
19.00	0.090	116.70	4.21	145.30	7.56	223.00	8.53	8.03	7.66
20.00	0.063	130.70	3.38	155.50	6.16	230.30	6.88	6.51	6.23
21.00	0.045	85.37	2.83	107.90	5.18	163.40	5.72	5.44	5.23
	Pan	444.90		572.20		801.00			
	Total mass	15709.47		11048.70		14012.30			
Size Distribution Interpolations									
	%passing 8 mm		92.64		97.26		96.03		96.66
	%passing 6 mm		84.80		92.36		90.92		91.66
	%passing 4 mm		70.37		80.48		80.06		80.28
	%passing 1 mm		22.88		32.14		35.44		33.74
	%passing 0.2 mm		6.36		11.62		13.28		12.43
	%passing 0.1 mm		4.42		7.94		8.98		8.44
Linear P80	[mm]		5.20		3.96		3.99		3.98
Linear P50	[mm]		2.45		1.89		1.76		1.83

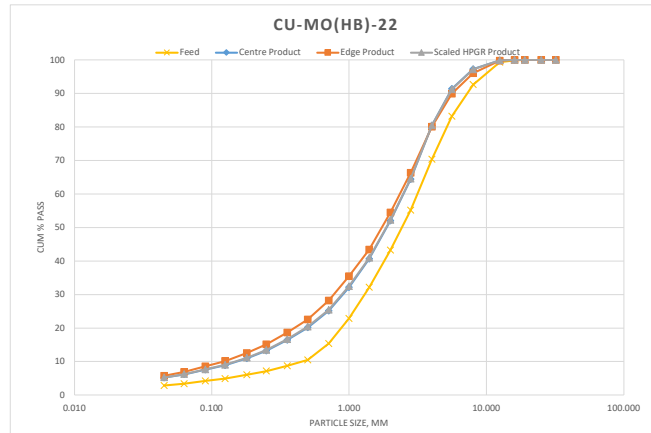


Figure A.6: Feed and product PSDs of test Cu-Mo(HB)-21

HPGR Test PSD Summary

Project	Cu-Mo (HB)		Total Feed	201.50	Kg
Sample ID	SAG feed belt cut		Center Product	92.00	Kg
Test ID	Cu-Mo(HB)-23		Edge Product	55.40	Kg
Moisture:	5.00	%			
Bulk:	1.74	g/cc	Waste	50.50	Kg
Dry Proctor:		g/cc	Center Product %	62%	
Pressure:	3.00	N/mm2	Edge Product %	38%	

Test No.		Feed		Centre Product		Edge Product		Experimental Full PSD	Scaled HPGR Product
Cu-Mo(HB)-23		Retained	Cum % Pass	Retained	Cum % Pass	Retained	Cum % Pass	Cum % Pass	90% Center + 10% Edge
Sieve #	Particle Size, mm								
1.00	32.000	0.00	100.00	0.00	100.00	0.00	100.00	100.00	100.00
2.00	25.000	0.00	100.00	0.00	100.00	0.00	100.00	100.00	100.00
3.00	19.000	0.00	100.00	0.00	100.00	0.00	100.00	100.00	100.00
4.00	16.000	17.00	99.85	0.00	100.00	0.00	100.00	100.00	100.00
5.00	12.500	53.40	99.36	5.10	99.96	0.00	100.00	99.98	99.96
6.00	8.000	628.40	93.70	258.60	97.93	303.40	97.66	97.83	97.91
7.00	5.600	921.80	85.38	570.10	93.46	659.70	92.59	93.13	93.37
8.00	4.000	1514.90	71.71	1462.30	82.00	1242.60	83.02	82.38	82.10
9.00	2.800	1657.80	56.76	1880.90	67.25	1897.70	68.42	67.69	67.36
10.00	2.000	1440.80	43.76	1611.60	54.61	1547.50	56.50	55.32	54.80
11.00	1.400	1283.60	32.18	1445.10	43.28	1549.20	44.58	43.77	43.41
12.00	1.000	962.90	23.50	993.80	35.48	1255.20	34.92	35.27	35.43
13.00	0.710	714.60	17.05	1032.70	27.39	1001.80	27.21	27.32	27.37
14.00	0.500	485.60	12.67	737.90	21.60	730.50	21.59	21.60	21.60
15.00	0.355	209.30	10.78	482.80	17.81	487.20	17.84	17.82	17.82
16.00	0.250	181.70	9.14	420.90	14.51	438.10	14.46	14.50	14.51
17.00	0.180	139.00	7.89	305.80	12.12	315.30	12.04	12.09	12.11
18.00	0.125	130.10	6.71	291.40	9.83	291.30	9.79	9.82	9.83
19.00	0.090	79.90	5.99	166.60	8.53	192.10	8.32	8.45	8.50
20.00	0.063	98.40	5.11	200.60	6.95	199.40	6.78	6.89	6.94
21.00	0.045	75.50	4.42	129.30	5.94	138.00	5.72	5.86	5.92
	Pan	490.50		757.30		743.00			
	Total mass	11085.20		12752.80		12992.00			
Size Distribution Interpolations									
	%passing 8 mm		93.70		97.93		97.66		97.83
	%passing 6 mm		86.77		94.21		93.43		93.92
	%passing 4 mm		71.71		82.00		83.02		82.38
	%passing 1 mm		23.50		35.48		34.92		35.43
	%passing 0.2 mm		8.25		12.80		12.73		12.77
	%passing 0.1 mm		6.20		8.90		8.74		8.84
Linear P80	[mm]		4.97		3.84		3.75		3.81
Linear P50	[mm]		2.38		1.76		1.67		1.72

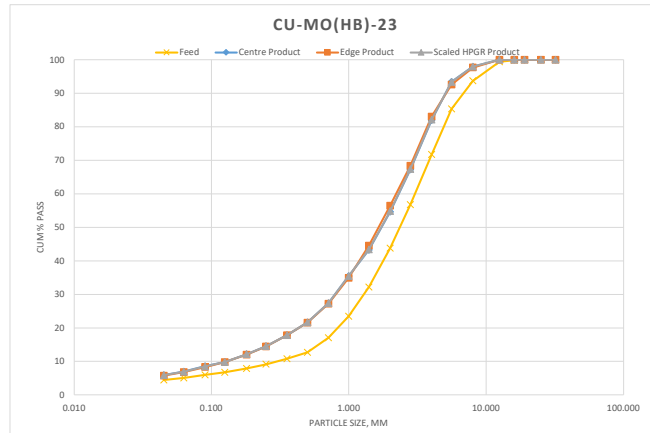


Figure A.7: Feed and product PSDs of test Cu-Mo(HB)-22

HPGR Test PSD Summary

Project	Cu-Mo (HB)		Total Feed	198.00	Kg
Sample ID	SAG feed belt cut		Center Product	78.60	Kg
Test ID	Cu-Mo(HB)-31		Edge Product	43.20	Kg
Moisture:	5.00	%			
Bulk:	1.74	g/cc	Waste	76.00	Kg
Dry Proctor:		g/cc	Center Product %	65%	
Pressure:	3.00	N/mm2	Edge Product %	35%	

Test No.		Feed		Centre Product		Edge Product		Experimental Full PSD	Scaled HPGR Product
Cu-Mo(HB)-31		Retained	Cum % Pass	Retained	Cum % Pass	Retained	Cum % Pass	Cum % Pass	90% Center + 10% Edge
Sieve #	Particle Size, mm								
1.00	32.000	0.00	100.00	0.00	100.00	0.00	100.00	100.00	100.00
2.00	25.000	0.00	100.00	0.00	100.00	0.00	100.00	100.00	100.00
3.00	19.000	0.00	100.00	0.00	100.00	0.00	100.00	100.00	100.00
4.00	16.000	0.00	100.00	0.00	100.00	0.00	100.00	100.00	100.00
5.00	12.500	0.10	99.90	6.50	99.93	14.90	99.78	99.88	99.92
6.00	8.000	3.90	96.00	295.00	96.93	312.50	95.10	96.28	96.74
7.00	5.600	7.60	88.40	603.60	90.77	535.40	87.09	89.46	90.40
8.00	4.000	11.50	76.90	851.30	82.09	668.90	77.08	80.31	81.59
9.00	2.800	14.60	62.30	1054.60	71.33	713.90	66.40	69.58	70.84
10.00	2.000	11.50	50.80	1087.50	60.24	787.80	54.62	58.25	59.68
11.00	1.400	9.60	41.20	930.10	50.75	633.30	45.14	48.76	50.19
12.00	1.000	7.60	33.60	918.00	41.39	524.20	37.30	39.94	40.98
13.00	0.710	6.70	26.90	731.90	33.93	417.00	31.06	32.91	33.64
14.00	0.500	4.80	22.10	496.90	28.86	322.50	26.23	27.93	28.60
15.00	0.355	3.80	18.30	539.30	23.36	291.50	21.87	22.83	23.21
16.00	0.250	3.90	14.40	431.30	18.96	281.10	17.67	18.50	18.83
17.00	0.180	2.70	11.70	347.00	15.42	204.10	14.61	15.13	15.34
18.00	0.125	2.60	9.10	544.70	9.87	132.50	12.63	10.85	10.14
19.00	0.090	1.50	7.60	220.60	7.62	150.00	10.39	8.60	7.89
20.00	0.063	1.50	6.10	339.50	4.15	359.20	5.01	4.46	4.24
21.00	0.045	1.00	5.10	331.30	0.77	180.90	2.31	1.32	0.93
	Pan	5.10		75.90		154.20			
	Total mass		100.00		9805.00		6683.90		
Size Distribution Interpolations									
	%passing 8 mm		96.00		96.93		95.10		96.28
	%passing 6 mm		89.67		91.80		88.43		90.60
	%passing 4 mm		76.90		82.09		77.08		80.31
	%passing 1 mm		33.60		41.39		37.30		39.94
	%passing 0.2 mm		12.47		16.43		15.49		16.10
	%passing 0.1 mm		8.03		8.26		11.03		8.54
Linear P80	[mm]		4.43		3.77		4.47		3.82
Linear P50	[mm]		1.95		1.37		1.71		1.48

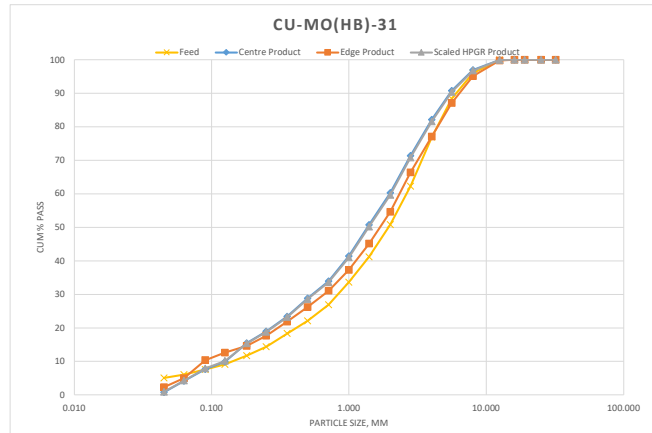


Figure A.8: Feed and product PSDs of test Cu-Mo(HB)-23

A.3 HPGR Test: Cu-Mo (HC) Ore

HPGR Test PSD Summary

Project	Cu-Mo (CH)		Total Feed	344.80	Kg
Sample ID	CompA		Center Product	144.90	Kg
Test ID	Cu-Mo(CH)-A11		Edge Product	59.30	Kg
Moisture:	1.40	%			
Bulk:	1.89	g/cc			
Dry Proctor:		g/cc	Waste	128.00	Kg
Pressure:	3.95	N/mm2	Center Product %	71%	
			Edge Product %	29%	

Test No.		Feed		Centre Product		Edge Product		Experimental Full PSD	Scaled HPGR Product	
Cu-Mo(CH)-A11		Retained	Cum % Pass	Retained	Cum % Pass	Retained	Cum % Pass	Cum % Pass	90% Center + 10% Edge	
Sieve #	Particle Size, mm									
1.00	32.000	0.00	100.00	0.00	100.00	0.00	100.00	100.00	100.00	
2.00	25.000	470.10	92.79	0.00	100.00	0.00	100.00	100.00	100.00	
3.00	19.000	937.60	78.41	0.00	100.00	0.00	100.00	100.00	100.00	
4.00	16.000	615.50	68.97	60.30	99.10	168.30	97.18	98.55	98.91	
5.00	12.500	562.50	60.35	79.80	97.92	385.60	90.73	95.83	97.20	
6.00	8.000	722.20	49.27	370.90	92.40	978.30	74.35	87.16	90.60	
7.00	5.600	442.70	42.48	451.80	85.68	649.80	63.47	79.23	83.46	
8.00	4.000	369.40	36.82	527.70	77.84	537.70	54.47	71.05	75.50	
9.00	2.800	329.20	31.77	518.00	70.13	445.10	47.02	63.42	67.82	
10.00	2.000	195.50	28.77	602.90	61.17	357.80	41.03	55.32	59.15	
11.00	1.400	276.10	24.54	541.80	53.11	374.10	34.76	47.78	51.28	
12.00	1.000	207.20	21.36	377.90	47.49	269.90	30.25	42.48	45.77	
13.00	0.710	185.50	18.52	426.10	41.16	260.70	25.88	36.72	39.63	
14.00	0.500	159.30	16.07	347.00	36.00	209.80	22.37	32.04	34.63	
15.00	0.355	146.70	13.82	321.00	31.22	206.30	18.92	27.65	29.99	
16.00	0.250	133.80	11.77	345.30	26.09	198.70	15.59	23.04	25.04	
17.00	0.180	112.60	10.05	284.00	21.87	158.10	12.94	19.27	20.97	
18.00	0.125	127.20	8.10	325.90	17.02	142.30	10.56	15.14	16.37	
19.00	0.090	94.40	6.65	255.00	13.23	121.20	8.53	11.86	12.76	
20.00	0.063	87.20	5.31	270.70	9.20	119.90	6.52	8.43	8.94	
21.00	0.045	20.60	4.99	44.10	8.55	96.20	4.91	7.49	8.18	
	Pan	325.70		574.80		293.50				
	Total mass	6521.00		6725.00		5973.30				
Size Distribution Interpolations										
	%passing 8 mm		49.27		92.40		74.35		87.16	90.60
	%passing 6 mm		43.62		86.80		65.28		80.55	84.65
	%passing 4 mm		36.82		77.84		54.47		71.05	75.50
	%passing 1 mm		21.36		47.49		30.25		42.48	45.77
	%passing 0.2 mm		10.54		23.07		13.70		20.35	22.14
	%passing 0.1 mm		7.06		14.31		9.11		12.80	13.79
	Linear P80 [mm]		19.66		4.44		9.55		5.83	4.90
	Linear P50 [mm]		8.30		1.18		3.28		1.58	1.31

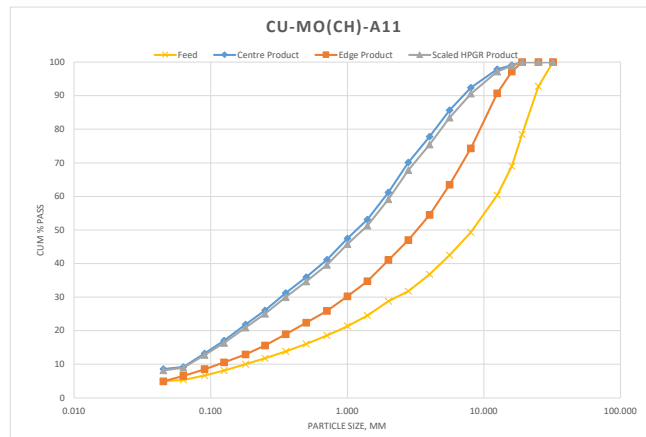


Figure A.9: Feed and product PSDs of test Cu-Mo(HC)-A11

HPGR Test PSD Summary

Project	Cu-Mo (CH)	Total Feed	342.90	Kg
Sample ID	CompA	Center Product	124.10	Kg
Test ID	Cu-Mo(CH)-A12	Edge Product	50.70	Kg
Moisture:	1.40			%
Bulk:	1.89	Waste	154.40	Kg
Dry Proctor:		Center Product %	71%	
Pressure:	3.05	Edge Product %	29%	

Test No.		Feed		Centre Product		Edge Product		Experimental Full PSD	Scaled HPGR Product
Cu-Mo(CH)-A12		Retained	Cum % Pass	Retained	Cum % Pass	Retained	Cum % Pass	Cum % Pass	90% Center + 10% Edge
Sieve #	Particle Size, mm								
1.00	32.000	0.00	100.00	0.00	100.00	0.00	100.00	100.00	100.00
2.00	25.000	470.10	92.79	0.00	100.00	0.00	100.00	100.00	100.00
3.00	19.000	937.60	78.41	0.00	100.00	0.00	100.00	100.00	100.00
4.00	16.000	615.50	68.97	75.00	98.99	282.60	95.39	97.95	98.63
5.00	12.500	562.50	60.35	130.60	97.23	521.20	86.89	94.23	96.20
6.00	8.000	722.20	49.27	669.10	88.21	1068.20	69.47	82.78	86.34
7.00	5.600	442.70	42.48	653.10	79.41	632.90	59.15	73.54	77.39
8.00	4.000	369.40	36.82	784.80	68.84	521.10	50.65	63.56	67.02
9.00	2.800	329.20	31.77	610.40	60.62	508.50	42.36	55.32	58.79
10.00	2.000	195.50	28.77	604.40	52.47	300.90	37.45	48.12	50.97
11.00	1.400	276.10	24.54	499.90	45.74	353.00	31.69	41.66	44.33
12.00	1.000	207.20	21.36	428.00	39.97	274.50	27.22	36.27	38.69
13.00	0.710	185.50	18.52	432.60	34.14	260.60	22.97	30.90	33.02
14.00	0.500	159.30	16.07	330.70	29.69	191.30	19.85	26.83	28.70
15.00	0.355	146.70	13.82	343.40	25.06	194.60	16.67	22.63	24.22
16.00	0.250	133.80	11.77	350.20	20.34	185.90	13.64	18.40	19.67
17.00	0.180	112.60	10.05	285.90	16.49	144.70	11.28	14.98	15.97
18.00	0.125	127.20	8.10	236.60	13.30	130.50	9.15	12.10	12.89
19.00	0.090	94.40	6.65	212.90	10.43	108.90	7.38	9.55	10.13
20.00	0.063	87.20	5.31	119.80	8.82	107.90	5.62	7.89	8.50
21.00	0.045	20.60	4.99	166.90	6.57	87.90	4.18	5.88	6.33
	Pan	325.70		487.50		256.50			
	Total mass	6521.00		7421.80		6131.70			
Size Distribution Interpolations									
	%passing 8 mm		49.27		88.21		69.47		82.78
	%passing 6 mm		43.62		80.88		60.87		75.08
	%passing 4 mm		36.82		68.84		50.65		63.56
	%passing 1 mm		21.36		39.97		27.22		36.27
	%passing 0.2 mm		10.54		17.59		11.95		15.95
	%passing 0.1 mm		7.06		11.25		7.88		10.27
Linear P80	[mm]		19.66		5.76		10.72		7.28
Linear P50	[mm]		8.20		1.78		3.91		2.21

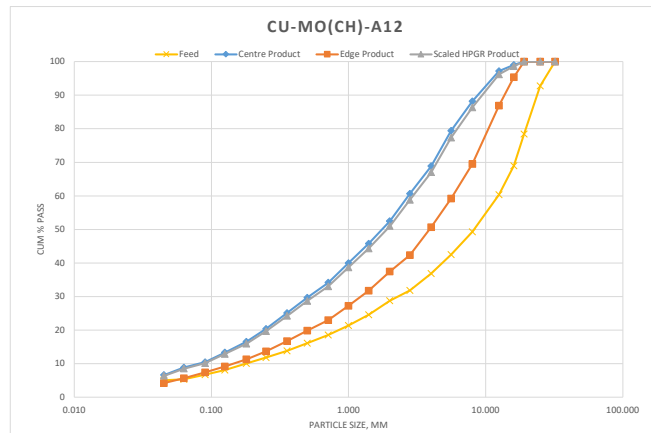


Figure A.10: Feed and product PSDs of test Cu-Mo(HC)-A12

HPGR Test PSD Summary

Project	Cu-Mo (CH)		Total Feed	304.20	Kg
Sample ID	CompA		Center Product	82.70	Kg
Test ID	Cu-Mo(CH)-A21		Edge Product	36.60	Kg
Moisture:	5.10	%			
Bulk:	1.53	g/cc	Waste	169.20	Kg
Dry Proctor:		g/cc	Center Product %	69%	
Pressure:	3.96	N/mm2	Edge Product %	31%	

Test No.		Feed		Centre Product		Edge Product		Experimental Full PSD	Scaled HPGR Product
Cu-Mo(CH)-A21		Retained	Cum % Pass	Retained	Cum % Pass	Retained	Cum % Pass	Cum % Pass	90% Center + 10% Edge
Sieve #	Particle Size, mm								
1.00	32.000	0.00	100.00	0.00	100.00	0.00	100.00	100.00	100.00
2.00	25.000	0.00	100.00	0.00	100.00	0.00	100.00	100.00	100.00
3.00	19.000	0.00	100.00	0.00	100.00	0.00	100.00	100.00	100.00
4.00	16.000	84.90	98.69	0.00	100.00	0.00	100.00	100.00	100.00
5.00	12.500	224.60	95.23	0.00	100.00	7.00	99.84	99.95	99.98
6.00	8.000	640.80	85.35	68.40	98.70	70.80	98.23	98.56	98.66
7.00	5.600	483.70	77.90	164.70	95.58	182.80	94.06	95.11	95.43
8.00	4.000	554.20	69.35	230.00	91.22	228.80	88.84	90.49	90.98
9.00	2.800	506.40	61.55	290.60	85.71	255.70	83.01	84.89	85.44
10.00	2.000	463.30	54.40	245.70	81.06	316.10	75.81	79.45	80.53
11.00	1.400	447.10	47.51	306.00	75.26	346.50	67.91	73.00	74.52
12.00	1.000	345.70	42.18	245.00	70.61	389.10	59.03	67.06	69.46
13.00	0.710	383.00	36.28	406.40	62.91	344.70	51.18	59.31	61.74
14.00	0.500	308.00	31.53	517.50	53.10	306.60	44.19	50.37	52.21
15.00	0.355	317.70	26.64	458.60	44.41	206.80	39.47	42.89	43.92
16.00	0.250	317.20	21.75	378.70	37.23	288.60	32.89	35.90	36.80
17.00	0.180	259.00	17.75	325.90	31.05	257.50	27.02	29.82	30.65
18.00	0.125	211.80	14.49	354.50	24.34	272.10	20.82	23.26	23.98
19.00	0.090	194.70	11.49	243.80	19.71	178.90	16.74	18.80	19.42
20.00	0.063	181.20	8.69	240.40	15.16	177.30	12.69	14.40	14.91
21.00	0.045	154.10	6.32	143.90	12.43	112.80	10.12	11.72	12.20
	Pan	409.90		655.80		444.00			
	Total mass	6487.30		5275.90		4386.10			

Size Distribution Interpolations					
%passing 8 mm		85.35	98.70	98.23	98.66
%passing 6 mm		79.14	96.10	94.75	95.97
%passing 4 mm		69.35	91.22	88.84	90.98
%passing 1 mm		42.18	70.61	59.03	67.06
%passing 0.2 mm		18.89	32.82	28.70	31.55
%passing 0.1 mm		12.34	21.03	17.90	20.72
Linear P80 [mm]		6.28	1.89	2.47	2.08
Linear P50 [mm]		1.62	0.45	0.67	0.46

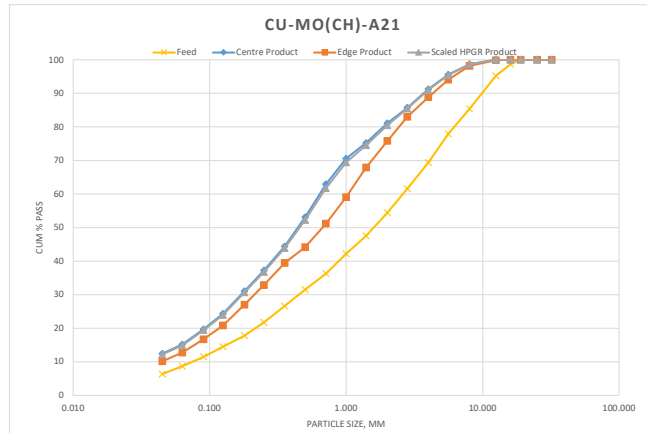


Figure A.11: Feed and product PSDs of test Cu-Mo(HC)-A21

HPGR Test PSD Summary

Project	Cu-Mo (CH)		Total Feed	284.80	Kg
Sample ID	CompA		Center Product	95.50	Kg
Test ID	Cu-Mo(CH)-A22		Edge Product	51.00	Kg
Moisture:	4.20	%			
Bulk:	1.67	g/cc	Waste	126.30	Kg
Dry Proctor:		g/cc	Center Product %	65%	
Pressure:	4.01	N/mm2	Edge Product %	35%	

Test No.		Feed		Centre Product		Edge Product		Experimental Full PSD	Scaled HPGR Product
Cu-Mo(CH)-A22		Retained	Cum % Pass	Retained	Cum % Pass	Retained	Cum % Pass	Cum % Pass	Cum % Pass
Sieve #	Particle Size, mm								
1.00	32.000	0.00	100.00	0.00	100.00	0.00	100.00	100.00	100.00
2.00	25.000	0.00	100.00	0.00	100.00	0.00	100.00	100.00	100.00
3.00	19.000	0.00	100.00	0.00	100.00	0.00	100.00	100.00	100.00
4.00	16.000	0.00	100.00	0.00	100.00	0.00	100.00	100.00	100.00
5.00	12.500	102.70	97.69	0.00	100.00	0.00	100.00	100.00	100.00
6.00	8.000	252.30	92.03	49.40	99.10	93.00	98.48	98.89	99.04
7.00	5.600	327.80	84.67	138.20	96.60	198.00	95.25	96.13	96.46
8.00	4.000	397.00	75.76	192.30	93.11	301.60	90.33	92.14	92.83
9.00	2.800	327.40	68.41	245.20	88.67	356.50	84.52	87.22	88.25
10.00	2.000	342.60	60.72	290.80	83.39	267.20	80.16	82.27	83.07
11.00	1.400	340.00	53.09	377.90	76.54	395.00	73.72	75.56	76.26
12.00	1.000	320.40	45.89	617.50	65.35	459.40	66.22	65.65	65.43
13.00	0.710	359.90	37.81	363.00	58.76	659.20	55.47	57.62	58.44
14.00	0.500	362.80	29.67	464.80	50.34	500.20	47.31	49.28	50.03
15.00	0.355	145.70	26.40	342.70	44.12	375.00	41.20	43.10	43.83
16.00	0.250	163.70	22.72	325.60	38.22	379.10	35.01	37.10	37.90
17.00	0.180	130.80	19.79	279.70	33.15	299.70	30.12	32.10	32.85
18.00	0.125	138.40	16.68	318.40	27.38	335.40	24.65	26.43	27.10
19.00	0.090	111.10	14.19	228.80	23.23	232.10	20.87	22.41	22.99
20.00	0.063	119.10	11.51	253.10	18.64	240.80	16.94	18.05	18.47
21.00	0.045	103.70	9.19	168.00	15.59	185.50	13.91	15.01	15.42
Pan		409.20		860.00		853.10			
Total mass		4454.60		5515.40		6130.80			
Size Distribution Interpolations									
%passing 8 mm			92.03		99.10		98.48		98.89
%passing 6 mm			85.90		97.02		95.79		96.89
%passing 4 mm			75.76		93.11		90.33		92.14
%passing 1 mm			45.89		65.35		66.22		65.65
%passing 0.2 mm			20.63		34.60		31.52		33.53
%passing 0.1 mm			14.90		24.41		21.95		23.56
Linear P80	[mm]		4.76		1.70		1.99		1.80
Linear P50	[mm]		1.23		0.49		0.57		0.50

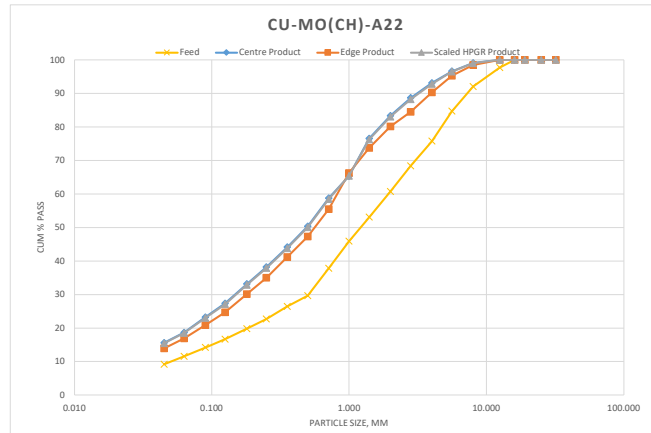


Figure A.12: Feed and product PSDs of test Cu-Mo(HC)-A22

HPGR Test PSD Summary

Project	Cu-Mo (CH)	Total Feed	283.20	Kg
Sample ID	CompA	Center Product	106.20	Kg
Test ID	Cu-Mo(CH)-A23	Edge Product	54.90	Kg
Moisture:	4.10			%
Bulk:	1.54	Waste	108.50	Kg
Dry Proctor:		Center Product %	66%	
Pressure:	4.00	Edge Product %	34%	

Test No.		Feed		Centre Product		Edge Product		Experimental Full PSD	Scaled HPGR Product
Cu-Mo(CH)-A23		Retained	Cum % Pass	Retained	Cum % Pass	Retained	Cum % Pass	Cum % Pass	90% Center + 10% Edge
Sieve #	Particle Size, mm								
1.00	32.000	0.00	100.00	0.00	100.00	0.00	100.00	100.00	100.00
2.00	25.000	0.00	100.00	0.00	100.00	0.00	100.00	100.00	100.00
3.00	19.000	0.00	100.00	0.00	100.00	0.00	100.00	100.00	100.00
4.00	16.000	37.60	99.24	0.00	100.00	0.00	100.00	100.00	100.00
5.00	12.500	60.10	98.03	0.00	100.00	0.00	100.00	100.00	100.00
6.00	8.000	259.40	92.82	48.10	98.58	130.30	97.96	98.37	98.52
7.00	5.600	309.10	86.60	79.80	96.24	216.60	94.57	95.67	96.07
8.00	4.000	455.90	77.43	124.40	92.57	274.40	90.28	91.79	92.34
9.00	2.800	331.00	70.77	125.90	88.87	333.70	85.06	87.57	88.49
10.00	2.000	346.90	63.79	182.90	83.49	333.30	79.84	82.24	83.12
11.00	1.400	360.80	56.53	190.40	77.88	391.90	73.71	76.46	77.46
12.00	1.000	383.20	48.82	241.00	70.79	336.50	68.44	69.99	70.55
13.00	0.710	535.60	38.05	439.80	57.84	634.40	58.52	58.07	57.91
14.00	0.500	424.00	29.52	330.90	48.10	594.30	49.22	48.48	48.22
15.00	0.355	183.30	25.83	251.70	40.70	428.60	42.51	41.32	40.88
16.00	0.250	194.10	21.93	217.60	34.29	418.00	35.97	34.86	34.46
17.00	0.180	158.40	18.74	180.50	28.98	331.20	30.79	29.60	29.16
18.00	0.125	163.10	15.46	184.70	23.54	360.90	25.14	24.09	23.70
19.00	0.090	117.40	13.10	147.20	19.21	235.90	21.45	19.97	19.43
20.00	0.063	139.00	10.30	134.90	15.24	255.30	17.46	16.00	15.46
21.00	0.045	88.60	8.52	100.00	12.30	171.90	14.77	13.14	12.54
	Pan	423.60		417.80		943.80			
	Total mass	4971.10		3397.60		6391.00			
Size Distribution Interpolations									
	%passing 8 mm		92.82		98.58		97.96		98.52
	%passing 6 mm		87.63		96.63		95.14		96.48
	%passing 4 mm		77.43		92.57		90.28		91.79
	%passing 1 mm		48.82		70.79		68.44		69.99
	%passing 0.2 mm		19.65		30.50		32.27		31.10
	%passing 0.1 mm		13.77		20.45		22.51		21.15
Linear P80	[mm]		4.45		1.63		2.02		1.77
Linear P50	[mm]		1.06		0.54		0.52		0.53

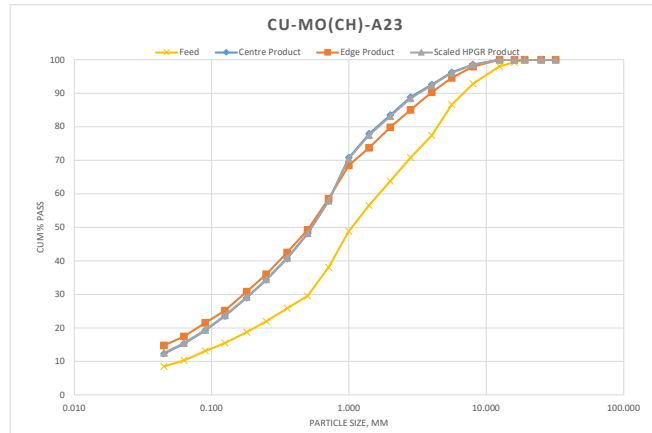


Figure A.13: Feed and product PSDs of test Cu-Mo(HC)-A23

HPGR Test PSD Summary

Project	Cu-Mo (CH)		Total Feed	302.00	Kg
Sample ID	CompC		Center Product	128.90	Kg
Test ID	Cu-Mo(CH)-C11		Edge Product	42.40	Kg
Moisture:	0.60	%			
Bulk:	1.86	g/cc	Waste	120.80	Kg
Dry Proctor:		g/cc	Center Product %	75%	
Pressure:	4.00	N/mm2	Edge Product %	25%	

Test No. Cu-Mo(CH)-C11		Feed		Centre Product		Edge Product		Experimental Full PSD	Scaled HPGR Product 90% Center + 10% Edge
Sieve #	Particle Size, mm	Retained	Cum % Pass	Retained	Cum % Pass	Retained	Cum % Pass	Cum % Pass	Cum % Pass
1.00	32.000	0.00	100.00	0.00	100.00	0.00	100.00	100.00	100.00
2.00	25.000	2105.10	86.47	0.00	100.00	0.00	100.00	100.00	100.00
3.00	19.000	1966.20	73.84	0.09	99.91	0.99	99.01	99.68	99.82
4.00	16.000	1562.50	63.79	0.74	99.17	4.46	94.55	98.03	98.71
5.00	12.500	1474.20	54.32	4.20	94.97	9.97	84.58	92.40	93.93
6.00	8.000	1660.10	43.65	9.00	85.97	14.44	70.14	82.05	84.39
7.00	5.600	982.50	37.34	7.48	78.49	9.37	60.77	74.11	76.72
8.00	4.000	787.20	32.28	9.02	69.48	8.14	52.64	65.31	67.79
9.00	2.800	709.10	27.72	5.40	64.08	6.28	46.35	59.69	62.31
10.00	2.000	582.60	23.98	7.14	56.94	6.28	40.07	52.76	55.25
11.00	1.400	546.40	20.47	7.04	49.90	6.56	33.51	45.84	48.26
12.00	1.000	414.90	17.80	5.59	44.31	3.04	30.47	40.89	42.93
13.00	0.710	380.10	15.36	6.02	38.29	4.19	26.29	35.32	37.09
14.00	0.500	320.90	13.30	5.61	32.68	3.73	22.55	30.17	31.66
15.00	0.355	284.80	11.47	4.27	28.41	2.94	19.61	26.23	27.53
16.00	0.250	282.10	9.65	4.62	23.79	2.84	16.77	22.05	23.09
17.00	0.180	241.60	8.10	3.84	19.95	2.34	14.43	18.58	19.40
18.00	0.125	277.10	6.32	4.26	15.68	2.95	11.48	14.64	15.26
19.00	0.090	188.00	5.11	2.51	13.18	1.79	9.69	12.31	12.83
20.00	0.063	207.70	3.78	2.73	10.45	1.90	7.79	9.79	10.18
21.00	0.045	125.20	2.97	0.94	9.51	0.27	7.52	9.02	9.31
	Pan	462.50		9.51		7.52			
	Total mass	15560.80		100.00		100.00			

Size Distribution Interpolations							
%passing 8 mm		43.65		85.97	70.14	82.05	84.39
%passing 6 mm		38.39		79.74	62.34	75.43	78.00
%passing 4 mm		32.28		69.48	52.64	65.31	67.79
%passing 1 mm		17.80		44.31	30.47	40.89	42.93
%passing 0.2 mm		8.54		21.04	15.10	19.57	20.45
%passing 0.1 mm		5.46		13.89	10.20	12.98	13.52
Linear P80 [mm]		21.93		6.08	11.07	7.38	6.63
Linear P50 [mm]		10.68		1.41	3.50	1.76	1.55

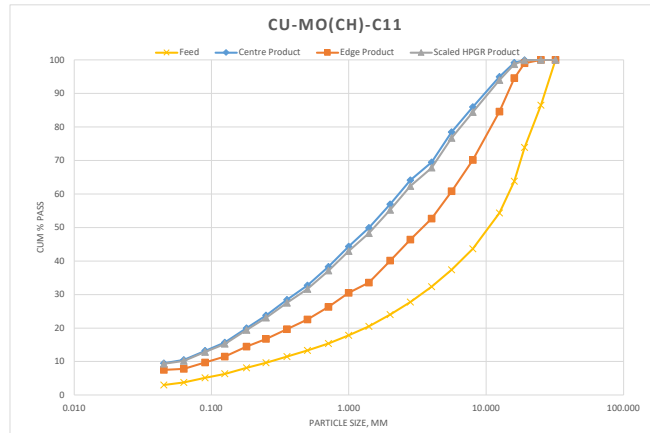


Figure A.14: Feed and product PSDs of test Cu-Mo(HC)-C11

HPGR Test PSD Summary

Project	Cu-Mo (CH)		Total Feed	310.00	Kg
Sample ID	CompC		Center Product	131.60	Kg
Test ID	Cu-Mo(CH)-C12		Edge Product	49.80	Kg
Moisture:	0.60	%			
Bulk:	1.86	g/cc	Waste	119.40	Kg
Dry Proctor:		g/cc	Center Product %	73%	
Pressure:	3.00	N/mm2	Edge Product %	27%	

Test No.		Feed		Centre Product		Edge Product		Experimental Full PSD	Scaled HPGR Product
Cu-Mo(CH)-C12		Retained	Cum % Pass	Retained	Cum % Pass	Retained	Cum % Pass	Cum % Pass	90% Center + 10% Edge
Sieve #	Particle Size, mm								
1.00	32.000	0.00	100.00	0.00	100.00	0.00	100.00	100.00	100.00
2.00	25.000	2105.10	86.47	0.00	100.00	0.00	100.00	100.00	100.00
3.00	19.000	1966.20	73.84	0.00	100.00	107.30	99.19	99.78	99.92
4.00	16.000	1562.50	63.79	225.90	98.61	624.10	94.46	97.47	98.19
5.00	12.500	1474.20	54.32	455.40	95.79	1071.70	86.35	93.20	94.85
6.00	8.000	1660.10	43.65	1629.10	85.73	1961.30	71.50	81.83	84.31
7.00	5.600	982.50	37.34	1119.50	78.82	1152.30	62.78	74.42	77.22
8.00	4.000	787.20	32.28	1566.10	69.15	1154.40	54.04	65.00	67.64
9.00	2.800	709.10	27.72	998.50	62.98	893.40	47.27	58.67	61.41
10.00	2.000	582.60	23.98	1144.70	55.91	831.70	40.98	51.81	54.42
11.00	1.400	546.40	20.47	1016.10	49.64	797.60	34.94	45.60	48.17
12.00	1.000	414.90	17.80	1143.60	42.58	575.00	30.59	39.29	41.38
13.00	0.710	380.10	15.36	953.90	36.69	563.80	26.32	33.84	35.65
14.00	0.500	320.90	13.30	795.00	31.78	451.40	22.90	29.34	30.89
15.00	0.355	284.80	11.47	691.10	27.51	405.80	19.83	25.40	26.74
16.00	0.250	282.10	9.65	732.10	22.99	390.50	16.87	21.31	22.38
17.00	0.180	241.60	8.10	631.00	19.09	336.00	14.33	17.78	18.62
18.00	0.125	277.10	6.32	671.80	14.94	396.10	11.33	13.95	14.58
19.00	0.090	188.00	5.11	402.20	12.46	243.90	9.48	11.64	12.16
20.00	0.063	207.70	3.78	460.20	9.62	274.20	7.41	9.01	9.40
21.00	0.045	125.20	2.97	139.40	8.76	40.20	7.10	8.30	8.59
	Pan	462.50		1418.00		938.40			
	Total mass	15560.80		16193.60		13209.10			
Size Distribution Interpolations									
	%passing 8 mm		43.65		85.73		71.50		81.83
	%passing 6 mm		38.39		79.97		64.23		75.65
	%passing 4 mm		32.28		69.15		54.04		65.00
	%passing 1 mm		17.80		42.58		30.59		39.29
	%passing 0.2 mm		8.54		20.20		15.06		18.79
	%passing 0.1 mm		5.46		13.17		10.01		12.30
Linear P80	[mm]		21.93		6.01		10.58		7.41
Linear P50	[mm]		10.68		1.43		3.28		1.82

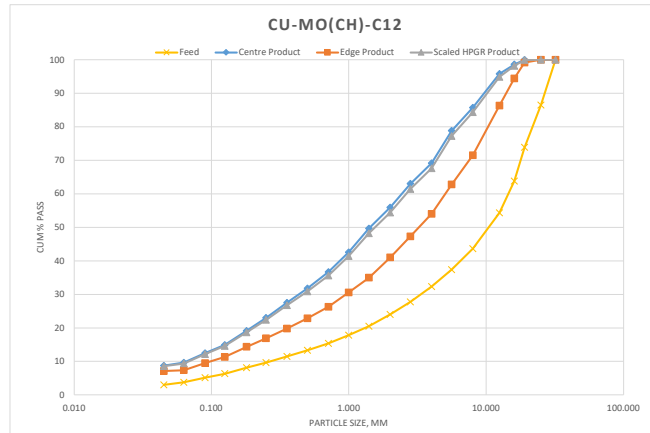


Figure A.15: Feed and product PSDs of test Cu-Mo(HC)-C12

HPGR Test PSD Summary

Project	Cu-Mo (CH)		Total Feed	315.50	Kg
Sample ID	CompC		Center Product	133.90	Kg
Test ID	Cu-Mo(CH)-C13		Edge Product	52.20	Kg
Moisture:	0.60	%			
Bulk:	1.86	g/cc	Waste	119.80	Kg
Dry Precor:		g/cc	Center Product %	72%	
Pressure:	2.50	N/mm2	Edge Product %	28%	

Test No.		Feed		Centre Product		Edge Product		Experimental Full PSD	Scaled HPGR Product
Cu-Mo(CH)-C13		Retained	Cum % Pass	Retained	Cum % Pass	Retained	Cum % Pass	Cum % Pass	90% Center + 10% Edge
Sieve #	Particle Size, mm								
1.00	32.000	0.00	100.00	0.00	100.00	0.00	100.00	100.00	100.00
2.00	25.000	2105.10	86.47	0.00	100.00	0.00	100.00	100.00	100.00
3.00	19.000	1966.20	73.84	116.60	99.33	144.70	98.85	99.19	99.28
4.00	16.000	1562.50	63.79	283.50	97.69	779.30	92.64	96.27	97.19
5.00	12.500	1474.20	54.32	715.90	93.56	1338.60	81.98	90.31	92.40
6.00	8.000	1660.10	43.65	2045.00	81.75	2109.30	65.19	77.10	80.09
7.00	5.600	982.50	37.34	1189.90	74.88	1045.30	56.87	69.83	73.08
8.00	4.000	787.20	32.28	1598.60	65.65	1034.10	48.63	60.88	63.95
9.00	2.800	709.10	27.72	977.40	60.01	845.20	41.90	54.93	58.20
10.00	2.000	582.60	23.98	1176.80	53.21	727.80	36.11	48.41	51.50
11.00	1.400	546.40	20.47	1201.50	46.28	728.10	30.31	41.80	44.68
12.00	1.000	414.90	17.80	963.00	40.72	492.70	26.39	36.70	39.28
13.00	0.710	380.10	15.36	992.40	34.99	481.70	22.55	31.50	33.74
14.00	0.500	320.90	13.30	922.80	29.66	383.80	19.49	26.81	28.64
15.00	0.355	284.80	11.47	748.70	25.34	339.30	16.79	22.94	24.48
16.00	0.250	282.10	9.65	718.80	21.19	318.60	14.26	19.24	20.49
17.00	0.180	241.60	8.10	610.70	17.66	270.20	12.10	16.10	17.10
18.00	0.125	277.10	6.32	671.90	13.78	291.30	9.79	12.66	13.38
19.00	0.090	188.00	5.11	412.20	11.40	195.40	8.23	10.51	11.08
20.00	0.063	207.70	3.78	439.50	8.86	222.00	6.46	8.19	8.62
21.00	0.045	125.20	2.97	104.20	8.26	32.70	6.20	7.68	8.06
	Pan	462.50		1431.10		778.80			
	Total mass	15560.80		17320.50		12558.90			
Size Distribution Interpolations									
	%passing 8 mm		43.65		81.75		65.19		77.10
	%passing 6 mm		38.39		76.03		58.25		71.04
	%passing 4 mm		32.28		65.65		48.63		60.88
	%passing 1 mm		17.80		40.72		26.39		39.28
	%passing 0.2 mm		8.54		18.67		12.72		17.00
	%passing 0.1 mm		5.46		12.08		8.67		11.13
Linear P80	[mm]		21.93		7.39		11.97		8.99
Linear P50	[mm]		10.68		1.72		4.27		2.19

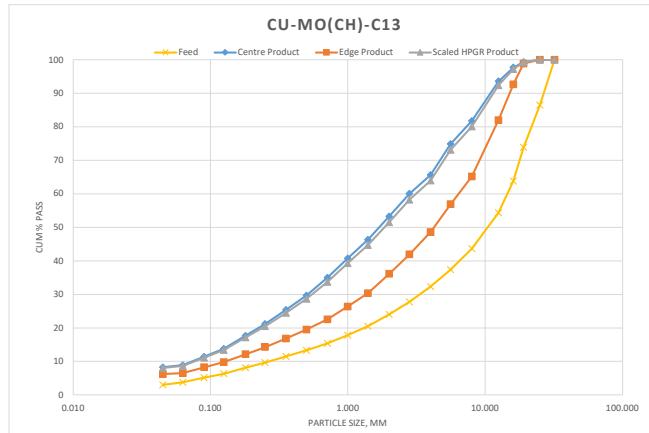


Figure A.16: Feed and product PSDs of test Cu-Mo(HC)-C13

HPGR Test PSD Summary

Project	Cu-Mo (CH)	Total Feed	246.60	Kg
Sample ID	CompC	Center Product	51.00	Kg
Test ID	Cu-Mo(CH)-C21	Edge Product	40.90	Kg
Moisture:	5.70	%		
Bulk:	1.39	g/cc		
Dry Proctor:		g/cc		
Pressure:	4.00	N/mm2	Waste	147.00
			Center Product %	55%
			Edge Product %	45%

Test No.		Feed		Centre Product		Edge Product		Experimental Full PSD	Scaled HPGR Product
Cu-Mo(CH)-C21		Retained	Cum % Pass	Retained	Cum % Pass	Retained	Cum % Pass	Cum % Pass	90% Center + 10% Edge
Sieve #	Particle Size, mm								
1.00	32.000	0.00	100.00	0.00	100.00	0.00	100.00	100.00	100.00
2.00	25.000	0.00	100.00	0.00	100.00	0.00	100.00	100.00	100.00
3.00	19.000	0.00	100.00	0.00	100.00	0.00	100.00	100.00	100.00
4.00	16.000	88.10	99.19	0.00	100.00	0.00	100.00	100.00	100.00
5.00	12.500	294.20	96.50	0.00	100.00	0.00	100.00	100.00	100.00
6.00	8.000	933.60	87.94	1.21	98.79	1.83	98.17	98.51	98.73
7.00	5.600	806.20	80.55	3.05	95.73	4.42	93.75	94.85	95.54
8.00	4.000	803.10	73.19	5.09	90.65	6.35	87.40	89.20	90.32
9.00	2.800	899.10	64.95	7.25	83.40	8.22	79.18	81.52	82.98
10.00	2.000	819.60	57.44	10.51	72.89	10.08	69.09	71.20	72.51
11.00	1.400	711.20	50.93	8.11	64.78	7.61	61.48	63.31	64.45
12.00	1.000	783.40	43.75	12.43	52.35	8.63	52.86	52.58	52.40
13.00	0.710	706.40	37.27	7.45	44.90	7.11	45.75	45.28	44.99
14.00	0.500	670.60	31.13	4.82	40.08	4.82	40.93	40.46	40.16
15.00	0.355	478.30	26.75	4.16	35.91	4.28	36.65	36.24	35.99
16.00	0.250	518.70	21.99	6.15	29.76	5.97	30.68	30.17	29.85
17.00	0.180	401.30	18.31	4.58	25.17	4.50	26.19	25.62	25.28
18.00	0.125	401.40	14.64	5.36	19.82	5.13	21.06	20.37	19.94
19.00	0.090	277.40	12.09	4.01	15.81	3.75	17.31	16.48	15.96
20.00	0.063	270.90	9.61	3.72	12.08	3.99	13.32	12.63	12.21
21.00	0.045	49.30	9.16	1.39	10.69	1.50	11.82	11.19	10.80
	Pan	999.50		10.69		11.82			
	Total mass	10912.30		100.00		100.00			
Size Distribution Interpolations									
	%passing 8 mm		87.94		98.79		98.17		98.51
	%passing 6 mm		81.78		96.24		94.48		95.46
	%passing 4 mm		73.19		90.65		87.40		89.20
	%passing 1 mm		43.75		52.35		52.86		52.40
	%passing 0.2 mm		19.36		26.48		27.47		26.58
	%passing 0.1 mm		12.82		16.95		18.38		17.09
Linear P80	[mm]		5.48		2.54		2.92		2.57
Linear P50	[mm]		1.35		0.91		0.88		0.91

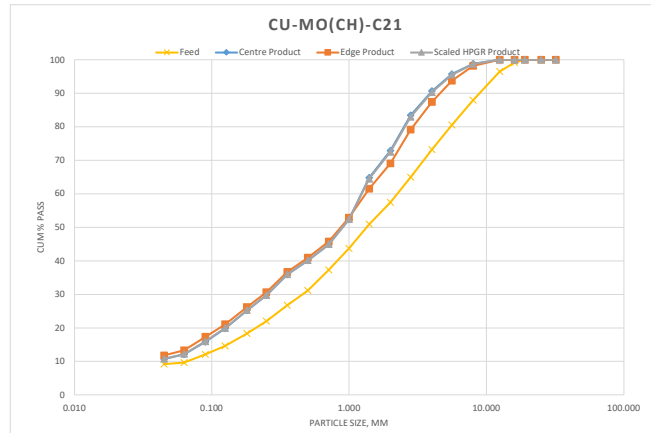


Figure A.17: Feed and product PSDs of test Cu-Mo(HC)-C21

HPGR Test PSD Summary

Project	Cu-Mo (CH)	Total Feed	240.50	Kg
Sample ID	CompC	Center Product	67.80	Kg
Test ID	Cu-Mo(CH)-C22	Edge Product	57.30	Kg
Moisture:	4.40			
Bulk:	1.41	Waste	109.70	Kg
Dry Proctor:		Center Product %	54%	
Pressure:	4.00	Edge Product %	46%	

Test No. Cu-Mo(CH)-C22		Feed		Centre Product		Edge Product		Experimental Full PSD	Scaled HPGR Product 90% Center + 10% Edge
Sieve #	Particle Size, mm	Retained	Cum % Pass	Retained	Cum % Pass	Retained	Cum % Pass	Cum % Pass	Cum % Pass
1.00	32.000	0.00	100.00	0.00	100.00	0.00	100.00	100.00	100.00
2.00	25.000	0.00	100.00	0.00	100.00	0.00	100.00	100.00	100.00
3.00	19.000	0.00	100.00	0.00	100.00	0.00	100.00	100.00	100.00
4.00	16.000	31.40	99.61	0.00	100.00	0.00	100.00	100.00	100.00
5.00	12.500	122.80	98.07	0.00	100.00	0.00	100.00	100.00	100.00
6.00	8.000	437.10	92.60	0.46	99.54	1.39	98.61	99.12	99.45
7.00	5.600	474.00	86.66	1.58	97.97	3.32	95.30	96.74	97.70
8.00	4.000	606.50	79.07	0.21	97.76	5.18	90.12	94.26	96.99
9.00	2.800	653.40	70.89	9.35	88.41	6.56	83.56	86.19	87.93
10.00	2.000	598.60	63.39	7.92	80.49	7.56	76.00	78.43	80.04
11.00	1.400	797.90	53.40	10.23	70.26	9.56	66.44	68.51	69.88
12.00	1.000	980.40	41.12	11.01	59.25	4.59	61.85	60.45	59.51
13.00	0.710	753.50	31.69	10.63	48.63	10.23	51.63	50.00	48.93
14.00	0.500	415.00	26.49	7.62	41.01	6.85	44.78	42.73	41.38
15.00	0.355	237.30	23.52	4.87	36.14	6.41	38.37	37.16	36.36
16.00	0.250	256.00	20.32	6.76	29.38	6.69	31.69	30.44	29.61
17.00	0.180	203.40	17.77	4.80	24.58	4.94	26.75	25.57	24.79
18.00	0.125	223.70	14.97	5.19	19.39	4.67	22.08	20.62	19.66
19.00	0.090	170.70	12.83	4.00	15.39	3.80	18.28	16.71	15.68
20.00	0.063	187.30	10.49	3.07	12.32	3.68	14.59	13.36	12.55
21.00	0.045	66.10	9.66	1.41	10.91	0.70	13.90	12.28	11.21
	Pan	771.40		10.91		13.90			
Total mass		7986.50		100.00		100.00			
Size Distribution Interpolations									
%passing 8 mm			92.60		99.54		98.61		99.12
%passing 6 mm			87.65		98.23		95.85		97.14
%passing 4 mm			79.07		97.76		90.12		94.26
%passing 1 mm			41.12		59.25		61.85		60.45
%passing 0.2 mm			18.50		25.95		28.16		26.96
%passing 0.1 mm			13.44		16.53		19.36		17.83
Linear P80	[mm]		4.20		1.97		2.42		2.16
Linear P50	[mm]		1.29		0.75		0.66		0.71

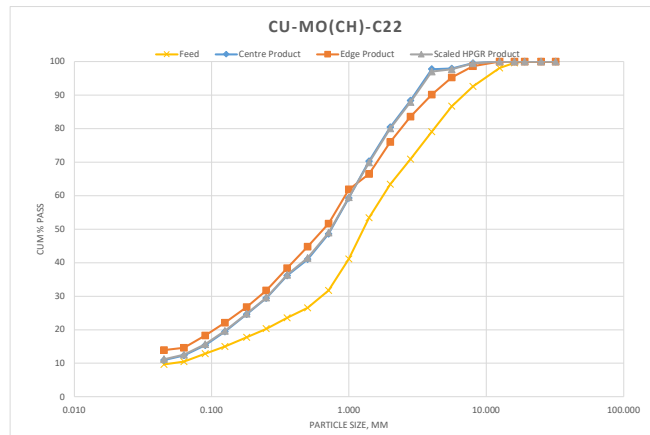


Figure A.18: Feed and product PSDs of test Cu-Mo(HC)-C22

HPGR Test PSD Summary

Project	Cu-Mo (CH)		Total Feed	242.50	Kg
Sample ID	CompC		Center Product	100.70	Kg
Test ID	Cu-Mo(CH)-C23		Edge Product	42.60	Kg
Moisture:	4.20	%			
Bulk:	1.42	g/cc	Waste	91.00	Kg
Dry Precator:		g/cc	Center Product %	70%	
Pressure:	4.00	N/mm2	Edge Product %	30%	

Test No. Cu-Mo(CH)-C23		Feed		Centre Product		Edge Product		Experimental Full PSD	Scaled HPGR Product 90% Center + 10% Edge
Sieve #	Particle Size, mm	Retained	Cum % Pass	Retained	Cum % Pass	Retained	Cum % Pass	Cum % Pass	Cum % Pass
1.00	32.000	0.00	100.00	0.00	100.00	0.00	100.00	100.00	100.00
2.00	25.000	0.00	100.00	0.00	100.00	0.00	100.00	100.00	100.00
3.00	19.000	0.00	100.00	0.00	100.00	0.00	100.00	100.00	100.00
4.00	16.000	80.20	98.82	0.00	100.00	0.00	100.00	100.00	100.00
5.00	12.500	114.80	97.12	0.00	100.00	0.00	100.00	100.00	100.00
6.00	8.000	422.90	90.88	65.40	98.91	102.00	97.98	98.64	98.82
7.00	5.600	409.50	84.84	125.00	96.84	210.00	93.83	95.95	96.54
8.00	4.000	560.00	76.57	155.50	94.26	234.30	89.20	92.75	93.75
9.00	2.800	525.80	68.81	249.30	90.12	298.40	83.30	88.09	89.44
10.00	2.000	530.80	60.97	417.60	83.19	333.20	76.71	81.26	82.54
11.00	1.400	751.20	49.89	790.00	70.08	605.30	64.74	68.49	69.54
12.00	1.000	472.60	42.91	723.50	58.07	294.90	58.91	58.32	58.15
13.00	0.710	762.40	31.66	600.70	48.10	477.70	49.46	48.50	48.24
14.00	0.500	375.00	26.12	390.60	41.62	329.80	42.94	42.01	41.75
15.00	0.355	196.80	23.22	320.20	36.30	279.20	37.42	36.63	36.41
16.00	0.250	247.30	19.57	427.90	29.20	346.90	30.56	29.60	29.34
17.00	0.180	180.30	16.91	296.80	24.27	244.00	25.73	24.71	24.42
18.00	0.125	196.30	14.01	321.60	18.94	254.00	20.71	19.46	19.11
19.00	0.090	152.80	11.75	235.60	15.03	179.10	17.17	15.66	15.24
20.00	0.063	157.20	9.43	192.00	11.84	177.70	13.66	12.38	12.02
21.00	0.045	84.90	8.18	54.10	10.94	49.80	12.67	11.46	11.11
	Pan	554.20		659.20		640.80			
	Total mass	6775.00		6025.00		5057.10			
Size Distribution Interpolations									
	%passing 8 mm		98.88		98.91		97.98		98.64
	%passing 6 mm		85.84		97.19		94.52		96.39
	%passing 4 mm		76.57		94.26		89.20		92.75
	%passing 1 mm		42.91		58.07		58.91		58.32
	%passing 0.2 mm		17.67		25.68		27.11		26.11
	%passing 0.1 mm		12.40		16.14		18.18		16.75
Linear P80	[mm]		4.66		1.85		2.40		1.94
Linear P50	[mm]		1.41		0.77		0.73		0.76

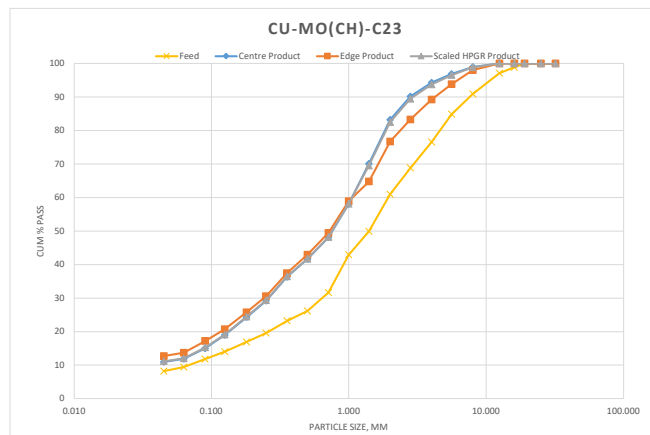


Figure A.19: Feed and product PSDs of test Cu-Mo(HC)-C23

HPGR Test PSD Summary

Project	Cu-Mo (CH)		Total Feed	292.50	Kg
Sample ID	CompD		Center Product	123.50	Kg
Test ID	Cu-Mo(CH)-D11		Edge Product	52.80	Kg
Moisture:	2.10	%			
Bulk:	1.62	g/cc	Waste	111.20	Kg
Dry Precorator:		g/cc	Center Product %	70%	
Pressure:	3.02	N/mm2	Edge Product %	30%	

Test No.		Feed		Centre Product		Edge Product		Experimental Full PSD	Scaled HPGR Product
Cu-Mo(CH)-D11		Retained	Cum % Pass	Retained	Cum % Pass	Retained	Cum % Pass	Cum % Pass	90% Center + 10% Edge
Sieve #	Particle Size, mm								Cum % Pass
1.00	32.000	0.00	100.00	0.00	100.00	0.00	100.00	100.00	100.00
2.00	25.000	611.50	89.16	0.00	100.00	0.00	100.00	100.00	100.00
3.00	19.000	1014.30	71.19	0.00	100.00	40.40	99.36	99.81	99.94
4.00	16.000	566.80	61.15	0.00	100.00	99.30	97.79	99.34	99.78
5.00	12.500	460.60	52.99	48.60	98.71	256.00	93.73	97.22	98.21
6.00	8.000	731.60	40.02	170.20	94.18	1019.50	77.56	89.20	92.52
7.00	5.600	358.50	33.67	277.40	86.81	718.40	66.17	80.63	84.74
8.00	4.000	275.00	28.80	315.00	78.43	583.80	56.92	71.99	76.28
9.00	2.800	229.50	24.73	339.60	69.40	521.10	48.65	63.19	67.33
10.00	2.000	201.40	21.16	321.00	60.86	373.00	42.74	55.44	59.05
11.00	1.400	164.80	18.24	232.10	54.69	373.60	36.82	49.34	52.91
12.00	1.000	136.60	15.82	189.70	49.65	334.70	31.51	44.22	47.84
13.00	0.710	114.40	13.79	270.10	42.47	269.10	27.24	37.91	40.94
14.00	0.500	107.30	11.89	260.50	35.54	266.00	23.03	31.79	34.29
15.00	0.355	94.10	10.23	177.70	30.82	192.90	19.97	27.57	29.73
16.00	0.250	86.90	8.69	188.20	25.81	193.60	16.90	23.14	24.92
17.00	0.180	74.60	7.36	147.50	21.89	159.40	14.37	19.64	21.14
18.00	0.125	82.60	5.90	160.40	17.62	171.00	11.66	15.84	17.03
19.00	0.090	62.80	4.79	121.50	14.39	125.90	9.66	12.98	13.92
20.00	0.063	65.40	3.63	115.10	11.33	133.10	7.55	10.20	10.95
21.00	0.045	55.00	2.65	92.80	8.87	102.90	5.92	7.98	8.57
	Pan	149.80		333.40		373.60			
	Total mass	5643.50		3760.80		6307.30			
Size Distribution Interpolations									
	%passing 8 mm		40.02		94.18		77.56		89.20
	%passing 6 mm		34.73		88.04		68.07		86.04
	%passing 4 mm		28.80		78.43		56.92		71.99
	%passing 1 mm		15.82		49.65		31.51		44.22
	%passing 0.2 mm		7.74		23.01		15.09		20.64
	%passing 0.1 mm		5.11		15.32		10.24		13.79
Linear P80	[mm]		21.94		4.30		8.68		5.48
Linear P50	[mm]		11.46		1.03		3.00		1.17

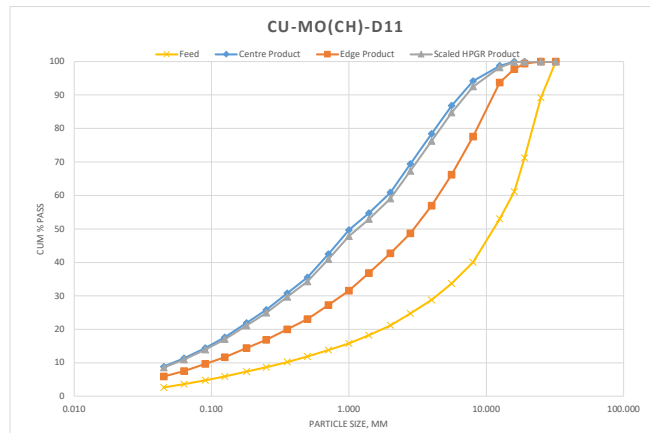


Figure A.20: Feed and product PSDs of test Cu-Mo(HC)-D11

HPGR Test PSD Summary

Project	Cu-Mo (CH)	Total Feed	255.60	Kg
Sample ID	CompD	Center Product	54.20	Kg
Test ID	Cu-Mo(CH)-D21	Edge Product	29.40	Kg
Moisture:	5.30			
	%			
Bulk:	1.59	Waste	164.00	Kg
	g/cc			
Dry Proctor:		Center Product %	65%	
	g/cc			
Pressure:	4.04	Edge Product %	35%	
	N/mm2			

Test No.		Feed		Centre Product		Edge Product		Experimental Full PSD	Scaled HPGR Product
Cu-Mo(CH)-D21		Retained	Cum % Pass	Retained	Cum % Pass	Retained	Cum % Pass	Cum % Pass	90% Center + 10% Edge
Sieve #	Particle Size, mm								
1.00	32.000	0.00	100.00	0.00	100.00	0.00	100.00	100.00	100.00
2.00	25.000	0.00	100.00	0.00	100.00	0.00	100.00	100.00	100.00
3.00	19.000	0.00	100.00	0.00	100.00	0.00	100.00	100.00	100.00
4.00	16.000	0.00	100.00	0.00	100.00	0.00	100.00	100.00	100.00
5.00	12.500	93.90	97.83	0.00	100.00	0.00	100.00	100.00	100.00
6.00	8.000	421.20	88.09	64.20	98.74	37.20	99.24	98.91	98.79
7.00	5.600	426.40	78.24	133.60	96.11	159.60	95.99	96.07	96.10
8.00	4.000	359.20	69.94	190.90	92.35	226.20	91.39	92.01	92.26
9.00	2.800	317.40	62.60	218.40	88.05	269.20	85.90	87.30	87.84
10.00	2.000	290.80	55.88	258.50	82.97	309.40	79.60	81.78	82.63
11.00	1.400	257.30	49.93	266.50	77.73	324.00	73.00	76.06	77.25
12.00	1.000	198.50	45.34	674.80	64.45	364.30	65.58	64.85	64.56
13.00	0.710	249.40	39.58	347.60	57.61	451.60	56.39	57.18	57.49
14.00	0.500	271.30	33.31	511.90	47.54	434.10	47.54	47.54	47.54
15.00	0.355	193.90	28.83	291.30	41.81	283.90	41.76	41.79	41.80
16.00	0.250	229.60	23.52	336.00	35.19	309.10	35.47	35.29	35.22
17.00	0.180	190.10	19.13	266.10	29.96	247.10	30.44	30.13	30.01
18.00	0.125	175.70	15.07	264.20	24.76	277.30	24.79	24.77	24.76
19.00	0.090	130.20	12.06	195.30	20.92	196.20	20.79	20.87	20.90
20.00	0.063	119.20	9.30	219.00	16.61	189.20	16.94	16.72	16.64
21.00	0.045	92.60	7.16	142.50	13.80	135.90	14.17	13.93	13.84
Pan		309.80		701.60		695.80			
Total mass		4326.50		5082.40		4910.10			

Size Distribution Interpolations					
%passing 8 mm		88.09	98.74	99.24	98.91
%passing 6 mm		79.88	96.55	96.53	96.54
%passing 4 mm		69.94	92.35	91.39	92.01
%passing 1 mm		45.34	64.45	65.58	64.85
%passing 0.2 mm		20.38	31.45	31.87	31.60
%passing 0.1 mm		12.92	22.02	21.93	21.99
Linear P80	[mm]	6.03	1.66	2.05	1.81
Linear P50	[mm]	1.41	0.55	0.56	0.55

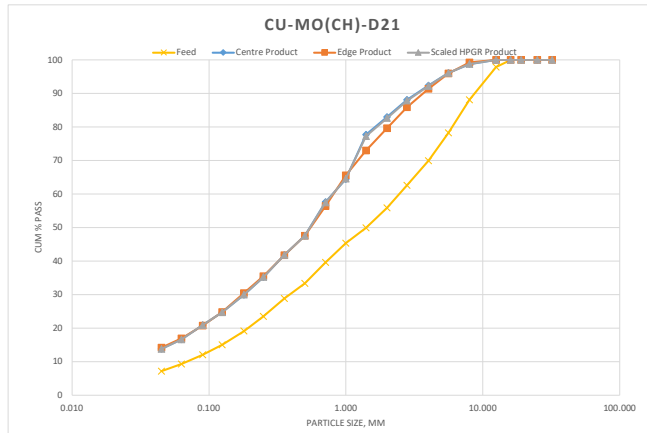


Figure A.21: Feed and product PSDs of test Cu-Mo(HC)-D21

A.4 HPGR Test: Cu-Au (C) Ore

HPGR Test PSD Summary

Project	Cu-Au (C)		Total Feed	265.70	Kg
Sample ID	SAG feed belt cut		Center Product	110.80	Kg
Test ID	Cu-Au(C)-01		Edge Product	47.60	Kg
Moisture:	3.49	%			
Bulk:	1.66	g/cc	Waste	99.00	Kg
Dry Proctor:		g/cc	Center Product %	70%	
Pressure:	5.00	N/mm2	Edge Product %	30%	

Test No.		Feed		Centre Product		Edge Product		Experimental Full PSD	Scaled HPGR Product
Cu-Au(C)-01		Retained	Cum % Pass	Retained	Cum % Pass	Retained	Cum % Pass	Cum % Pass	Cum % Pass
Sieve #	Particle Size, mm								
1.00	32.000	0.00	100.00	0.00	100.00	0.00	100.00	100.00	100.00
2.00	25.000	2002.60	88.28	0.00	100.00	0.00	100.00	100.00	100.00
3.00	19.000	1653.00	78.60	0.00	100.00	0.00	100.00	100.00	100.00
4.00	16.000	1491.00	69.88	71.20	99.49	162.50	98.65	99.23	99.40
5.00	12.500	2037.20	57.96	258.20	97.62	851.50	91.55	95.80	97.02
6.00	8.000	3054.10	40.08	1176.50	89.14	2134.30	73.76	84.51	87.60
7.00	5.600	1622.40	30.59	1167.20	80.72	1393.90	62.14	75.13	78.86
8.00	4.000	1158.00	23.81	1302.00	71.32	1140.40	52.63	65.71	69.46
9.00	2.800	992.60	18.00	1469.40	60.72	1108.60	43.39	55.52	58.99
10.00	2.000	651.70	14.18	1405.20	50.59	863.90	36.19	46.26	49.15
11.00	1.400	520.80	11.14	1344.40	40.89	820.40	29.35	37.42	39.74
12.00	1.000	364.20	9.00	877.20	34.56	515.10	25.06	31.71	33.61
13.00	0.710	248.50	7.55	743.20	29.20	520.80	20.72	26.65	28.35
14.00	0.500	197.50	6.39	775.80	23.60	417.90	17.23	21.69	22.97
15.00	0.355	158.50	5.47	636.50	19.01	397.10	13.92	17.48	18.50
16.00	0.250	131.30	4.70	508.30	15.35	302.40	11.40	14.16	14.95
17.00	0.180	84.30	4.21	230.72	13.68	199.40	9.74	12.50	13.29
18.00	0.125	93.24	3.66	296.42	11.54	254.40	7.62	10.36	11.15
19.00	0.090	64.05	3.28	202.34	10.08	185.30	6.07	8.88	9.68
20.00	0.063	70.60	2.87	194.13	8.68	167.80	4.68	7.48	8.28
21.00	0.045	58.98	2.53	144.85	7.64	98.70	3.85	6.50	7.26
	Pan	431.64		1058.76		462.20			
	Total mass	17086.20		13862.33		11996.60			
Size Distribution Interpolations									
	%passing 8 mm		40.08		89.14		73.76		84.51
	%passing 6 mm		32.17		82.12		64.07		76.70
	%passing 4 mm		23.81		71.32		52.63		65.71
	%passing 1 mm		9.00		34.56		25.06		31.71
	%passing 0.2 mm		4.35		14.16		10.21		12.97
	%passing 0.1 mm		3.39		10.50		6.52		9.30
Linear P80	[mm]		19.87		5.48		9.58		6.84
Linear P50	[mm]		10.50		1.96		3.66		2.32

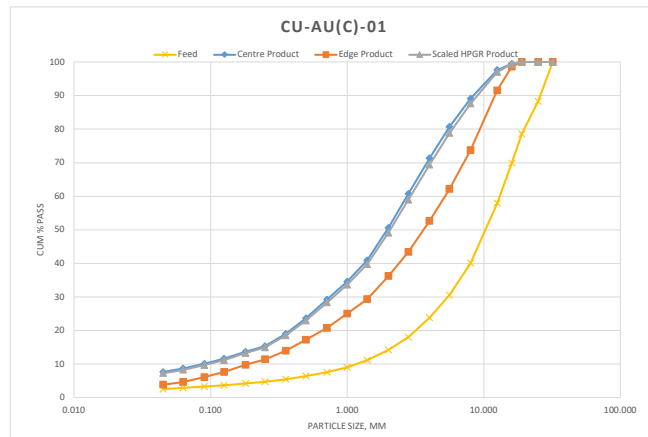


Figure A.22: Feed and product PSDs of test Cu-Au(C)-01

HPGR Test PSD Summary

Project	Cu-Au (C)		Total Feed	259.10	Kg
Sample ID	SAG feed belt cut		Center Product	88.40	
Test ID	Cu-Au(C)-02		Edge Product	34.10	Kg
Moisture:	3.72	%			
Bulk:	1.72	g/cc	Waste	128.80	Kg
Dry Proctor:		g/cc	Center Product %	72%	
Pressure:	4.09	N/mm2	Edge Product %	28%	

Test No. Cu-Au(C)-02		Feed		Centre Product		Edge Product		Experimental Full PSD	Scaled HPGR Product 90% Center + 10% Edge
Sieve #	Particle Size, mm	Retained	Cum % Pass	Retained	Cum % Pass	Retained	Cum % Pass	Cum % Pass	Cum % Pass
1.00	32.000	0.00	100.00	0.00	100.00	0.00	100.00	100.00	100.00
2.00	25.000	2002.60	88.28	21.30	99.80	0.00	100.00	99.86	99.82
3.00	19.000	1653.00	78.60	46.80	99.37	29.30	99.64	99.44	99.40
4.00	16.000	1491.00	69.88	98.60	98.45	234.80	96.78	97.99	98.29
5.00	12.500	2037.20	57.96	293.20	95.73	655.70	88.79	93.80	95.04
6.00	8.000	3054.10	40.08	1022.20	86.25	1428.90	71.38	82.11	84.77
7.00	5.600	1622.40	30.59	1031.50	76.69	1009.20	59.08	71.79	74.93
8.00	4.000	1158.00	23.81	1073.50	66.73	854.00	48.67	61.70	64.93
9.00	2.800	992.60	18.00	1181.00	55.78	802.60	38.89	51.08	54.09
10.00	2.000	651.70	14.18	839.90	47.99	496.90	32.83	43.77	46.48
11.00	1.400	520.80	11.14	891.10	39.73	465.20	27.16	36.23	38.47
12.00	1.000	364.20	9.00	689.70	33.33	372.40	22.62	30.35	32.26
13.00	0.710	248.50	7.55	479.40	28.88	295.50	19.02	26.14	27.90
14.00	0.500	197.50	6.39	519.40	24.07	257.70	15.88	21.79	23.25
15.00	0.355	158.50	5.47	566.00	18.82	259.00	12.73	17.12	18.21
16.00	0.250	131.30	4.70	455.20	14.60	182.30	10.50	13.46	14.19
17.00	0.180	84.30	4.21	143.99	13.26	89.82	9.41	12.19	12.88
18.00	0.125	93.24	3.66	217.53	11.24	107.30	8.10	10.37	10.93
19.00	0.090	64.05	3.28	143.47	9.91	69.59	7.25	9.17	9.65
20.00	0.063	70.60	2.87	139.84	8.62	75.76	6.33	7.98	8.39
21.00	0.045	58.98	2.53	116.54	7.54	65.48	5.53	6.98	7.34
	Pan	431.64		812.64		453.89			
	Total mass	17086.20		10782.81		8205.34			
Size Distribution Interpolations									
	%passing 8 mm	40.08		86.25		71.38		82.11	84.77
	%passing 6 mm	32.17		78.28		61.13		73.51	76.57
	%passing 4 mm	23.81		66.73		48.67		61.70	64.93
	%passing 1 mm	9.00		33.33		22.62		30.35	32.26
	%passing 0.2 mm	4.35		13.64		9.72		12.55	13.25
	%passing 0.1 mm	3.39		10.29		7.50		9.52	10.01
Linear P80	[mm]	19.87		6.43		10.23		7.51	6.84
Linear P50	[mm]	10.50		2.21		4.20		2.68	2.37

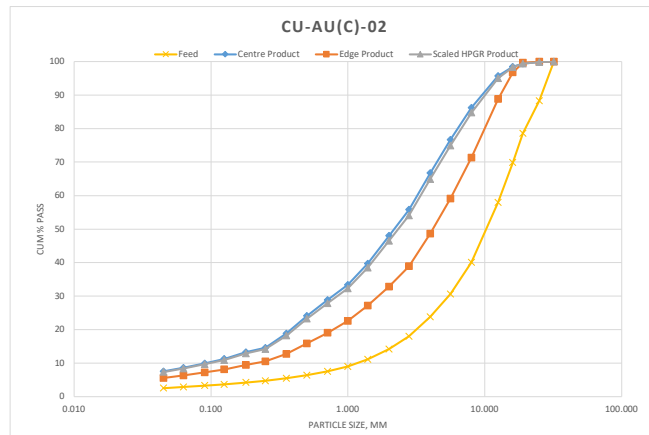


Figure A.23: Feed and product PSDs of test Cu-Au(C)-02

HPGR Test PSD Summary

Project	Cu-Au (C)	Total Feed	261.20	Kg
Sample ID	SAG feed belt cut	Center Product	119.10	Kg
Test ID	Cu-Au(C)-03	Edge Product	46.40	Kg
Moisture:	4.10			%
Bulk:	1.57	Waste	89.50	Kg
Dry Proctor:		Center Product %	72%	
Pressure:	3.09	Edge Product %	28%	

Test No.		Feed		Centre Product		Edge Product		Experimental Full PSD	Scaled HPGR Product
Cu-Au(C)-03		Retained	Cum % Pass	Retained	Cum % Pass	Retained	Cum % Pass	Cum % Pass	Cum % Pass
Sieve #	Particle Size, mm								
1.00	32.000	0.00	100.00	0.00	100.00	0.00	100.00	100.00	100.00
2.00	25.000	2002.60	88.28	0.00	100.00	0.00	100.00	100.00	100.00
3.00	19.000	1653.00	78.60	41.30	99.67	108.30	99.04	99.49	99.60
4.00	16.000	1491.00	69.88	68.60	99.11	391.10	95.56	98.12	98.76
5.00	12.500	2037.20	57.96	467.60	95.35	1403.20	83.09	91.91	94.12
6.00	8.000	3054.10	40.08	1451.10	83.65	2369.50	62.02	77.59	81.49
7.00	5.600	1622.40	30.59	1388.70	72.46	1456.50	49.08	65.91	70.12
8.00	4.000	1158.00	23.81	1275.10	62.19	1056.00	39.69	55.88	59.94
9.00	2.800	992.60	18.00	1384.70	51.03	938.40	31.35	45.51	49.06
10.00	2.000	651.70	14.18	953.00	43.35	605.40	25.97	38.48	41.61
11.00	1.400	520.80	11.14	1009.70	35.28	539.60	21.17	31.33	33.87
12.00	1.000	364.20	9.00	705.60	29.60	377.50	17.82	26.30	28.42
13.00	0.710	248.50	7.55	530.90	25.32	272.20	15.40	22.54	24.33
14.00	0.500	197.50	6.39	504.50	21.25	272.20	12.98	18.93	20.43
15.00	0.355	158.50	5.47	563.80	16.71	268.70	10.59	14.99	16.10
16.00	0.250	131.30	4.70	464.60	12.97	199.10	8.82	11.80	12.55
17.00	0.180	84.30	4.21	138.64	11.85	123.59	7.72	10.69	11.44
18.00	0.125	93.24	3.66	185.95	10.35	139.68	6.48	9.27	9.96
19.00	0.090	64.05	3.28	131.42	9.29	95.18	5.63	8.27	8.93
20.00	0.063	70.60	2.87	123.53	8.30	100.38	4.74	7.30	7.94
21.00	0.045	58.98	2.53	99.88	7.49	78.13	4.04	6.53	7.15
	Pan	431.64		929.77		455.04			
	Total mass	17086.20		12409.40		11249.70			
Size Distribution Interpolations									
	%passing 8 mm		40.08		83.65		62.02		77.59
	%passing 6 mm		32.17		74.33		51.24		67.85
	%passing 4 mm		23.81		62.19		39.69		55.88
	%passing 1 mm		9.00		29.60		17.82		26.30
	%passing 0.2 mm		4.35		12.17		8.03		11.01
	%passing 0.1 mm		3.39		9.60		5.87		8.55
Linear P80	[mm]		19.87		7.22		11.84		8.76
Linear P50	[mm]		10.50		2.69		5.77		3.32

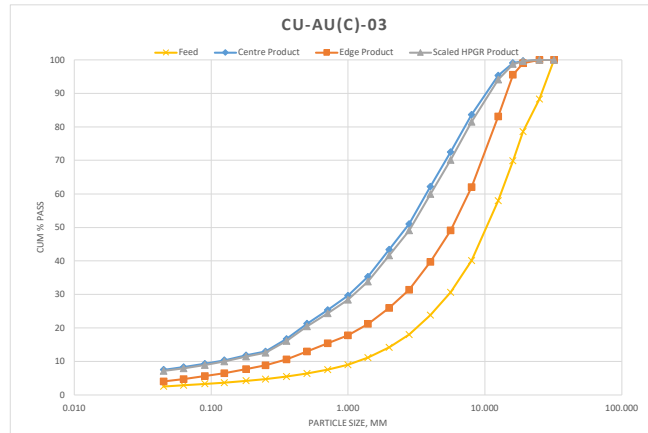


Figure A.24: Feed and product PSDs of test Cu-Au(C)-03

HPGR Test PSD Summary

Project	Cu-Au (C)		Total Feed	259.60	Kg
Sample ID	SAG feed belt cut		Center Product	117.30	Kg
Test ID	Cu-Au(C)-04		Edge Product	49.10	Kg
Moisture:	1.12	%			
Bulk:		g/cc	Waste	90.80	Kg
Dry Proctor:		g/cc	Center Product %	70%	
Pressure:	3.92	N/mm2	Edge Product %	30%	

Test No.		Feed		Centre Product		Edge Product		Experimental Full PSD	Scaled HPGR Product
Cu-Au(C)-04		Retained	Cum % Pass	Retained	Cum % Pass	Retained	Cum % Pass	Cum % Pass	Cum % Pass
Sieve #	Particle Size, mm								
1.00	32.000	233.60	98.72	0.00	100.00	0.00	100.00	100.00	100.00
2.00	25.000	2058.00	87.48	0.00	100.00	30.10	99.76	99.76	99.98
3.00	19.000	2681.80	72.84	33.00	99.76	124.40	98.78	99.47	99.66
4.00	16.000	1545.00	64.40	55.60	99.36	442.30	95.28	98.16	98.96
5.00	12.500	2249.50	52.11	374.20	96.68	921.60	87.99	94.12	95.81
6.00	8.000	3112.60	35.11	1430.80	86.42	2850.10	65.43	80.23	84.32
7.00	5.600	1558.40	26.60	1258.30	77.40	1484.90	53.68	70.40	75.03
8.00	4.000	1082.60	20.69	1380.00	67.50	1269.30	43.64	60.46	65.12
9.00	2.800	876.40	15.90	1428.30	57.26	1114.00	34.83	50.64	55.02
10.00	2.000	593.80	12.66	1250.30	48.30	768.10	28.75	42.53	46.34
11.00	1.400	501.40	9.92	1328.80	38.77	761.70	22.72	34.03	37.16
12.00	1.000	332.50	8.10	901.90	32.30	516.80	18.63	28.27	30.93
13.00	0.710	214.70	6.93	638.90	27.72	353.00	15.84	24.21	26.53
14.00	0.500	195.60	5.86	679.20	22.85	344.20	13.12	19.98	21.88
15.00	0.355	189.60	4.83	608.50	18.49	309.90	10.66	16.18	17.70
16.00	0.250	146.00	4.03	482.00	15.03	251.90	8.67	13.15	14.39
17.00	0.180	75.15	3.62	256.97	13.19	138.00	7.58	11.53	12.63
18.00	0.125	93.44	3.11	307.87	10.98	156.80	6.34	9.61	10.52
19.00	0.090	67.60	2.74	210.17	9.47	109.38	5.47	8.29	9.07
20.00	0.063	67.60	2.37	206.07	7.99	108.09	4.62	7.00	7.66
21.00	0.045	54.87	2.07	156.81	6.87	81.18	3.98	6.02	6.58
	Pan	378.94		958.10		502.45			
	Total mass	18309.10		13945.80		12638.20			
Size Distribution Interpolations									
	%passing 8 mm		35.11		86.42		65.43		80.23
	%passing 6 mm		28.02		78.90		55.64		72.04
	%passing 4 mm		20.69		67.50		43.64		60.46
	%passing 1 mm		8.10		32.30		18.63		28.27
	%passing 0.2 mm		3.74		13.71		7.89		12.00
	%passing 0.1 mm		2.84		9.90		5.72		8.67
Linear P80	[mm]		21.93		6.29		10.91		7.94
Linear P50	[mm]		11.94		2.15		5.01		2.74

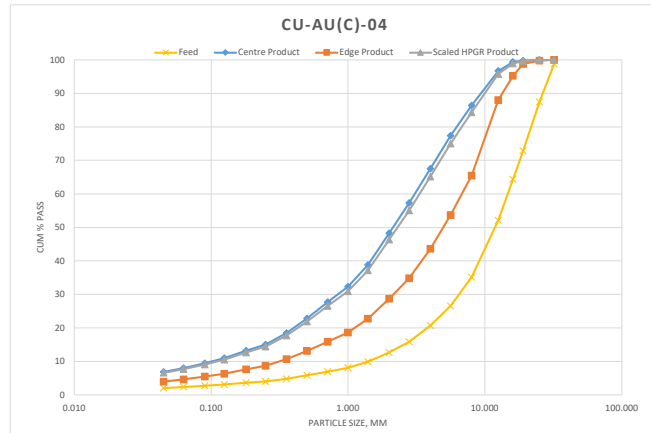


Figure A.25: Feed and product PSDs of test Cu-Au(C)-04

HPGR Test PSD Summary

Project	Cu-Au (C)		Total Feed	276.30	Kg
Sample ID	SAG feed belt cut		Center Product	117.60	Kg
Test ID	Cu-Au(C)-05		Edge Product	44.00	Kg
Moisture:	5.55	%			
Bulk:		g/cc	Waste	102.20	Kg
Dry Proctor:		g/cc	Center Product %	73%	
Pressure:	4.01	N/mm2	Edge Product %	27%	

Test No.		Feed		Centre Product		Edge Product		Experimental Full PSD	Scaled HPGR Product
Cu-Au(C)-05		Retained	Cum % Pass	Retained	Cum % Pass	Retained	Cum % Pass	Cum % Pass	90% Center + 10% Edge
Sieve #	Particle Size, mm								
1.00	32.000	0.00	100.00	0.00	100.00	0.00	100.00	100.00	100.00
2.00	25.000	2663.80	85.65	0.00	100.00	26.50	99.75	99.93	99.98
3.00	19.000	2800.40	70.56	0.00	100.00	9.00	99.67	99.91	99.97
4.00	16.000	1579.80	62.04	51.50	99.58	307.80	96.82	98.83	99.30
5.00	12.500	2119.40	50.62	331.50	96.86	684.40	90.48	95.12	96.22
6.00	8.000	2927.30	34.85	1364.50	85.68	2321.10	68.99	81.13	84.01
7.00	5.600	1498.10	26.78	1349.80	74.61	1334.50	56.63	69.72	72.82
8.00	4.000	1057.10	21.08	1287.90	64.06	1138.30	46.09	59.17	62.26
9.00	2.800	852.90	16.48	1908.00	48.42	1126.40	35.66	44.95	47.14
10.00	2.000	621.80	13.13	638.30	43.19	578.40	30.30	39.68	41.90
11.00	1.400	469.30	10.60	926.10	35.60	592.10	24.82	32.66	34.52
12.00	1.000	320.00	8.88	672.90	30.08	438.10	20.76	27.55	29.15
13.00	0.710	137.90	8.14	499.00	25.99	320.00	17.80	23.76	25.17
14.00	0.500	317.90	6.42	503.00	21.87	288.50	15.13	20.03	21.20
15.00	0.355	162.20	5.55	471.30	18.01	238.70	12.92	16.62	17.50
16.00	0.250	143.40	4.78	367.00	15.00	209.90	10.98	13.90	14.60
17.00	0.180	100.87	4.23	194.29	13.41	127.89	9.79	10.42	13.05
18.00	0.125	105.41	3.66	227.55	11.54	142.02	8.48	10.71	11.23
19.00	0.090	74.82	3.26	154.03	10.28	102.61	7.53	9.53	10.00
20.00	0.063	76.48	2.85	164.53	8.93	100.38	6.60	8.29	8.70
21.00	0.045	67.38	2.49	129.53	7.87	84.02	5.82	7.31	7.66
	Pan	461.34		960.07		628.29			
	Total mass	18557.60		12200.80		10798.90			
Size Distribution Interpolations									
	%passing 8 mm		34.85		85.68		68.99		81.13
	%passing 6 mm		28.12		76.46		58.69		71.62
	%passing 4 mm		21.08		64.06		46.09		59.17
	%passing 1 mm		8.88		30.08		20.76		27.55
	%passing 0.2 mm		4.39		13.86		10.13		12.85
	%passing 0.1 mm		3.38		10.64		7.80		9.87
Linear P80	[mm]		22.76		6.77		10.31		7.76
Linear P50	[mm]		12.32		2.92		4.59		3.23

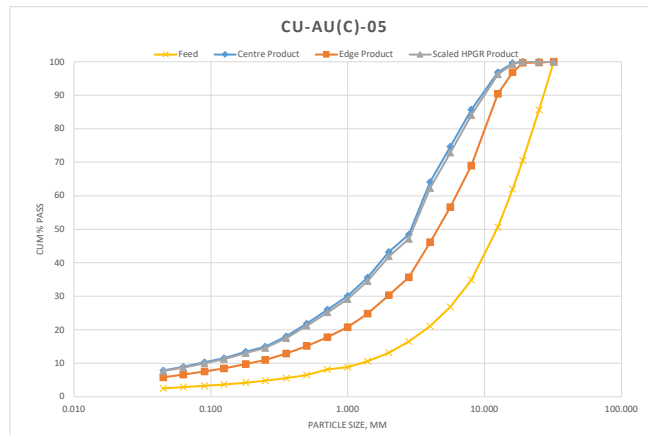


Figure A.26: Feed and product PSDs of test Cu-Au(C)-05

A.5 HPGR Test: Au (G) Ore

HPGR Test PSD Summary

Project	Au (G)	Total Feed	264.30	Kg
Sample ID	Comp1	Center Product	105.50	Kg
Test ID	Au(G)-D01	Edge Product	46.00	Kg
Moisture:	2.50			%
Bulk:	1.51	Waste	108.80	Kg
Dry Proctor:		Center Product %	70%	
Pressure:	5.05	Edge Product %	30%	

Test No.		Feed		Centre Product		Edge Product		Experimental Full PSD	Scaled HPGR Product
Au(G)-D01		Retained	Cum % Pass	Retained	Cum % Pass	Retained	Cum % Pass	Cum % Pass	90% Center + 10% Edge
Sieve #	Particle Size, mm								
1.00	32.000	239.10	98.65	0.00	100.00	0.00	100.00	100.00	100.00
2.00	25.000	4362.00	73.93	0.00	100.00	16.80	99.85	99.95	99.98
3.00	19.000	2859.20	57.73	0.00	100.00	55.10	99.35	99.80	99.94
4.00	16.000	1540.20	49.00	40.60	99.69	73.20	98.69	99.39	99.59
5.00	12.500	1943.30	37.99	188.60	98.27	520.30	94.00	96.97	97.84
6.00	8.000	2543.60	23.57	922.50	91.30	1664.90	78.97	87.56	90.07
7.00	5.600	988.60	17.97	1109.00	82.93	1145.50	68.64	78.59	81.50
8.00	4.000	690.20	14.06	865.40	76.39	817.00	61.26	71.80	74.88
9.00	2.800	481.00	11.33	1162.80	67.61	994.60	52.29	62.96	66.08
10.00	2.000	319.80	9.52	1345.90	57.44	918.60	44.00	53.36	56.10
11.00	1.400	278.70	7.94	1359.20	47.18	833.30	36.48	43.93	46.11
12.00	1.000	187.60	6.88	870.90	40.60	536.10	31.64	37.88	39.70
13.00	0.710	165.50	5.94	946.52	33.45	439.10	27.68	31.70	32.87
14.00	0.500	113.30	5.30	686.50	28.27	317.30	24.82	27.22	27.92
15.00	0.355	97.30	4.75	547.50	24.13	395.40	21.25	23.26	23.84
16.00	0.250	82.30	4.28	452.60	20.71	330.10	18.27	19.97	20.47
17.00	0.180	61.00	3.93	327.20	18.24	218.80	16.30	17.65	18.05
18.00	0.125	99.80	3.37	352.20	15.58	341.30	13.22	14.86	15.34
19.00	0.090	119.30	2.69	293.30	13.37	207.60	11.34	12.75	13.16
20.00	0.063	118.20	2.02	235.70	11.59	164.40	9.86	11.06	11.41
21.00	0.045	91.30	1.51	133.10	10.58	59.80	9.32	10.20	10.45
	Pan	265.80		1400.80		1032.80			
	Total mass	17647.10		13240.32		11082.00			
Size Distribution Interpolations									
	%passing 8 mm		23.57		91.30		78.97		87.56
	%passing 6 mm		18.90		84.32		70.36		80.08
	%passing 4 mm		14.06		76.39		61.26		71.80
	%passing 1 mm		6.88		40.60		31.64		37.88
	%passing 0.2 mm		4.03		18.95		16.86		18.74
	%passing 0.1 mm		2.89		14.00		11.88		13.79
Linear P80	[mm]		26.72		4.88		8.31		5.98
Linear P50	[mm]		16.34		1.57		2.58		1.79

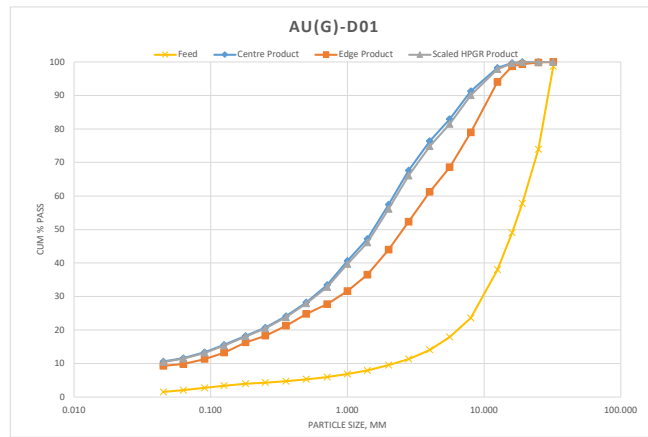


Figure A.27: Feed and product PSDs of test Au(G)-D01

HPGR Test PSD Summary

Project	Au (G)	Total Feed	275.50	Kg
Sample ID	Compl	Center Product	111.10	Kg
Test ID	Au(G)-D02	Edge Product	45.60	Kg
Moisture:	2.50			%
Bulk:	1.51	Waste	111.50	Kg
Dry Proctor:		Center Product %	71%	
Pressure:	4.01	Edge Product %	29%	

Test No. Au(G)-D02		Feed		Centre Product		Edge Product		Experimental Full PSD	Scaled HPGR Product 90% Center + 10% Edge
Sieve #	Particle Size, mm	Retained	Cum % Pass	Retained	Cum % Pass	Retained	Cum % Pass	Cum % Pass	Cum % Pass
1.00	32.000	127.10	99.30	0.00	100.00	0.00	100.00	100.00	100.00
2.00	25.000	5167.70	70.81	0.00	100.00	0.00	100.00	100.00	100.00
3.00	19.000	2138.50	59.02	0.00	100.00	137.20	98.76	99.64	99.88
4.00	16.000	1690.00	49.70	108.20	99.17	735.30	92.11	97.11	98.46
5.00	12.500	1931.20	39.05	239.70	97.32	708.50	85.71	93.94	96.16
6.00	8.000	2653.10	24.42	1090.50	88.91	1968.50	67.92	82.80	86.81
7.00	5.600	1072.30	18.51	1046.50	80.83	1112.00	57.86	74.15	78.54
8.00	4.000	739.50	14.43	1009.90	73.05	1087.20	48.04	65.77	70.54
9.00	2.800	532.20	11.50	1430.10	62.02	842.00	40.43	55.73	59.86
10.00	2.000	420.80	9.18	1231.10	52.52	719.20	33.93	47.11	50.66
11.00	1.400	286.70	7.60	1186.80	43.37	447.00	29.88	39.44	42.02
12.00	1.000	203.50	6.47	657.20	38.30	513.50	25.24	34.50	36.99
13.00	0.710	174.80	5.51	786.70	32.23	394.20	21.68	29.16	31.17
14.00	0.500	127.90	4.80	569.60	27.84	285.80	19.10	25.29	26.96
15.00	0.355	109.10	4.20	492.60	24.04	308.20	16.31	21.79	23.26
16.00	0.250	94.00	3.68	435.40	20.68	244.50	14.10	18.76	20.02
17.00	0.180	71.20	3.29	298.50	18.38	183.70	12.44	16.65	17.78
18.00	0.125	103.80	2.72	374.10	15.49	197.10	10.66	14.09	15.01
19.00	0.090	117.40	2.07	272.80	13.39	187.20	8.97	12.10	12.95
20.00	0.063	94.90	1.55	233.10	11.59	147.70	7.63	10.44	11.19
21.00	0.045	56.60	1.24	227.50	9.83	53.40	7.15	9.05	9.57
	Pan	224.40		1275.10		790.90			
	Total mass	18136.70		12965.40		11063.10			
Size Distribution Interpolations									
	%passing 8 mm	24.42		88.91		67.92		82.80	86.81
	%passing 6 mm	19.49		82.18		59.54		75.59	79.92
	%passing 4 mm	14.43		73.05		48.04		65.77	70.54
	%passing 1 mm	6.47		38.30		25.24		34.50	36.99
	%passing 0.2 mm	3.40		19.03		12.91		17.25	18.42
	%passing 0.1 mm	2.26		13.99		9.45		12.67	13.53
Linear P80	[mm]	27.26		5.43		11.06		7.22	6.02
Linear P50	[mm]	16.10		1.83		4.32		2.27	1.95

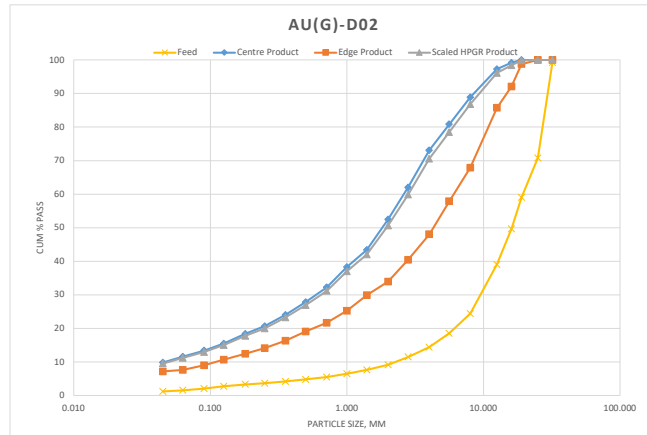


Figure A.28: Feed and product PSDs of test Au(G)-D02

HPGR Test PSD Summary

Project	Au (G)	Total Feed	255.50	Kg
Sample ID	Comp1	Center Product	118.90	Kg
Test ID	Au(G)-D03	Edge Product	46.80	Kg
Moisture:	2.50			%
Bulk:	1.51	Waste	84.80	Kg
Dry Proctor:		Center Product %	72%	
Pressure:	2.58	Edge Product %	28%	

Test No. Au(G)-D03		Feed		Centre Product		Edge Product		Experimental Full PSD	Scaled HPGR Product 90% Center + 10% Edge
Sieve #	Particle Size, mm	Retained	Cum % Pass	Retained	Cum % Pass	Retained	Cum % Pass	Cum % Pass	Cum % Pass
1.00	32.000	224.90	98.59	0.00	100.00	0.00	100.00	100.00	100.00
2.00	25.000	3595.00	76.12	0.00	100.00	49.70	99.55	99.87	99.96
3.00	19.000	2776.80	58.76	38.10	99.73	453.20	95.47	98.53	99.31
4.00	16.000	1665.80	48.34	128.40	98.83	731.80	88.88	96.02	97.84
5.00	12.500	1643.80	38.07	395.00	96.06	1047.30	79.44	91.37	94.40
6.00	8.000	2278.00	23.82	1494.80	85.57	2003.60	61.39	78.74	83.15
7.00	5.600	937.50	17.96	1276.20	76.62	1165.50	50.89	69.35	74.04
8.00	4.000	614.40	14.12	1123.90	68.73	925.70	42.55	61.34	66.11
9.00	2.800	465.40	11.21	1451.20	58.55	860.80	34.80	51.84	56.17
10.00	2.000	350.20	9.02	1283.10	49.54	690.70	28.58	43.62	47.45
11.00	1.400	225.20	7.61	1044.40	42.21	542.60	23.69	36.98	40.36
12.00	1.000	198.00	6.38	820.00	36.46	401.10	20.08	31.83	34.82
13.00	0.710	144.80	5.47	751.20	31.19	292.70	17.44	27.31	29.81
14.00	0.500	104.80	4.81	543.40	27.38	211.90	15.53	24.03	26.19
15.00	0.355	95.30	4.22	563.80	23.42	246.80	13.31	20.56	22.41
16.00	0.250	78.50	3.73	459.40	20.20	201.60	11.49	17.74	19.33
17.00	0.180	62.90	3.33	320.60	17.95	144.30	10.19	15.76	17.17
18.00	0.125	118.40	2.59	326.20	15.66	217.30	8.23	13.56	14.92
19.00	0.090	125.60	1.81	326.10	13.37	145.00	6.93	11.55	12.73
20.00	0.063	81.60	1.30	220.40	11.82	111.10	5.93	10.16	11.23
21.00	0.045	42.20	1.04	80.10	11.26	37.50	5.59	9.66	10.69
	Pan	165.60		1604.90		620.40			
	Total mass	15994.70		14251.20		11100.60			
Size Distribution Interpolations									
	%passing 8 mm		23.82		85.57		61.39		78.74
	%passing 6 mm		18.94		78.11		52.64		70.92
	%passing 4 mm		14.12		68.73		42.55		61.34
	%passing 1 mm		6.38		36.46		20.08		31.83
	%passing 0.2 mm		3.45		18.59		10.56		16.32
	%passing 0.1 mm		2.03		14.02		7.30		12.13
Linear P80	[mm]		26.21		6.51		12.71		8.45
Linear P50	[mm]		16.48		2.04		5.43		2.62

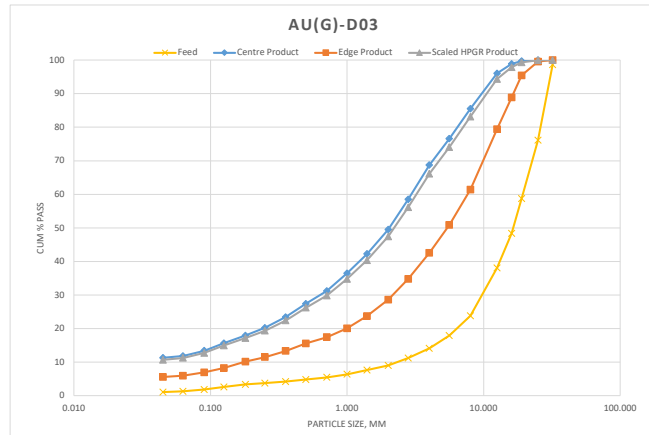


Figure A.29: Feed and product PSDs of test Au(G)-D03

HPGR Test PSD Summary

Project	Au (G)	Total Feed	264.50	Kg
Sample ID	Comp1	Center Product	110.40	Kg
Test ID	Au(G)-D04	Edge Product	44.30	Kg
Moisture:	5.00			%
Bulk:	1.56	Waste	99.30	Kg
Dry Proctor:		Center Product %	71%	
Pressure:	4.00	Edge Product %	29%	

Test No. Au(G)-D04		Feed		Centre Product		Edge Product		Experimental Full PSD	Scaled HPGR Product 90% Center + 10% Edge
Sieve #	Particle Size, mm	Retained	Cum % Pass	Retained	Cum % Pass	Retained	Cum % Pass	Cum % Pass	Cum % Pass
1.00	32.000	256.00	98.54	0.00	100.00	0.00	100.00	100.00	100.00
2.00	25.000	3606.20	77.91	0.00	100.00	0.00	100.00	100.00	100.00
3.00	19.000	3014.00	60.68	0.00	100.00	12.10	99.88	99.97	99.99
4.00	16.000	1832.70	50.20	24.00	99.79	133.70	98.55	99.44	99.67
5.00	12.500	1725.10	40.33	203.30	98.05	533.50	93.26	96.67	97.57
6.00	8.000	2582.20	25.57	843.20	90.80	1633.20	77.04	86.86	89.42
7.00	5.600	1136.80	19.06	893.70	83.12	1027.50	66.84	78.46	81.49
8.00	4.000	757.60	14.73	1038.80	74.19	864.40	58.26	69.63	72.60
9.00	2.800	590.10	11.36	1263.80	63.33	926.90	49.06	59.24	61.90
10.00	2.000	376.70	9.20	1066.50	54.16	749.20	41.62	50.57	52.91
11.00	1.400	271.10	7.65	1029.80	45.31	721.10	34.46	42.21	44.23
12.00	1.000	208.90	6.46	530.70	40.75	420.20	30.29	37.76	39.71
13.00	0.710	159.20	5.55	610.30	35.51	395.60	26.37	32.89	34.59
14.00	0.500	129.50	4.81	618.10	30.20	386.80	22.53	28.00	29.43
15.00	0.355	109.30	4.18	506.30	25.84	312.70	19.42	24.01	25.20
16.00	0.250	86.70	3.69	394.50	22.45	261.80	16.82	20.84	21.89
17.00	0.180	67.80	3.30	264.30	20.18	188.70	14.95	18.68	19.66
18.00	0.125	93.20	2.77	331.60	17.33	190.40	13.06	16.11	16.91
19.00	0.090	128.20	2.03	281.40	14.91	210.40	10.97	13.78	14.52
20.00	0.063	71.10	1.63	205.40	13.15	157.50	9.41	12.08	12.77
21.00	0.045	27.80	1.47	63.90	12.60	48.70	8.92	11.55	12.23
	Pan	256.50		1466.10		898.80			
Total mass		17486.70		11635.70		10073.20			
Size Distribution Interpolations									
%passing 8 mm			25.57		90.80		77.04		86.86
%passing 6 mm			20.15		84.40		68.54		79.86
%passing 4 mm			14.73		74.19		58.26		69.63
%passing 1 mm			6.46		40.75		30.29		37.76
%passing 0.2 mm			3.41		20.83		15.48		19.30
%passing 0.1 mm			2.24		15.61		11.57		14.45
Linear P80	[mm]		25.71		5.04		8.82		6.04
Linear P50	[mm]		15.93		1.72		2.92		1.80

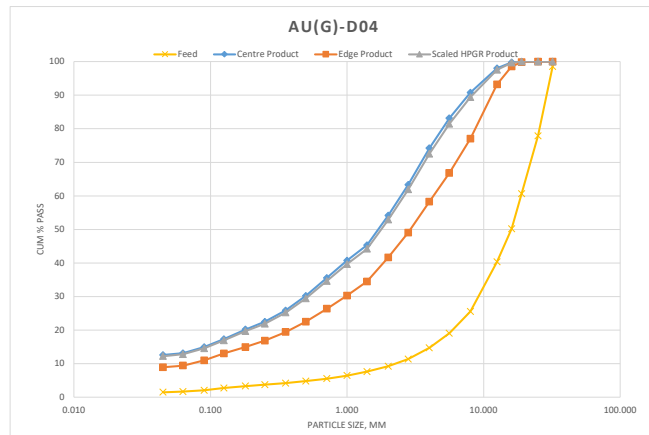


Figure A.30: Feed and product PSDs of test Au(G)-D04

HPGR Test PSD Summary

Project	Au (G)	Total Feed	277.50	Kg
Sample ID	Comp2	Center Product	138.50	Kg
Test ID	Au(G)-P01	Edge Product	56.60	Kg
Moisture:	2.50			%
Bulk:	1.59	Waste	76.20	Kg
Dry Proctor:		Center Product %	71%	
Pressure:	4.52	Edge Product %	29%	

Test No. Au(G)-P01		Feed		Centre Product		Edge Product		Experimental Full PSD	Scaled HPGR Product 90% Center + 10% Edge
Sieve #	Particle Size, mm	Retained	Cum % Pass	Retained	Cum % Pass	Retained	Cum % Pass	Cum % Pass	Cum % Pass
1.00	32.000	105.80	99.46	0.00	100.00	0.00	100.00	100.00	100.00
2.00	25.000	4909.60	74.48	0.00	100.00	15.40	99.80	99.94	99.98
3.00	19.000	3032.00	59.05	0.00	100.00	111.30	98.39	99.53	99.84
4.00	16.000	1972.20	49.02	19.90	99.76	136.70	96.64	98.86	99.45
5.00	12.500	2154.40	38.06	200.20	97.39	580.00	89.26	95.03	96.58
6.00	8.000	2802.00	23.80	857.50	87.21	1272.00	73.05	83.11	85.80
7.00	5.600	1176.90	17.81	764.50	78.14	837.20	62.39	73.57	76.57
8.00	4.000	865.10	13.41	735.00	69.42	676.30	53.77	64.88	67.86
9.00	2.800	531.50	10.71	712.70	60.97	602.10	46.10	56.66	59.48
10.00	2.000	452.90	8.40	667.30	53.05	596.00	38.51	48.83	51.60
11.00	1.400	290.00	6.93	589.50	46.06	425.20	33.09	42.30	44.76
12.00	1.000	183.60	5.99	644.60	38.41	282.60	29.49	35.82	37.52
13.00	0.710	182.50	5.06	454.20	33.02	333.00	25.25	30.77	32.24
14.00	0.500	123.60	4.44	339.70	28.99	234.50	22.26	27.04	28.32
15.00	0.355	118.60	3.83	364.50	24.67	279.70	18.70	22.93	24.07
16.00	0.250	96.10	3.34	319.20	20.88	221.10	15.88	19.43	20.38
17.00	0.180	78.90	2.94	233.20	18.11	163.70	13.80	16.86	17.68
18.00	0.125	77.90	2.55	299.40	14.56	218.70	11.01	13.53	14.20
19.00	0.090	83.60	2.12	196.20	12.23	148.30	9.12	11.33	11.92
20.00	0.063	87.10	1.68	215.50	9.68	141.00	7.32	8.99	9.44
21.00	0.045	32.70	1.51	75.10	8.78	57.10	6.60	8.15	8.57
	Pan	296.80		740.40		517.80			
	Total mass	19653.80		8428.60		7849.70			
Size Distribution Interpolations									
	%passing 8 mm	23.80		87.21		73.05		83.11	85.80
	%passing 6 mm	18.81		79.66		64.16		75.16	78.11
	%passing 4 mm	13.41		69.42		53.77		64.88	67.86
	%passing 1 mm	5.99		38.41		29.49		35.82	37.52
	%passing 0.2 mm	3.06		18.90		14.39		17.59	18.45
	%passing 0.1 mm	2.24		12.90		9.66		11.96	12.57
Linear P80	[mm]	26.55		6.09		9.93		7.22	6.49
Linear P50	[mm]	16.29		1.74		3.41		2.12	1.86

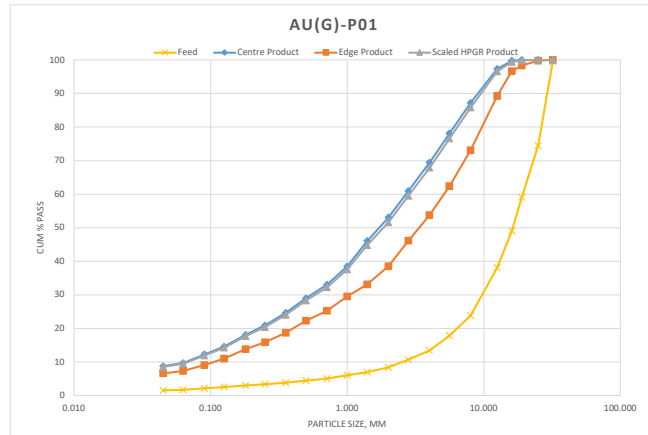


Figure A.31: Feed and product PSDs of test Au(G)-P01

HPGR Test PSD Summary

Project	Au (G)	Total Feed	286.50	Kg
Sample ID	Comp2	Center Product	101.20	Kg
Test ID	Au(G)-P02	Edge Product	43.90	Kg
Moisture:	2.50			%
Bulk:	1.59	Waste	138.20	Kg
Dry Proctor:		Center Product %	70%	
Pressure:	3.61	Edge Product %	30%	

Test No. Au(G)-P02		Feed		Centre Product		Edge Product		Experimental Full PSD	Scaled HPGR Product 90% Center + 10% Edge
Sieve #	Particle Size, mm	Retained	Cum % Pass	Retained	Cum % Pass	Retained	Cum % Pass	Cum % Pass	Cum % Pass
1.00	32.000	183.10	98.84	0.00	100.00	0.00	100.00	100.00	100.00
2.00	25.000	4050.10	73.23	0.00	100.00	0.00	100.00	100.00	100.00
3.00	19.000	2535.90	57.20	21.00	99.83	113.70	98.86	99.54	99.74
4.00	16.000	1593.90	47.12	108.40	98.97	283.80	96.03	98.08	98.68
5.00	12.500	1801.40	35.73	433.10	95.52	1041.00	85.62	92.53	94.53
6.00	8.000	2194.90	21.86	1408.00	84.32	1742.10	68.19	79.44	82.71
7.00	5.600	882.50	16.28	1113.80	75.46	1102.10	57.17	69.93	73.63
8.00	4.000	589.90	12.55	1125.80	66.50	892.20	48.25	60.98	64.68
9.00	2.800	447.00	9.72	1148.40	57.36	776.40	40.49	52.26	55.67
10.00	2.000	314.80	7.73	1072.10	48.83	696.40	33.52	44.20	47.30
11.00	1.400	206.10	6.43	1108.40	40.01	588.70	27.64	36.27	38.77
12.00	1.000	136.90	5.56	790.00	33.73	465.90	22.98	30.47	32.65
13.00	0.710	125.40	4.77	600.50	28.95	354.20	19.44	26.07	28.00
14.00	0.500	90.20	4.20	412.90	25.66	254.10	16.89	23.01	24.78
15.00	0.355	85.00	3.66	493.30	21.74	245.90	14.44	19.53	21.01
16.00	0.250	69.60	3.22	412.10	18.46	200.60	12.43	16.63	17.85
17.00	0.180	57.00	2.86	341.20	15.74	157.10	10.86	14.26	15.25
18.00	0.125	56.20	2.50	364.20	12.84	216.60	8.69	11.59	12.43
19.00	0.090	91.60	1.92	256.00	10.81	163.10	7.06	9.67	10.43
20.00	0.063	85.70	1.38	237.40	8.92	127.10	5.79	7.97	8.61
21.00	0.045	24.10	1.23	90.00	8.20	56.70	5.22	7.30	7.90
	Pan	194.60		1030.80		522.40			
	Total mass	15815.90		12567.40		10000.10			
Size Distribution Interpolations									
	%passing 8 mm	21.86		84.32		68.19		79.44	82.71
	%passing 6 mm	17.21		76.94		59.01		71.51	75.14
	%passing 4 mm	12.55		66.50		48.25		60.98	64.68
	%passing 1 mm	5.56		33.73		22.98		30.47	32.65
	%passing 0.2 mm	2.96		16.52		11.31		14.94	16.00
	%passing 0.1 mm	2.09		11.39		7.53		10.22	11.00
Linear P80	[mm]	26.85		6.83		11.05		8.19	7.28
Linear P50	[mm]	16.86		2.11		4.31		2.58	2.26

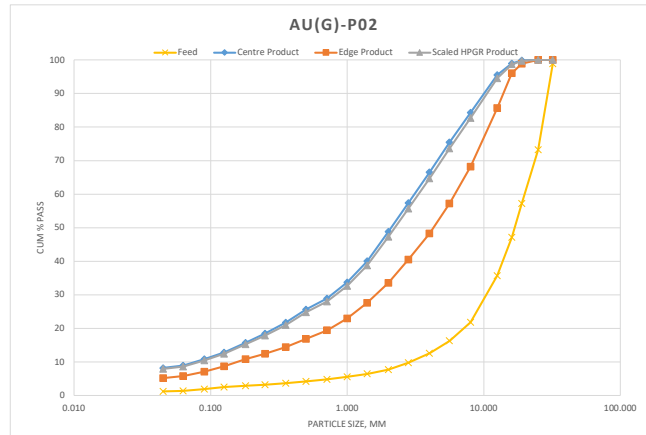


Figure A.32: Feed and product PSDs of test Au(G)-P02

HPGR Test PSD Summary

Project	Au (G)	Total Feed	290.00	Kg
Sample ID	Comp2	Center Product	112.90	Kg
Test ID	Au(G)-P03	Edge Product	44.20	Kg
Moisture:	2.50			%
Bulk:	1.59	Waste	127.20	Kg
Dry Proctor:		Center Product %	72%	
Pressure:	2.61	Edge Product %	28%	

Test No. Au(G)-P03		Feed		Centre Product		Edge Product		Experimental Full PSD	Scaled HPGR Product 90% Center + 10% Edge
Sieve #	Particle Size, mm	Retained	Cum % Pass	Retained	Cum % Pass	Retained	Cum % Pass	Cum % Pass	Cum % Pass
1.00	32.000	27.20	99.78	0.00	100.00	0.00	100.00	100.00	100.00
2.00	25.000	3121.20	74.88	0.00	100.00	0.00	100.00	100.00	100.00
3.00	19.000	1887.00	59.82	145.30	98.91	308.90	97.17	98.42	98.74
4.00	16.000	1153.90	50.61	182.40	97.54	730.90	90.47	95.55	96.83
5.00	12.500	1377.40	39.62	677.70	92.46	1485.70	76.84	88.07	90.90
6.00	8.000	1763.20	25.55	1924.00	78.03	2226.10	56.43	71.96	75.87
7.00	5.600	763.60	19.46	1332.00	68.04	1093.60	46.40	61.96	65.88
8.00	4.000	543.50	15.13	1296.60	58.32	904.00	38.11	52.64	56.30
9.00	2.800	425.80	11.73	1208.20	49.26	749.40	31.24	44.19	47.46
10.00	2.000	305.00	9.29	1068.20	41.25	599.20	25.75	36.89	39.70
11.00	1.400	238.70	7.39	973.70	33.95	484.10	21.31	30.39	32.69
12.00	1.000	153.00	6.17	749.10	28.33	358.90	18.02	25.43	27.30
13.00	0.710	112.30	5.27	583.90	23.95	276.10	15.49	21.57	23.11
14.00	0.500	88.40	4.57	499.30	20.21	219.90	13.47	18.31	19.54
15.00	0.355	81.50	3.92	380.00	17.36	211.80	11.53	15.72	16.78
16.00	0.250	65.70	3.39	347.10	14.76	182.40	9.86	13.38	14.27
17.00	0.180	53.70	2.96	270.00	12.73	141.80	8.56	11.56	12.32
18.00	0.125	53.80	2.53	344.20	10.15	193.50	6.78	9.20	9.81
19.00	0.090	64.50	2.02	210.60	8.57	141.60	5.48	7.70	8.26
20.00	0.063	53.20	1.60	242.70	6.75	118.70	4.39	6.09	6.52
21.00	0.045	22.80	1.41	85.30	6.11	50.60	3.93	5.50	5.89
	Pan	177.20		815.20		428.70			
Total mass		12532.60		13335.50		10905.90			
Size Distribution Interpolations									
%passing 8 mm		25.55		78.03		56.43		71.96	75.87
%passing 6 mm		20.48		69.71		48.07		63.62	67.55
%passing 4 mm		15.13		58.32		38.11		52.64	56.30
%passing 1 mm		6.17		28.33		18.02		25.43	27.30
%passing 0.2 mm		3.09		13.31		8.93		12.08	12.87
%passing 0.1 mm		2.17		9.02		5.85		8.13	8.71
Linear P80	[mm]	26.44		8.61		13.31		10.25	9.24
Linear P50	[mm]	15.80		2.90		6.46		3.63	3.14

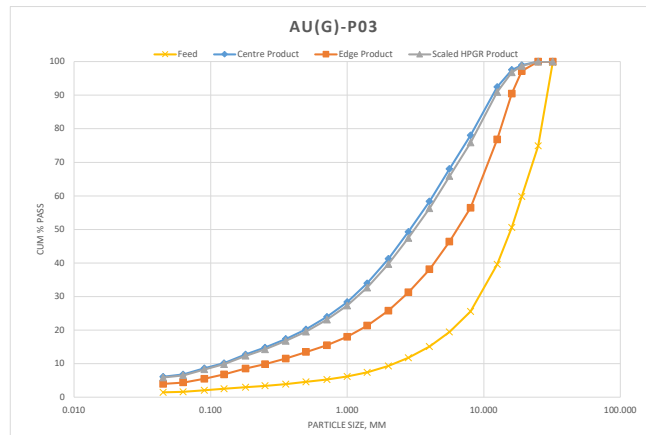


Figure A.33: Feed and product PSDs of test Au(G)-P03

HPGR Test PSD Summary

Project	Au (G)	Total Feed	271.50	Kg
Sample ID	Comp2	Center Product	105.20	Kg
Test ID	Au(G)-P04	Edge Product	42.50	Kg
Moisture:	5.00			%
Bulk:	1.70	Waste	111.40	Kg
Dry Precor:		Center Product %	71%	
Pressure:	3.59	Edge Product %	29%	

Test No.		Feed		Centre Product		Edge Product		Experimental Full PSD	Scaled HPGR Product
Au(G)-P04		Retained	Cum % Pass	Retained	Cum % Pass	Retained	Cum % Pass	Cum % Pass	90% Center + 10% Edge
Sieve #	Particle Size, mm								
1.00	32.000	373.50	97.97	0.00	100.00	0.00	100.00	100.00	100.00
2.00	25.000	4652.00	72.65	0.00	100.00	0.00	100.00	100.00	100.00
3.00	19.000	2894.90	56.90	26.50	99.75	64.30	99.36	99.64	99.72
4.00	16.000	1714.70	47.57	43.10	99.36	254.90	96.82	98.63	99.10
5.00	12.500	1985.90	36.76	316.90	96.42	890.20	87.94	93.98	95.58
6.00	8.000	2438.50	23.49	1305.30	84.35	1889.70	69.10	79.96	82.82
7.00	5.600	1080.60	17.61	990.20	75.18	1139.90	57.74	70.17	73.44
8.00	4.000	709.60	13.75	919.20	66.68	940.20	48.37	61.41	64.85
9.00	2.800	543.50	10.79	1077.80	56.71	827.90	40.11	51.93	55.05
10.00	2.000	376.20	8.74	949.40	47.92	743.80	32.70	43.54	46.40
11.00	1.400	293.30	7.15	869.00	39.88	507.50	27.64	36.36	38.66
12.00	1.000	203.80	6.04	701.90	33.39	422.20	23.43	30.52	32.39
13.00	0.710	161.30	5.16	442.60	29.29	328.40	20.16	26.66	28.38
14.00	0.500	116.90	4.52	410.70	25.49	273.30	17.43	23.17	24.69
15.00	0.355	120.50	3.87	416.00	21.64	229.50	15.15	19.77	20.99
16.00	0.250	90.80	3.37	340.40	18.49	209.50	13.06	16.93	17.95
17.00	0.180	76.60	2.96	264.70	16.04	167.00	11.39	14.71	15.58
18.00	0.125	72.60	2.56	293.40	13.33	261.70	8.78	12.02	12.88
19.00	0.090	97.80	2.03	235.40	11.15	151.40	7.27	10.04	10.76
20.00	0.063	74.70	1.62	196.70	9.33	177.70	5.50	8.23	8.95
21.00	0.045	30.10	1.46	90.40	8.50	64.00	4.86	7.45	8.13
	Pan	268.30		918.20		487.90			
	Total mass	18376.10		10807.80		10031.00			
Size Distribution Interpolations									
	%passing 8 mm		23.49		84.35		69.10		79.96
	%passing 6 mm		18.59		76.71		59.63		71.80
	%passing 4 mm		13.75		66.68		48.37		61.41
	%passing 1 mm		6.04		33.39		23.43		30.52
	%passing 0.2 mm		3.08		16.74		11.87		16.26
	%passing 0.1 mm		2.18		11.77		7.70		11.37
Linear P80	[mm]		27.03		6.86		10.60		8.01
Linear P50	[mm]		16.78		2.19		4.28		2.62

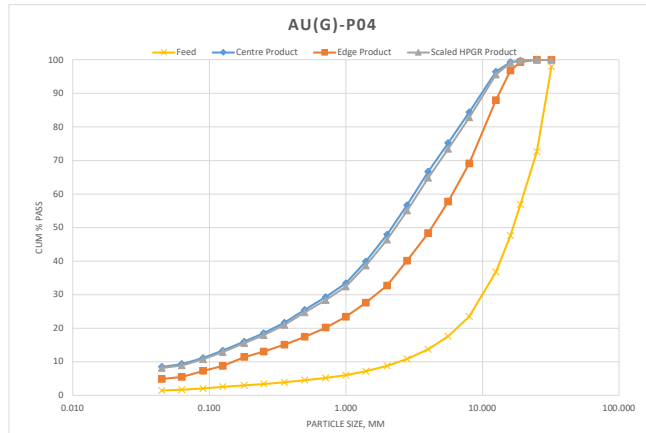


Figure A.34: Feed and product PSDs of test Au(G)-P04

HPGR Test PSD Summary

Project	Au (G)	Total Feed	327.30	Kg
Sample ID	Comp2	Center Product	99.10	Kg
Test ID	Au(G)-P05	Edge Product	43.80	Kg
Moisture:	2.50			%
Bulk:	1.59	Waste	178.90	Kg
Dry Proctor:		Center Product %	69%	
Pressure:	3.54	Edge Product %	31%	

Test No. Au(G)-P05		Feed		Centre Product		Edge Product		Experimental Full PSD	Scaled HPGR Product 90% Center + 10% Edge
Sieve #	Particle Size, mm	Retained	Cum % Pass	Retained	Cum % Pass	Retained	Cum % Pass	Cum % Pass	Cum % Pass
1.00	32.000	0.00	100.00	0.00	100.00	0.00	100.00	100.00	100.00
2.00	25.000	2582.80	74.22	0.00	100.00	0.00	100.00	100.00	100.00
3.00	19.000	1749.10	56.75	0.00	100.00	0.00	100.00	100.00	100.00
4.00	16.000	890.70	47.86	200.20	98.21	138.00	97.35	97.95	98.13
5.00	12.500	955.90	38.32	250.90	95.98	304.80	91.49	94.60	95.53
6.00	8.000	1447.30	23.87	1316.00	84.24	996.00	72.36	80.60	83.05
7.00	5.600	605.00	17.83	1078.40	74.62	526.40	62.24	70.82	73.38
8.00	4.000	387.90	13.96	1105.60	64.76	494.00	52.75	61.08	63.55
9.00	2.800	291.50	11.05	1091.80	55.02	414.40	44.79	51.88	53.99
10.00	2.000	219.50	8.86	916.80	46.84	339.50	38.27	44.21	45.98
11.00	1.400	148.50	7.37	754.00	40.11	298.80	32.53	37.79	39.35
12.00	1.000	105.00	6.33	746.00	33.46	239.00	27.93	31.76	32.91
13.00	0.710	88.90	5.44	540.70	28.63	227.00	23.57	27.08	28.13
14.00	0.500	53.50	4.90	380.50	25.24	137.50	20.93	23.92	24.81
15.00	0.355	78.90	4.12	497.20	20.81	195.50	17.17	19.69	20.44
16.00	0.250	49.90	3.62	408.70	17.16	147.50	14.34	16.30	16.88
17.00	0.180	46.00	3.16	262.50	14.82	97.50	12.47	14.10	14.58
18.00	0.125	72.90	2.43	423.50	11.04	141.80	9.74	10.64	10.91
19.00	0.090	15.80	2.27	247.80	8.83	58.00	8.63	8.77	8.81
20.00	0.063	28.50	1.99	317.70	6.00	71.90	7.25	6.38	6.12
21.00	0.045	33.30	1.66	237.00	3.88	88.20	5.55	4.39	4.05
	Pan	166.00		435.20		289.00			
	Total mass	10016.90		11210.50		5204.80			
Size Distribution Interpolations									
	%passing 8 mm		23.87		84.24		72.36		80.60
	%passing 6 mm		18.84		76.22		63.93		72.45
	%passing 4 mm		13.96		64.76		52.75		61.08
	%passing 1 mm		6.33		33.46		27.93		31.76
	%passing 0.2 mm		3.29		15.49		13.00		14.73
	%passing 0.1 mm		2.32		9.46		8.95		9.30
Linear P80	[mm]		26.57		6.94		9.80		7.85
Linear P50	[mm]		16.72		2.31		3.59		2.60

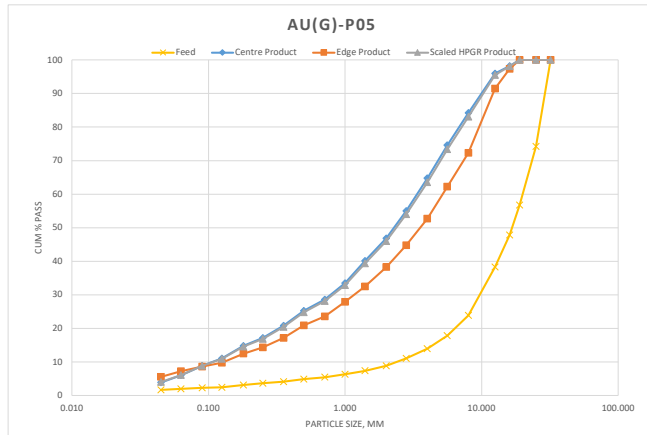


Figure A.35: Feed and product PSDs of test Au(G)-P05

A.6 HPGR Test: Quarry Sample

HPGR Test PSD Summary									
Project	Quarry		Total Feed	292.00	Kg				
Sample ID	CH_crushed		Center Product	40.20	Kg				
Test ID	SD01		Edge Product	16.50	Kg				
Moisture:	3.10	%							
Bulk:	1.76	g/cc	Waste			230.00	Kg		
Dry Proctor:		g/cc	Center Product %			71%			
Pressure:	4.02	N/mm2	Edge Product %			29%			

Test No.	Feed		Centre Product		Edge Product		Experimental Full PSD	Scaled HPGR Product	
SD01	Retained	Cum % Pass	Retained	Cum % Pass	Retained	Cum % Pass	Cum % Pass	90% Center + 10% Edge	
Sieve #	Particle Size, mm								
1.00	32.000	0.00	100.00	0.00	100.00	0.00	100.00	100.00	100.00
2.00	25.000	0.00	100.00	0.00	100.00	0.00	100.00	100.00	100.00
3.00	19.000	0.00	100.00	0.00	100.00	0.00	100.00	100.00	100.00
4.00	16.000	0.00	100.00	0.00	100.00	0.00	100.00	100.00	100.00
5.00	12.500	44.50	99.57	0.00	100.00	9.20	99.88	99.97	99.99
6.00	8.000	1391.90	86.02	244.50	97.41	526.80	93.16	96.17	96.98
7.00	5.600	2439.10	62.28	605.70	90.98	968.90	80.81	88.02	89.96
8.00	4.000	1945.10	43.35	828.20	82.19	1082.50	67.00	77.77	80.67
9.00	2.800	1293.40	30.76	824.50	73.44	848.10	56.18	68.42	71.71
10.00	2.000	664.00	24.30	740.40	65.58	620.70	48.27	60.54	63.85
11.00	1.400	377.20	20.63	571.90	59.51	420.70	42.90	54.68	57.85
12.00	1.000	263.60	18.07	504.90	54.16	340.50	38.56	49.62	52.60
13.00	0.710	194.80	16.17	507.10	48.77	311.40	34.59	44.65	47.36
14.00	0.500	168.10	14.53	409.30	44.43	258.90	31.28	40.61	43.12
15.00	0.355	150.40	13.07	420.40	39.97	240.50	28.22	36.55	38.79
16.00	0.250	202.20	11.10	583.20	33.78	311.00	24.25	31.01	32.83
17.00	0.180	206.20	9.10	498.20	28.49	294.80	20.49	26.17	27.69
18.00	0.125	243.70	6.72	612.40	22.00	380.30	15.64	20.15	21.36
19.00	0.090	225.70	4.53	511.50	16.57	319.00	11.57	15.11	16.07
20.00	0.063	179.10	2.78	371.20	12.63	258.00	8.28	11.36	12.19
21.00	0.045	89.30	1.92	288.10	9.57	168.60	6.13	8.57	9.23
	Pan	196.80		902.00		480.60			
	Total mass	10275.10		9423.50		7840.50			

Size Distribution Interpolations										
%passing 8 mm		86.02		97.41			93.16		96.17	96.98
%passing 6 mm		66.24		92.05			82.87		89.38	91.13
%passing 4 mm		43.35		82.19			67.00		77.77	80.67
%passing 1 mm		18.07		54.16			38.56		49.62	52.60
%passing 0.2 mm		9.67		30.01			21.56		27.55	29.16
%passing 0.1 mm		5.16		18.12			12.73		16.55	17.58
Linear P80	[mm]	7.39		3.70			5.51		4.35	3.91
Linear P50	[mm]	4.56		0.78			2.18		1.03	0.86

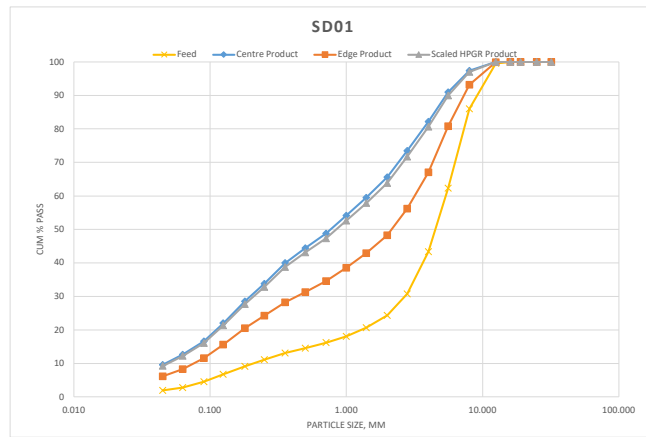


Figure A.36: Feed and product PSDs of test Quarry SD-01

HPGR Test PSD Summary

Project	Quarry	Total Feed	290.80	Kg
Sample ID	CH_crushed	Center Product	38.90	Kg
Test ID	SD02	Edge Product	17.70	Kg
Moisture:	2.15	%		
Bulk:	1.76	g/cc	Waste	224.00
Dry Precorator:		g/cc	Center Product %	69%
Pressure:	4.01	N/mm2	Edge Product %	31%

Test No. SD02		Feed		Centre Product		Edge Product		Experimental Full PSD	Scaled HPGR Product 90% Center + 10% Edge
Sieve #	Particle Size, mm	Retained	Cum % Pass	Retained	Cum % Pass	Retained	Cum % Pass	Cum % Pass	Cum % Pass
1.00	32.000	0.00	100.00	0.00	100.00	0.00	100.00	100.00	100.00
2.00	25.000	0.00	100.00	0.00	100.00	0.00	100.00	100.00	100.00
3.00	19.000	0.00	100.00	0.00	100.00	0.00	100.00	100.00	100.00
4.00	16.000	0.00	100.00	0.00	100.00	0.00	100.00	100.00	100.00
5.00	12.500	45.90	99.48	0.00	100.00	10.60	99.87	99.96	99.99
6.00	8.000	856.00	89.74	117.30	98.67	533.70	93.23	96.97	98.13
7.00	5.600	1889.30	68.25	472.60	93.31	1139.90	79.05	88.85	91.88
8.00	4.000	1967.10	45.88	737.20	84.95	1037.90	66.14	79.07	83.07
9.00	2.800	1324.30	30.81	799.70	75.88	913.50	54.78	69.28	73.77
10.00	2.000	1041.10	18.97	733.90	67.56	714.70	45.89	60.78	65.39
11.00	1.400	406.20	14.35	696.60	59.66	454.10	40.24	53.59	57.72
12.00	1.000	150.00	12.64	536.60	53.57	314.90	36.33	48.18	51.85
13.00	0.710	124.50	11.23	508.60	47.80	328.40	32.24	42.94	46.25
14.00	0.500	103.70	10.05	400.30	43.26	266.30	28.93	38.78	41.83
15.00	0.355	86.40	9.06	395.70	38.78	249.40	25.83	34.73	37.48
16.00	0.250	103.40	7.89	458.90	33.57	257.10	22.63	30.15	32.48
17.00	0.180	119.10	6.53	457.60	28.38	367.30	18.06	25.16	27.35
18.00	0.125	137.10	4.97	577.00	21.84	347.10	13.74	19.31	21.03
19.00	0.090	143.30	3.34	502.40	16.14	267.00	10.42	14.35	15.57
20.00	0.063	77.60	2.46	442.60	11.12	251.10	7.30	9.93	10.74
21.00	0.045	62.60	1.75	204.10	8.81	146.20	5.48	7.77	8.48
	Pan	153.80		776.70		440.60			
Total mass		8791.40		8817.80		8039.80			
Size Distribution Interpolations									
%passing 8 mm			89.74		98.67		93.23		98.13
%passing 6 mm			71.83		94.20		81.41		92.92
%passing 4 mm			45.88		84.95		66.14		79.07
%passing 1 mm			12.64		53.57		36.33		48.18
%passing 0.2 mm			6.92		29.87		19.37		26.58
%passing 0.1 mm			3.81		17.77		11.37		17.13
Linear P80	[mm]		6.91		3.35		5.76		4.15
Linear P50	[mm]		4.29		0.82		2.37		1.13

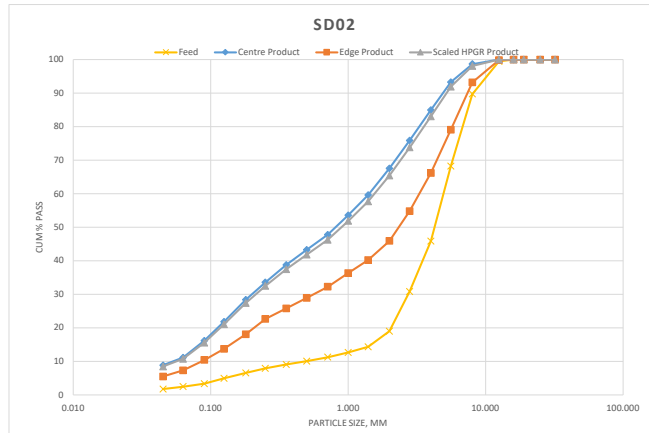


Figure A.37: Feed and product PSDs of test Quarry SD-02

HPGR Test PSD Summary

Project	Quarry		Total Feed	298.80	Kg
Sample ID	VS crushed		Center Product	43.50	Kg
Test ID	SD03		Edge Product	18.40	Kg
Moisture:	1.55	%			
Bulk:	1.76	g/cc	Waste	230.00	Kg
Dry Proctor:		g/cc	Center Product %	70%	
Pressure:	4.02	N/mm ²	Edge Product %	30%	

Test No. SD03		Feed		Centre Product		Edge Product		Experimental Full PSD	Scaled HPGR Product 90% Center + 10% Edge
Sieve #	Particle Size, mm	Retained	Cum % Pass	Retained	Cum % Pass	Retained	Cum % Pass	Cum % Pass	Cum % Pass
1.00	32.000	0.00	100.00	0.00	100.00	0.00	100.00	100.00	100.00
2.00	25.000	0.00	100.00	0.00	100.00	0.00	100.00	100.00	100.00
3.00	19.000	87.90	99.01	0.00	100.00	0.00	100.00	100.00	100.00
4.00	16.000	282.80	95.82	0.00	100.00	70.50	99.16	99.75	99.92
5.00	12.500	787.00	87.30	78.50	99.22	323.50	95.33	98.06	98.83
6.00	8.000	2540.00	58.68	670.50	92.57	1779.20	74.22	87.11	90.73
7.00	5.600	1278.80	44.27	800.90	84.62	1115.20	60.99	77.60	82.26
8.00	4.000	618.40	37.31	784.90	76.83	751.60	52.08	69.47	74.36
9.00	2.800	317.70	33.73	721.80	69.67	525.00	45.85	62.59	67.29
10.00	2.000	369.20	29.57	603.30	63.68	443.30	40.59	56.82	61.37
11.00	1.400	337.10	25.77	526.90	58.45	351.40	36.42	51.90	56.25
12.00	1.000	234.30	23.13	465.50	53.83	270.70	33.21	47.70	51.77
13.00	0.710	190.80	20.98	600.70	47.87	290.20	29.77	42.49	46.06
14.00	0.500	172.40	19.04	411.70	43.79	231.90	27.02	38.80	42.11
15.00	0.355	173.10	17.09	449.80	39.32	225.20	24.35	34.87	37.83
16.00	0.250	198.50	14.85	473.00	34.63	252.40	21.35	30.68	33.30
17.00	0.180	203.90	12.55	599.60	28.68	261.70	18.25	25.58	27.64
18.00	0.125	253.20	9.70	625.20	22.47	342.80	14.18	20.01	21.65
19.00	0.090	205.00	7.39	532.40	17.19	264.40	11.05	15.36	16.58
20.00	0.063	179.90	5.36	519.90	12.03	269.70	7.85	10.79	11.61
21.00	0.045	121.10	4.00	243.20	9.62	146.10	6.11	8.58	9.27
	Pan	355.10		969.30		515.40			
Total mass		8876.20		10077.10		8430.20			
Size Distribution Interpolations									
%passing 8 mm			58.68		92.57		74.22		87.11
%passing 6 mm			46.67		85.94		63.20		79.18
%passing 4 mm			37.31		76.83		52.08		69.47
%passing 1 mm			23.13		53.83		33.21		47.70
%passing 0.2 mm			13.21		30.38		19.14		27.04
%passing 0.1 mm			8.05		18.70		11.94		16.69
Linear P80	[mm]		11.35		4.65		9.23		6.21
Linear P50	[mm]		6.55		0.81		3.60		1.22

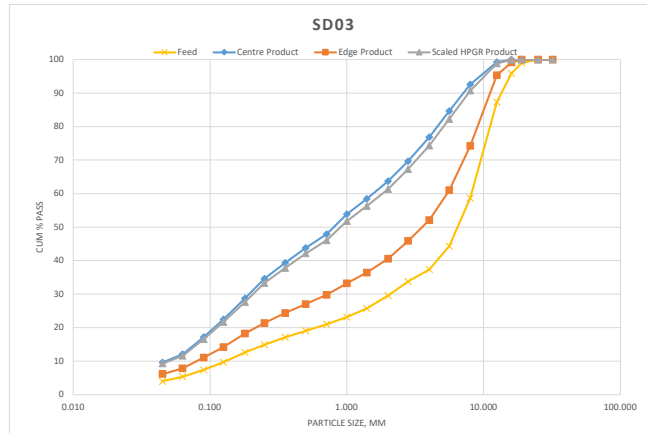


Figure A.38: Feed and product PSDs of test Quarry SD-03

HPGR Test PSD Summary

Project	Quarry	Total Feed	295.00	Kg
Sample ID	VS crushed	Center Product	38.60	Kg
Test ID	SD04	Edge Product	18.70	Kg
Moisture:	1.13			%
Bulk:	1.76			g/cc
Dry Proctor:		Waste	232.10	Kg
		Center Product %	67%	
Pressure:	4.01	Edge Product %	33%	

Test No.		Feed		Centre Product		Edge Product		Experimental Full PSD	Scaled HPGR Product	
SD04		Retained	Cum % Pass	Retained	Cum % Pass	Retained	Cum % Pass	Cum % Pass	90% Center + 10% Edge	
Sieve #	Particle Size, mm									
1.00	32.000	0.00	100.00	0.00	100.00	0.00	100.00	100.00		100.00
2.00	25.000	0.00	100.00	0.00	100.00	0.00	100.00	100.00		100.00
3.00	19.000	31.50	99.68	0.00	100.00	0.00	100.00	100.00		100.00
4.00	16.000	259.20	97.00	6.80	99.93	48.50	99.53	99.80		99.89
5.00	12.500	762.30	89.15	52.40	99.37	218.00	97.39	98.72		99.17
6.00	8.000	2905.60	59.21	471.40	94.36	1408.90	83.59	90.85		93.29
7.00	5.600	1730.70	41.38	581.50	88.19	1187.20	71.97	82.89		86.56
8.00	4.000	1068.40	30.37	671.10	81.06	1047.10	61.71	74.74		79.12
9.00	2.800	713.40	23.02	685.50	73.77	845.80	53.43	67.14		71.74
10.00	2.000	613.60	16.70	681.40	66.54	788.70	45.71	59.74		64.45
11.00	1.400	258.10	14.04	750.30	58.57	566.40	40.16	52.56		56.73
12.00	1.000	136.90	12.63	517.90	53.06	436.20	35.89	47.46		51.35
13.00	0.710	96.60	11.63	533.20	47.40	273.00	33.21	42.77		45.98
14.00	0.500	100.40	10.60	430.30	42.83	355.20	29.74	38.56		41.52
15.00	0.355	96.80	9.60	379.30	38.80	343.50	26.37	34.74		37.56
16.00	0.250	107.50	8.49	505.60	33.43	385.10	22.60	29.89		32.35
17.00	0.180	121.50	7.24	429.10	28.87	366.50	19.01	25.65		27.88
18.00	0.125	149.70	5.70	625.70	22.22	475.30	14.36	19.66		21.44
19.00	0.090	152.80	4.12	455.20	17.39	350.80	10.92	15.28		16.74
20.00	0.063	122.00	2.87	475.00	12.34	312.90	7.86	10.88		11.89
21.00	0.045	74.20	2.10	238.30	9.81	213.80	5.76	8.49		9.41
	Pan	204.10		923.50		588.50				
	Total mass	9705.30		9413.50		10211.40				
Size Distribution Interpolations										
	%passing 8 mm		59.21		94.36		83.59		90.85	93.29
	%passing 6 mm		44.35		89.22		73.90		84.22	87.68
	%passing 4 mm		30.37		81.06		61.71		74.74	79.12
	%passing 1 mm		12.63		53.06		35.89		47.46	51.35
	%passing 0.2 mm		7.60		30.17		20.04		26.86	29.16
	%passing 0.1 mm		4.57		18.77		11.90		16.53	18.08
Linear P80	[mm]		11.12		3.83		7.26		5.03	4.19
Linear P50	[mm]		6.76		0.84		2.44		1.20	0.93

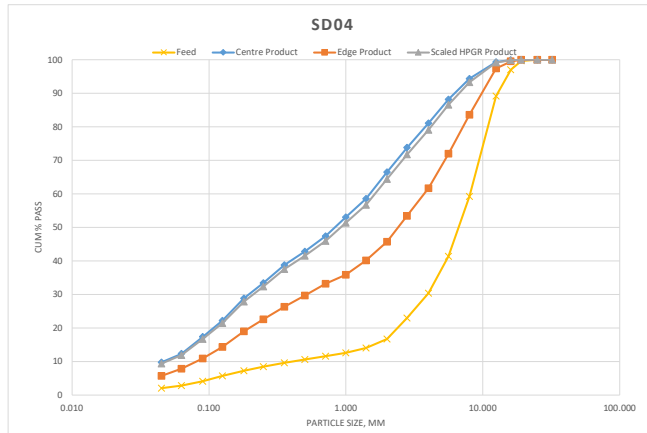


Figure A.39: Feed and product PSDs of test Quarry SD-04

HPGR Test PSD Summary

Project	Quarry		Total Feed	425.00	Kg
Sample ID	HH Feed		Center Product	62.40	Kg
Test ID	SD05		Edge Product	26.00	Kg
Moisture:	1.14	%			
Bulk:	1.49	g/cc			
Dry Proctor:		g/cc	Waste	325.00	Kg
Pressure:	3.55	N/mm ²	Center Product %	71%	
			Edge Product %	29%	

Test No. SD05		Feed		Centre Product		Edge Product		Experimental Full PSD	Scaled HPGR Product 90% Center + 10% Edge	
Sieve #	Particle Size, mm	Retained	Cum % Pass	Retained	Cum % Pass	Retained	Cum % Pass	Cum % Pass	Cum % Pass	Cum % Pass
1.00	32.000	0.00	100.00	0.00	100.00	0.00	100.00	100.00		100.00
2.00	25.000	0.00	100.00	0.00	100.00	0.00	100.00	100.00		100.00
3.00	19.000	470.90	94.41	0.00	100.00	0.00	100.00	100.00		100.00
4.00	16.000	1064.80	81.77	0.00	100.00	20.30	99.65	100.00		99.97
5.00	12.500	2170.10	56.00	47.70	99.41	149.40	97.10	100.00		99.18
6.00	8.000	2973.70	20.70	558.60	92.47	1100.30	78.29	100.00		91.05
7.00	5.600	1324.20	4.97	696.00	83.83	982.10	61.50	100.00		81.60
8.00	4.000	112.90	3.63	786.40	74.07	645.10	50.47	100.00		71.71
9.00	2.800	23.60	3.35	689.80	65.50	498.80	41.94	100.00		63.14
10.00	2.000	13.60	3.19	568.30	58.44	376.20	35.51	100.00		56.15
11.00	1.400	9.00	3.09	515.00	52.05	281.80	30.70	100.00		49.91
12.00	1.000	6.90	3.00	397.80	47.11	200.70	27.27	100.00		45.13
13.00	0.710	5.60	2.94	369.80	42.52	153.40	24.64	100.00		40.73
14.00	0.500	5.20	2.88	313.60	38.62	145.60	22.15	100.00		36.98
15.00	0.355	6.00	2.80	289.30	35.03	131.80	19.90	100.00		33.52
16.00	0.250	9.20	2.70	347.80	30.71	145.80	17.41	100.00		29.38
17.00	0.180	12.00	2.55	361.90	26.22	146.30	14.91	100.00		25.09
18.00	0.125	26.00	2.24	452.80	20.60	186.10	11.73	100.00		19.71
19.00	0.090	38.80	1.78	419.90	15.38	166.70	8.88	100.00		14.73
20.00	0.063	39.30	1.32	354.10	10.99	148.10	6.34	100.00		10.52
21.00	0.045	32.70	0.93	176.70	8.79	73.30	5.09	100.00		8.42
	Pan	78.20		708.20		297.80		100.00		
	Total mass	8422.70		8053.70		5849.60				
Size Distribution Interpolations										
	%passing 8 mm		20.70		92.47		78.29		88.30	91.05
	%passing 6 mm		7.59		85.27		64.30		79.10	83.17
	%passing 4 mm		3.63		74.07		50.47		67.13	71.71
	%passing 1 mm		3.00		47.11		27.27		41.27	45.13
	%passing 0.2 mm		2.59		27.50		15.62		24.01	26.32
	%passing 0.1 mm		1.91		16.87		9.69		14.76	16.16
Linear P80	[mm]		15.76		4.97		8.41		6.20	5.34
Linear P50	[mm]		11.73		1.23		3.93		1.83	1.41



Figure A.40: Feed and product PSDs of test Quarry SD-05

HPGR Test PSD Summary

Project	Quarry		Total Feed	418.00	Kg
Sample ID	HH Feed		Center Product	67.30	Kg
Test ID	SD06		Edge Product	27.50	Kg
Moisture:	1.14	%			
Bulk:	1.49	g/cc	Waste	315.00	Kg
Dry Precorator:		g/cc	Center Product %	71%	
Pressure:	4.53	N/mm2	Edge Product %	29%	

Test No. SD06		Feed		Centre Product		Edge Product		Experimental Full PSD	Scaled HPGR Product 90% Center + 10% Edge
Sieve #	Particle Size, mm	Retained	Cum % Pass	Retained	Cum % Pass	Retained	Cum % Pass	Cum % Pass	Cum % Pass
1.00	32.000	0.00	100.00	0.00	100.00	0.00	100.00	100.00	100.00
2.00	25.000	0.00	100.00	0.00	100.00	0.00	100.00	100.00	100.00
3.00	19.000	470.90	94.41	0.00	100.00	0.00	100.00	100.00	100.00
4.00	16.000	1064.80	81.77	8.50	99.88	23.50	99.61	99.81	99.86
5.00	12.500	2170.10	56.00	52.90	99.16	153.90	97.07	98.56	98.95
6.00	8.000	2973.70	20.70	501.60	92.34	1019.60	80.23	88.82	91.13
7.00	5.600	1324.20	4.97	600.50	84.17	940.60	64.69	78.52	82.22
8.00	4.000	112.90	3.63	631.20	75.58	668.80	53.64	69.21	73.38
9.00	2.800	23.60	3.35	568.50	67.84	518.00	45.08	61.24	65.57
10.00	2.000	13.60	3.19	433.50	61.94	319.00	39.81	55.52	59.73
11.00	1.400	9.00	3.09	400.20	56.50	287.10	35.07	50.28	54.35
12.00	1.000	6.90	3.00	319.00	52.16	195.60	31.84	46.26	50.12
13.00	0.710	5.60	2.94	414.20	46.52	223.10	28.15	41.19	44.68
14.00	0.500	5.20	2.88	315.50	42.23	154.90	25.59	37.40	40.56
15.00	0.355	6.00	2.80	283.30	38.37	155.00	23.03	33.92	36.84
16.00	0.250	9.20	2.70	359.50	33.48	173.10	20.17	29.62	32.15
17.00	0.180	12.00	2.55	323.20	29.08	172.60	17.32	25.67	27.91
18.00	0.125	26.00	2.24	485.20	22.48	204.90	13.93	20.00	21.63
19.00	0.090	38.80	1.78	427.60	16.66	256.20	9.70	14.64	15.97
20.00	0.063	39.30	1.32	371.30	11.61	163.40	7.00	10.27	11.15
21.00	0.045	32.70	0.93	126.40	9.89	67.60	5.89	8.73	9.49
	Pan	78.20		726.70		356.30			
	Total mass	8422.70		7348.80		6053.20			
Size Distribution Interpolations									
	%passing 8 mm	20.70		92.34		80.23		88.82	91.13
	%passing 6 mm	7.59		85.53		67.28		80.23	83.70
	%passing 4 mm	3.63		75.58		53.64		69.21	73.38
	%passing 1 mm	3.00		52.16		31.84		46.26	50.12
	%passing 0.2 mm	2.59		30.34		18.13		26.80	29.12
	%passing 0.1 mm	1.91		18.32		10.91		16.17	17.58
Linear P80	[mm]	15.76		4.82		7.97		5.95	5.20
Linear P50	[mm]	11.73		0.89		3.49		1.37	0.99

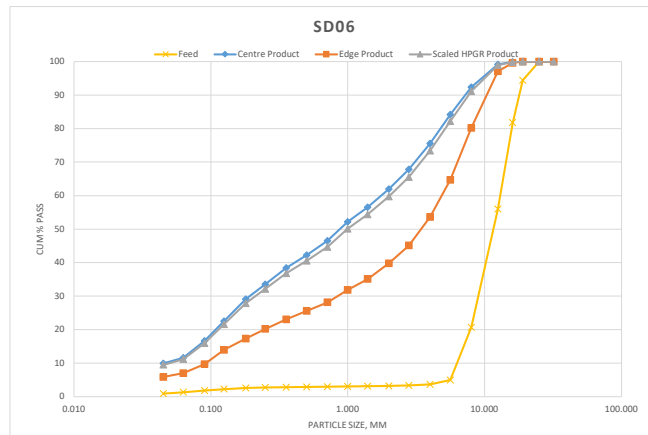


Figure A.41: Feed and product PSDs of test Quarry SD-06

HPGR Test PSD Summary

Project	Quarry		Total Feed	246.60	Kg
Sample ID	HH Feed		Center Product	53.10	Kg
Test ID	SD07		Edge Product	24.10	Kg
Moisture:	3.43	%			
Bulk:	1.76	g/cc	Waste	161.30	Kg
Dry Precorator:		g/cc	Center Product %	69%	
Pressure:	4.01	N/mm2	Edge Product %	31%	

Test No. SD07		Feed		Centre Product		Edge Product		Experimental Full PSD	Scaled HPGR Product 90% Center + 10% Edge
Sieve #	Particle Size, mm	Retained	Cum % Pass	Retained	Cum % Pass	Retained	Cum % Pass	Cum % Pass	Cum % Pass
1.00	32.000	0.00	100.00	0.00	100.00	0.00	100.00	100.00	100.00
2.00	25.000	0.00	100.00	0.00	100.00	0.00	100.00	100.00	100.00
3.00	19.000	0.00	100.00	0.00	100.00	0.00	100.00	100.00	100.00
4.00	16.000	25.50	99.68	0.00	100.00	0.00	100.00	100.00	100.00
5.00	12.500	70.30	98.81	5.20	99.92	35.30	99.35	99.74	99.86
6.00	8.000	655.40	90.67	184.70	97.15	319.20	93.51	96.01	96.78
7.00	5.600	771.90	81.08	254.90	93.31	366.70	86.79	91.28	92.66
8.00	4.000	698.80	72.40	380.80	87.59	421.30	79.07	84.93	86.74
9.00	2.800	650.90	64.31	393.40	81.68	383.10	72.05	78.67	80.71
10.00	2.000	496.60	58.15	318.70	76.89	287.10	66.79	73.73	75.88
11.00	1.400	445.50	52.61	339.70	71.78	261.60	62.00	68.73	70.80
12.00	1.000	378.00	47.92	289.40	67.43	210.60	58.14	64.53	66.50
13.00	0.710	373.80	43.27	437.80	60.85	175.10	54.93	59.00	60.26
14.00	0.500	302.30	39.52	280.20	56.64	250.00	50.35	54.67	56.01
15.00	0.355	317.50	35.57	326.70	51.72	263.70	45.52	49.79	51.10
16.00	0.250	370.90	30.97	439.60	45.12	309.30	39.85	43.47	44.59
17.00	0.180	373.20	26.33	417.90	38.83	300.30	34.35	37.43	38.39
18.00	0.125	550.80	19.49	601.90	29.79	457.20	25.98	28.60	29.41
19.00	0.090	387.00	14.68	445.90	23.08	367.70	19.24	21.88	22.70
20.00	0.063	349.30	10.34	546.60	14.87	352.90	12.77	14.21	14.66
21.00	0.045	170.30	8.23	121.40	13.04	146.50	10.09	12.12	12.75
	Pan	662.30		867.60		550.70			
	Total mass	8050.30		6652.40		5458.30			
Size Distribution Interpolations									
	%passing 8 mm		90.67		97.15		93.51		96.01
	%passing 6 mm		82.68		93.95		87.91		92.07
	%passing 4 mm		72.40		87.59		79.07		84.93
	%passing 1 mm		47.92		67.43		58.14		64.53
	%passing 0.2 mm		27.66		40.63		35.92		39.16
	%passing 0.1 mm		16.05		25.00		21.16		23.80
Linear P80	[mm]		5.40		2.52		4.19		3.05
Linear P50	[mm]		1.18		0.33		0.49		0.36

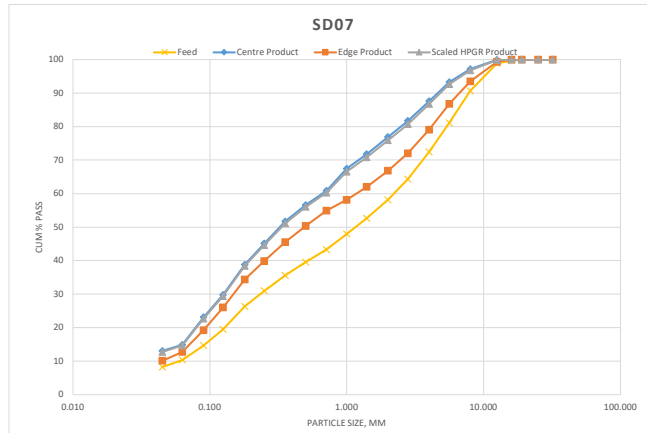


Figure A.42: Feed and product PSDs of test Quarry SD-07

HPGR Test PSD Summary

Project	Quarry	Total Feed	245.60	Kg
Sample ID	HH Feed	Center Product	51.00	Kg
Test ID	SD08	Edge Product	21.70	Kg
Moisture:	2.83			%
Bulk:	1.76	Waste	167.30	Kg
Dry Proctor:		Center Product %	70%	
Pressure:	4.02	Edge Product %	30%	

Test No. SD08		Feed		Centre Product		Edge Product		Experimental Full PSD	Scaled HPGR Product 90% Center + 10% Edge
Sieve #	Particle Size, mm	Retained	Cum % Pass	Retained	Cum % Pass	Retained	Cum % Pass	Cum % Pass	Cum % Pass
1.00	32.000	0.00	100.00	0.00	100.00	0.00	100.00	100.00	100.00
2.00	25.000	0.00	100.00	0.00	100.00	0.00	100.00	100.00	100.00
3.00	19.000	0.00	100.00	0.00	100.00	0.00	100.00	100.00	100.00
4.00	16.000	0.00	100.00	0.00	100.00	0.00	100.00	100.00	100.00
5.00	12.500	71.10	99.05	0.00	100.00	13.30	99.75	99.93	99.98
6.00	8.000	563.10	91.52	143.90	97.68	257.70	95.00	96.88	97.41
7.00	5.600	807.30	80.72	260.30	93.47	392.80	87.76	91.77	92.90
8.00	4.000	924.40	68.36	378.50	87.35	467.70	79.14	84.90	86.53
9.00	2.800	876.70	56.63	438.50	80.27	448.30	70.87	77.47	79.33
10.00	2.000	716.70	47.05	398.10	73.84	382.20	63.83	70.85	72.84
11.00	1.400	429.90	41.30	397.60	67.41	303.70	58.23	64.67	66.49
12.00	1.000	320.00	37.02	301.10	62.55	285.60	52.96	59.69	61.59
13.00	0.710	153.40	34.97	399.80	56.09	147.00	50.25	54.35	55.51
14.00	0.500	248.20	31.65	320.30	50.91	236.00	45.90	49.42	50.41
15.00	0.355	218.10	28.73	274.20	46.48	233.70	41.60	45.02	45.99
16.00	0.250	265.90	25.17	365.30	40.58	301.90	36.03	39.22	40.13
17.00	0.180	275.20	21.49	308.50	35.60	281.20	30.85	34.18	35.12
18.00	0.125	389.00	16.29	545.90	26.78	383.40	23.78	25.88	26.48
19.00	0.090	343.40	11.70	430.00	19.83	373.00	16.90	18.96	19.54
20.00	0.063	294.30	7.76	496.00	11.82	231.40	12.63	12.06	11.90
21.00	0.045	106.90	6.33	153.50	9.34	127.00	10.29	9.62	9.43
	Pan	473.40		577.80		558.30			
Total mass		7477.00		6189.30		5424.20			
Size Distribution Interpolations									
%passing 8 mm			91.52		97.68		95.00		96.88
%passing 6 mm			82.52		94.17		88.97		92.62
%passing 4 mm			68.36		87.35		79.14		84.90
%passing 1 mm			37.02		62.55		52.96		59.69
%passing 0.2 mm			22.54		37.02		32.33		35.62
%passing 0.1 mm			13.01		21.81		18.86		20.93
Linear P80	[mm]		5.51		2.77		4.16		3.21
Linear P50	[mm]		2.25		0.47		0.70		0.52

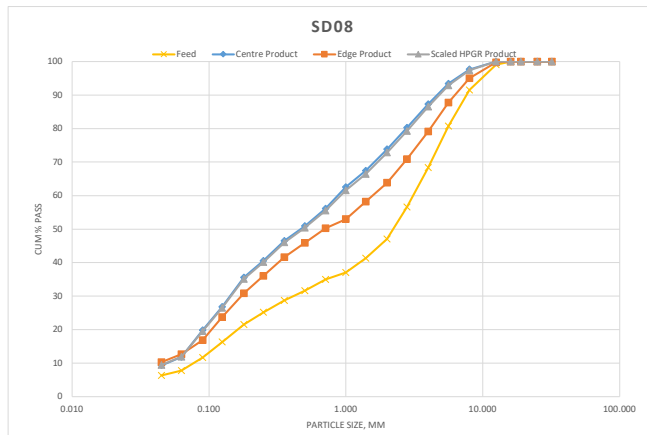


Figure A.43: Feed and product PSDs of test Quarry SD-08

Appendix B

Piston-die Press Test Data

B.1 Piston-die Press Procedure

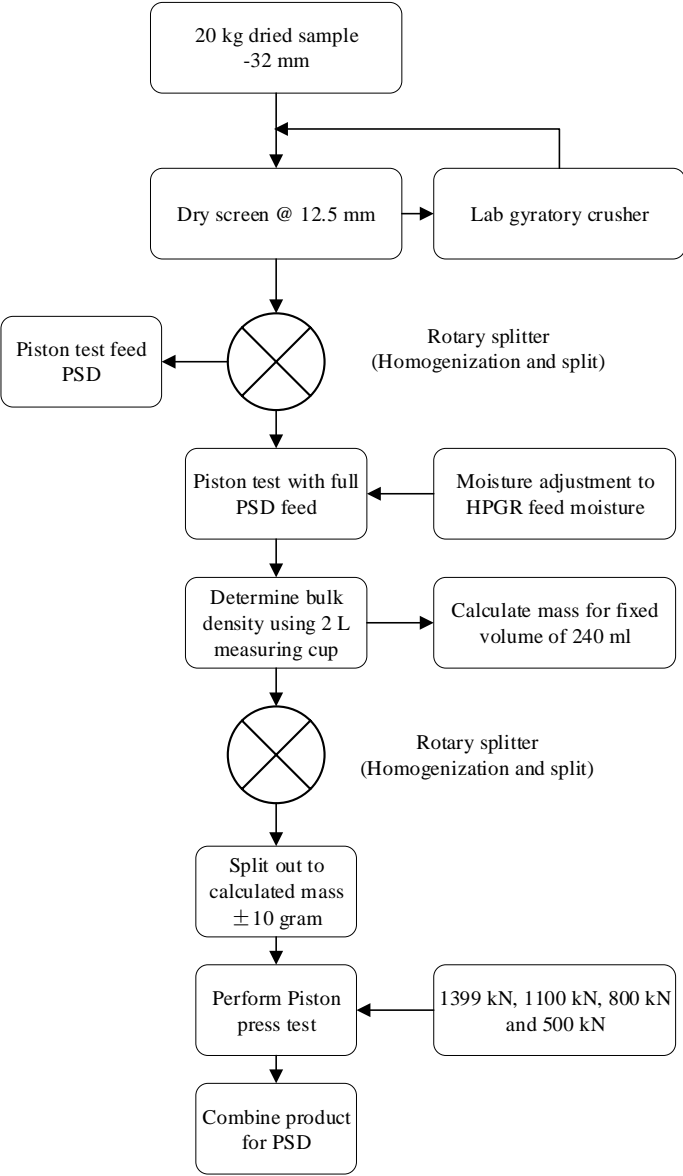


Figure B.1: Piston-die press calibration test procedure

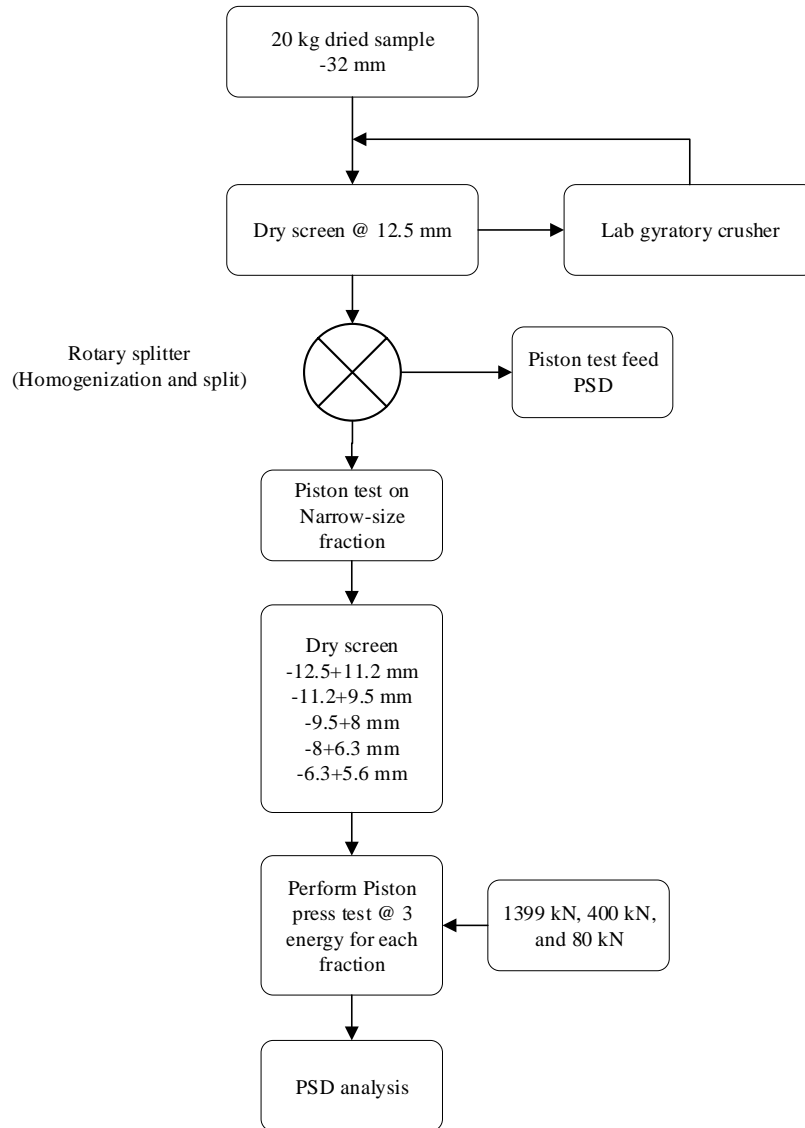


Figure B.2: Piston-die press simulation test procedure

B.2 PPT Calibration Tests

		C_1A_Feed		C_1A_P1			C_1A_P2			C_1A_P3			C_1A_P4		
Sample															
Moisture		3.49 %		3.49 %			3.49 %			3.49 %			3.49 %		
Force				1396.41 kN			1099.23 kN			798.88 kN			499.49 kN		
Pressure				240.39 MPa			189.24 MPa			137.53 MPa			85.99 MPa		
Specific Energy, kW/t				2.087 kWh/t			1.694 kWh/t			1.265 kWh/t			0.947 kWh/t		
Thickness				26.55 mm			27.15 mm			27.52 mm			28.21 mm		
Density				2.82 g/cc			2.76 g/cc			2.71 g/cc			2.60 g/cc		
Sieve #	Size (mm)	Weight (g)	Cum. % passing	Weight (g)	Cum. % passing	Normalized	Weight (g)	Cum. % passing	Normalized	Weight (g)	Cum. % passing	Normalized	Weight (g)	Cum. % passing	Normalized
1/2 inch	12.5	0	100.00	0.00	100.00	10.620	0.00	100.00	9.287	0.00	100.00	7.827	0.00	100.00	6.326
7/16 inch	11.2	61	94.21	0.00	100.00	9.515	0.00	100.00	8.321	2.80	99.26	7.013	0.00	100.00	5.668
3/8 inch	9.5	76.4	86.95	5.00	98.70	8.071	0.00	100.00	7.058	6.60	97.52	5.948	6.80	98.25	4.807
1/4 inch	6.7	234.4	64.68	26.00	91.93	5.692	25.20	93.48	4.978	32.40	88.96	4.195	32.80	89.81	3.391
4 Mesh	4.75	244	41.50	28.40	84.54	4.035	45.00	81.84	3.529	37.50	79.05	2.974	52.10	76.41	2.404
6 Mesh	3.36	113.1	30.76	36.40	75.07	2.855	36.70	72.34	2.496	39.30	68.67	2.104	42.30	65.53	1.700
8 Mesh	2.36	83.6	22.82	34.20	66.16	2.005	33.80	63.60	1.753	36.00	59.15	1.478	40.40	55.13	1.194
10 Mesh	1.7	50.4	18.03	31.10	58.07	1.444	32.10	55.29	1.263	29.10	51.47	1.064	35.40	46.03	0.860
14 Mesh	1.18	33.5	14.85	30.80	50.05	1.002	31.10	47.24	0.877	30.30	43.46	0.739	32.50	37.66	0.597
20 Mesh	0.85	33.3	11.68	24.60	43.65	0.722	24.00	41.03	0.632	22.90	37.41	0.532	21.80	32.06	0.430
28 Mesh	0.6	21	9.69	21.90	37.95	0.510	21.70	35.42	0.446	20.50	31.99	0.376	18.50	27.30	0.304
35 Mesh	0.425	16.8	8.09	21.50	32.35	0.361	20.80	30.04	0.316	18.80	27.03	0.266	18.10	22.64	0.215
48 Mesh	0.3	12.2	6.93	16.00	28.19	0.255	14.80	26.21	0.223	13.60	23.43	0.188	11.90	19.58	0.152
65 Mesh	0.212	10	5.98	14.30	24.47	0.180	13.00	22.85	0.158	11.90	20.29	0.133	10.50	16.88	0.107
150 Mesh	0.106	14.6	4.60	22.00	18.74	0.090	20.00	17.67	0.079	17.70	15.61	0.066	16.10	12.73	0.054
Pan		48.4		72.00			68.30			59.10			49.50		
Total wt.		1052.70		384.2			386.5			378.5			388.7		
P50		5.49		1.18			1.35			1.60			1.98		
P80		8.61		4.04			4.46			4.92			5.24		
RR Piston, RR50				4.66			4.08			3.44			2.78		
RR Piston, RR80				2.13			1.93			1.75			1.64		
P1mm		13.122													

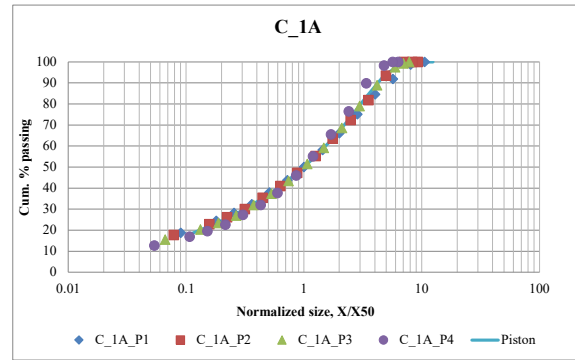
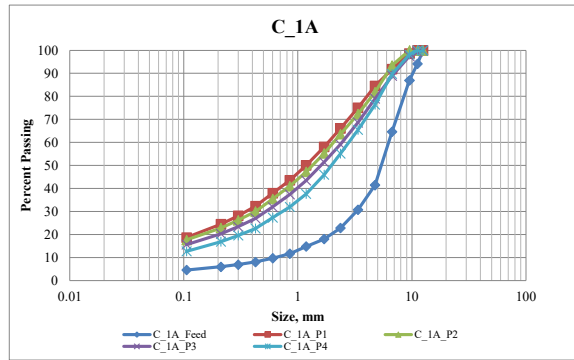


Figure B.3: PPT calibration test results - Cu-Au(C)-1A

		C_1B_Feed		C_1B_P1			C_1B_P2			C_1B_P3			C_1B_P4		
Sample															
Moisture		3.49	%	3.49	%	3.49	%	3.49	%	3.49	%	3.49	%	3.49	%
Force				1395.94	kN	1098.60	kN	799.39	kN	499.29	kN	85.95	MPa	499.29	kN
Pressure				240.31	MPa	189.13	MPa	137.62	MPa	85.95	MPa	2.74	MPa	137.62	MPa
Specific Energy, kW/t				2.040	kWh/t	1.682	kWh/t	1.338	kWh/t	0.949	kWh/t	0.949	kWh/t	1.682	kWh/t
Thickness				26.84	mm	26.67	mm	27.64	mm	28.58	mm	28.58	mm	26.84	mm
Density				2.82	g/cc	2.77	g/cc	2.68	g/cc	2.59	g/cc	2.59	g/cc	2.82	g/cc
Sieve #	Size (mm)	Weight (g)	Cum. % passing	Weight (g)	Cum. % passing	Normalized	Weight (g)	Cum. % passing	Normalized	Weight (g)	Cum. % passing	Normalized	Weight (g)	Cum. % passing	Normalized
1/2 inch	12.5	0	100.00	0.00	100.00	10.650	0.00	100.00	9.016	0.00	100.00	8.133	0.00	100.00	6.250
7/16 inch	11.2	61	94.21	0.00	100.00	9.543	0.00	100.00	8.079	2.80	99.27	7.287	0.00	100.00	5.600
3/8 inch	9.5	76.4	86.95	5.20	98.66	8.094	6.10	98.42	6.853	6.00	97.70	6.181	6.40	98.27	4.750
1/4 inch	6.7	234.4	64.68	23.10	92.72	5.708	19.70	93.32	4.833	23.70	91.49	4.359	30.40	90.07	3.350
4 Mesh	4.75	244	41.50	27.30	85.70	4.047	42.90	82.20	3.426	42.30	80.41	3.090	45.80	77.71	2.375
6 Mesh	3.36	113.1	30.76	37.90	75.95	2.863	38.70	72.18	2.424	40.50	69.81	2.186	48.10	64.73	1.680
8 Mesh	2.36	83.6	22.82	35.10	66.92	2.011	34.30	63.29	1.702	34.40	60.80	1.535	38.10	54.45	1.180
10 Mesh	1.7	50.4	18.03	33.60	58.27	1.448	32.90	54.77	1.226	32.10	52.40	1.106	31.40	45.98	0.850
14 Mesh	1.18	33.5	14.85	31.70	50.12	1.005	31.80	46.53	0.851	31.20	44.23	0.768	30.00	37.88	0.590
20 Mesh	0.85	33.3	11.68	25.70	43.50	0.724	25.10	40.03	0.613	24.50	37.81	0.553	21.20	32.16	0.425
28 Mesh	0.6	21	9.69	23.80	37.38	0.511	21.90	34.35	0.433	21.70	32.13	0.390	19.20	26.98	0.300
35 Mesh	0.425	16.8	8.09	21.80	31.77	0.362	20.90	28.94	0.307	20.00	26.89	0.277	17.00	22.40	0.212
48 Mesh	0.3	12.2	6.93	15.30	27.84	0.256	15.30	24.97	0.216	14.60	23.07	0.195	12.10	19.13	0.150
65 Mesh	0.212	10	5.98	14.10	24.21	0.181	13.60	21.45	0.153	12.60	19.77	0.138	10.40	16.32	0.106
150 Mesh	0.106	14.6	4.60	19.00	19.32	0.090	20.20	16.22	0.076	19.00	14.79	0.069	15.50	12.14	0.053
Pan		48.4		75.10			62.60			56.50			45.00		
Total wt.		1052.70		388.7			386.0			381.9			370.6		
P50		5.49		1.17			1.39			1.54			2.00		
P80		8.61		3.90			4.42			4.69			5.08		
RR Piston, RR50				4.68			3.96			3.57			2.74		
RR Piston, RR80				2.21			1.95			1.84			1.69		
P1mm		13.122													

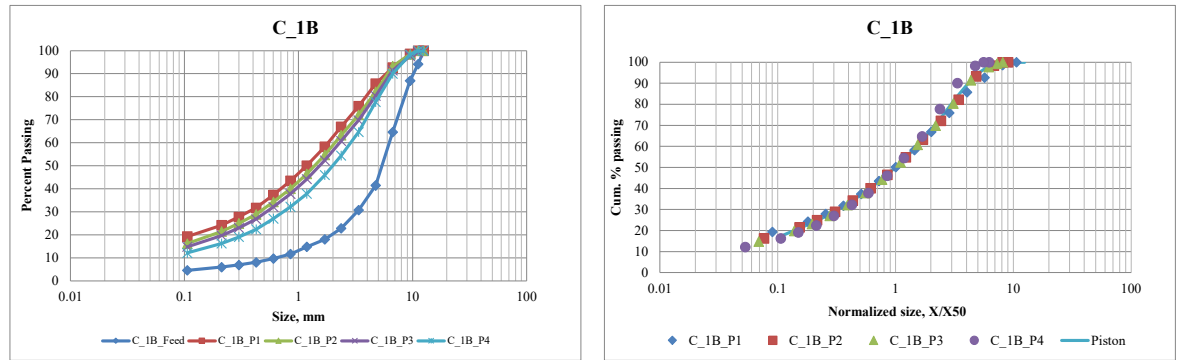


Figure B.4: PPT calibration test results - Cu-Au(C)-1B

		C 2A Feed		C 2A P1			C 2A P2			C 2A P3			C 2A P4		
Sample															
Moisture		3.49	%	3.49	%	3.49	%	3.49	%	3.49	%	3.49	%	3.49	
Force				1396.01	kN	1098.68	kN	799.08	kN	499.51	kN	85.99	MPa	1.001	
Pressure				240.33	MPa	189.14	MPa	137.56	MPa	1.470	kWh/t	25.28	mm	25.76	
Specific Energy, kW/t				2.242	kWh/t	1.839	kWh/t	1.470	kWh/t	2.82	g/cc	2.70	g/cc	2.70	
Thickness				24.27	mm	24.98	mm	25.28	mm	25.76	mm	25.76	mm	25.76	
Density				3.00	g/cc	2.91	g/cc	2.82	g/cc	2.82	g/cc	2.82	g/cc	2.70	
Sieve #	Size (mm)	Weight (g)	Cum. % passing	Weight (g)	Cum. % passing	Normalized	Weight (g)	Cum. % passing	Normalized	Weight (g)	Cum. % passing	Normalized	Weight (g)	Cum. % passing	Normalized
1/2 inch	12.5	0	100.00	0.00	100.00	10.855	0.00	100.00	9.865	0.00	100.00	8.083	0.00	100.00	6.499
7/16 inch	11.2	45.8	96.26	0.00	100.00	9.726	0.00	100.00	8.839	2.80	99.28	7.243	0.00	100.00	5.823
3/8 inch	9.5	99.3	88.15	5.60	98.56	8.250	8.20	97.91	7.497	11.40	96.34	6.143	7.00	98.17	4.939
1/4 inch	6.7	259.8	66.94	22.00	92.88	5.818	23.60	91.89	5.288	22.50	90.54	4.333	29.70	90.40	3.483
4 Mesh	4.75	264.4	45.35	36.30	83.53	4.125	38.90	81.97	3.749	38.60	80.60	3.072	45.40	78.51	2.469
6 Mesh	3.36	141.3	33.81	32.00	75.28	2.918	36.00	72.79	2.652	36.30	71.24	2.173	42.90	67.29	1.747
8 Mesh	2.36	104.6	25.27	36.90	65.76	2.049	36.60	63.45	1.863	40.10	60.91	1.526	43.10	56.01	1.227
10 Mesh	1.7	67.7	19.74	32.30	57.44	1.476	31.40	55.45	1.342	35.40	51.79	1.099	35.60	46.69	0.884
14 Mesh	1.18	43	16.23	26.30	50.66	1.025	26.20	48.76	0.931	25.50	45.22	0.763	25.40	40.04	0.613
20 Mesh	0.85	41.4	12.85	31.60	42.51	0.738	33.40	40.24	0.671	28.90	37.77	0.550	28.00	32.71	0.442
28 Mesh	0.6	25.5	10.76	24.90	36.09	0.521	22.80	34.43	0.474	22.10	32.08	0.388	20.00	27.48	0.312
35 Mesh	0.425	19.6	9.16	23.40	30.06	0.369	18.70	29.66	0.335	19.80	26.98	0.275	18.00	22.77	0.221
48 Mesh	0.3	14.5	7.98	16.50	25.81	0.261	17.10	25.30	0.237	14.00	23.37	0.194	12.20	19.58	0.156
65 Mesh	0.212	11.9	7.01	14.00	22.20	0.184	16.00	21.22	0.167	11.90	20.30	0.137	10.30	16.88	0.110
150 Mesh	0.106	18	5.54	21.50	16.65	0.092	20.80	15.91	0.084	18.80	15.46	0.069	16.60	12.54	0.055
Pan		67.8		64.60			62.40			60.00			47.90		
Total wt.		1224.60		387.9			392.1			388.1			382.1		
P50			5.18		1.15			1.27			1.55			1.92	
P80			8.40		4.11			4.43			4.65			4.97	
RR Piston, RR50					4.50			4.09			3.35			2.69	
RR Piston, RR80					2.04			1.90			1.81			1.69	
P1mm			14.382												

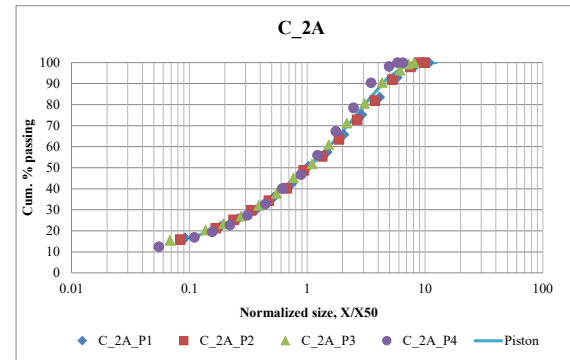
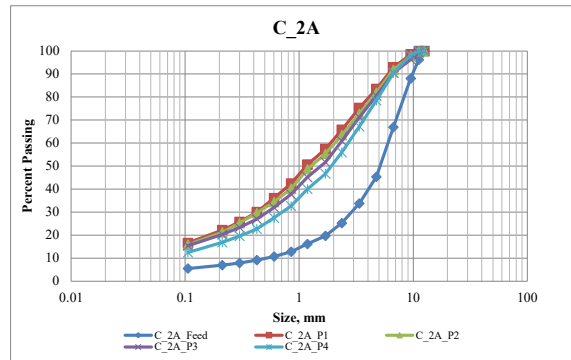


Figure B.5: PPT calibration test results - Cu-Au(C)-2A

		C 2B Feed			C 2B P1			C 2B P2			C 2B P3			C 2B P4		
Sample																
Moisture		3.49 %			3.49 %			3.49 %			3.49 %			3.49 %		
Force					1394.89 kN			1098.57 kN			799.15 kN			499.35 kN		
Pressure					240.13 MPa			189.12 MPa			137.58 MPa			85.96 MPa		
Specific Energy, kW/t					2.390 kWh/t			1.850 kWh/t			1.427 kWh/t			1.015 kWh/t		
Thickness					26.90 mm			24.34 mm			25.06 mm			26.00 mm		
Density					2.67 g/cc			2.93 g/cc			2.82 g/cc			2.70 g/cc		
Sieve #	Size (mm)	Weight (g)	Cum. % passing	Weight (g)	Cum. % passing	Normalized	Weight (g)	Cum. % passing	Normalized	Weight (g)	Cum. % passing	Normalized	Weight (g)	Cum. % passing	Normalized	
1/2 inch	12.5	0	100.00	0.00	100.00	11.059	0.00	100.00	8.578	0.00	100.00	7.358	4.30	98.89	6.329	
7/16 inch	11.2	45.8	96.26	0.00	100.00	9.909	2.80	99.24	7.686	5.70	98.52	6.593	6.80	97.13	5.671	
3/8 inch	9.5	99.3	88.15	3.10	99.20	8.405	7.70	97.16	6.519	12.80	95.21	5.592	2.50	96.48	4.810	
1/4 inch	6.7	259.8	66.94	20.90	93.78	5.928	17.60	92.39	4.598	29.20	87.64	3.944	26.30	89.67	3.392	
4 Mesh	4.75	264.4	45.35	34.00	84.97	4.203	38.10	82.08	3.260	41.30	76.94	2.796	48.70	77.07	2.405	
6 Mesh	3.36	141.3	33.81	34.50	76.02	2.973	36.70	72.14	2.306	36.00	67.61	1.978	41.90	66.23	1.701	
8 Mesh	2.36	104.6	25.27	37.40	66.33	2.088	38.00	61.86	1.620	36.30	58.20	1.389	43.10	55.07	1.195	
10 Mesh	1.7	67.7	19.74	32.00	58.04	1.504	32.60	53.03	1.167	31.60	50.01	1.001	34.70	46.09	0.861	
14 Mesh	1.18	43	16.23	26.30	51.22	1.044	25.50	46.13	0.810	24.30	43.72	0.695	25.60	39.47	0.597	
20 Mesh	0.85	41.4	12.85	33.10	42.64	0.752	29.10	38.25	0.583	30.10	35.92	0.500	27.50	32.35	0.430	
28 Mesh	0.6	25.5	10.76	23.10	36.65	0.531	22.50	32.16	0.412	20.60	30.58	0.353	20.10	27.15	0.304	
35 Mesh	0.425	19.6	9.16	19.30	31.65	0.376	21.00	26.48	0.292	16.40	26.33	0.250	17.80	22.54	0.215	
48 Mesh	0.3	14.5	7.98	18.10	26.96	0.265	15.10	22.39	0.206	15.00	22.44	0.177	12.10	19.41	0.152	
65 Mesh	0.212	11.9	7.01	16.00	22.81	0.188	12.90	18.90	0.145	13.00	19.07	0.125	10.20	16.77	0.107	
150 Mesh	0.106	18	5.54	22.90	16.87	0.094	19.50	13.62	0.073	18.30	14.33	0.062	16.10	12.60	0.054	
Pan		67.8		65.10			50.30			55.30			48.70			
Total wt.		1224.60			385.8			369.4			385.9			386.4		
P50		5.18			1.13			1.46			1.70			1.98		
P80		8.40			3.94			4.43			5.27			5.17		
RR Piston, RR50					4.58			3.55			3.05			2.62		
RR Piston, RR80					2.13			1.89			1.60			1.62		
P1mm		14.382														

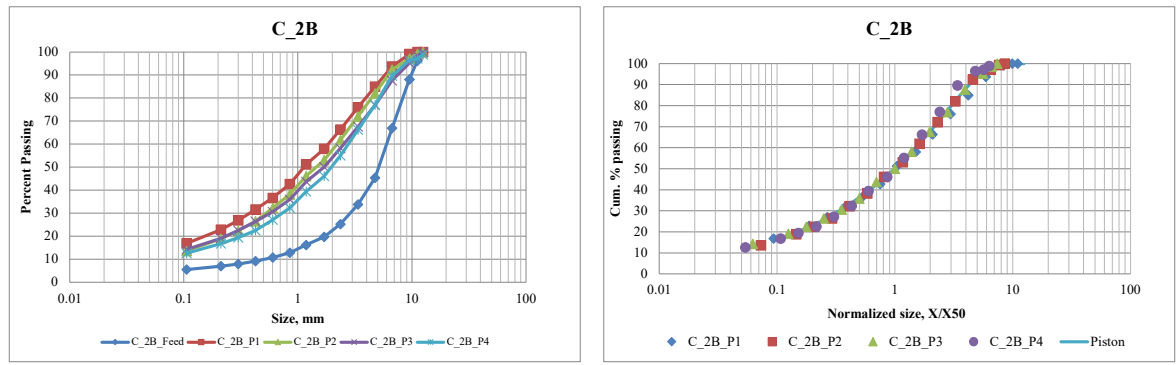


Figure B.6: PPT calibration test results - Cu-Au(C)-2B

		C_3A_Feed		C_3A_P1			C_3A_P2			C_3A_P3			C_3A_P4		
Sample															
Moisture		3.49 %		3.49 %			3.49 %			3.49 %			3.49 %		
Force				1396.20 kN			1098.77 kN			799.30 kN			499.66 kN		
Pressure				240.36 MPa			189.16 MPa			137.60 MPa			86.02 MPa		
Specific Energy, kW/t				2.433 kWh/t			1.959 kWh/t			1.497 kWh/t			1.028 kWh/t		
Thickness				23.99 mm			24.77 mm			25.48 mm			26.39 mm		
Density				2.97 g/cc			2.90 g/cc			2.80 g/cc			2.67 g/cc		
Sieve #	Size (mm)	Weight (g)	Cum. % passing	Weight (g)	Cum. % passing	Normalized	Weight (g)	Cum. % passing	Normalized	Weight (g)	Cum. % passing	Normalized	Weight (g)	Cum. % passing	Normalized
1/2 inch	12.5	0	100.00	0.00	100.00	10.617	0.00	100.00	9.389	0.00	100.00	7.549	0.00	100.00	5.921
7/16 inch	11.2	54	96.21	0.00	100.00	9.513	0.00	100.00	8.413	4.60	98.82	6.764	2.40	99.38	5.306
3/8 inch	9.5	143.3	86.14	2.30	99.40	8.069	3.30	99.15	7.136	2.70	98.12	5.737	8.10	97.29	4.500
1/4 inch	6.7	317	63.88	15.20	95.40	5.691	25.50	92.58	5.033	25.00	91.69	4.046	39.00	87.23	3.174
4 Mesh	4.75	343.7	39.75	38.70	85.23	4.035	38.70	82.60	3.568	46.80	79.64	2.869	48.50	74.72	2.250
6 Mesh	3.36	150.6	29.17	36.10	75.74	2.854	34.50	73.70	2.524	37.70	69.94	2.029	43.80	63.42	1.592
8 Mesh	2.36	110.2	21.43	38.90	65.52	2.005	39.00	63.65	1.773	43.20	58.82	1.425	39.90	53.12	1.118
10 Mesh	1.7	66.6	16.76	32.10	57.08	1.444	34.40	54.78	1.277	32.30	50.50	1.027	33.60	44.45	0.805
14 Mesh	1.18	43.5	13.70	26.70	50.07	1.002	27.10	47.80	0.886	25.40	43.96	0.713	25.00	38.00	0.559
20 Mesh	0.85	42.2	10.74	33.00	41.39	0.722	31.30	39.73	0.638	31.70	35.80	0.513	27.70	30.86	0.403
28 Mesh	0.6	25.2	8.97	23.40	35.24	0.510	24.10	33.51	0.451	21.70	30.22	0.362	20.40	25.59	0.284
35 Mesh	0.425	19.4	7.61	19.30	30.17	0.361	22.20	27.79	0.319	17.70	25.66	0.257	18.10	20.92	0.201
48 Mesh	0.3	14.4	6.59	17.80	25.49	0.255	15.50	23.79	0.225	16.00	21.54	0.181	12.00	17.83	0.142
65 Mesh	0.212	11.7	5.77	15.70	21.37	0.180	13.30	20.37	0.159	13.70	18.02	0.128	10.10	15.22	0.100
150 Mesh	0.106	17.7	4.53	21.10	15.82	0.090	20.30	15.13	0.080	18.80	13.18	0.064	15.80	11.15	0.050
Pan		64.5		60.20			58.70			51.20			43.20		
Total wt.		1424.00		380.5			387.9			388.5			387.6		
P50		5.61		1.18			1.33			1.66			2.11		
P80		8.71		3.94			4.31			4.80			5.53		
RR Piston, RR50				4.76			4.21			3.39			2.66		
RR Piston, RR80				2.21			2.02			1.81			1.58		
P1mm		12.084													

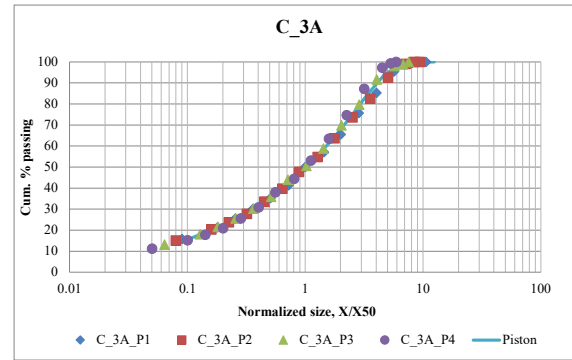
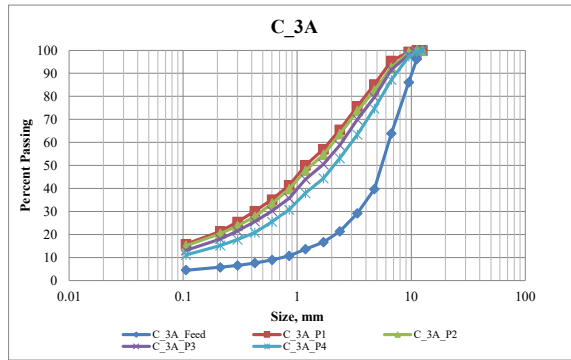


Figure B.7: PPT calibration test results - Cu-Au(C)-3A

		C 3B Feed		C 3B P1			C 3B P2			C 3B P3			C 3B P4		
Sample		3.49 %		3.49 %			3.49 %			3.49 %			3.49 %		
Moisture		3.49 %		3.49 %			3.49 %			3.49 %			3.49 %		
Force		1396.26 kN		1098.63 kN			799.36 kN			499.24 kN			85.95 MPa		
Pressure		240.37 MPa		189.13 MPa			137.61 MPa			90.90 MPa			26.32 mm		
Specific Energy, kW/t		2.400 kWh/t		2.400 kWh/t			1.933 kWh/t			1.411 kWh/t			0.990 kWh/t		
Thickness		23.84 mm		24.87 mm			25.66 mm			26.32 mm			2.68 g/cc		
Density		2.98 g/cc		2.91 g/cc			2.80 g/cc			2.68 g/cc			2.68 g/cc		
Sieve #	Size (mm)	Weight (g)	Cum. % passing	Weight (g)	Cum. % passing	Normalized	Weight (g)	Cum. % passing	Normalized	Weight (g)	Cum. % passing	Normalized	Weight (g)	Cum. % passing	Normalized
1/2 inch	12.5	0	100.00	0.00	100.00	10.394	0.00	100.00	9.320	0.00	100.00	7.760	0.00	100.00	6.369
7/16 inch	11.2	54	96.21	0.00	100.00	9.313	0.00	100.00	8.351	5.00	98.73	6.953	0.00	100.00	5.706
3/8 inch	9.5	143.3	86.14	4.90	98.71	7.900	4.50	98.84	7.083	10.70	96.01	5.898	5.20	98.66	4.840
1/4 inch	6.7	317	63.88	19.90	93.47	5.571	26.10	92.14	4.996	21.70	90.49	4.159	26.60	91.79	3.414
4 Mesh	4.75	343.7	39.75	35.60	84.10	3.950	46.00	80.32	3.542	42.70	79.63	2.949	54.90	77.62	2.420
6 Mesh	3.36	150.6	29.17	35.10	74.86	2.794	32.60	71.94	2.505	39.10	69.69	2.086	43.50	66.39	1.712
8 Mesh	2.36	110.2	21.43	36.20	65.32	1.962	36.90	62.46	1.760	39.40	59.67	1.465	44.70	54.85	1.202
10 Mesh	1.7	66.6	16.76	32.80	56.69	1.414	31.30	54.42	1.268	34.00	51.03	1.055	32.30	46.52	0.866
14 Mesh	1.18	43.5	13.70	26.70	49.66	0.981	25.90	47.76	0.880	25.90	44.44	0.733	25.70	39.88	0.601
20 Mesh	0.85	42.2	10.74	30.70	41.57	0.707	32.70	39.36	0.634	29.70	36.89	0.528	29.70	32.21	0.433
28 Mesh	0.6	25.2	8.97	24.20	35.20	0.499	23.40	33.35	0.447	22.80	31.10	0.372	19.80	27.10	0.306
35 Mesh	0.425	19.4	7.61	22.80	29.20	0.353	19.00	28.47	0.317	20.60	25.86	0.264	15.50	23.10	0.217
48 Mesh	0.3	14.4	6.59	16.20	24.93	0.249	17.60	23.95	0.224	14.30	22.22	0.186	13.70	19.57	0.153
65 Mesh	0.212	11.7	5.77	14.00	21.25	0.176	15.20	20.04	0.158	12.10	19.15	0.132	11.60	16.57	0.108
150 Mesh	0.106	17.7	4.53	22.00	15.46	0.088	20.70	14.72	0.079	19.90	14.09	0.066	16.20	12.39	0.054
Pan		64.5		58.70		0.088	57.30		0.079	55.40		0.066	48.00		0.054
Total wt.		1424.00		379.8			389.2			393.3			387.4		
P50		5.61		1.20			1.34			1.61			1.96		
P80		8.71		4.09			4.69			4.81			5.05		
RR Piston, RR50				4.66			4.18			3.48			2.86		
RR Piston, RR80				2.13			1.86			1.81			1.72		
P1mm		12.084													

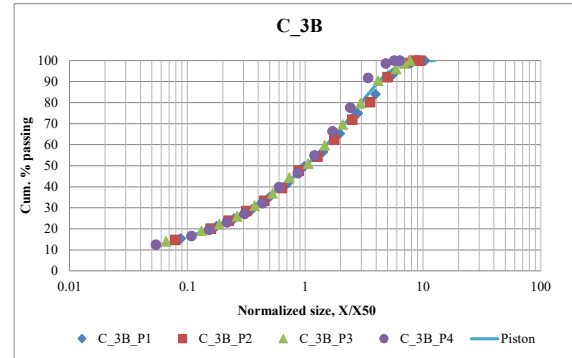
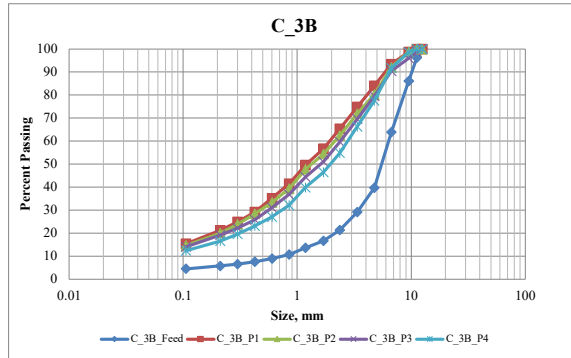


Figure B.8: PPT calibration test results - Cu-Au(C)-3B

		C_4A_Feed		C_4A_P1			C_4A_P2			C_4A_P3			C_4A_P4		
Sample		1.11641791 %		1.11641791 %			1.11641791 %			1.11641791 %			1.11641791 %		
Moisture		1.11641791 %		1.11641791 %			1.11641791 %			1.11641791 %			1.11641791 %		
Force		1396.55 kN		1396.55 kN			1098.65 kN			799.30 kN			499.22 kN		
Pressure		240.42 MPa		240.42 MPa			189.14 MPa			137.60 MPa			85.94 MPa		
Specific Energy, kW/t		2.493 kWh/t		2.493 kWh/t			1.918 kWh/t			1.458 kWh/t			1.003 kWh/t		
Thickness		30.06 mm		30.06 mm			26.26 mm			27.17 mm			28.41 mm		
Density		2.38 g/cc		2.38 g/cc			2.76 g/cc			2.65 g/cc			2.52 g/cc		
Sieve #	Size (mm)	Weight (g)	Cum. % passing	Weight (g)	Cum. % passing	Normalized	Weight (g)	Cum. % passing	Normalized	Weight (g)	Cum. % passing	Normalized	Weight (g)	Cum. % passing	Normalized
1/2 inch	12.5	0	100.00	0.00	100.00	10.789	0.00	100.00	9.568	0.00	100.00	7.896	0.00	100.00	5.339
7/16 inch	11.2	79.2	93.70	4.30	98.93	9.667	2.50	99.38	8.573	5.20	98.69	7.074	9.90	97.51	4.783
3/8 inch	9.5	156	81.30	4.50	97.81	8.199	6.20	97.83	7.272	7.30	96.84	6.001	22.20	91.94	4.057
1/4 inch	6.7	280.7	58.98	27.30	91.03	5.783	29.50	90.51	5.128	26.60	90.11	4.232	31.40	84.06	2.862
4 Mesh	4.75	195.5	43.44	33.00	82.82	4.100	39.50	80.65	3.656	48.50	77.85	3.000	54.00	70.50	2.029
6 Mesh	3.36	114.5	34.34	34.00	74.37	2.900	34.30	72.08	2.572	35.00	69.00	2.122	38.40	60.86	1.435
8 Mesh	2.36	88.7	27.29	36.60	65.27	2.037	34.90	63.37	1.806	38.20	59.34	1.491	42.40	50.21	1.008
10 Mesh	1.7	60.3	22.49	33.40	56.97	1.467	34.10	54.86	1.301	31.40	51.40	1.074	32.40	42.08	0.726
14 Mesh	1.18	42	19.15	26.10	50.48	1.018	26.50	48.24	0.903	26.90	44.60	0.745	24.50	35.93	0.504
20 Mesh	0.85	46.1	15.49	32.30	42.46	0.734	32.00	40.25	0.651	33.40	36.16	0.537	29.00	28.65	0.363
28 Mesh	0.6	32.1	12.94	25.50	36.12	0.518	25.30	33.93	0.459	22.90	30.37	0.379	19.70	23.70	0.256
35 Mesh	0.425	26.5	10.83	24.00	30.15	0.367	23.20	28.14	0.325	18.50	25.69	0.268	15.40	19.83	0.182
48 Mesh	0.3	20.1	9.23	17.30	25.85	0.259	16.20	24.09	0.230	16.70	21.47	0.189	13.50	16.44	0.128
65 Mesh	0.212	16.3	7.93	14.90	22.15	0.183	13.90	20.62	0.162	14.00	17.93	0.134	11.40	13.58	0.091
150 Mesh	0.106	22.9	6.11	24.30	16.11	0.091	22.00	15.13	0.081	19.40	13.02	0.067	15.90	9.59	0.045
Pan		76.9		64.80			60.60			51.50			38.20		
Total wt.		1257.80		402.3			400.5			395.5			398.3		
P50		5.56		1.16			1.31			1.58			2.34		
P80		9.33		4.25			4.63			5.06			6.08		
RR Piston, RR50				4.80			4.26			3.51			2.38		
RR Piston, RR80				2.20			2.01			1.84			1.53		
P1mm		17.153													

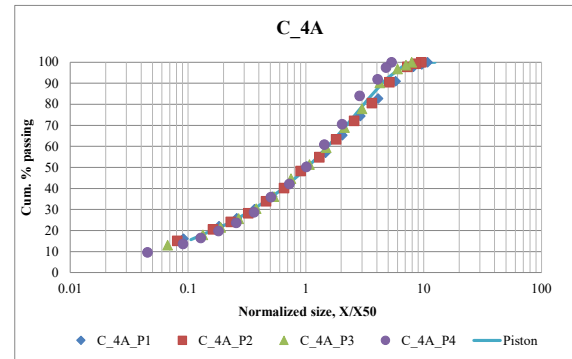
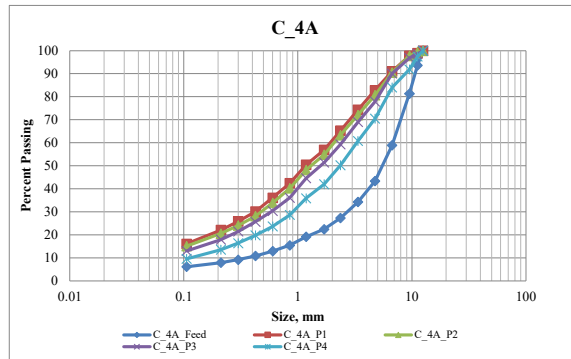


Figure B.9: PPT calibration test results - Cu-Au(C)-4A

		C_4B_Feed			C_4B_P1			C_4B_P2			C_4B_P3			C_4B_P4		
Sample		1.11641791 %			1.11641791 %			1.11641791 %			1.11641791 %			1.11641791 %		
Moisture		1.11641791 %			1.11641791 %			1.11641791 %			1.11641791 %			1.11641791 %		
Force		1396.43 kN			1098.61 kN			798.97 kN			499.59 kN			86.00 kN		
Pressure		240.40 MPa			189.13 MPa			148.5 MPa			137.54 MPa			86.00 MPa		
Specific Energy, kW/t		2.438			1.940			1.485			2.622			2.789		
Thickness		30.44 mm			25.60 mm			26.22 mm			27.89 mm			27.89 mm		
Density		2.37 g/cc			2.79 g/cc			2.69 g/cc			2.54 g/cc			2.54 g/cc		
Sieve #	Size (mm)	Weight (g)	Cum. % passing	Weight (g)	Cum. % passing	Normalized	Weight (g)	Cum. % passing	Normalized	Weight (g)	Cum. % passing	Normalized	Weight (g)	Cum. % passing	Normalized	
1/2 inch	12.5	0	100.00	0.00	100.00	10.999	0.00	100.00	9.150	0.00	100.00	7.048	0.00	100.00	6.008	
7/16 inch	11.2	79.2	93.70	0.00	100.00	9.855	6.70	98.34	8.198	8.80	97.83	6.315	2.20	99.46	5.383	
3/8 inch	9.5	156	81.30	7.00	98.23	8.359	8.90	96.14	6.954	15.50	94.00	5.357	11.90	96.53	4.566	
1/4 inch	6.7	280.7	58.98	28.80	90.96	5.895	28.10	89.18	4.904	29.40	86.74	3.778	42.50	86.08	3.220	
4 Mesh	4.75	195.5	43.44	35.00	82.13	4.180	39.10	79.49	3.477	43.00	76.12	2.678	44.90	75.04	2.283	
6 Mesh	3.36	114.5	34.34	33.60	73.65	2.957	34.30	70.99	2.459	37.40	66.89	1.895	44.90	64.00	1.615	
8 Mesh	2.36	88.7	27.29	34.00	65.07	2.077	38.90	61.36	1.727	38.40	57.41	1.331	43.80	53.23	1.134	
10 Mesh	1.7	60.3	22.49	30.40	57.40	1.496	30.20	53.88	1.244	34.10	48.99	0.959	32.60	45.22	0.817	
14 Mesh	1.18	42	19.15	25.60	50.93	1.038	25.50	47.56	0.864	26.00	42.57	0.665	25.80	38.87	0.567	
20 Mesh	0.85	46.1	15.49	30.10	43.34	0.748	32.40	39.53	0.622	29.10	35.38	0.479	30.20	31.45	0.409	
28 Mesh	0.6	32.1	12.94	24.60	37.13	0.528	23.20	33.79	0.439	22.30	29.88	0.338	20.50	26.41	0.288	
35 Mesh	0.425	26.5	10.83	23.50	31.20	0.374	19.20	29.03	0.311	20.40	24.84	0.240	16.20	22.42	0.204	
48 Mesh	0.3	20.1	9.23	16.90	26.93	0.264	17.50	24.70	0.220	14.20	21.33	0.169	14.20	18.93	0.144	
65 Mesh	0.212	16.3	7.93	14.60	23.25	0.187	15.30	20.91	0.155	12.10	18.35	0.120	12.10	15.96	0.102	
150 Mesh	0.106	22.9	6.11	23.60	17.29	0.093	21.90	15.48	0.078	19.20	13.60	0.060	17.00	11.78	0.051	
	Pan	76.9		68.50			62.50			55.10			47.90			
Total wt.		1257.80			396.2			403.7			405			406.7		
P50		5.56			1.14			1.37			1.77			2.08		
P80		9.33			4.37			4.84			5.41			5.58		
RR Piston, RR50		4.90			4.90			4.07			3.14			2.67		
RR Piston, RR80		2.14			2.14			1.93			1.72			1.67		
P1mm		17.153														

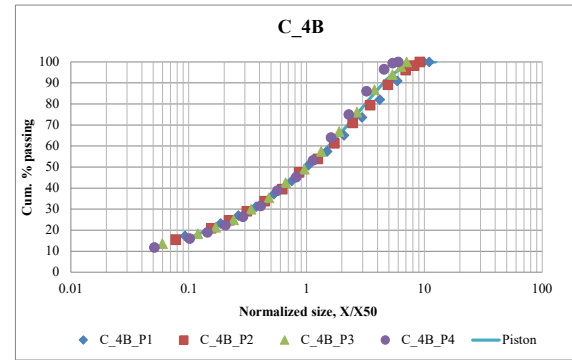
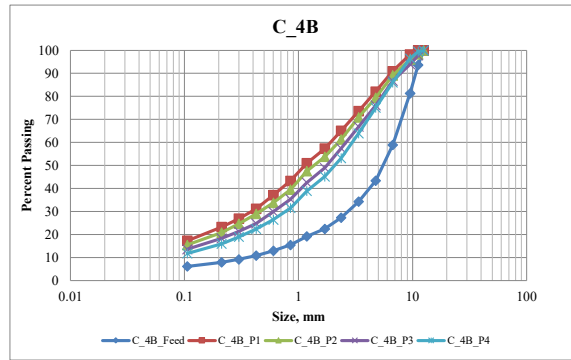


Figure B.10: PPT calibration test results - Cu-Au(C)-4B

		C_Geo1_Feed			C_Geo1_P1			C_Geo1_P2			C_Geo1_P3			C_Geo1_P4		
Sample																
Moisture		2.5 %			2.5 %			2.5 %			2.5 %			2.5 %		
Force		1396.17 kN			1098.51 kN			799.41 kN			499.11 kN					
Pressure		240.35 MPa			189.11 MPa			137.62 MPa			85.92 MPa					
Specific Energy, kW/t		2.501 kWh/t			1.978 kWh/t			1.493 kWh/t			1.056 kWh/t					
Thickness		24.08 mm			23.66 mm			25.30 mm			26.76 mm					
Density		2.89 g/cc			2.81 g/cc			2.71 g/cc			2.56 g/cc					
Sieve #	Size (mm)	Weight (g)	Cum. % passing	Weight (g)	Cum. % passing	Normalized	Weight (g)	Cum. % passing	Normalized	Weight (g)	Cum. % passing	Normalized	Weight (g)	Cum. % passing	Normalized	
1/2 inch	12.5	0	100.00	0.00	100.00	11.336	0.00	100.00	9.410	0.00	100.00	8.072	0.00	100.00	6.576	
7/16 inch	11.2	2.3	99.79	0.00	100.00	10.157	0.00	100.00	8.432	0.00	100.00	7.232	0.00	100.00	5.892	
3/8 inch	9.5	41.3	95.95	0.00	100.00	8.615	0.00	100.00	7.152	3.50	99.09	6.134	0.00	100.00	4.997	
1/4 inch	6.7	290.6	68.96	9.60	97.50	6.076	15.80	95.73	5.044	21.00	93.64	4.326	25.30	93.48	3.525	
4 Mesh	4.75	281.6	42.81	37.40	87.74	4.308	48.10	82.72	3.576	46.00	81.71	3.067	58.80	78.33	2.499	
6 Mesh	3.36	144.6	29.38	41.80	76.84	3.047	40.70	71.71	2.529	44.80	70.08	2.170	48.40	65.86	1.768	
8 Mesh	2.36	85.7	21.42	35.70	67.53	2.140	33.10	62.75	1.777	37.00	60.48	1.524	39.60	55.66	1.241	
10 Mesh	1.7	51.6	16.62	31.00	59.44	1.542	27.50	55.32	1.280	32.30	52.10	1.098	32.40	47.31	0.894	
14 Mesh	1.18	41.7	12.75	30.80	51.41	1.070	28.40	47.63	0.888	29.90	44.34	0.762	30.70	39.40	0.621	
20 Mesh	0.85	26.4	10.30	24.80	44.94	0.771	22.50	41.55	0.640	23.50	38.25	0.549	25.10	32.93	0.447	
28 Mesh	0.6	20.5	8.40	23.00	38.94	0.544	20.50	36.00	0.452	20.80	32.85	0.387	19.90	27.80	0.316	
35 Mesh	0.425	16.5	6.86	19.70	33.80	0.385	17.50	31.27	0.320	17.70	28.26	0.274	16.20	23.63	0.224	
48 Mesh	0.3	12.4	5.71	15.90	29.66	0.272	14.10	27.45	0.226	13.80	24.68	0.194	12.40	20.43	0.158	
65 Mesh	0.212	9.8	4.80	15.20	25.69	0.192	12.70	24.02	0.160	12.00	21.56	0.137	10.60	17.70	0.112	
150 Mesh	0.106	13.9	3.51	22.40	19.85	0.096	18.90	18.91	0.080	17.70	16.97	0.068	15.20	13.79	0.056	
Pan		37.8		76.10			69.90			65.40			53.50			
Total wt.		1076.70			583.4			369.7			385.4			388.1		
P50		5.31			1.10			1.33			1.55			1.90		
P80		7.84			3.73			4.38			4.53			4.95		
RR Piston, RR50					4.82			4.00			3.43			2.79		
RR Piston, RR80					2.10			1.79			1.73			1.58		
P1mm		11.415														

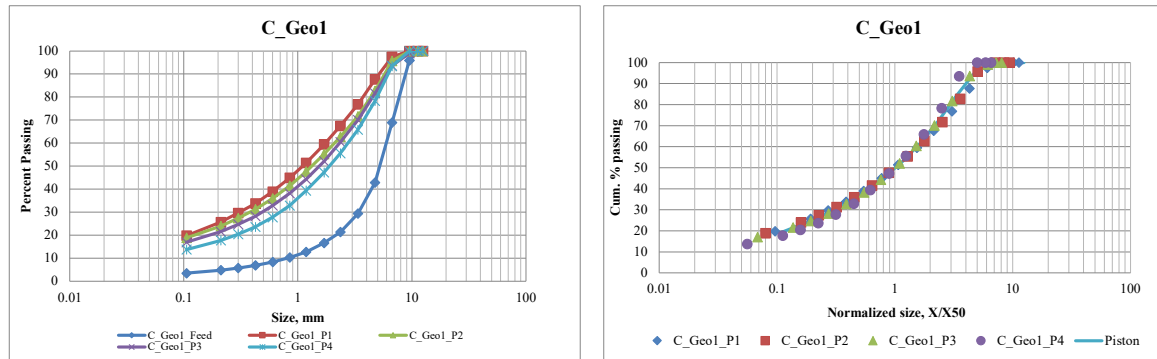


Figure B.11: PPT calibration test results - Cu-Au(C)-Geo1

		C_Geo2_Feed		C_Geo2_P1			C_Geo2_P2			C_Geo2_P3			C_Geo2_P4		
Sample															
Moisture		2.5 %		2.5 %			2.5 %			2.5 %			2.5 %		
Force				1396.12 kN			1098.82 kN			799.14 kN			498.87 kN		
Pressure				240.35 MPa			189.17 MPa			137.57 MPa			85.88 MPa		
Specific Energy, kWh/t				2.622 kWh/t			2.059 kWh/t			1.528 kWh/t			1.148 kWh/t		
Thickness				24.20 mm			24.35 mm			23.88 mm			26.96 mm		
Density				2.74 g/cc			2.67 g/cc			2.71 g/cc			2.41 g/cc		
Sieve #	Size (mm)	Weight (g)	Cum. % passing	Weight (g)	Cum. % passing	Normalized	Weight (g)	Cum. % passing	Normalized	Weight (g)	Cum. % passing	Normalized	Weight (g)	Cum. % passing	Normalized
1/2 inch	12.5	0	100.00	0.00	100.00	11.941	0.00	100.00	9.323	0.00	100.00	8.038	0.00	100.00	5.969
7/16 inch	11.2	49.1	94.34	0.00	100.00	10.699	9.90	97.26	8.353	0.00	100.00	7.202	5.29	98.57	5.348
3/8 inch	9.5	135.6	78.70	3.80	98.96	9.075	5.00	95.88	7.085	12.40	96.58	6.109	19.68	93.23	4.536
1/4 inch	6.7	228.2	52.38	17.40	94.19	6.400	24.80	89.02	4.997	28.50	88.72	4.308	34.23	83.96	3.199
4 Mesh	4.75	140.8	36.14	32.60	85.26	4.538	35.90	79.10	3.543	39.50	77.83	3.054	42.27	72.50	2.268
6 Mesh	3.36	82.1	26.67	33.00	76.22	3.210	29.50	70.94	2.506	34.90	68.21	2.161	38.20	62.15	1.604
8 Mesh	2.36	55.1	20.31	31.10	67.70	2.254	32.30	62.01	1.760	32.00	59.39	1.518	34.55	52.79	1.127
10 Mesh	1.7	34.6	16.32	27.20	60.25	1.624	26.00	54.82	1.268	25.80	52.27	1.093	26.95	45.48	0.812
14 Mesh	1.18	30.1	12.85	28.50	52.44	1.127	26.20	47.58	0.880	31.60	43.56	0.759	26.60	38.27	0.563
20 Mesh	0.85	19.8	10.57	23.40	46.03	0.812	21.70	41.58	0.634	25.10	36.64	0.547	19.70	32.93	0.406
28 Mesh	0.6	16.3	8.69	22.00	40.00	0.573	20.10	36.02	0.447	23.00	30.30	0.386	17.80	28.11	0.286
35 Mesh	0.425	13.2	7.16	19.60	34.63	0.406	17.70	31.13	0.317	19.70	24.87	0.273	15.70	23.86	0.203
48 Mesh	0.3	10.3	5.97	15.90	30.27	0.287	14.20	27.20	0.224	15.20	20.68	0.193	11.90	20.63	0.143
65 Mesh	0.212	8.4	5.01	15.50	26.03	0.203	13.30	23.53	0.158	13.80	16.87	0.136	10.30	17.84	0.101
150 Mesh	0.106	12.6	3.55	22.60	19.84	0.101	19.30	18.19	0.079	19.00	11.63	0.068	14.90	13.80	0.051
Pan		30.8		72.40			65.80			42.20			50.93		
Total wt.		867.00		365.0			361.7			362.7			369.0		
P50		6.42		1.05			1.34			1.56			2.09		
P80		9.64		3.90			4.91			5.11			5.98		
RR Piston, RR50				6.13			4.79			4.13			3.06		
RR Piston, RR80				2.47			1.96			1.89			1.61		
P1mm		11.603													

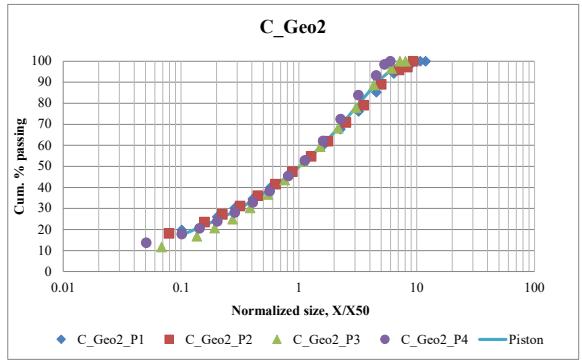
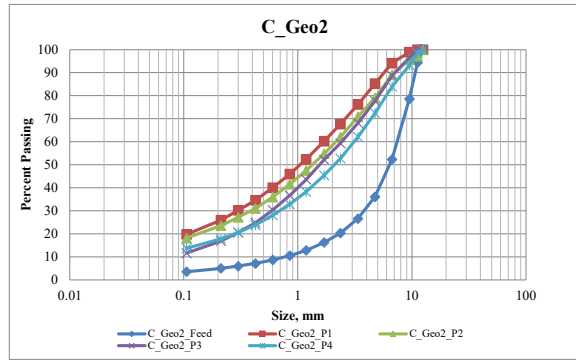


Figure B.12: PPT calibration test results - Cu-Au(C)-Geo2

		C_Geo3_Feed		C_Geo3_P1			C_Geo3_P2			C_Geo3_P3			C_Geo3_P4		
Sample															
Moisture		2.5	%	2.5	%		2.5	%		2.5	%		2.5	%	
Force				1394.27	kN		1097.01	kN		798.79	kN		499.21	kN	
Pressure				240.03	MPa		188.85	MPa		137.51	MPa		85.94	MPa	
Specific Energy, kW/t				2.542	kWh/t		2.114	kWh/t		1.602	kWh/t		1.104	kWh/t	
Thickness				25.07	mm		25.45	mm		26.33	mm		27.41	mm	
Density				2.80	g/cc		2.73	g/cc		2.61	g/cc		2.48	g/cc	
Sieve #	Size (mm)	Weight (g)	Cum. % passing	Weight (g)	Cum. % passing	Normalized	Weight (g)	Cum. % passing	Normalized	Weight (g)	Cum. % passing	Normalized	Weight (g)	Cum. % passing	Normalized
1/2 inch	12.5	0	100.00	0.00	100.00	11.136	0.00	100.00	9.931	0.00	100.00	8.488	0.00	100.00	6.823
7/16 inch	11.2	8.8	99.25	0.00	100.00	9.978	0.00	100.00	8.898	0.00	100.00	7.605	0.00	100.00	6.114
3/8 inch	9.5	40.3	95.82	0.00	100.00	8.463	1.10	99.72	7.548	1.40	99.64	6.451	4.19	98.91	5.186
1/4 inch	6.7	302	70.14	19.40	94.99	5.969	20.70	94.36	5.323	16.80	95.29	4.549	21.49	93.34	3.657
4 Mesh	4.75	311.1	43.68	38.80	84.97	4.232	40.70	83.84	3.774	49.60	82.47	3.225	55.74	78.90	2.593
6 Mesh	3.36	157.4	30.29	38.90	74.92	2.993	38.00	74.01	2.670	46.10	70.55	2.281	46.06	66.96	1.834
8 Mesh	2.36	95.7	22.15	33.10	66.37	2.102	34.70	65.04	1.875	36.90	61.01	1.602	39.30	56.77	1.288
10 Mesh	1.7	62.9	16.80	28.60	58.98	1.515	31.70	56.84	1.351	31.70	52.82	1.154	33.22	48.16	0.928
14 Mesh	1.18	51.7	12.40	30.60	51.07	1.051	31.70	48.64	0.938	26.60	45.94	0.801	33.90	39.37	0.644
20 Mesh	0.85	31.7	9.70	25.70	44.43	0.757	25.60	42.02	0.675	21.90	40.28	0.577	25.00	32.89	0.464
28 Mesh	0.6	24.1	7.66	24.60	38.08	0.535	24.30	35.74	0.477	19.40	35.26	0.407	21.90	27.22	0.328
35 Mesh	0.425	18.3	6.10	21.90	32.42	0.379	21.00	30.31	0.338	17.10	30.84	0.289	18.10	22.52	0.232
48 Mesh	0.3	13.2	4.98	17.60	27.87	0.267	16.90	25.94	0.238	13.60	27.33	0.204	13.80	18.95	0.164
65 Mesh	0.212	10.1	4.12	16.80	23.53	0.189	15.50	21.93	0.168	12.20	24.17	0.144	11.00	16.10	0.116
150 Mesh	0.106	13.9	2.93	23.60	17.44	0.094	21.60	16.34	0.084	17.80	19.57	0.072	15.10	12.18	0.058
Pan		34.5		67.50			63.20			75.70			47.00		
Total wt.		1175.70		387.1			386.7			386.8			385.8		
P50			5.24		1.12			1.26			1.47			1.83	
P80			7.76		4.03			4.17			4.44			4.89	
RR Piston, RR50					4.67			4.16			3.56			2.86	
RR Piston, RR80					1.93			1.86			1.75			1.59	
P1mm			10.930												

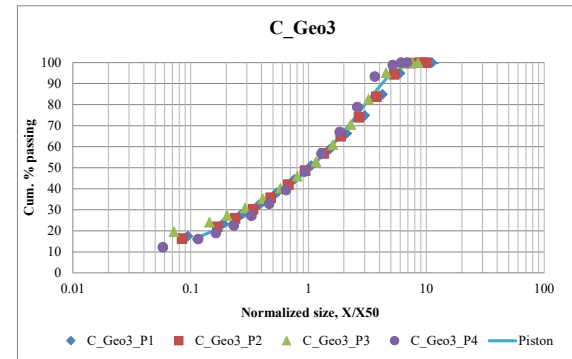
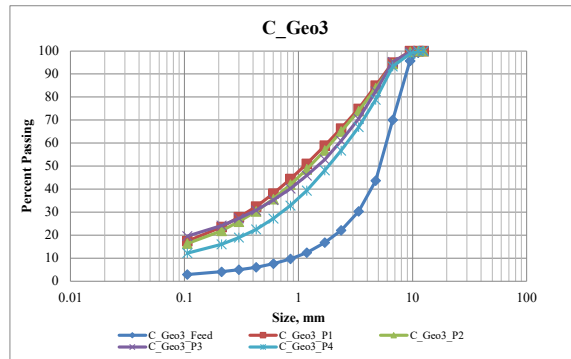


Figure B.13: PPT calibration test results - Cu-Au(C)-Geo3

		C_Geo4_Feed		C_Geo4_P1			C_Geo4_P2			C_Geo4_P3			C_Geo4_P4		
Sample															
Moisture		2.5	%	2.5	%	2.5	%	2.5	%	2.5	%	2.5	%	2.5	%
Force				1396.06	kN	1098.52	kN	799.24	kN	498.98	kN	85.90	MPa	1.085	kWh/t
Pressure				240.33	MPa	189.11	MPa	137.59	MPa	26.68	mm	27.82	mm	2.48	g/cc
Specific Energy, kW/t				2.467	kWh/t	1.939	kWh/t	1.564	kWh/t	2.59	g/cc				
Thickness				26.10	mm	25.87	mm	26.68	mm						
Density				2.78	g/cc	2.72	g/cc								
Sieve #	Size (mm)	Weight (g)	Cum. % passing	Weight (g)	Cum. % passing	Normalized	Weight (g)	Cum. % passing	Normalized	Weight (g)	Cum. % passing	Normalized	Weight (g)	Cum. % passing	Normalized
1/2 inch	12.5	0	100.00	0.00	100.00	9.298	0.00	100.00	8.021	0.00	100.00	7.293	0.00	100.00	5.431
7/16 inch	11.2	52.3	94.05	0.00	100.00	8.331	0.00	100.00	7.186	2.69	99.31	6.534	6.05	98.45	4.866
3/8 inch	9.5	124.2	79.93	5.80	98.55	7.067	14.70	96.25	6.096	6.37	97.67	5.542	6.88	96.70	4.127
1/4 inch	4.75	248.8	51.63	34.90	89.86	4.984	38.00	86.56	4.299	40.97	87.11	3.909	53.88	82.93	2.911
4 Mesh	4.75	140.3	35.68	39.40	80.04	3.533	38.80	76.66	3.048	44.66	75.61	2.771	50.38	70.07	2.064
6 Mesh	3.36	83.6	26.17	35.90	71.09	2.499	34.80	67.78	2.156	38.52	65.69	1.960	41.25	59.53	1.460
8 Mesh	2.36	55.7	19.83	35.20	62.32	1.755	34.90	58.88	1.514	34.82	56.72	1.377	35.00	50.59	1.025
10 Mesh	1.7	36.3	15.71	29.80	54.90	1.265	27.70	51.81	1.091	26.70	49.84	0.992	28.28	43.37	0.739
14 Mesh	1.18	30.9	12.19	29.80	47.47	0.878	28.20	44.62	0.757	28.80	42.42	0.688	28.00	36.21	0.513
20 Mesh	0.85	19.5	9.97	23.80	41.54	0.632	22.60	38.85	0.545	21.70	36.83	0.496	20.30	31.03	0.369
28 Mesh	0.6	15.8	8.18	22.20	36.01	0.446	20.70	33.57	0.385	19.70	31.75	0.350	18.50	26.30	0.261
35 Mesh	0.425	12.8	6.72	19.60	31.12	0.316	18.00	28.98	0.273	16.80	27.43	0.248	15.50	22.34	0.185
48 Mesh	0.3	9.7	5.62	15.90	27.16	0.223	14.40	25.31	0.192	13.40	23.97	0.175	11.90	19.31	0.130
65 Mesh	0.212	8.1	4.70	15.60	23.27	0.158	13.60	21.84	0.136	11.60	20.99	0.124	10.00	16.75	0.092
150 Mesh	0.106	12	3.33	22.60	17.64	0.079	19.80	16.79	0.068	17.50	16.48	0.062	14.70	13.00	0.046
Pan		29.3		70.80			65.80			63.97			50.88		
Total wt.		879.30		401.3			392.0			388.2			391.5		
P50		6.50		1.34			1.56			1.71			2.30		
P80		9.51		4.74			5.36			5.45			6.23		
RR Piston, RR50				4.84			4.17			3.79			2.83		
P1mm		10.982		2.00			1.77			1.75			1.53		

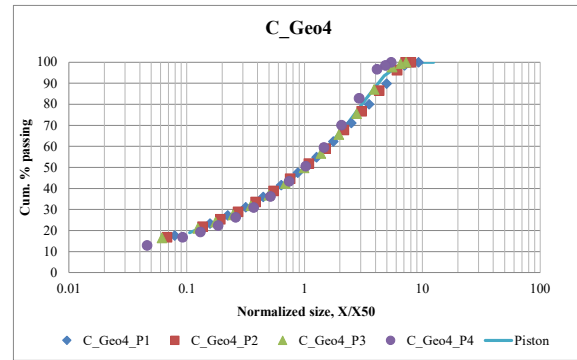
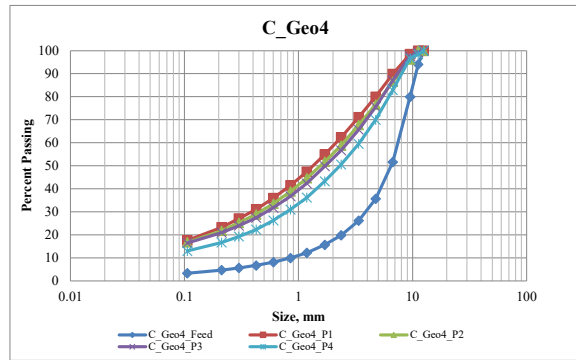


Figure B.14: PPT calibration test results - Cu-Au(C)-Geo4

		C_Geo5_Feed		C_Geo5_P1			C_Geo5_P2			C_Geo5_P3			C_Geo5_P4		
Sample		2.5 %		2.5 %			2.5 %			2.5 %			2.5 %		
Moisture		2.5 %		2.5 %			2.5 %			2.5 %			2.5 %		
Force		1396.68 kN		1396.68 kN			1099.04 kN			799.01 kN			499.29 kN		
Pressure		240.44 MPa		240.44 MPa			189.20 MPa			137.55 MPa			85.95 MPa		
Specific Energy, kW/t		2.406		2.406			1.956			1.524			1.096		
Thickness		24.87 mm		24.87 mm			25.51 mm			25.85 mm			26.96 mm		
Density		2.84 g/cc		2.84 g/cc			2.77 g/cc			2.66 g/cc			2.54 g/cc		
Sieve #	Size (mm)	Weight (g)	Cum. % passing	Weight (g)	Cum. % passing	Normalized	Weight (g)	Cum. % passing	Normalized	Weight (g)	Cum. % passing	Normalized	Weight (g)	Cum. % passing	Normalized
1/2 inch	12.5	3.7	99.67	0.00	100.00	11.894	0.00	100.00	10.392	0.00	100.00	8.271	0.00	100.00	6.778
7/16 inch	11.2	8.3	98.93	0.00	100.00	10.657	0.00	100.00	9.312	0.00	100.00	7.411	0.00	100.00	6.073
3/8 inch	9.5	39	95.45	0.00	100.00	9.039	0.00	100.00	7.898	0.00	100.00	6.286	1.70	99.56	5.151
1/4 inch	6.7	290.6	69.50	13.30	96.59	6.375	17.40	95.58	5.570	21.20	94.51	4.433	29.03	92.09	3.633
4 Mesh	4.75	314.4	41.43	38.60	86.69	4.520	45.20	84.10	3.949	50.20	81.51	3.143	50.39	79.12	2.576
6 Mesh	3.36	146.5	28.35	39.00	76.68	3.197	39.30	74.11	2.793	46.30	69.52	2.223	50.04	66.24	1.822
8 Mesh	2.36	84.7	20.79	34.40	67.86	2.246	35.20	65.17	1.962	35.30	60.38	1.562	39.55	56.06	1.280
10 Mesh	1.7	52.2	16.13	29.50	60.29	1.618	30.50	57.42	1.413	29.80	52.67	1.125	30.74	48.15	0.922
14 Mesh	1.18	44.1	12.19	30.90	52.36	1.123	30.70	49.62	0.981	30.30	44.82	0.781	31.10	40.14	0.640
20 Mesh	0.85	27.2	9.76	25.00	45.95	0.809	25.10	43.24	0.707	23.60	38.71	0.562	23.10	34.20	0.461
28 Mesh	0.6	20.8	7.90	23.50	39.92	0.571	22.80	37.45	0.499	21.70	33.09	0.397	20.40	28.94	0.325
35 Mesh	0.425	16.4	6.44	20.70	34.61	0.404	19.90	32.39	0.353	18.40	28.33	0.281	17.10	24.54	0.230
48 Mesh	0.3	12	5.37	16.60	30.35	0.285	15.90	28.35	0.249	14.50	24.57	0.198	12.90	21.22	0.163
65 Mesh	0.212	9.4	4.53	16.30	26.17	0.202	14.80	24.59	0.176	12.40	21.36	0.140	11.00	18.39	0.115
150 Mesh	0.106	13.9	3.29	23.00	20.27	0.101	21.50	19.13	0.088	18.30	16.62	0.070	15.90	14.30	0.057
	Pan	36.8		79.00			75.30			64.20			55.55		
Total wt.		1120.00		389.8			393.6			386.2			388.5		
P50		5.38		1.05			1.20			1.51			1.84		
P80		7.82		3.79			4.14			4.56			4.87		
RR Piston, RR50				5.12			4.48			3.56			2.92		
RR Piston, RR80				2.07			1.89			1.72			1.61		
P1mm		10.863													

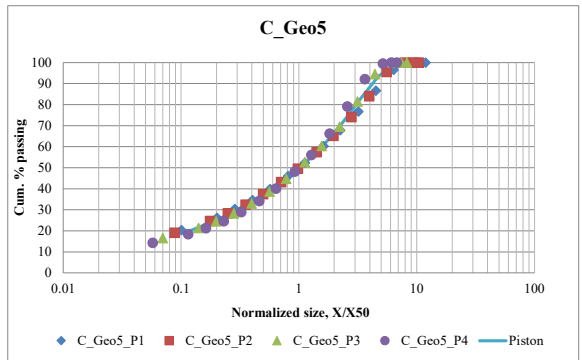
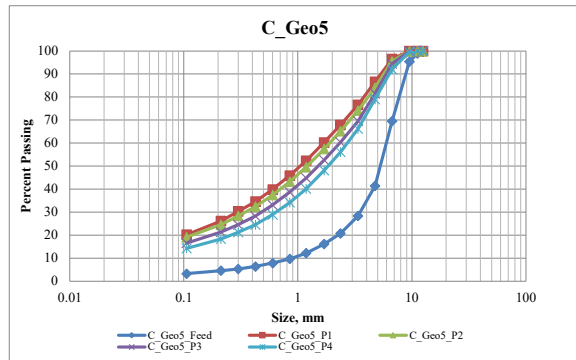


Figure B.15: PPT calibration test results - Cu-Au(C)-Geo5

		C_Geo6_Feed		C_Geo6_P1			C_Geo6_P2			C_Geo6_P3			C_Geo6_P4		
Sample															
Moisture		2.5 %		2.5 %			2.5 %			2.5 %			2.5 %		
Force				1395.80 kN			1098.52 kN			799.38 kN			499.13 kN		
Pressure				240.29 MPa			189.11 MPa			137.62 MPa			85.93 MPa		
Specific Energy, kW/t				2.604 kWh/t			2.173 kWh/t			1.659 kWh/t			1.154 kWh/t		
Thickness				24.58 mm			24.48 mm			25.54 mm			26.21 mm		
Density				2.85 g/cc			2.78 g/cc			2.66 g/cc			2.54 g/cc		
Sieve #	Size (mm)	Weight (g)	Cum. % passing	Weight (g)	Cum. % passing	Normalized	Weight (g)	Cum. % passing	Normalized	Weight (g)	Cum. % passing	Normalized	Weight (g)	Cum. % passing	Normalized
1/2 inch	12.5	0	100.00	0.00	100.00	10.137	0.00	100.00	8.871	0.00	100.00	7.686	0.00	100.00	5.889
7/16 inch	11.2	9.1	99.08	0.00	100.00	9.082	0.00	100.00	7.949	0.00	100.00	6.886	0.00	100.00	5.277
3/8 inch	9.5	41.4	94.88	0.00	100.00	7.704	1.40	99.63	6.742	0.00	100.00	5.841	0.00	100.00	4.476
1/4 inch	6.7	289.5	65.56	13.60	96.48	5.433	14.00	95.93	4.755	15.80	95.87	4.120	26.12	93.07	3.157
4 Mesh	4.75	303.7	34.79	46.40	84.45	3.852	43.00	84.56	3.371	53.90	81.77	2.921	56.73	78.01	2.238
6 Mesh	3.36	128.5	21.77	38.00	74.60	2.725	44.40	72.83	2.385	45.40	69.89	2.066	55.41	63.30	1.583
8 Mesh	2.36	66.2	15.06	35.30	65.46	1.914	39.10	62.49	1.675	39.30	59.61	1.451	39.18	52.90	1.112
10 Mesh	1.7	38.4	11.17	31.70	57.24	1.379	30.90	54.32	1.207	32.70	51.06	1.045	31.85	44.44	0.801
14 Mesh	1.18	29	8.24	31.50	49.08	0.957	30.60	46.23	0.837	31.00	42.95	0.726	30.50	36.34	0.556
20 Mesh	0.85	17	6.51	25.50	42.47	0.689	24.10	39.86	0.603	24.10	36.65	0.523	23.00	30.24	0.400
28 Mesh	0.6	12.8	5.22	23.10	36.49	0.487	21.80	34.10	0.426	21.20	31.10	0.369	18.30	25.38	0.283
35 Mesh	0.425	9.6	4.24	20.10	31.28	0.345	18.60	29.18	0.302	17.70	26.47	0.261	15.30	21.32	0.200
48 Mesh	0.3	6.9	3.55	15.50	27.26	0.243	14.50	25.35	0.213	13.50	22.94	0.184	11.30	18.32	0.141
65 Mesh	0.212	5.3	3.01	14.50	23.50	0.172	13.10	21.89	0.150	11.60	19.91	0.130	8.70	16.01	0.100
150 Mesh	0.106	7.4	2.26	19.10	18.55	0.086	17.70	17.21	0.075	15.60	15.83	0.065	12.10	12.80	0.050
Pan		22.3		71.60			65.10			60.50			48.21		
Total wt.		987.10		385.9			378.3			382.3			376.7		
P50		5.78		1.23			1.41			1.63			2.12		
P80		8.09		4.08			4.18			4.53			4.99		
RR Piston, RR50				4.69			4.10			3.56			2.72		
RR Piston, RR80				1.98			1.94			1.79			1.62		
P1mm		7.297													

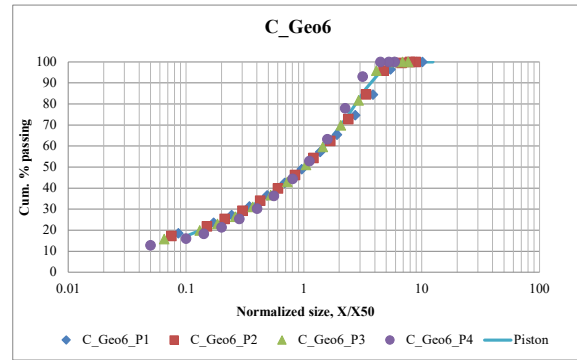
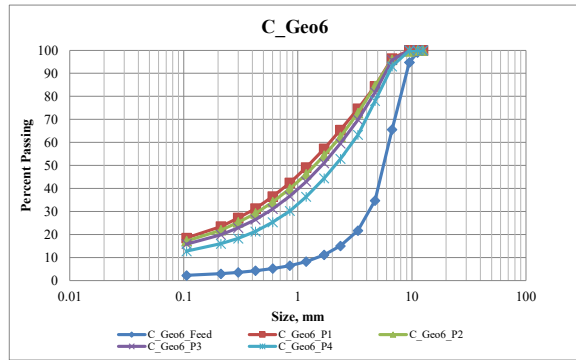


Figure B.16: PPT calibration test results - Cu-Au(C)-Geo6

Appendix C

HPGR and PPT Reproducibility

C.1 HPGR Test Reproducibility

C.1.1 Reproducibility testing

To assess the reproducibility of sample blending and splitting processes to prepare feed for HPGR tests, a suite of duplicate tests were performed on two selected bulk samples. The Cu-Au (C) sample represents a tertiary HPGR test feed, and the Fe (SA) sample corresponds to a finer feed for quaternary stage HPGR testing. The two bulk samples were split to obtain respective sub-samples for PSD analysis. The PSDs of 5 Cu-Au (C) sub-samples and 9 Fe (SA) sub-samples are plotted in Figure C.1, from which it can be seen that all reproducibility tests yielded consistent results except one Cu-Au (C) sample with a small deviation.

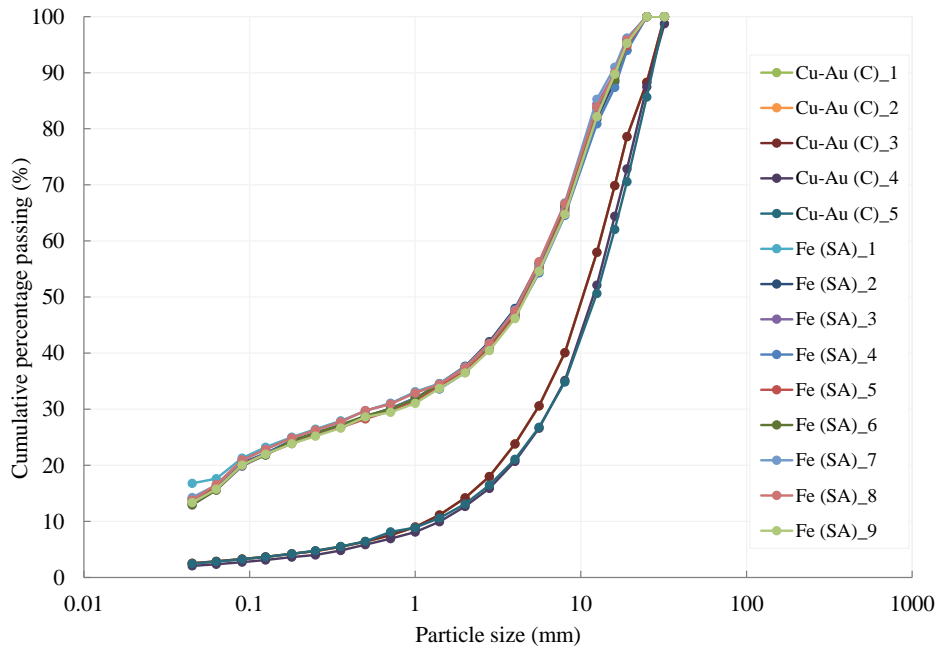


Figure C.1: Variation in PSD of the sub-sampled HPGR feed

Statistical analysis of the tests is summarized in Table C.1 and Table C.2. The results show that parameters F_{80} , F_{50} , and percent below 1 mm have high degrees of repeatability. The means of the P_{80} for the Cu-Au (C) and Fe (SA) sub-samples were 20.86 ± 1.72 mm and 11.72 ± 0.25 mm with 95% confidence, respectively. The measurement precision improved as the PSD became finer, for example, the Relative Standard Error (RSE) for P_{80} measurement improved from 3.0% to 0.9%.

Due to the large sample requirement for HPGR pilot testing, only a limited number of HPGR duplicate tests were performed to evaluate the testing reproducibility. Table C.3 summarizes the results of those HPGR reproducibility tests. Overall, the results indicate good precision for pilot-scale HPGR testing at UBC, particularly for the key machine sizing parameters namely the specific pressing force (F_{sp}), net specific energy consumption (E_{sp}) and specific throughput constant (m).

Table C.1: Five replicates of HPGR feed PSDs - Cu-Au (C)

Statistics	F ₈₀ (mm)	F ₅₀ (mm)	F _{1mm} (%)
No. data points	5	5	5
Mean	20.86	11.15	8.80
Standard Deviation (SD)	1.39	0.91	0.39
Standard Error (SE)	0.62	0.40	0.18
Relative Standard Error (RSE)	3.0%	3.6%	2.0%
Coefficient of Variation (COV)	6.7%	8.1%	4.5%
95% Confidence Interval (CI)	1.72	1.12	0.49

Table C.2: Nine replicates of HPGR feed PSDs - Fe (SA)

Statistics	F ₈₀ (mm)	F ₅₀ (mm)	F _{1mm} (%)
No. data points	9	9	9
Mean	11.72	4.56	32.15
Standard Deviation (SD)	0.33	0.12	0.71
Standard Error (SE)	0.11	0.04	0.24
Relative Standard Error (RSE)	0.9%	0.9%	0.7%
Coefficient of Variation (COV)	2.8%	2.7%	2.2%
95% Confidence Interval (CI)	0.25	0.09	0.54

Table C.3: Summary of HPGR repeat tests

Description	Unit	Test 1	Test 1 repeat	Test 2	Test 2 repeat
F_{sp}	[N/mm ²]	4.04	4.03	4.05	4.04
E_{sp}	[kWh/t]	1.67	1.68	1.89	1.89
x_g	[mm]	22.99	22.63	23.52	23.30
\dot{m}	[ts/hm ³]	336	332	344	347
F_{80}	[mm]	8.86	9.48	14.84	14.86
F_{50}	[mm]	3.28	3.64	5.61	5.75
P_{80}	[mm]	4.31	3.78	4.43	5.37
P_{50}	[mm]	0.49	0.45	0.46	0.64

C.1.2 Reproducibility between labs

A comparison of HPGR testing using a different HPGR machine was conducted to confirm the performance of high pressure comminution for a given ore sample. The comparative tests were performed on the duplicate feed samples provided to the testing facility Lab C, where a Weir HPGR was installed. Table C.4 compares the machine specifications of the Weir unit at Lab C to the Köppern machine at UBC.

Table C.4: HPGR testing facilities

Description	Unit	Köppern/UBC	Weir/Lab C
Roll diameter	[mm]	750	800
Roll length	[mm]	220	250
Roll wear surface	[-]	Hexadur®	Studded
Roll edge design	[-]	Cheek plate	Cheek plate
Installed power	[kW]	200	500 (250 each)
Variable speed drive	[rpm]	up to 40	11-24

Figure C.2 compares the specific throughput constant (\dot{m}) recorded from the test programs conducted at the two facilities. The specific pressing force (F_{sp}) appeared to have a limited impact on the specific throughput constant for the tested ore sample. Although the Köppern HPGR showed a slight decrease in \dot{m} with the increase of F_{sp} due to reduced operating gap, no clear trend was identified for the Weir HPGR testing at Lab C. One question arose as to why the Weir HPGR achieved consistently higher \dot{m} than the Köppern unit. This can be largely explained by the difference in the surface lining between the two units. The Weir HPGR with studded liner yields higher throughput than a smooth surface due to higher friction provided by the autogenous layer (Klymowsky et al., 2006). It is of particular note that industrial Köppern HPGRs use studded liners as well, hence similar \dot{m} can be expected.

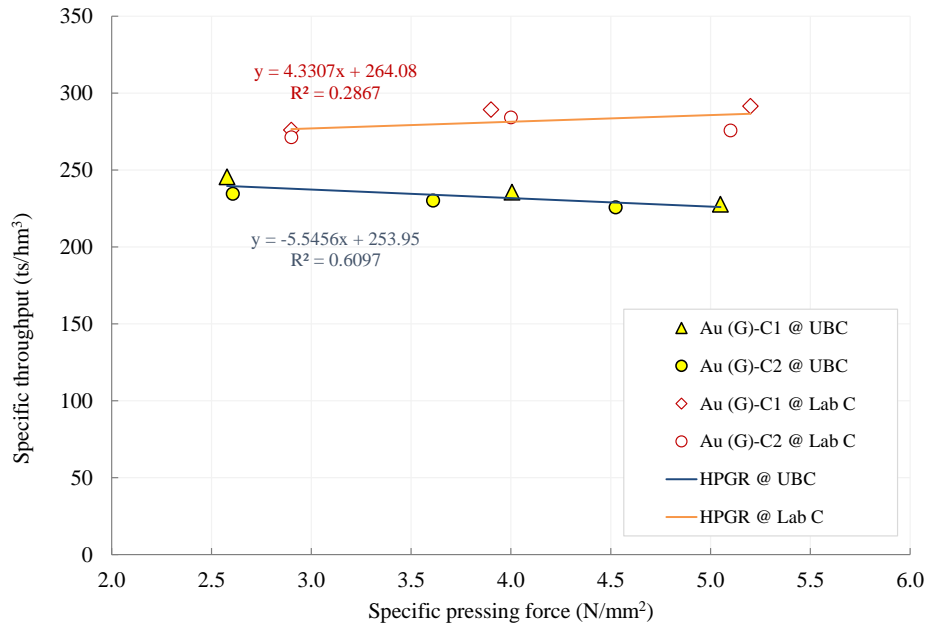


Figure C.2: Specific throughput versus specific pressing force with UBC Köppern HPGR vs Lab C Weir HPGR

Figure C.3 reveals that the total specific energy consumption increased linearly with the increase of the applied specific pressing force for the HPGR testing performed at the UBC and lab C. A good agreement is observed between the two testing facilities, suggesting that both HPGRs would provide a similar amount of specific energy input at a given specific pressing force setting.

Figure C.4 shows that an increase in net specific energy consumption as a result of higher specific pressing force produced finer product as represented by the P_{80} and P_{50} sizes. It is also shown in Figure C.5 that the percent passing 6 mm in the product increased with higher net specific energy input. It is evident that the UBC and Lab C testing facilities provide similar HPGR performance, so that improved confidence in using either testing results for HPGR performance evaluation was gained.

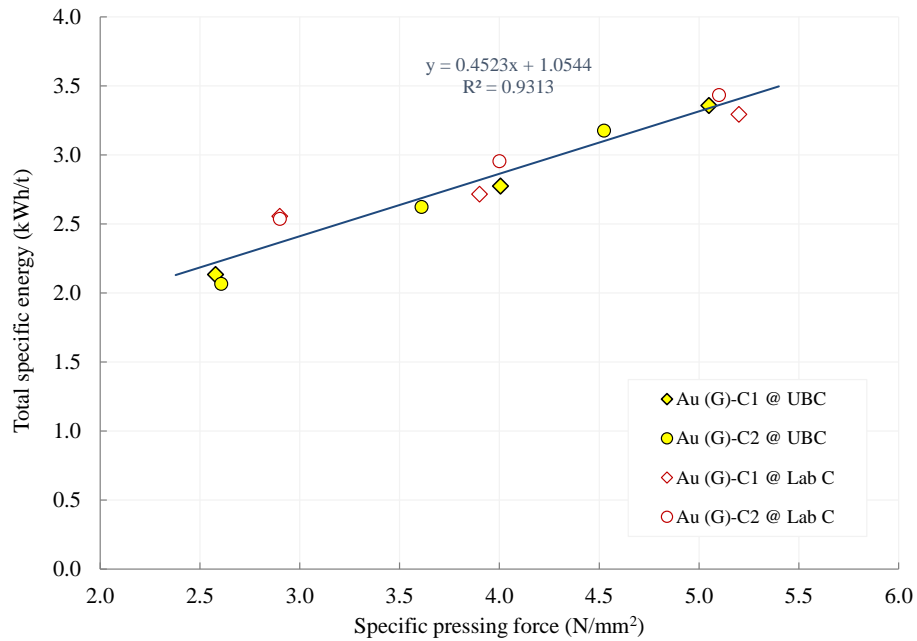


Figure C.3: Total specific energy versus specific pressing force with UBC Köppern HPGR and Lab C Weir HPGR

C.2 PPT Test Reproducibility

C.2.1 PPT calibration test

Reproducibility of the PPT calibration testing was evaluated through performing 6 repeat tests using feed samples prepared from a single bulk sample. Figure C.6 shows the feed PSD of 6 sub-samples for the PPT reproducibility tests and their resulting product PSD. The statistics of the PSD data are summarized in Table C.5. The analysis suggests that parameters F_{80} , F_{50} , and percent below 1 mm have satisfactory repeatability using the current subsampling procedure. The means of the F_{80} and F_{50} were 8.59 ± 0.14 mm and 5.40 ± 0.20 mm with 95% confidence, respectively. The percent below 1 mm parameter (F-1mm) has a slightly lower precision, having a mean of 13.2% with Coefficient of Variation (COV) being 7.8% and Relative Standard Error (RSE) being 3.2%.

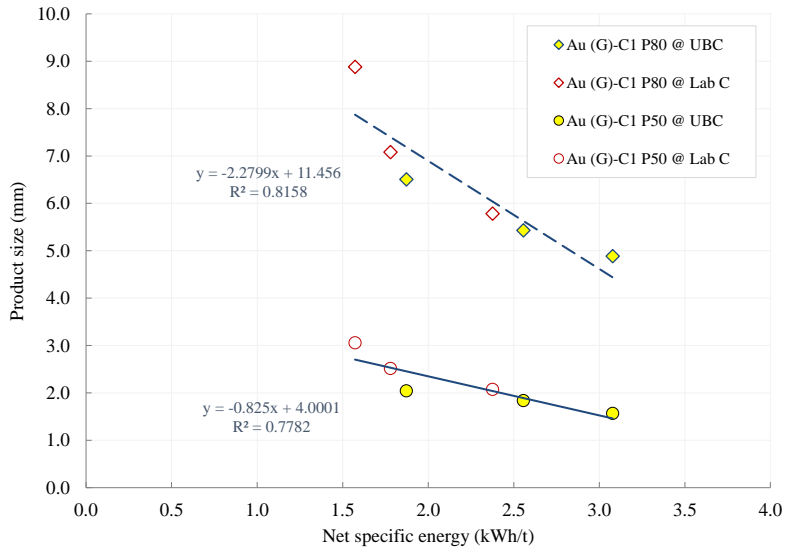


Figure C.4: Center product size P_{80} and P_{50} versus net specific energy with UBC Köppern HPGR and Lab C Weir HPGR

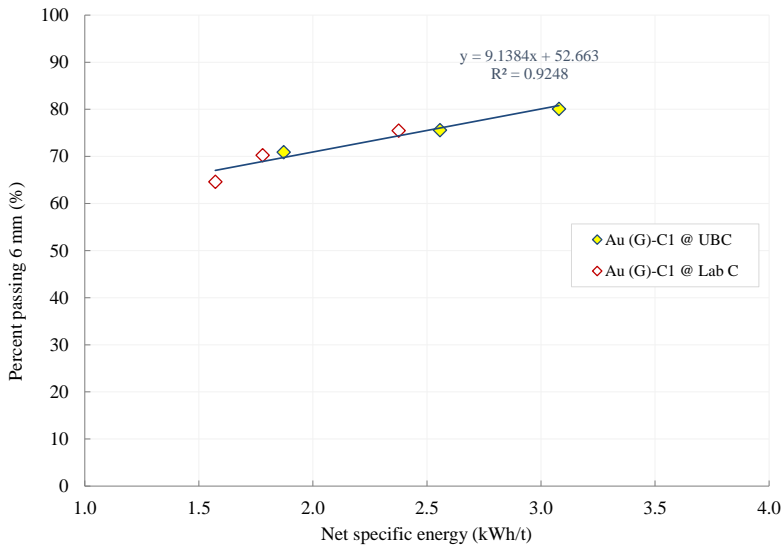


Figure C.5: Percent passing 6 mm in the product of UBC Köppern HPGR and Lab C Weir HPGR

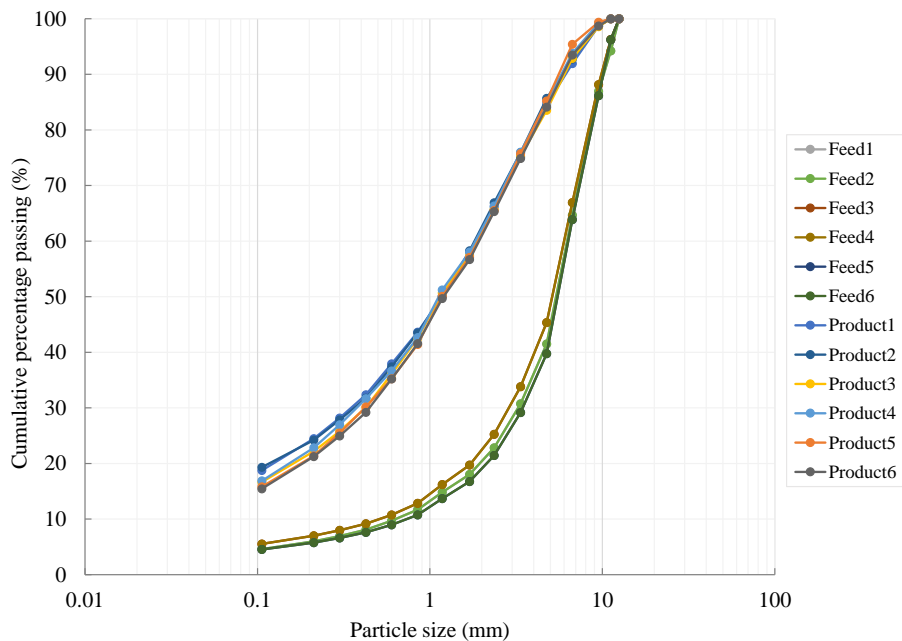


Figure C.6: Variation in PSD of the repeat PPT feed and product

Table C.5: Six replicates of PPT feed and product sizes

Statistics	F₈₀ (mm)	F₅₀ (mm)	F_{1mm} (%)	P₈₀ (mm)	P₅₀ (mm)	P_{1mm} (%)
No. data points	6	6	6	6	6	6
Mean	8.59	5.40	13.20	4.05	1.17	46.07
SD	0.14	0.19	1.03	0.09	0.02	0.61
SE	0.06	0.08	0.42	0.04	0.01	0.25
RSE	0.7%	1.4%	3.2%	0.9%	0.9%	0.5%
COV	1.6%	3.5%	7.8%	2.2%	2.1%	1.3%
95% CI	0.14	0.20	1.08	0.10	0.03	0.64

Table C.6 provides additional results of the 6 PPT calibration repeat tests, including applied piston pressure, estimated specific energy from the force-displacement curve and particle size reduction (F_{80}/P_{80} and F_{50}/P_{50}). Overall, the results indicate a good precision for the PPT calibration testing.

Table C.6: Summary of PPT calibration repeat tests

Statistics	Pressure (Mpa)	Esp (kWh/t)	F ₈₀ /P ₈₀	F ₅₀ /P ₅₀
No. data points	6	6	6	6
Mean	240.3	2.37	4.64	2.14
SD	0.09	0.07	0.09	0.06
SE	0.04	0.03	0.04	0.03
RSE	0%	1.2%	0.8%	1.2%
COV	0%	3.1%	2.0%	2.9%
95% CI	0.10	0.08	0.10	0.07

C.2.2 PPT simulation test

Repeat tests have also been performed to assess the reproducibility of the PPT simulation testing. Two sub-samples were prepared from the Au (T9) ore sample for the reproducibility tests. Figure C.7 presents the scatter plots of t_{10} values as a function of the input energy for specific particle sizes obtained from the two repeat tests, along with the fitted t_{10} breakage curve to both of the PPT simulation tests.

Table C.7 lists the fitted breakage and appearance parameters, clearly showing excellent consistency between the repeat tests.

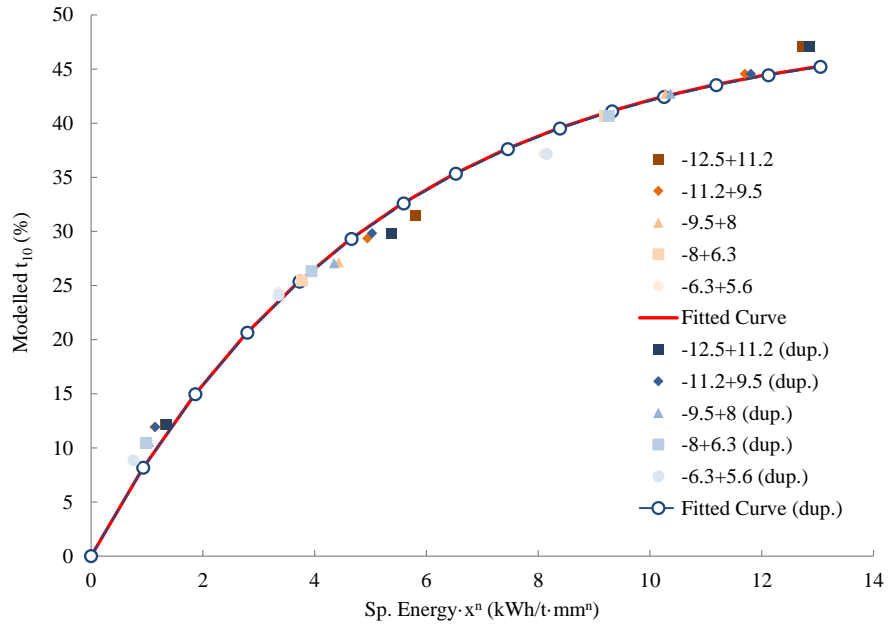


Figure C.7: PPT simulation repeat tests - breakage curves

Table C.7: Breakage and appearance parameters for the repeat simulation tests

Test	Au (T9)	Au (T9)-dup	Delta
M	49.1	49.0	-0.1%
f_{mat}	0.20	0.20	-0.2%
n	0.60	0.61	0.6%
$M \cdot f_{mat}$	9.61	9.58	-0.3%
β_1	109.91	109.60	-0.3%
β_2	8.00	7.90	-1.2%
β_3	130.58	129.67	-0.7%
β_4	29.40	29.06	-1.2%
β_5	202.63	203.90	0.6%
β_6	98.77	99.81	1.1%
β_7	0.66	0.65	0.0%
β_8	0.49	0.49	0.1%
β_9	0.41	0.42	0.2%

Appendix D

Machine Learning Approach for m Prediction

D.1 Introduction

In Chapter 5, the multi-variable linear regression models failed to predict the HPGR specific throughput constant (m) parameter with a reasonable accuracy. Due to the advances in data science and computing power in the recent years, one can now implement more algorithm-intensive models for predicting and forecasting the desired response variables using a large set of predictor variables. Such models are commonly referred to as the machine learning models, or analytical models (McCoy and Auret, 2019). Some examples of these data-driven models in the comminution field are the ore grindability identification (Gonzalez et al., 2008), grinding mill liner prediction (Ahmadzadeh and Lundberg, 2013), and SAG mill power forecasting (Hoseinian et al., 2017; Li et al., 2019).

In this research study, the data-driven approach is adopted to develop an improved model for m prediction using the same database obtained from the UBC HPGR database. Having a more accurate prediction of the m increases the confidence of the HPGR sizing and circuit design based on limited information on the feed characteristics and operating conditions. The methodology can also be applied to the HPGR operation, where the developed model can be integrated into the existing process control system to improve the operational performance.

D.2 Methodology

The overall workflow to achieving a machine learning model solution is shown in Figure D.1. The overall procedure involves data collection, data pre-processing, model training and testing, and final model selection. If the developed models meet the target prediction accuracy and model reliability, further deployment can be considered.

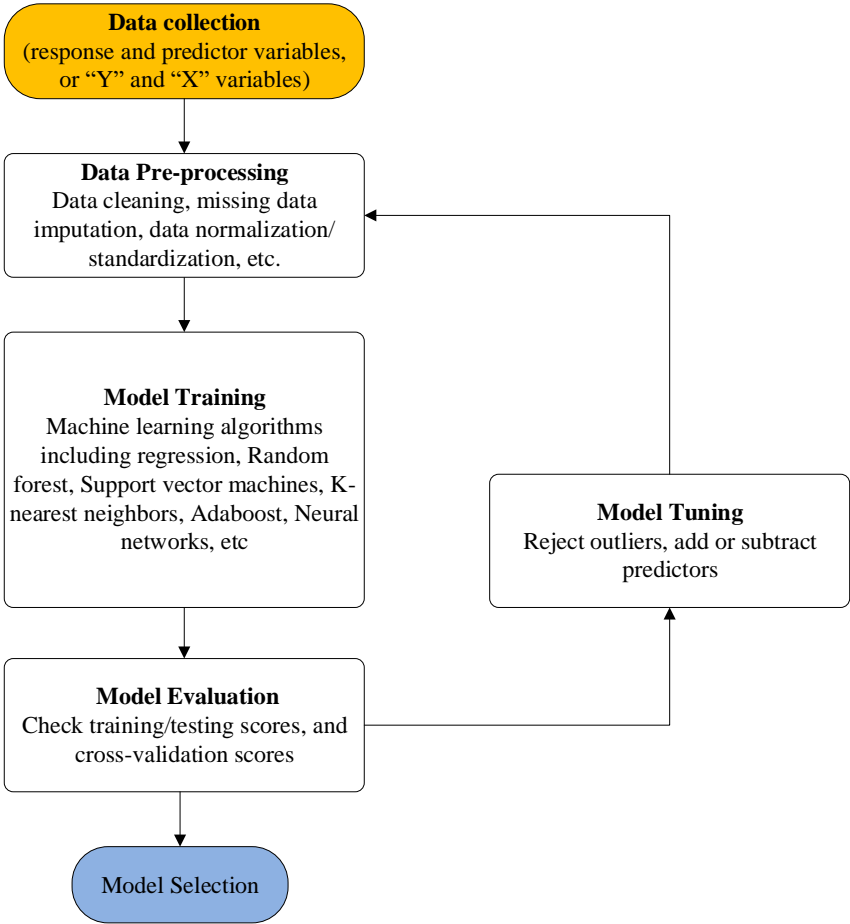


Figure D.1: Workflow for machine learning model development

D.2.1 Data collection

The same dataset used to build the multiple-linear regression models in Chapter 5 was used to develop the machine learning models for m . The detail description and basic statistics for each of the predictor variables can be found in Chapter 5. It should be noted that the database contains both qualitative or quantitative variables. The qualitative variables were introduced as dummy variables during the modeling process.

D.2.2 Data pre-processing

Similar to the steps followed in Chapter 5, the first requirement was to perform data pre-processing, which include data cleaning and missing data imputation. The data pre-processing is an essential step to ensure the prepared database is in a logical structure for data mining process and subsequent analytical modeling. The general tools utilized in data pre-processing include data interpolation, dimensions reduction, normalization and standardization, and features selection and creation.

D.2.3 Analytical modeling

The analytical modeling is based on machine learning algorithms. Once the database was prepared, various machine learning algorithms were applied to the data set to develop the m models. A brief description about some commonly used machine learning algorithms is provided in this section, including Regression (linear and non-linear), Random forest, Support Vector Machines (SVM), K-Nearest Neighbors (KNN), AdaBoost, and Neural Networks (NN).

Random Forest

The random forest (Breiman, 2001) is an algorithm that uses multiple trees. It uses bagging and feature randomness when building each individual tree to try to create a forest of trees whose prediction by committee is more accurate than that of any individual tree.

Support Vector Machine

The Support Vector Machines (SVM) algorithm tries to find the boundary between the data points that will create a maximized margin (Cortes and Vapnik, 1995). In the machine learning field, most datasets are in high dimensional space, although it is not possible to visualize, the general principle is the same.

K-Nearest Neighbors

The K-Nearest Neighbors is one of the simpler machine learning methods. The KNN algorithm (Altman, 1992) simply counts and identifies the nearest neighbors of a new data point. It classifies the new point based on the most common neighbor.

AdaBoost

The AdaBoost algorithm (Freund and Schapire, 1995), short for adaptive boosting, works alongside other models to improve their results. By using an ensemble of smaller models, it can create a new classifier with improved accuracy.

Neural Network

The Long Short-Term Memory (LSTM) neural network, is capable of learning long term dependencies on its own. This is accomplished with learning “blocks” and “gates” that can open and close based on the required or given data.

D.2.4 Model evaluation and selection

Each of the selected machine learning models was trained and tested based on training/testing and cross-validation procedures. The testing results provide the key statistics for the model evaluation, from which the best performing model can be selected for prediction of the desired response variable.

D.3 Results and Discussion

Machine learning modeling with training/testing dataset (based on 80/20 random split) and 5-fold CV was performed using the cleaned dataset. Table D.1 summarizes the testing and evaluation results for those selected models. The AdaBoost algorithm appeared to provide the best scores, with R^2 being 0.798 and 0.809 for the training/testing evaluation and 5-fold CV evaluation, respectively. The respective MAE are 12.5 ts/hm³ and 13.0 ts/hm³. It was found that the linear regression model produced a negative R^2 , which is often the indication that the regression model has a high bias and/or high variance. The result is aligned with the findings from Chapter 5, concluding that the most simple linear regression model is not suitable for the \dot{m} prediction. It was also noted that the Neural Networks (NN) model produced a negative R^2 . The major limitation of NN in this case is the lack of samples for training. Typically, NN models are trained on thousands of data points, whereas this study was limited to only a few hundred data points.

Table D.1: Testing scores for potential mdot models

Model	Training/Testing (80/20 split)			5-fold Cross-validation		
	RMSE	MAE	R^2	RMSE	MAE	R^2
kNN	35.6	26.3	0.293	36.2	26.1	0.316
SVM	39.4	27.9	0.136	40.8	29.4	0.130
Random Forest	20.7	14.7	0.761	22.6	16.4	0.734
Neural Network	196.6	192.8	-20.554	196.0	191.7	-19.098
Linear Regression	263.6	37.8	-37.719	118.8	23.4	-6.385
AdaBoost	19.0	12.5	0.798	19.1	13.0	0.809

Figure D.2 compares the Adaboost predicted \dot{m} to the measured values, with the 95% confidence intervals of the regression line and the predictions. The distribution of error between the AdaBoost prediction and actual observation is presented in Figure D.3. The resulting standard deviation is under 4.4 ts/hm³. Statistically, this suggests that 95% of the error estimates fall within 8.8 ts/hm³ of the true value, based on 2 standard deviations estimate.

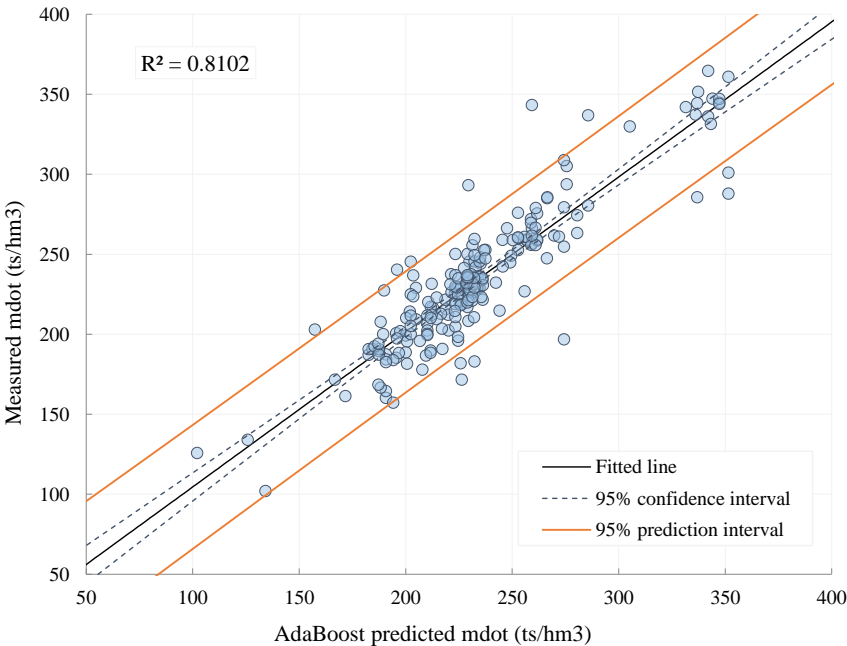


Figure D.2: Prediction vs observation using the AdaBoost model

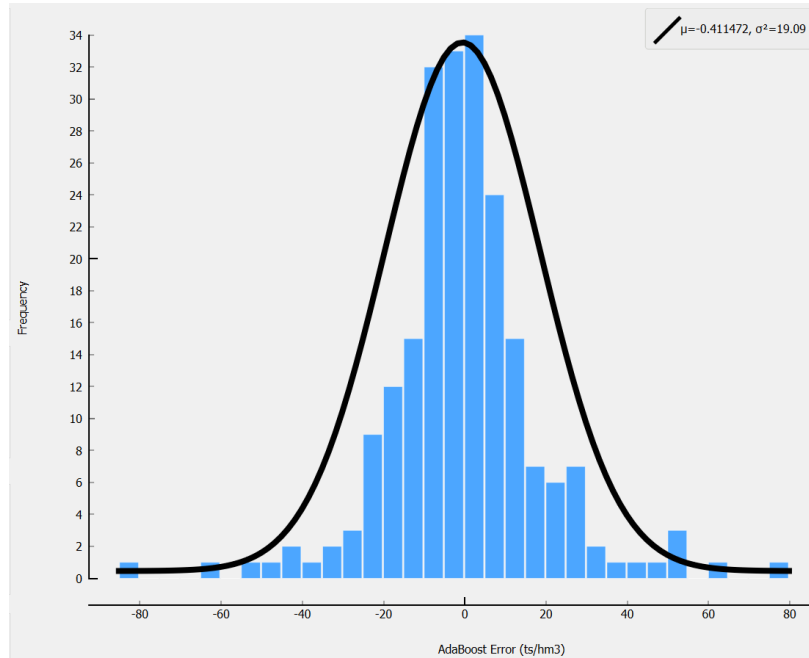


Figure D.3: Distribution of AdaBoost prediction error

D.4 Summary and Conclusions

This study presented a data-driven approach for modeling of the pilot HPGR \dot{m} based on available predictor variables from the UBC HPGR database. The results showed that the best machine learning model for the \dot{m} prediction was the AdaBoost model, capable of predicting the \dot{m} with an average error of 12.5 ts/hm^3 , and the prediction error has a standard deviation of 4.4 ts/hm^3 . The model accuracy is considered sufficient for implementation to estimate the throughput capacity of the pilot HPGR operating at varying conditions for given materials.

To further improve the machine learning model, a larger data set would be required that allows for better training and testing and potentially using other machine learning models, such as the Neural Networks (NN). Overall, the machine learning approach shows promising potential for the prediction of the \dot{m} parameter. Other opportunities of using the data-driven modeling are the development of real time measurement of the key HPGR performance indicators for the HPGR operation, which can be included in the advanced process control system for the operation.